DOCTORAL THESIS

DEVELOPMENT OF GENE-THERAPY TOOLS FOR BERNARD-SOULIER SYNDROME TYPE C TREATMENT

GONZALO MARTÍNEZ NAVAJAS

Director: Pedro José Real Luna

July 2023

UNIVERSITY OF GRANADA ‖ ***DOCTORATE PROGRAMME OF BIOMEDICINE***

UNIVERSIDAD DE GRANADA

Genyo

Editor: Universidad de Granada. Tesis Doctorales
Autor: Gonzalo Martínez Navajas
ISBN: 978-84-1117-025-1
URI: https://hdl.handle.net/10481/84671

El doctorando / *The doctoral candidate* **D. Gonzalo Martínez Navajas** y el director de la tesis / *and the thesis supervisor/s:* **Dr. Pedro José Real Luna.**

Garantizamos, al firmar esta tesis doctoral, que el trabajo ha sido realizado por el doctorando bajo la dirección de los directores de la tesis y hasta donde nuestro conocimiento alcanza, en la realización del trabajo, se han respetado los derechos de otros autores a ser citados, cuando se han utilizado sus resultados o publicaciones.

/

Guarantee, by signing this doctoral thesis, that the work has been done by the doctoral candidate under the direction of the thesis supervisor/s and, as far as our knowledge reaches, in the performance of the work, the rights of other authors to be cited (when their results or publications have been used) have been respected.

Lugar y fecha / Place and date:

Granada, 22 de junio de 2023.

Director de la Tesis — Doctorando

Thesis supervisor — *Doctoral candidate.*

Dr. Pedro José Real Luna — D. Gonzalo Martínez Navajas

DEVELOPMENT OF GENE-THERAPY TOOLS FOR BERNARD-SOULIER SYNDROME TYPE C TREATMENT.

~Resumen de Tesis~

Las plaquetas son fragmentos celulares anucleados liberados de los megacariocitos, sus células precursoras, que residen en la médula ósea. Las plaquetas participan en una gran variedad de procesos, como la cicatrización de heridas, el papel en el cáncer y la respuesta inmunitaria, entre otros. Sin embargo, su función principal y mejor definida es la regulación de la hemostasia.

Cuando se produce una lesión vascular, las células endoteliales se desprenden y queda expuesta la membrana basal y, más concretamente, las fibras de colágeno. El factor von Willebrand (VWF) circulante se adhiere a estas fibras formando un complejo que es reconocido por el receptor GPIb-V-IX de la superficie de las plaquetas. Esta interacción induce un efecto de rodamiento de las plaquetas circulantes sobre la zona lesionada, hasta detenerlas. Este proceso induce la activación, reclutamiento y agregación de las plaquetas circundantes sobre la zona afectada, formando un tapón plaquetario y poniendo fin a la hemorragia al interaccionar con los factores de coagulación.

El complejo GPIb-V-IX resulta del ensamblaje de cuatro subunidades, GPIbα, GPIbβ, GPIX y GPV. Las variantes patogénicas que afectan a sus genes codificantes, excepto *GP5*, dan lugar a la manifestación de un trastorno plaquetario hereditario, el síndrome de Bernard-Soulier (SBS). Según el gen afectado podemos distinguir el SBS Tipo A1 cuando la

variante aparece en *GP1BA*, Tipo B (*GP1BB*) y Tipo C (*GP9*). Significativamente, el *GP9* presenta un mayor número de variantes patogénicas que conducen al SBS.

Como resultado de estas variantes patogénicas, el receptor GPIb-V-IX es incapaz de exteriorizarse completamente en la superficie plaquetaria. En consecuencia, esto genera plaquetas no funcionales que son incapaces de reconocer las zonas de lesión y continuar con la cascada de coagulación. Los pacientes que padecen SBS se caracterizan por frecuentes episodios de sangrados mucocutáneos y hemorragias graves. Además, experimentan macrotrombocitopenia, es decir, un recuento reducido de plaquetas gigantes. La ausencia del receptor explica el fenotipo hemorrágico observado.

Estos pacientes sólo pueden recurrir a medidas de prevención para evitar los episodios hemorrágicos, y beneficiarse de tratamientos paliativos para disminuir la gravedad de la hemorragia. Sin embargo, siguen enfrentándose a una enfermedad de por vida que merma la calidad de ésta. En casos excepcionales, el trasplante de células madre hematopoyéticas (CMH) entre hermanos afectados y no afectados por el SBS ha conseguido revertir la enfermedad. Sin embargo, el número limitado de donantes HLA compatibles y el riesgo de aloinmunización limitan su uso frecuente como abordaje terapéutico.

Utilizando la revolucionaria tecnología CRISPR-Cas9, desarrollamos knockouts para cada gen codificador de subunidad en dos líneas celulares megacarioblásticas que expresan constitutivamente el receptor GPIb-V-IX. Estos knockouts informaron sobre la importancia que cada subunidad tiene para el ensamblaje de todo el receptor en un microambiente humano fisiológico y replicaron la mayoría de los fenotipos descritos en la literatura, estos son, ausencia o alteración de la externalización de GPIb-V-IX para genes inductores de SBS. En cuanto a GP5-KOs, confirmamos que este gen no impide la externalización del receptor GPIb-IX pero disminuye la presencia de GPIbβ. Este hecho dentro del ensamblaje del receptor no impidió su funcionalidad uniendo VWF pero se redujo ligeramente.

A medida que avanza la investigación, la terapia génica adquiere cada vez más importancia en el tratamiento de las enfermedades monogénicas. Concretamente, la terapia génica que utiliza vectores integradores en las CMH, que son la fuente de todos los componentes celulares de la sangre, está cobrando importancia en el campo de la hematología como enfoque curativo para abordar las neoplasias malignas en su origen. De hecho, actualmente se están investigando numerosas enfermedades en ensayos clínicos, empleando diversos tratamientos basados en vectores lentivirales autoinactivantes. Estos ensayos pretenden corregir deficiencias primarias observadas en afecciones como el

síndrome de Wiskott-Aldrich, SCID-X1 o ADA-SCID.

Además, a finales de 2022, la “Food and Drug Administration” ya ha concedido la aprobación para la comercialización y distribución de dos terapias génicas basadas en la tecnología de vectores lentivirales. Estas terapias están dirigidas al tratamiento de la β-Talasemia y al de la Adrenoleucodistrofia Cerebral, marcando avances significativos en este campo.

En cuanto al SBS, algunos estudios han aportado pruebas convincentes de la reversión fenotípica y la restauración de la funcionalidad de las plaquetas mediante la generación de plaquetas producidas *in vitro* a partir de células madre pluripotentes inducidas derivadas de pacientes con mutaciones en *GP1BA* y *GP1BB*. Además, la transducción de CMHs con vectores lentivirales que expresan *GP1BA* y *GP1BB*, seguida de su infusión en modelos murinos *in vivo* carentes de sus respectivos genes (*Gp1ba*^{null} y *Gp1bb*^{null}), ha demostrado de forma consistente una recuperación de los tiempos de sangrado y un alivio significativo de la macrotrombocitopenia.

Estos hallazgos nos han inspirado para investigar la idoneidad potencial del SBS tipo C como candidato a ser corregido mediante un enfoque similar. La estrategia terapéutica propuesta consiste en tratar a los pacientes con SBS tipo C que albergan variantes patogénicas de *GP9* con

un vector lentiviral autoinactivante que sobreexpresa *GP9* en las CMH del paciente. Estas CMH se tratarían *ex vivo* y posteriormente se reinfundirían en el paciente una vez corregidas.

Para lograr una expresión de GPIX estable y específica de tejido, es crucial la integración de nuestro casete terapéutico en las CMH del paciente. Estas CMH son responsables de la producción de megacariocitos (MK) y plaquetas anormales en individuos con EVC. Sin embargo, debido a la limitada disponibilidad de pacientes y a la singularidad de sus características hemorrágicas, puede que no sea factible aislar las CMH como herramienta donde optimizar nuestras herramientas de terapia génica. Por lo tanto, son necesarios modelos preclínicos alternativos para evaluar la eficacia de nuestras estrategias de sustitución génica antes de aplicarlas a nuestras células diana finales.

Además, también desarrollamos otro modelo de enfermedad de SBS tipo C mediante la eliminación de *GP9* en células madre pluripotentes inducidas (iPSCs). Este modelo añadió un paso más de sofisticación, ya que, mientras que el modelo de células megacarioblásticas sirvió para explorar la biología de los receptores, en este caso pudimos reproducir el desarrollo hematopoyético y megacariocítico completo, desde las CMH hasta la producción de MKs y plaquetas. Pudimos confirmar que las iPSCs carentes de *GP9* generaban *in vitro* plaquetas gigantes similares a las plaquetas de los pacientes

con SBS, convirtiéndose en una alternativa perfecta a las CMHs de los pacientes.

El siguiente paso crucial de nuestra investigación fue el desarrollo de vectores lentivirales autoinactivantes (LV) que expresan GPIX bajo promotores fisiológicos, asegurando una expresión megacariocítica específica adecuada para su aplicación clínica. Los modelos de enfermedad *GP9*-KO previamente establecidos sirvieron como valiosas herramientas preclínicas para evaluar la funcionalidad de nuestros LVs en la restauración de la expresión de GPIX. Sorprendentemente, los GPIX-LVs transdujeron con éxito células GP9-KO, conduciendo a la recuperación de niveles de expresión de GPIX comparables a los de las células de tipo salvaje (WT). Es importante destacar que esta expresión era específica de tejido, ya que era indetectable en otras líneas celulares no megacarioblásticas.

Además, la introducción exógena de GPIX facilitó la externalización de las subunidades restantes, en particular GPIbα, que actúa como subunidad funcional del complejo. Estos receptores rescatados genéticamente recuperaron su capacidad funcional, incluido el reconocimiento de VWF soluble, la aglutinación en presencia de ristocetina y la adhesión firme a recubrimientos de VWF en presencia de botrocetina.

De forma similar, en nuestro modelo de enfermedad de SBS tipo C basado en iPSCs, la transducción no sólo restauró

la expresión de GPIX en la membrana de los MKs sino que también recuperó su expresión en las plaquetas, lo que resultó en una reversión a su tamaño normal. En ambos casos, los niveles de expresión fueron comparables a los de las células WT. Es importante destacar que nuestras LVs exhibieron actividad funcional a lo largo de todo el proceso de diferenciación, sin estar sujetas a silenciamiento epigenético.

Una vez demostrada la funcionalidad de nuestras herramientas de terapia génica, quisimos validar su eficacia recuperando la expresión de GPIX, ahora en nuestras futuras células diana, CMHs aisladas de pacientes con SBS Tipo C portadores de diferentes variantes patogénicas de *GP9*. A través de su aislamiento a partir de sangre periférica no movilizada, transducción y posterior diferenciación en MKs y plaquetas, validamos la reversión del fenotipo SBS *ex vivo*. Por lo tanto, estos resultados confirman el prometedor potencial terapéutico de nuestro enfoque de terapia génica.

Por último, desarrollamos un modelo murino específicamente diseñado para evaluar la eficacia de nuestros LVs en la restauración de funciones fisiológicas normales, como el tiempo de sangrado. Este modelo tiene una gran relevancia como estudio preclínico definitivo antes de pasar a la fase clínica. No sólo nos permitirá seguir evaluando la eficacia de nuestros LVs que expresan GPIX, sino también valorar la bioseguridad integradora de nuestros LVs y evaluar la presencia de posibles autoanticuerpos contra el complejo GPIb-V-IX rescatado genéticamente.

Los hallazgos previos de nuestra propia investigación, junto con descubrimientos relevantes realizados por otros investigadores en modelos murinos *Gp1ba*^{null} y *Gp1bb*^{null}, nos llenan de optimismo respecto a los posibles resultados al tratar modelos de ratón *Gp9*^{null} SBS en un futuro próximo.

En conclusión, los hallazgos significativos presentados en este trabajo de investigación establecen firmemente el síndrome de Bernard-Soulier tipo C como un trastorno hereditario que tiene el potencial de ser curado mediante estrategias de terapia génica.

~Thesis Summary~

Platelets are anucleate cell fragments released from megakaryocytes, their precursor cells which reside within the bone marrow. Platelets participate in a wide variety of processes like wound healing, role in cancer, immune response, among others. However, their main and best-defined function is in the regulation of hemostasia.

Once a vascular injury occurs, endothelial cells become detached and the basal membrane, and more specifically, collagen fibers, become exposed. Circulating von Willebrand factor (VWF) adhere to these fibers forming a complex which is recognized by the platelet surface receptor GPIb-V-IX. This interaction induces a rolling effect of circulating platelets over the injury zone, till arresting them. This process induces the activation, recruitment, and aggregation of surrounding platelets over the affected area, forming a platelet plug and ending the hemorrhage when interacting with the coagulation factors.

GPIb-V-IX complex results from the assembly of four subunits, GPIbα, GPIbβ, GPIX and GPV. Pathogenic variants affecting their coding genes except for *GP5* results in the manifestation of an inherited platelet disorder, Bernard-Soulier Syndrome (BSS). Accordingly to the affected gene we can distinguish BSS Type A1 when the variant appears in *GP1BA*, Type B (*GP1BB*) and Type C (*GP9*). Significantly, *GP9* exhibits a higher number of pathogenic variants that lead to BSS.

As a result of those pathogenic variants, GPIb-V-IX receptor is unable to fully externalize on the platelet surface. Consequently, this generates non-functional platelets that are incapable of recognizing injury zones and performing subsequent following necessary steps. Patients suffering for BSS are characterized by frequent mucocutaneous bleeding episodes and severe hemorrhages. Additionally, they experience macrothrombocytopenia, this is, reduced count of giant platelets. Pathogenic variants affecting the assembly of the receptor explains the observed bleeding phenotype.

These patients uniquely can take advantage of prevention, to avoid the bleeding episodes, and palliative treatments in order to diminish the hemorrhage severity. However, they still face a lifetime disease which diminish their life quality. In exceptional cases, hematopoietic stem cells (HSCs) transplantation among siblings affected and non-affected by BSS has been successful in reversing the disease. Nevertheless, the limited number of compatible HLA donors and the risk of alloimmunization limits its frequent use as a therapeutic approach.

Utilizing the revolutionary CRISPR-Cas9 technology, we developed knockouts for each subunit coding gene in two megakaryoblastic cell lines that constitutively express the GPIb-V-IX receptor. These knockouts shed light on the importance that each subunit makes for the assemblage of the entire receptor in a physiological human microenvironment and replicated most of the phenotypes described in the literature,

these are, absence or impaired GPIb-V-IX externalization for BSS driver genes. Regarding *GP5*-KOs, we confirmed that this gene does not impede GPIb-IX receptor externalization but decreases GPIbβ presence. This fact within the receptor assembly did not hinder its functionality by binding VWF but it was slightly reduced.

As research progresses, gene therapy is becoming increasingly important in the treatment of monogenic diseases. Specifically, gene therapy utilizing integrative vectors on HSCs, which are the source of all blood cellular components, is gaining significance in the field of hematology as a curative approach for addressing malignancies at their origin. In fact, numerous diseases are currently being investigated in clinical trials, employing various treatments based on self-inactivating lentiviral vectors. These trials aim to correct primary deficiencies seen in conditions such as Wiskott-Aldrich Syndrome, SCID-X1, or ADA-SCID.

Moreover, by the end of 2022, the Food and Drug Administration has already granted approval for the marketing and distribution of two gene therapies based on lentiviral vector technology. These therapies target β-Thalassemia and Cerebral Adrenoleukodystrophy, marking significant advancements in the field.

Regarding BSS, numerous studies have provided compelling evidence of the phenotypical reversion and restoration of platelet functionality through the generation of *in*

vitro-produced platelets from induced pluripotent stem cells derived from patients with *GP1BA* and *GP1BB* mutations. Furthermore, the transduction of HSCs with lentiviral vectors expressing *GP1BA* and *GP1BB*, followed by their infusion into *in vivo* murine models lacking their respective genes (*Gp1ba*^{null} and *Gp1bb*^{null}), has consistently demonstrated a recovery of bleeding times and a significant alleviation of macrothrombocytopenia.

These findings have inspired us to investigate the potential suitability of BSS type C as candidate for being corrected using a similar approach. The proposed therapeutic strategy involves treating BSS type C patients harboring *GP9* pathogenic variants with a self-inactivating lentiviral vector that overexpresses *GP9* in the patient's HSCs. These HSCs would be treated *ex vivo* and subsequently reinfused into the patient once they have been corrected.

To achieve stable and tissue-specific expression of GPIX, the integration of our therapeutic cassette into the patient's HSCs is crucial. These HSCs are responsible for the production of abnormal megakaryocytes (MKs) and platelets in individuals with BSS. However, due to the limited availability of patients and the uniqueness of their bleeding characteristics, it may not be feasible to isolate HSCs for testing our gene therapy tools. Therefore, alternative preclinical models are necessary to evaluate the effectiveness of our gene replacement strategies before applying them on our final target cells.

Additionally, we also developed another BSS type C disease model by knocking-out *GP9* in induced pluripotent stem cells (iPSCs). This model added one step more of sophistication, because, while megakaryoblastic cell model served to explore receptor biology, in this case we were able to reproduce whole hematopoietic and megakaryocytic development, from HSCs to produce MKs and platelets. We could confirm that iPSCs lacking *GP9* generated *in vitro* giant platelets similar to BSS patients' platelets, becoming a perfect alternative to patients' HSCs.

The next crucial step involved in our research was the development of self-inactivating lentiviral vectors (LV) that express GPIX under physiological promoters, ensuring megakaryocytic-specific expression suitable for clinical application. The previously established *GP9*-KO disease models served as valuable preclinical tools for assessing the functionality of our LVs in restoring GPIX expression. Remarkably, GPIX-LVs successfully transduced *GP9*-KO cells, leading to the recovery of GPIX expression levels comparable to wild-type (WT) cells. Importantly, this expression was tissue-specific, as it was undetectable in other non-megakaryoblastic cell lines.

Furthermore, the introduction of exogenous GPIX facilitated the externalization of the remaining subunits, particularly GPIbα, which serves as the functional subunit of the complex. These genetically rescued receptors regained their functional capacity, including the recognition of soluble

VWF, agglutination in the presence of ristocetin and firm adhesion to coated VWF in the presence of botrocetin.

Similarly, in our BSS Type C disease model based on iPSCs, the transduction not only restored GPIX expression on the membrane of MKs but also recovered its expression in platelets, resulting in a reversion to their normal size. In both cases, the expression levels were comparable to those of WT cells. Importantly, our LVs exhibited functional activity throughout the entire differentiation process, without being subject to epigenetic silencing.

Once proved the functionality of our gene therapy tools, we wanted to validate its efficacy by recovering the GPIX expression, now in our future target cells, HSCs isolated from BSS Type C patients carrying different *GP9* pathogenic variants. Through its isolation from non-mobilized peripheral blood, transduction, and subsequent differentiation into MKs and platelets, we validated the reversal of the BSS phenotype *ex vivo*. Therefore, these results confirm the promising therapeutic potential of our gene therapy approach.

Lastly, we developed a novel murine model specifically designed to evaluate the effectiveness of our LVs in restoring normal physiological functions, such as bleeding time. This model holds significant relevance as the definitive preclinical study before progressing to the clinical phase. It will not only allow us to further evaluate the efficacy of our GPIX-expressing LVs, but also assess the integrative biosafety of our LVs and

evaluate the presence of possible autoantibodies against the genetically rescued GPIb-V-IX complex.

The previous findings from our own research, along with relevant discoveries made by other researchers in *Gp1ba*^{null} and *Gp1bb*^{null} murine models, fill us with a sense of optimism regarding the potential outcomes when treating BSS *Gp9*^{null} mouse models in the near future.

In conclusion, the significant findings presented in this research work firmly establish Bernard-Soulier Syndrome type C as an inherited disorder that holds the potential to be cured through gene therapy strategies.

LEGEND OF FIGURES

LEGEND OF TABLES

Abbreviation	Meaning
µg	Micrograms
µL	Microliters
µM	Micromolar
7AAD	7-Amino Actinomycin D
AAV	Adeno-Associated Virus
AONs	Antisense Oligonucleotides
ATCC	American Type Culture Collection
AVs	Adenoviruses
bp	Base Pairs
BSS	Bernard-Soulier Syndrome
CDS	Coding DNA Sequence
CHO	Chinese Hamster Ovary
CML	Chronic Myelogenous Leukemia
CRISPR	Clustered Regularly Interspaced Short Palindromic Repeat
CT	Cytosolic Domain
CTCs	Circulating Tumor Cells
D	Digested
DAMP	Damage-Associated Molecular Patterns
ddH_2O	Double Distilled Water
DMD	Duchenne Muscular Dystrophy
DMSO	Dymethil Sulfoxide
DSB	Double Strand Break
dsDNA	Double Stranded DNA
ED	Extracellular Domain
EDTA	Ethylenediaminetetraacetic Acid

eGFP	Enhanced Green Fluorescent Protein
EMA	European Medicines Agency
EMT	Epithelial-to-Mesenchymal Transition
EP	Enrichment Pool
ESC	Embryonic Stem Cells
FACS	Fluorescence-Activated Cell Sorting
FDA	Food and Drug Administration
FSC	Forward Scatter
FW	Forward
gDNA	Genomic DNA
GP	General Pool
GP1BA	Glycoprotein Ibα [gene]
GP1BB	Glycoprotein Ibβ [gene]
GP5	Glycoprotein V [gene]
GP6	Glycoprotein VI [gene]
GP9	Glycoprotein IX [gene]
Gp9	Murine Glycoprotein IX [gene]
GPIbα	Glycoprotein Ibα [protein]
GPIbβ	Glycoprotein Ibβ [protein]
GPIX	Glycoprotein IX [protein]
GPV	Glycoprotein VI [protein]
GT	Glanzmann's Thrombasthenia
GVHD	Graft Versus Host Disease
HDR	Homology Directed Repair
h*GP6*(p)	Promoter of h*GP6*
HPA	Human Platelet Antigens
HSCs	Hematopoietic Stem Cell

indels	Insertion-Deletion Mutation
IPD	Inherited Platelet Disorder
iPSC	Induced Pluripotent Stem Cell
IPTG	β-D-1-thiogalactopyranoside
IS2	Insulator 2
ITR	Inverted Terminal Repeat
KO	Knockout
L	Lane
LBD	Ligand Binding Domain
LRR	Leucine Rich Repeats
LTR	Long Terminal Repeat
LV	Lentiviral Vector
MCS	Multicloning Site
MEP	Megakaryocyte Erythroid Progenitor
MFI	Mean Fluorescence intensities
MK	Megakaryocyte
mL	Milliliter
MOI	Multiplicity Of Infection
MPV	Mean Platelet Volume
mRNA	Messenger RNA
MSD	Mechanosensitive Domain
ND	Non-Digested
ng	Nanograms
NHEJ	Non-Homologous End Joining
NK	Natural Killer
ºC	Celsius Degrees
OCS	Open Canalicular System

pA	PolyA Tail
PAM	Protospacer Adjacent Motif
PAMP	Pathogen-Associated Molecular Patterns
PBS	Phosphate Buffered Saline
PCR	Polymerase Chain Reaction
PID	Platelet Immunodeficiency
PFA	Paraformaldehyde
PNK	Phosphonucleotide Kinase
PRP	Platelet-Rich Plasma
PS	Phosphatidyl Serine
PX-458	pSpCas9BB-2A-GFP
RE	Restriction Enzyme
R-EV	Reporter Empty Vector- (eGFP)
R-GPIX	Reporter Vector- (GPIX-eGFP)
RIPA assay	Ristocetin-Induced Platelet Aggregation
RNAi	RNA Interference
RPM	Revolutions Per Minute
RT	Reverse Transcriptase
RV	Reverse
RVs	Retroviruses
SD	Standard Deviation
SFFV	Spleen Forming Focus Virus
sgRNA	Single Strand RNA
SIN	Self-Inactivating Vector
SP	Signal Peptide
SSC	Side Scatter
ssDNA	Single Stranded DNA

ssODN	Single Stranded Oligodeoxynucleotide
ssRNA	Single Stranded RNA
TALEN	Transcription Activator-Like Effector Nuclease
TD	Transmembrane Domain
T-EV	Therapeutic Empty Vector
TF	Tissue Factor
T-GPIX	Therapeutic Vector- (GPIX)
TPO	Trombopoietin
VSVg	Vesicular Stomatitis Virus
VWF	Von Willebrand Factor
WT	Wild Type
X-GAL	5-bromo-4-chloro-3-indolyl-β-D-galactopyranoside
ZFN	Zinc-Finger Nuclease

CHAPTER I

INTRODUCTION

1. Platelets: Characterization and role in hemostasis.

1.1. Components of platelets: Description and functions.

Platelets are cytoplasmic fragments shed from their precursors, megakaryocytes (MKs), residing in the bone marrow[1]. They are the smallest blood cells, their size ranges from 2-5 µm, with discoid morphology when they are not activated and are anucleated[2,3]. Platelets circulate in the bloodstream close to the apical surface of the vessel wall, allowing to have a rapid response when a vascular injury occurs[1].

1.1.1. Platelet production: Thrombopoiesis.

Platelets circulate through the bloodstream in concentrations ranging from 1.50-4.00x10^{11} platelets/L. It is estimated that MKs, their precursor cells, can generate around 10^{11} platelets per day.

Thrombopoiesis is the bone marrow process responsible for producing platelets from Hematopoietic Stem Cells (HSCs) which resides in it. These stem cells differentiate into megakaryoblasts, which undergo multiple rounds of DNA replication without cell division, leading to the formation of large MKs with multilobulated nuclei. Reached this stage, MKs undergo maturation, during which platelet-specific organelles are formed. The mature MKs produce cytoplasmic extensions called proplatelets, which enter the sinusoidal vessels and are

released into the bloodstream. The proplatelets then reach their mature form through fragmentation[1,4–6] (**Figure 1**).

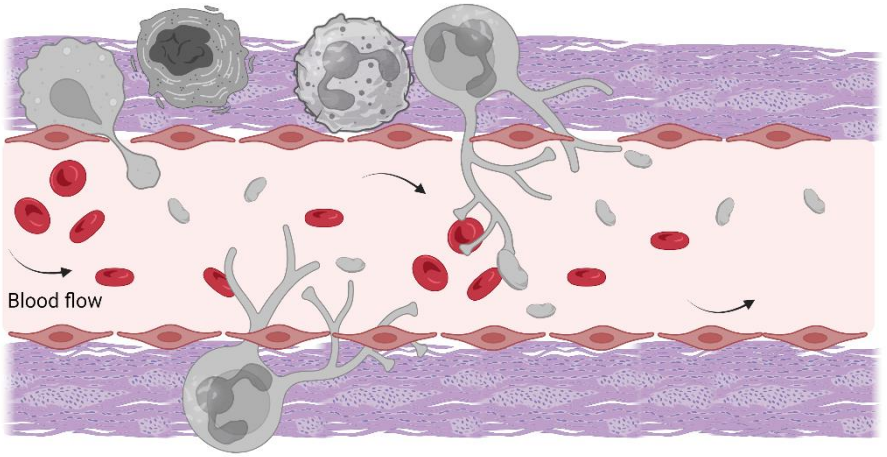

Figure 1. Proplatelets generation.

Schematic view of megakaryocytes extending pseudopodia through sinusoidal vessels releasing proplatelets into the bloodstream. Image created by Martínez-Navajas, G. -Author.

Thrombopoiesis is regulated by various growth factors, with thrombopoietin (TPO) being the primary regulator. TPO promotes the growth and maturation of MKs, thereby stimulating platelet production[5–7].

1.1.2. Platelet clearance.

Platelets have a relatively short lifespan of about 7-10 days. Platelet clearance involves the elimination of senescent platelets from circulation when they reach the end of their lifespan or become damaged. The primary site of platelet clearance is the spleen, although the liver and lungs also contribute to a lesser extent[1,4].

During clearance, specialized immune cells called macrophages perform phagocytosis, engulfing and digesting the platelets. In the spleen, macrophages reside in the red pulp, particularly within the splenic sinusoids. As platelets age or sustain damage, their surface markers undergo changes that make them recognizable to macrophages. Among these markers, it is possible to highlight the phosphatidyl serine (PS) exposure after platelet activation or degradation or the gradual loss of their RNA contents as platelets age. Altered platelets are then captured by macrophages in the splenic sinusoids. Once captured, macrophages internalize the platelets through phagocytosis, enclosing them within phagosomes [4,8].

Another possible mechanism for platelet clearance is the glycoprotein desyalilation, specifically affecting the GPIbα subunit of the GPIb-V-IX receptor. Sialidases can recognize senescent platelets, removing the sialic acid from the glycoprotein. This absence is recognized by the hepatic asialoglycoprotein receptor-1, removing them from the bloodstream. This recognition induces the expression of TPO, which promotes the platelet generation and regulates the number of platelets in the blood[1,8].

Platelet clearance serves a vital role in maintaining proper platelet levels and functionality in the bloodstream, thereby ensuring effective blood clotting and hemostasis.

1.1.3. Platelet structure.

The structure of the platelets can be divided in peripheral zone, sol-gel zone, organelle zone and membrane system[7].

1.1.3.1. Peripheral zone

- ***Principal transmembrane proteins***

The platelet's glycocalyx is dynamic and contains multiple glycoproteins and integrins responsible for the interaction with subendothelial structures of the injured vessel walls, for the platelet activation and aggregation, as long as for the clot retraction. Despite there are several integrins and glycoproteins involved in these processes, we are going to focus on few of the membrane proteins that are essential for platelet adhesion, activation and aggregation:

GPIb-V-IX receptor.

This glycoprotein plays a crucial role in both normal hemostasis and arterial thrombosis. It facilitates platelet adhesion to areas of injury by recognizing its main substrate, von Willebrand factor (VWF) (**Figure 2**), which can bind to collagen through its A1 domain under high shear rates. In addition, the complex can also bind to thrombospondin, promoting platelet adhesion in the absence of VWF. It has the ability to interact with P-selectin, facilitating interactions between endothelial cells and platelets, as well as platelet-to-platelet interactions[7,9].

Furthermore, GPIb-V-IX contributes to procoagulant activity on activated platelets by providing binding sites for α-thrombin, factor XI, and high-molecular-weight kininogen. Additionally, the cross-linking of GPIb-V-IX by VWF or other multivalent ligands initiates complex signaling processes that ultimately result in the activation of IIb-IIIa and shedding of the GPIbα ectodomain (**Figure 2**)[1,7].

Glycoprotein IIb-IIIa.

This protein, also known as integrin αIIbβIII (**Figure 2**), is responsible for platelet aggregation when activated. In its resting state, it exists in a low-affinity form, but it transitions to a high-affinity state upon platelet activation. It is the most abundant glycoprotein on the surface of platelets and is also stored in α-granules[7].

The protein is composed of a heterodimer formed by the interaction of two transmembrane subunits, αIIb and β3. Following platelet activation, a signaling cascade triggers a conformational change in the extracellular domain of the integrin, turning it into a high-affinity receptor for fibrinogen and VWF, which it shares with the GPIb-V-IX receptor. Binding to divalent fibrinogen or multivalent VWF allows activated IIb-IIIa to facilitate platelet-platelet interactions and the formation of platelet aggregates[9].

Additionally, activated IIb-IIIa can bind to vitronectin and fibronectin (**Figure 2**), enabling platelet adhesion to

subendothelial structures and contributing to the regulation of platelet aggregation[9].

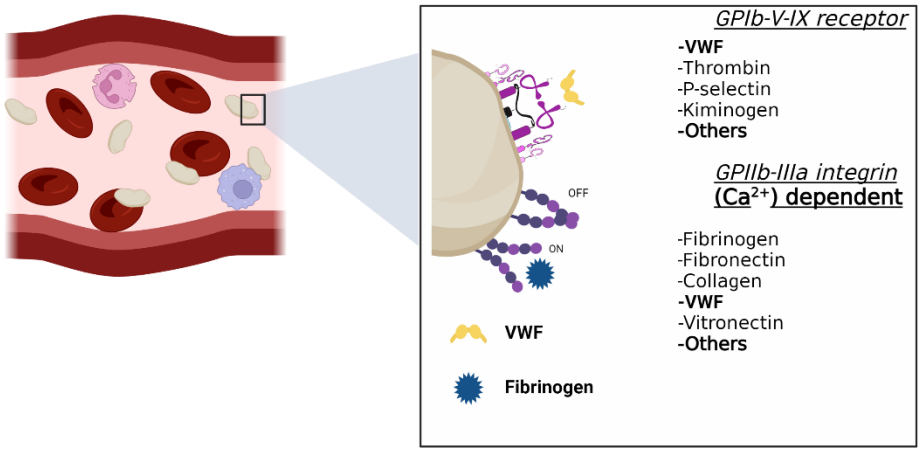

Figure 2. GPIb-V-IX and GPIIb-IIIa, main proteins on platelet surface.

Zoom of the main and most abundant platelet surface glycoproteins-integrins. Indicating main substrates and two-conformational-states of the integrin. To note, both are capable to interact with VWF. Image created by Martínez-Navajas, G. -Author.

GPVI receptor

GPVI is a crucial receptor belonging to the immunoglobulin superfamily, serving as the primary signaling receptor for collagen on human platelets. It plays crucial roles in hemostasis and various platelet-mediated processes. GPVI forms a complex with the FcRγ-chain, which is found on platelets in both monomeric and dimeric forms. The monomeric form is predominantly present on resting platelets, exhibiting insufficient affinity for collagen to initiate activation in response to physiological levels. In contrast, the dimeric form displays increased collagen affinity and collagen binding to this dimeric

complex triggers intracellular signals, leading to the production of additional dimers[10,11].

In the absence of the FcRγ-chain, GPVI cannot reach the platelet surface, thus preventing collagen-induced platelet activation. Platelets adhere to exposed collagen fibers by binding immobilized VWF to GPIb-V-IX. This facilitates the binding of collagen to low-affinity GPVI, generating intracellular signals that subsequently induce inside-out activation of integrins, including αÌIβI and IIb-IIIa. As a result, GPVI activation is reinforced, promoting stable platelet adhesion and spreading through the binding of αÌIβI to collagen and IIb-IIIa to VWF, respectively. Following activation by collagen and other agonists, GPVI is rapidly shed from the platelet surface, likely as a preventive measure against excessive collagen-induced activation[7,10].

Integrin αIIβI.

Platelet integrin αÌIβI, also called glycoprotein Ia/IIa, is a receptor located on the surface of platelets. It consists of two subunits, α2 and β1, and belongs to a family of cell adhesion molecules known as integrins.

The main role of integrin αÌIβI is to function as a receptor for collagen, a key component of the extracellular matrix found in blood vessel walls and connective tissues. The interaction between αÌIβI and collagen is crucial for platelet adhesion to exposed collagen fibers at sites of vascular injury or damage[10].

When platelets come into contact with collagen, the binding of immobilized VWF to the platelet receptor GPIb-V-IX facilitates the attachment of collagen to the low-affinity state of integrin αÌIβI. This interaction triggers intracellular signaling, leading to the inside-out activation of integrins. Activated αÌIβI integrins enable platelets to firmly adhere to collagen, promoting stable platelet adhesion and spreading. This process not only enhances the activation of GPVI but also facilitates platelet aggregation by allowing the binding of IIb-IIIa to fibrinogen and other adhesive molecules[10–12].

In summary, integrin αÌIβI on platelets acts as a receptor for collagen, facilitating platelet adhesion and interaction with the extracellular matrix. Its activation contributes to stable platelet adhesion and spreading, reinforcing GPVI activation and enabling platelet aggregation through the binding of IIb-IIIa to fibrinogen and other adhesive substances.

P-selectin.

Platelet CD62P, also known as P-selectin, is a cell surface protein that plays a significant role in hemostasis. CD62P is involved in the initial response to vascular injury. When blood vessels are damaged, platelets are activated and undergo changes that include the translocation of CD62P from α-granules to the platelet's membrane[13].

Additionally, endothelial cells that line the blood vessels can express P-selectin molecules on their surface in response to various triggers like inflammation or injury. The binding of

CD62P on activated platelets to P-selectin on endothelial cells initiates a process called platelet rolling. This rolling motion allows platelets to interact with the endothelium and establish a connection. It can also bind to GPIbα subunit from GPIb-V-IX receptor, favoring platelet activation cascade[9,13,14].

Additionally, CD62P participates in platelet-leukocyte interactions during hemostasis. Activated platelets can bind to leukocytes by interacting with CD62P and its ligand, P-selectin glycoprotein ligand-1 (PSGL-1), which is present on the surface of leukocytes. This interaction facilitates the recruitment and activation of leukocytes at the site of vascular injury, contributing to the formation of a stable blood clot[9,13].

- ***Other components and structures of the peripheral zone***

Below the glycocalyx we can find the lipid bilayer, which is asymmetrical, consisting in an inner membrane layer containing negative charged aminophospholipids such as PS, and an external layer containing neutral phospholipids. Once activated, negative charged PS can flip to the outer membrane promoting their pro-coagulant activity, of important note during the secondary hemostasia[7].

The peripheral zone also exhibits the open canalicular system (OCS), which consists in a series of channels in their plasma membrane communicating with the exterior. This system allows for the uptake of plasma components through endocytosis and the release of granule contents through

exocytosis. When platelets are activated, their granules move towards the plasma membrane or the OCS releasing their content through exocytosis, where they diffuse into the extracellular environment. In addition, OCS can be evaginated providing an increase in plasmatic membrane required for platelet spreading over injury zones after the platelet adhesion to the basal membrane. Consequently, activated platelets can increase their surface up to 4-times in comparison to resting platelets[1,7].

The submembrane area of platelets is located directly under the lipid bilayer and plays a crucial role in platelet function. It contains a network of thin actin filaments known as the membrane contractile cytoskeleton, which is essential for platelet morphological change and the movement of receptors and particles across the platelet's surface. Within the submembrane compartment, the cytoplasmic domains of transmembrane receptors interact with various proteins, including those associated with calmodulin, myosin, and actin filaments that make up the cytoskeleton. These interactions regulate the signaling processes necessary for platelet activation[7,15].

1.1.3.2. Sol-Gel zone.

This zone is located beneath the peripheral zone. It has gel-like consistency and contains a meshwork of cytoskeletal proteins, including actin filaments (responsible of shape change after activation) and microtubules (after platelet

activation, centralize the granules to favors its externalization via OCS) (**Figure 3**), which provide structural support and help maintain the shape of the platelet[7,16].

1.1.3.3. Granular zone

This zone contents three different components: α-granules, dense granules and cellular contents (**Figure 3**).

α-granules are the most frequent organelles, and they contain a variety of proteins, including membrane proteins like IIb-IIIa integrin, P-selectin, and CD36. They also contain adhesive molecules such as fibrinogen, VWF, vitronectin, and multimerin 1, which play roles in hemostasis and thrombosis. Additionally, platelet α granules store chemokines that have direct antimicrobial properties, contributing to host defense against pathogens. They also store pro- and anti-angiogenic factors that regulate angiogenesis[16].

Dense granules serve to store small molecules such us Ca^{2+}, ADP, bioactive amines, and polyphosphates[3,17].

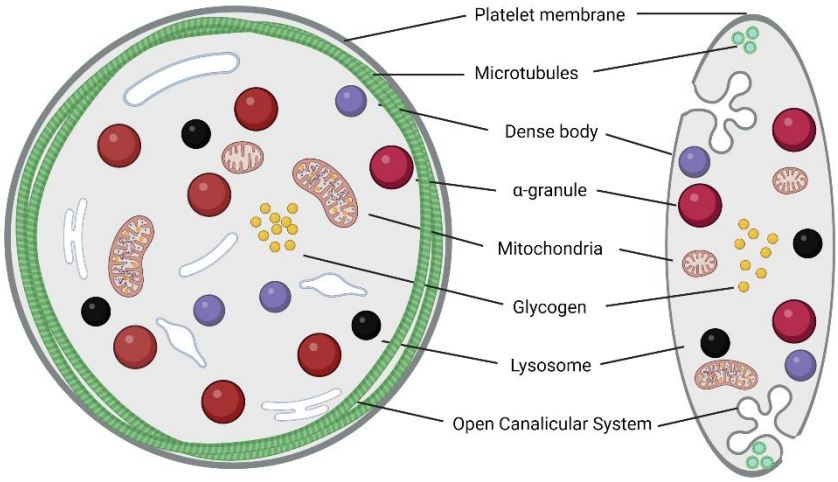

Figure 3. Platelet ultrastructure.

Schematic view of main components that are observable within soft-gel and granular zones of platelets. Image created by Martínez-Navajas, G. -Author (inspired in Beavo et al., 2012)[18].

Within platelets, lysosomes and mitochondria are present, and they play essential roles in platelet function. Lysosomes store enzymes and other molecules that are crucial for various platelet processes. Mitochondria, on the other hand, contain ATP and ADP, which are important energy sources for platelet activation and function [2,18].

1.1.4. Platelet proteome and sheddome.

Despite most of the proteins present in the platelets are inherited from their megakaryocytic precursors or endocytosed from plasma, platelets can also synthetize their own proteins thanks to the RNA storage that they conserve after their

release from the MK. Activated platelets can synthesize a wide variety of proteins such as B cell lymphoma 3 (Bcl-3), interleukin (IL)-1b, tissue factor (TF), P-selectin, among others. These proteins could be involved in the regulation of many processes, such as coagulation, clot retraction, inflammation, cancer metastasis, among other processes[1,19].

Interestingly, platelets can shed surface proteins during ligand binding or activation. Platelet ectodomain shedding has emerged as a potential mechanism to modulate platelet activity and produce bioactive protein fragments. Metalloproteinases like ADAM17 and ADAM10 can negatively regulate platelet adhesion and activation by cleaving platelet glycoproteins GPIb-V-IX and GPVI, respectively. Shedding of molecules such as CD40L and semaphoring-4D generates bioactive fragments that affect other cells function through receptor binding, contributing to inflammation and wound healing. Shedding of soluble P-selectin is important for inflammatory markers, but the mechanisms behind P-selectin shedding from platelets still require further investigation. While the constituents of the platelet sheddome are gradually being characterized, more research is needed to understand the impacts of ectodomain shedding on platelet function[1].

1.2. Hemostasis phases: Role of platelets in vascular injury and clot formation.

Platelets are involved in many processes, with growing impact as long as they are researched, however, hemostasia is considered their main function. Hemostasis can be defined as the set of processes aimed at counteracting bleeding caused by vascular injury. This process can be divided into four phases: vasoconstriction, primary hemostasis, secondary hemostasis, and fibrinolysis[20,21].

1.2.1. Vasoconstriction

Following vascular injury, the damaged blood vessel undergoes vasoconstriction, which helps to minimize the blood loss. This constriction is facilitated by the release of vasoconstrictor molecules from the injured endothelial cells, such as endothelin. Endothelin acts to promote the contraction of smooth muscle fibers surrounding the endothelial cells, contributing to the narrowing of the blood vessel and the reduction of blood flow. Furthermore, endothelial cells also release other molecules such as VWF, facilitating platelet recruitment and activation[22,23].

1.2.2. Primary hemostasia

This phase will be thoroughly explained due to the significance of platelet membrane receptors in our research. After vessel vasoconstriction, the primary hemostasis is initiated (**Figure 4**), encompassing the initial stages of the

coagulation process and culminating in the formation of a platelet plug[24].

When a vessel ruptures, endothelial cells become detached, exposing the collagen-rich extracellular matrix. At this point, VWF, a molecule circulating within the blood plasma and released by activated endothelial cells[23], recognizes and bind to the collagen-rich matrix through its A1 domain, mainly under high shear rates[24,25].

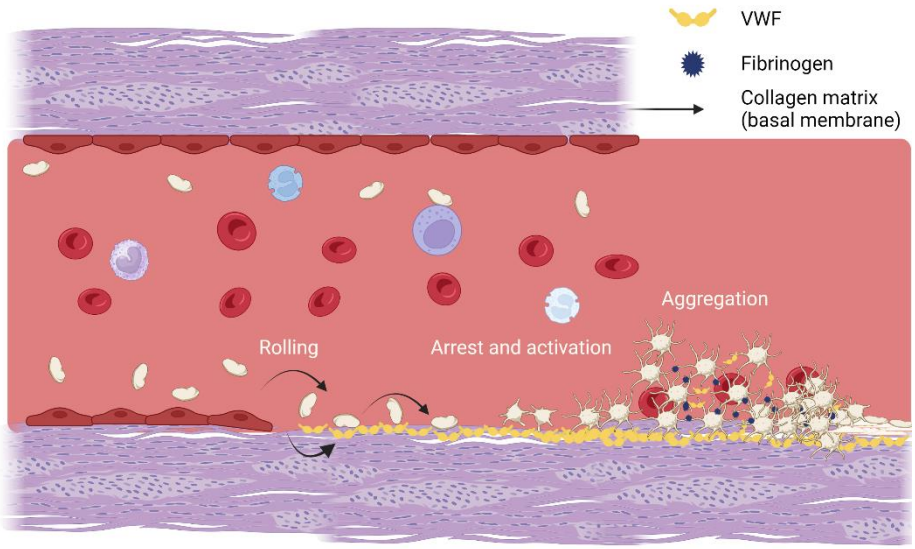

Figure 4. Primary hemostasia.

Schematic view of the primary hemostasia, phase where surface glycoproteins are the main responsible for adhering to vascular injury zones, becoming activated and inducing an aggregation response which culminates with platelet plug formation. Image created by Martínez-Navajas, G. -Author.

Simultaneously, platelets circulate in the bloodstream in an inactive conformation carrying the GPIb-V-IX complex on their surface. This receptor enables them to sense vascular injury by interacting with VWF adhered to collagen. Although

this interaction is weak, it is sufficient to induce platelet deceleration. Platelets begin to roll over the subendothelium until they eventually stop and cover the injured region (**Figure 4**). During this process, the interaction between the GPIb-V-IX receptor and VWF, along with the interaction of other platelet receptors with their agonist molecules such as GPVI and Integrin αÌIβI, which specifically recognize collagen, assist in platelet adhesion to the matrix. This step is crucial in initiating a signaling cascade that leads to the activation of platelet integrins (Integrin αÌIβI and IIb-IIIa), transitioning them from a resting state to a high affinity for their respective substrates. This process is denominated platelet activation (**Figure 4**). Subsequently, platelets undergo a morphological change, extending pseudopods and releasing the contents of their granules outward and externalizing new adhesion proteins like P-selectin and IIb-IIIa, incrementing its presence on the platelet surface. This phenomenon enhances the activation of neighboring platelets[9,14,20,21,24–27].

The most relevant integrin on the platelet membrane is GPIIb-IIIa[20,26]. Once activated, it exhibits high affinity for molecules such as fibrinogen, which has two binding sites for the integrin, or VWF. This enables platelets to interact with each other through the formation of interplatelet bridges, culminating in platelet aggregation and the formation of the platelet plug [20,21,24–26] (**Figure 4**).

1.2.3. Secondary hemostasia.

The secondary phase of hemostasis, known as the coagulation phase, plays a crucial role in strengthening and stabilizing the platelet plug formed during the primary phase. It involves a complex cascade of reactions that culminate in the formation of a fibrin clot.

After platelets have adhered to the injured vessel wall and created a plug, the coagulation cascade is initiated. This cascade consists of a series of enzymatic reactions triggered by tissue factor (TF) and activated platelets. TF is released by damaged cells, particularly in the subendothelial tissue[15,22].

The coagulation cascade can be divided into the intrinsic and extrinsic pathways, which eventually converge to form a common pathway leading to the formation of a fibrin clot. In the intrinsic pathway, factors present in the plasma, such as Factor XII, Factor XI, and Factor VIII, are sequentially activated upon exposure to subendothelial components and activated platelets. In the extrinsic pathway, tissue factor released by damaged cells combines with Factor VII to initiate coagulation[1].

Both pathways eventually activate Factor X, which plays a critical role in converting prothrombin to thrombin. Notably, platelets also participate in this phase. Following platelet activation, platelets flip negatively charged PS to their outer membrane. PS exposure subsequently facilitates the assembly of the pro-thrombinase complex near the developing

blood clot and promotes thrombin generation. Thrombin, in turn, transforms soluble fibrinogen into insoluble fibrin strands, creating a meshwork that traps platelets and stabilizes the platelet plug. Thrombin also enhances platelet activation and amplifies the coagulation cascade by activating additional clotting factors[1].

The clotting process is regulated by various anticoagulant mechanisms to prevent excessive clot formation and maintain blood flow. Natural anticoagulants like Antithrombin III, protein C, and protein S inhibit clotting factors and restrict clot formation to the site of injury [28,29].

1.2.4. Fibrinolysis phase

Finally, coagulation factors also play a role in the dissolution of the platelet thrombus, a process known as fibrinolysis. During this phase, the enzyme plasminogen is converted into its active form called plasmin. Plasmin then acts on the fibrin meshwork that forms the blood clot and breaks it down into smaller fragments. Thrombus dissolution plays a key role in blood flow reestablishment to guarantee the oxygen supply to the different tissues and organs and to favor the repairment of the damaged areas by facilitating the access to immune cells and other types involved in the wound healing process[28,29].

1.3. Platelet's role in other processes.

Despite platelets have been characterized by their function in hemostasia, last decade new roles of platelet function have been elucidated.

1.3.1. Inflammation and wound healing.

Platelets are known as "first responders", because they usually are the first who reach the affected area and releasing a wide range of molecules. This is possible thanks to their reduced size, their highly active cytoskeleton and the absence of nuclei which could limit their movement throughout the damaged area. The absence of nuclei impedes a continued action; thus, they participate as releaser of different types of molecules from their granules with different finalities[3,30].

It has been reported that platelets are able to migrate withing inflamed vessels in response to different stimuli like SDF1 or CXCL12, released by stromal cells[31]. Recruited platelets within the damaged tissue now release new chemokines and cytokines from their granules with role in inducing a tropism to the damaged area for new platelets, more specialized immune cells, bone marrow progenitor and endothelial progenitor cells. These cells will sterilize the surrounding area from pathogens and will aid to regenerate the affected tissue or organ[3].

Additionally, platelets help to induce the inflammation response as "first responder" when they reach the affected area by releasing molecules such as TGF-β, P-selectin,

CD40L, among others[32]. These are a heterogeneous mixture of cytokines and adhesion molecules which bind, activate or induce homing responses for monocytes, neutrophils or T-lymphocytes[33,34].

Platelet's TGF-β also chemoattract non-immune resident cells like fibroblasts, activating them and making them to evolve through myofibroblasts. This culminates with the remodeling and occlusion of the injury area. It also promotes mesenchymal stem cells differentiation, aiding to recover the tissue[35].

1.3.2. Tumor progression and metastasis.

Having seen all the features where platelets participate by promoting cell grown and regeneration, it is important to note that tumor cells can also take advantage of these characteristics.

A tumor can grow to various cubic millimeters until it reaches a certain size limit. At this point, it needs to expand its vascularization to ensure a continuous supply of oxygen and nutrients. By releasing cytokines and growth factors like VEGF (vascular endothelial growth factor), it can activate endothelial cells. These activated endothelial cells expose molecules such as P-selectin, VWF, tissue factor, and different integrins, eventually leading to the recruitment of platelets[3].

Additionally, tumor cells can induce vascular permeabilization by releasing proangiogenic factors, which help detach perivascular cells. This detachment is a critical step that promotes platelet arrest at these exposed sites. When platelets interact with these molecules, they initiate signaling cascades and eventually release their granule cargo, thereby assisting tumor cells in remodeling the surrounding tissue and inducing inflammation. Tumor cells can also exploit pro-tumorigenic molecules like TGF-β (transforming growth factor-beta) to their advantage[36,37].

Additionally, they can also get access to the circulation by escaping the tumoral mass. To do this, they adopt an invasive phenotype, phenomena known as “epithelial-to-mesenchymal transition” (EMT). It is characterized by fibroblastic (stem) morphology, expression of matrix-degrading enzymes, increment of their motility and acquired resistance to apoptosis. All these adaptations, not surge uniquely in an autonomous manner, but also are influenced by factors released by the microenvironment, where mesenchymal stem cells, macrophages and also activated platelets have been seen to contribute to this phenomenon[38].

When tumor cells invade blood vessels, they leave the supportive tumor microenvironment and face challenging conditions within the bloodstream. The high shear stresses in blood vessels can damage cancer cells, and the blood contains immune cells, such as natural killer (NK) cells, which can detect and kill circulating tumor cells (CTCs). Platelets play a

crucial role in the early interaction with CTCs. They bind to CTCs and quickly form aggregates around them upon entering the bloodstream (**Figure 5**). CTCs actively enhance aggregate formation by releasing substances that activate platelets. Platelets act as a protective shield for CTCs, safeguarding them from shear stress and providing defense against NK cells[3,36].

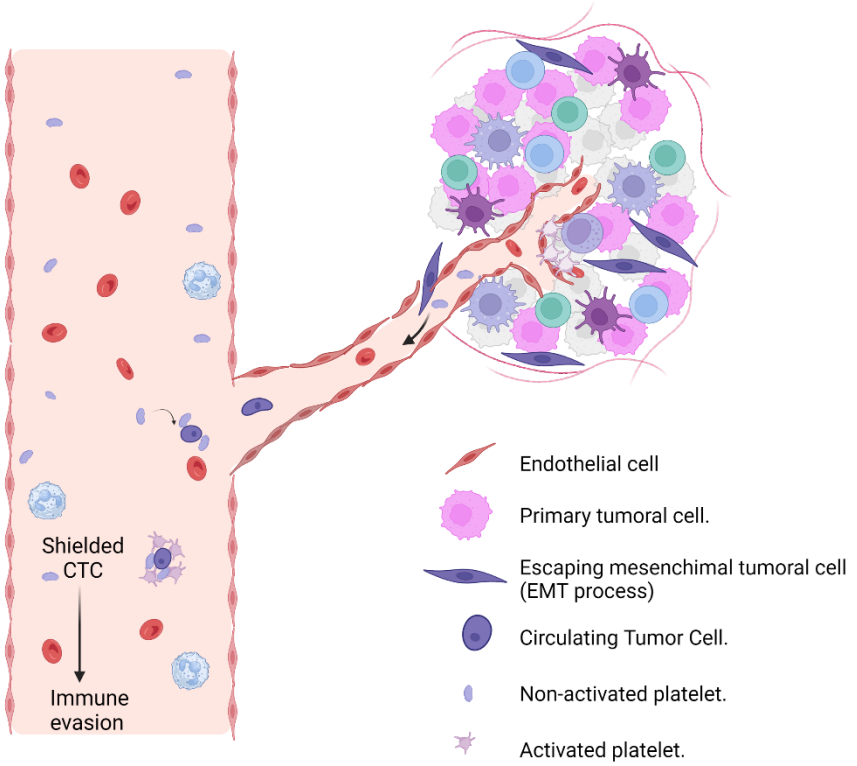

Figure 5. Platelet-aided tumor progression.

Schematic view of the scaping process from the tumoral mass. Tumor cell undergoes EMT, acquiring stemness features and escaping in direction to the bloodstream where it can interact with platelets, using them as core to be protected from the action of immune cells. Image created by Martínez-Navajas, G. -Author.

Platelets can also hinder NK cell activity by transferring HLA-I molecules to the surface of tumor cells, thereby inhibiting NK cell cytotoxicity. Additionally, platelets suppress NK cell antitumor function by downregulating the NKG2D receptor, which is responsible for recognizing and eliminating transformed cells, through TGFβ-mediated signaling[36].

1.3.3. Sensing pathogens.

Immune cells must be able to distinguish own tissue from pathogens, in order to eliminate them from the organism. To do this, they have developed pattern recognition receptors which can detect highly conserved pathogen-associated molecular patterns (PAMPs) or damage-associated molecular patterns (DAMPs), that are released by affected or damaged host cells. Platelet, as first responders, can also recognize these PAMPs and DAMPs at the injured place and inducing the expression of TLRs. Additionally, platelets also express receptor which directly interact with the pathogens and activate themselves to release microbicidal peptides, defensines, among other molecules, which are content in their α-granules[36].

Platelets can also recognize viruses. In this case, platelets interact with them through surface lectins, TLR or integrins. This recognition facilitates the internalization of the virus within the platelet, its activation, degranulation and, in last term, induces a neutrophil-mediated phagocytosis[39].

Similarly, platelets can also recognize and bind bacteria in the bloodstream through these specialized receptors. Platelets have the ability to attach to surface proteins of bacteria either through direct contact or indirectly via plasma proteins like fibrinogen or VWF, which interact with the bacteria. Additionally, platelets can interact with bacterial toxins or secreted substances. The outcomes of the interaction between platelets and bacteria are varied and can lead to complete or partial activation of platelets, thus releasing microbicidal molecules or immune-related responses that will end in the clearance of the platelet-bacteria-complex from the blood flow[36,40].

2. Inherited platelet disorders: Importance and clinical management.

2.1. General classification of bleeding disorders.

As we have seen, numerous platelet receptors, plasma proteins, and coagulation factors participate in hemostasis. Dysfunction of any of these elements can lead to bleeding disorders. Bleeding disorders encompass a spectrum of conditions that disrupt the regular functionality of the coagulation process. These disorders can be caused by a variety of factors, including medications, underlying medical conditions or inherited genetic mutations[22].

When a bleeding disorder originates from a genetic cause, it is categorized as an inherited bleeding disorder, known for their heightened vulnerability to spontaneous or prolonged bleeding. These disorders can be classified into three main subtypes: factor deficiencies, which impact plasma coagulation factors; platelet disorders, which affect platelet formation or function; and fibrinolytic disorders, which disrupt the final phase of hemostasis[41].

(i) **Factor deficiencies**, there are several cases according to the factor that is missing, such as Hemophilia A (Deficiency of factor VIII), which is the most frequent coagulation disorder. Less commonly, it is possible to identify Hemophilia B (Deficiency of factor IX), Hemophilia C (Deficiency of factor XI), Factor VII deficiency

(Also known as proconvertin deficiency), Factor V deficiency (Owren's disease), Factor X deficiency (Stuart-Prower factor deficiency).

(ii) **Inherited platelet disorders**, characterized by abnormalities in platelet biology, leading to an inability to recognize or respond to injury responses, impairing the clot formation. This field is of further importance for our research and will be explained in detail in the next section.

(iii) **Fibrinolytic disorders**, these disorders involve abnormalities in the fibrinolytic system, which is responsible for breaking down clots. Few examples of known disorders described affecting this phase are plasminogen deficiency (plasminogen is converted to plasmin, the enzyme that degrades fibrin) and Alpha-2-antiplasmin deficiency (enzyme that inhibits plasmin activity, and its deficiency results in excessive fibrinolysis).

(iv) **Combined disorders**, when two or more categories are involved in the disorder.

2.2. Inherited platelet disorders.

Inherited platelet disorders (IPDs) are caused by pathogenic variants affecting genes involved in platelet production, structure, or functionality [2]. Its genetic cause makes them to be inheritable from parents to their children.

Patients with factor deficiencies exhibit distinctive symptoms such as delayed and deep muscular bleeding. For these cases, laboratory tests which measure different plasma factors are useful aiding to distinguish the specific factor deficiency and its underlying cause[42].

Individuals with IPDs experience abundant mucocutaneous bleeding after an injury or medical procedure[43]. The symptomatology of patients experiencing IPDs is similar despite the different causes that could be altering the platelet function. Typical signs include easy bruising, nosebleeds (epistaxis), bleeding gums (gingival bleeding), heavy menstrual bleeding (menorrhagia), and postpartum bleeding. The severity of symptoms can vary among individuals with the same disorder [44,45]. Additionally, in the case of IPDs, clinical and laboratory features can be indistinct and overlapping with other bleeding disorders or even normal variations. This can lead to diagnostic confusion and misinterpretation of test results. Furthermore, some individuals with IPDs may not present with obvious bleeding symptoms or may have mild manifestations that are easily overlooked. As a result, specific IPDs may go undiagnosed or misdiagnosed for an extended period[46–48].

Obtaining an accurate molecular diagnosis holds significant importance in facilitating informed clinical decision-making and effective disease management. It guides treatment choices such as gene correction, factor replacement, stem cell transplantation, or active monitoring. Additionally, a molecular

diagnosis aids in predicting the progression of associated conditions such as deafness, kidney failure, myelofibrosis, lung fibrosis, or malignancy. Furthermore, it can also provide valuable information for family planning purposes.

2.2.1. Diagnosis of inherited platelets disorders.

The true prevalence of IPDs remains unknown, but estimations suggest they affect between one in 10.000 to one in 1.000.000 individuals. Mild disorders are likely more common as patients often are undiagnosed or misdiagnosed. A recent survey of the general population found that approximately 3 in 1,000 individuals carry clinically significant loss-of-function variants in genes associated with IPDs. Typically, IPDs can be categorized into two main groups:

(i) **Inherited thrombocytopenias**: These disorders affect the number of circulating platelets which can be normal, large, or small-sized[46].

(ii) **Inherited platelet function disorders**: These disorders result in dysfunctional platelets with reduced function. They stem from defects in membrane receptors, granules, signaling elements, or other components of the biochemical machinery within platelets. Thrombocytopenia and impaired platelet function are commonly associated with these disorders[46].

Accurate diagnosis of IPDs requires several laboratory tests, including:

I. **Complete blood count and peripheral blood smear:** These initial tests provide crucial information about the quantity, size, and morphology of blood cells. Abnormal findings may include large platelets in Bernard-Soulier Syndrome (BSS). However, the presence of thrombocytopenia alone does not exclude IPDs, requiring further evaluation.
II. **Platelet function analyzer-100 (PFA-100):** This simple and rapid screening tool measures *in vitro* bleeding time by using a membrane coated with collagen/epinephrine or collagen/ADP. Interpretation should consider variables such as platelet function, VWF level, platelet count, and hematocrit level.
III. **Platelet aggregation test using a light transmission aggregometer:** Widely used, this test determines platelet function by observing aggregation patterns in response to agonists like ADP, epinephrine, ristocetin, and collagen. Specific aggregation patterns can aid in the diagnosis of various IPDs, including Glanzmann's thrombasthenia (GT), BSS, pseudo-von Willebrand disease, ADP receptor defect, and gray platelet syndrome.
IV. **Flow cytometry:** This method measures the expression of molecules, such as glycoproteins, phospholipids, and granules within platelets. Flow cytometry effectively diagnoses surface glycoprotein

defects like GT and BSS and requires only a small blood sample.

V. **Electron microscopy:** Electron microscopy is utilized to diagnose platelet structure and granule defects.
VI. **Genetic testing:** Although not widely available, genetic tests are crucial for IPD diagnosis, particularly in identifying genetic alterations in family members. Next-generation sequencing, including targeted gene panels, is effective for both diagnosis and differential diagnosis of IPDs.

Commonly, steps I-III are widely used as the initial diagnostic approach for an IPD, while steps IV-VI are employed as a secondary and more concise approach to confirm the cause of the IPD.

2.2.2. Classification of inherited platelets disorders.

Over the past decades, the identification of genes causing IPDs has primarily relied on conventional Sanger sequencing and laboratory methodologies. However, these approaches have limitations in terms of their identification and association capabilities due to inherent technical constraints, so many IPDs remained with unclear origin and diagnostic. However, continuous evolve of DNA sequencing methodologies like the development of next-generation sequencing overcame these limitations thanks to it reduced cost and rapid sequencing of entire genomes[49–51].

To date and thanks to this continue evolve, it has been detected a wide variety of pathogenic variants affecting up to 75 genes that are associated to 60 different types of IPDs[46].

From a molecular perspective, IPDs are caused by pathogenic variants affecting coding genes of various platelet components involved in the hemostasis process. Depending on the affected component, different pathologies can be distinguished. We have subclassified the main diseases based on the specific platelet function that is affected. Despite many of them can be interlinked, they can generally be categorized into defects in granule formation, trafficking or secretion; defects in cytoskeleton regulation; defects in platelets adhesion; defects in platelets activation; defects in platelets aggregation or defects in platelet's procoagulant activity (Refer to **Table 1** and **Figure 6**).

Table 1. Classification of inherited platelet disorders.

Main characteristic inherited platelet disorders classified according to defects in platelet function or biological process. Modified from Shim Y, 2020[51].

Affected platelet process/function	Gene	Locus	Protein	Phenotype (OMIM number)	Inheritance	Clinical characteristics
Defects in granule formation, trafficking, or secretion	*HPS1*	10q24.2		Hermansky-Pudlak syndrome (OMIM #203300, #608233, #614072, #614073, #614074, #614075, #614076, #614077, #614171)	AR	Normal platelet count Platelet aggregation defect or abnormal response Platelet dense granule defect Oculocutaneous albinism Congenital neutropenia Pulmonary fibrosis Granulomatous colitis
	AP3B1	5q14.1				
	HPS3	3q24				
	HPS4	22q12.1				
	HPS5	11p15.1				
	HPS6	10q24.32				
	DTNBP1	6p22.3				
	BLOC1S3	19q13.32				
	BLOC1S6	15q21.1				
	LYST	1q42.3	Lysosomal trafficking regulator	Chediak-Higashi syndrome (OMIM #214500)	AR	Normal platelet count Platelet aggregation defect or abnormal response Platelet dense granule defect Oculocutaneous albinism Severe immunological deficiency Lack of NK cell function
	PLAU	10q22.2	Urinary plasminogen activator	Quebec platelet disorder (OMIM #601709)	AD	Gain-of-function defect in fibrinolysis Thrombocytopenia or normal platelet count Degradation of platelet α-granule contents Platelet aggregation defect or abnormal response

Table 1. Classification of inherited platelet disorders.

Cont.

	NBEAL2	3p21.31	Beige and Chediak-Higashidomain protein	Gray platelet syndrome (OMIM #139090)	AR	Thrombocytopenia Platelet α-granule defect Large-sized platelets Platelet aggregation defect Gray platelets on light microscopy of Wright-stain Myelofibrosis
Defects in cytoskeleton regulation	*MYH9*	22q12.3	Nonmuscle myosin heavy chain IIa	MYH9-related thrombocytopenia syndromes (OMIM #155100)	AD	Thrombocytopenia or normal platelet count Large-sized platelets Nephritis Sensorineural hearing loss
	WAS	Xp11.23	WAS protein	Wiskott-Aldrich syndrome (OMIM #301000)	XR	Thrombocytopenia Small-sized platelets Immunodeficiency Eczema
				Thrombocytopenia 1 (OMIM #313900)= X-linked thrombocytopenia	XR	Thrombocytopenia Small-sized platelets Without profound immunodeficiency Defects of white blood cell cytoskeleton Transient eczema
Defects in platelet-vessel wall interactions (disorders of adhesion)	*GP1BA*	17p13.2	GPIbα	Bernard-Soulier syndrome (OMIM #231200) type A1, B and C.	AR	Thrombocytopenia or normal platelet count Large-sized platelet Platelet adhesion defect
	GP1BB	22q11.2	GPIbβ			
	GP9	13q21.3	GPIX			
	GP1BA	17p13.2	GPIbα	Pseudo-von Willebrand disease (OMIM #177820)	AD	Thrombocytopenia Large-sized platelet Platelet adhesion defect

Table 1. Classification of inherited platelet disorders.

Cont.

	GP1BB	22q11.21	GPIbβ	22q11 deletion syndrome De George syndrome (OMIM Velocardiofacial syndrome	AD	Thrombocytopenia or normal platelet count Large-sized platelet Platelet adhesion defect
	GP6	19q13.42	GPVI	GPVI collagen receptor defect.	AR	Normal platelet count and morphology. Platelet adhesion defect. Bleeding mostly associated withantiplatelet intake, dental interventions, or other hemostatic challenges
Defects in platelet activation (transduction cascade affection)	*P2RY12*	3q25.1	ADP receptor	Bleeding disorder, platelettype, 8 (OMIM #609821)	AR	Platelet aggregation defect
	TBXA2R	19p13.3	Thromboxane A2 receptor	Bleeding disorder, platelettype, 13 (OMIM #614009)	AD	Platelet aggregation defect
	TBXAS1	7q34	Thromboxane synthase	Thromboxane synthase deficiency (OMIM #614158)	AD	Platelet aggregation defect
				Ghosal hematodiaphyseal syndrome (OMIM #231095)	AR	Platelet aggregation defect
Defects in platelet-platelet interactions (disorders of aggregation)	*ITGA2B*	17q21.31	GPIIb	Glanzmann thrombasthenia (OMIM #273800)	AR	Normal platelet count
	ITGB3	17q21.32	GPIIIa			Platelet aggregation defect
Defects in procoagulant activity	*ANO6*	12q12	Transmembrane protein 16F	Scott syndrome (OMIM #262890)	AR	Impaired surface exposure of phosphatidylserine of platelets

AD, autosomal dominant; ADP, adenosine 5'-diphosphate; AR, autosomal recessive; GP, glycoprotein; GPCR, G-protein-coupled receptors; XR, X-linked recessive.

Briefly, we are describing the historically well-known inherited platelet disorders. These are considered particularly significant and pose a higher risk of severe bleeding:

Glanzmann's thrombasthenia (GT): This disorder arises from a deficiency or dysfunction of the glycoprotein IIb-IIIa receptor on platelets (**Figure 6**), crucial for platelet aggregation. Individuals with GT commonly face severe bleeding symptoms, including spontaneous bleeding, prolonged bleeding after injuries or surgeries, and recurring episodes of mucocutaneous bleeding[2,41].

Bernard-Soulier Syndrome (BSS): This rare disorder occurs due to a deficiency or dysfunction of the GPIb-V-IX receptor on platelets (**Figure 6**), resulting in impaired platelet adhesion. It carries a heightened risk of bleeding, and affected individuals may experience severe bleeding episodes such as excessive bruising, prolonged nosebleeds, and gastrointestinal bleeding[52–54].

Hermansky-Pudlak Syndrome: This syndrome is characterized by abnormalities in platelet granule formation and function, as well as pigmentation and other organ abnormalities. Bleeding symptoms can vary, but some individuals may experience significant bleeding complications, including gastrointestinal bleeding, pulmonary hemorrhage, and excessive menstrual bleeding[49–51].

Chediak-Higashi Syndrome: This rare disorder affects various aspects of cellular function, including platelets. Platelet

function abnormalities lead to an increased tendency to bleed, and individuals with Chediak-Higashi syndrome may encounter spontaneous bleeding, prolonged bleeding after minor trauma, and easy bruising[47,55,56].

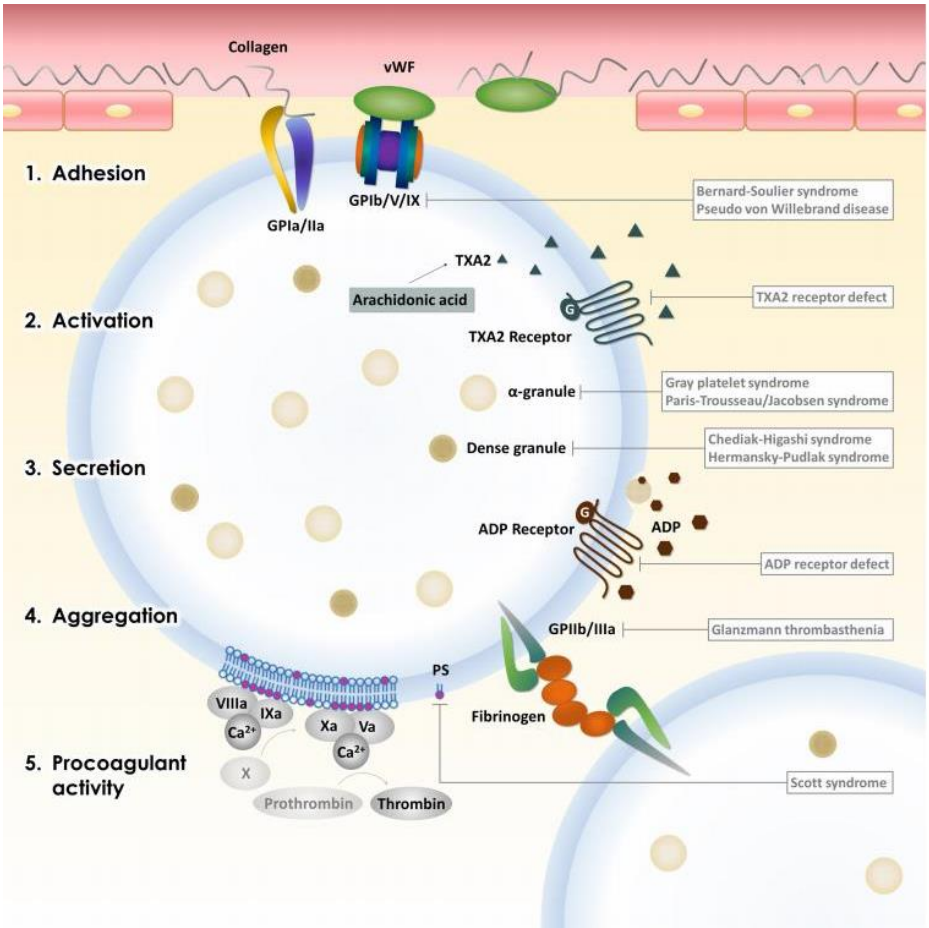

Figure 6. Examples of inherited platelet disorders.

Schematic view of main inherited platelet disorders according to defects in specific platelet proteins or altered function-process. Modified from Jung N & Shim Y, 2020[49].

As mentioned, patients experiencing IPDs exhibit similar signs, all of them involving bleeding tendencies. Among these inherited platelet disorders, the ones that affect the GPIb-V-IX receptor are particularly interesting for this research project. It exhibits one of the most severe bleeding phenotypes among all IPDs [2,44,45]. The study will focus in-depth on BSS, analyzing its origin, current treatment options to alleviate its effects, and future treatment directions aimed at finding a curative solution for this disease.

3. Bernard-Soulier Syndrome.

BSS is an extremely rare bleeding disorder that affects platelet functionality[57,58]. Its prevalence is less than 1 in 1 million, although recent studies suggest that its incidence might be higher due to potential misdiagnosis[44,59]. BSS follows an autosomal recessive inheritance pattern when present in its biallelic form. Affected individuals experience macrothrombocytopenia, characterized by a reduced number of abnormally large platelets in the blood, which leads to prolonged bleeding episodes. The syndrome is caused by the absence or dysfunction of the platelet membrane receptor GPIb-V-IX[2,57,58].

3.1. GPIb-V-IX receptor: Deep explanation and role in BSS.

3.1.1. Structure of the receptor.

The GPIb-V-IX receptor is expressed on the surface of MKs and mature platelets. This receptor is result of the assembly of four subunits: GPIbα, GPIbβ, GPIX and GPV (**Figure 7**) encoded by *GP1BA*, *GP1BB*, *GP9* and *GP5*, respectively. These subunits are transmembrane proteins which belong to the leucine-rich repeat protein family.

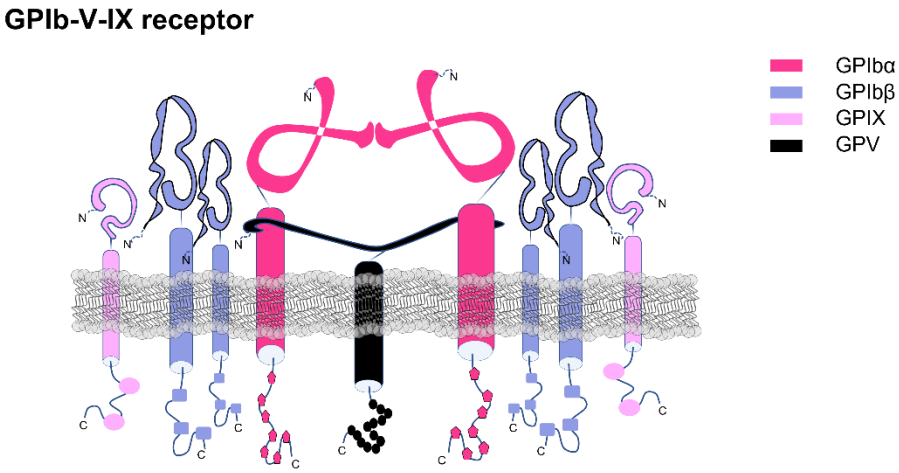

Figure 7. GPIb-V-IX receptor.

Schematic view of the GPIb-V-IX receptor composed by the assembly of four different subunits: GPIbα, GPIbβ, GPIX and GPV. Image created by Martínez-Navajas, G. -Author.

Molecularly, GPIbα is covalently bound to two GPIbβ polypeptides (**Figure 7**), constituting the GPIb subunit[60]. Then, GPIb is non-covalently bound to GPIX. Finally, GPIb-IX is weakly associated to GPV by transmembrane associations [61], conforming the GPIb-V-IX receptor[52,62,63], achieving a stoichiometry of 2:4:2:1 (GPIbα:GPIbβ:GPIX:GPV). The ultrastructure for each subunit is following indicated and can be contrasted in the **Figure 8**:

- **GPIbα (135 kDa):** It is the main component of the complex, harboring binding domains for VWF, as well as other molecules involved in hemostasis, thrombosis, and inflammation processes[64]. GPIbα is the largest subunit of the GPIb-IX complex. It plays a crucial role in binding to various ligands, such as VWF, thrombin, P-selectin, the integrin MAC-1 (αMβ2),

coagulation factors XI and XII, high molecular weight kininogen, and thrombospondin (**Figure 8**)[63,65–68]. The N-terminal domain of GPIbα consists of eight leucine-rich repeats, forming an elongated shape above the platelet surface, known as the ligand binding domain (LBD)[69]. Close to this region, there is a negatively charged portion that contains sulfated tyrosine residues, important for thrombin binding[66,70]. GPIbα also has a mucin-like macroglycopeptide with sialylated carbohydrate chains, contributing to its exposed position and facilitating ligand binding. Adjacent to the macroglycopeptide region is the mechanosensitive domain (MSD)[71], which can be cleaved by ADAM17, releasing soluble GPIbα fragments (glycocalicin) into the plasma. The cytoplasmic tail of GPIbα contains binding sites for intracellular signaling molecules and connects the receptor complex to actin filaments[63,65–68].

- **GPIbβ (25 kDa):** This subunit is much smaller containing a single LRR that interacts intracellularly with calmodulin. GPIbβ is palmitoylated on cysteine residues in the transmembrane region[57,72].
- **GPIX (17 kDa):** It is the smallest receptor subunit, which does not associate with any intracellular molecule. GPIX has a cytoplasmic tail of only eight residues, containing a myristoylated one at the junction of the transmembrane and cytoplasmic

domain, which potentially localizes the receptor in lipid rafts[60,73].

- **GPV (83 kDa):** Contains 15 leucine-rich repeats, a transmembrane domain, and a short cytoplasmic tail is weakly associated with the GPIb-IX complex by transmembrane domain interactions with GPIbα[61].

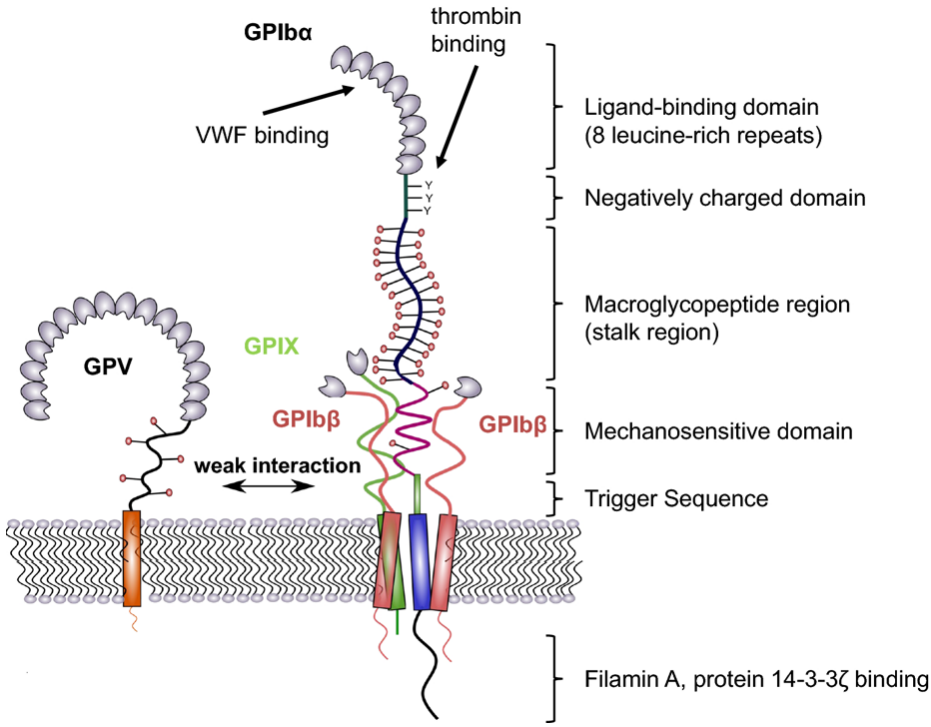

Figure 8. Ultrastructure of GPIb-V-IX receptor.

Detailed scheme of the GPIb-V-IX receptor indicating components and main structures of GPIbα. Modified from Bendas G & Schlesinger M, 2022[64].

3.1.2. Receptor functionality.

As mentioned previously, this receptor serves a crucial function in primary hemostasis by facilitating platelet adhesion to areas of vascular damage under conditions of intense shear stress. It exhibits a strong attraction to the A1 domain of VWF. Following a vascular injury, VWF identifies and binds to subendothelial collagen, resulting in the creation of an unfolded-VWF layer that is subsequently recognized by the GPIb-V-IX platelet receptor, aiding to decelerate inactive circulating platelets, recruiting them, and inducing a cascade of intracellular signaling that culminates in platelet activation and aggregation[20,21,24–26]. Therefore, the absence of this receptor impairs proper platelet adhesion and vascular injury recognition, leading to the characteristic bleeding problems[1,26,57,58,64].

This complex also binds thrombin through the negatively charged region, interacting with two-GPIbα molecules, aiding to fully activate platelets through signaling cascades, together with PAR-1 and PAR-4 receptors. In addition, once bound, thrombin acts on other targets in the blood clotting cascade, such as fibrinogen, to convert it into fibrin, which forms the meshwork of a blood clot[63,69,74].

Another function of the receptor is to participate in maintaining platelet morphology through the interaction of Filamin A (**Figure 8**) and platelet cytoskeleton[57,58].

This receptor also has a key role in platelet clearance. Removal of terminal sialic acid from platelet glycans leads to exposure of multiple galactose residues on glycans which are subsequently recognized by the hepatic Ashwell-Morell receptor (AMR). The AMR is a multi-complex receptor and contains several lectin domains for interaction with galactose or galactosamine. Binding to the AMR leads to platelet internalization and subsequent elimination. Relatedly, platelet uptake by AMR stimulates hepatic thrombopoietin (TPO) generation and release which induces thrombopoiesis by MKs in the bone marrow to replace the eliminated platelets[63,75,76].

Additionally, this receptor likely plays an important role during thrombopoiesis and platelet turnover due to the reduced number and abnormally large size of platelets in BSS patients [64].

3.2. BSS typologies according to the affected gene: Genotype and phenotype correlations.

Pathogenic variants responsible for BSS can disrupt the synthesis, processing, or expression of the receptor, resulting in its absence or dysfunction from the surface of MKs and platelets[59]. According to the causal pathogenic variant and the affected gene, we can classify BSS into different typologies.

3.2.1. Classical Biallelic BSS.

DNA sequencing of BSS patients has allowed the identification of more than 100 different pathogenic variants underlying the disease associated to *GP1BA*, *GP1BB* and *GP9* (**Figure 9**). Of them, pathogenic variants are equally distributed among *GP1BA* and *GP1BB* (28% each), being more represented when associated to *GP9* (44%)[77]. According to the gene affected by the variants, we refer to it as type 1A BSS (*GP1BA)*, type 1B BSS (*GP1BB*), or type C BSS (*GP9*)[52,64,77,78].

To date there has not been reported any pathogenic variant associated to *GP5* which could lead to BSS[2,52,57,58,64,77].

It is predominantly an autosomal recessive disorder, meaning that both alleles at a given *locus* must be mutated. These mutations can be homozygous (the same mutation appears on both alleles at a *locus*) or compound heterozygous (different mutations occur on each allele at a *locus*). Typically,

these mutations are *missense*, *nonsense*, or *deletions/insertions* that can disrupt the reading frame [2,52,57,64].

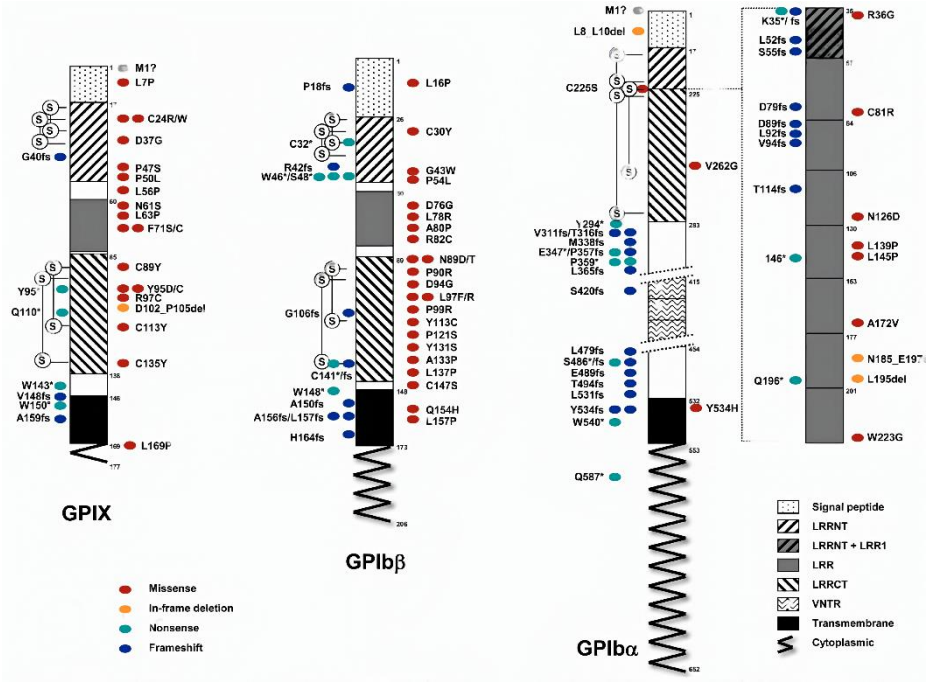

Figure 9. Main Bernard-Soulier Syndrome pathogenic variants described until 2014.

Schematic representation of GPIbα, GPIbβ and GPIX protein structures indicating functional domains and associated positions of inducer Bernard-Soulier syndrome pathogenic variants that are described until 2014. Savoia A, et al. 2014[80].

3.2.2. Monoallelic form of BSS.

Heterozygous carriers are usually asymptomatic and have normal platelet counts, although in occasions slightly enlarged platelets and decreased platelet glycoprotein GPIb-V-IX complex expression can be found, as well as a moderately reduced Ristocetin-Induced Platelet Aggregation (RIPA) response, a test triggering the binding of VWF to GPIbα.

In addition, there have been reported cases of mild forms of BSS with intermedial platelet size between biallelic BSS and controls. Typically, these patients can exhibit decreased expression levels of a pseudo-functional receptor on their surface[79].

These cases are inherited in an autosomal dominant form and uniquely associated to *GP1BA* and *GP1BB*, but not *GP9* to date. It was first described for individuals in Italy carrying the mutation p.A172V associated to *GP1BA*, best known as Bolzano variant. Then, around 12 *missense* mutations affecting to *GP1BA* (in all these cases, the pathogenic variants uniquely affect the LRR-VWF binding domain) and 14 associated to *GP1BB* have been described to date, both inducing the monoallelic BSS[51,80].

3.2.3. Platelet type Von Willebrand Disease.

Although the reference to BSS is not applicable here, it is important to note that not all pathogenic variants associated with the GPIb-V-IX complex result in BSS. This is the case of

platelet-type von Willebrand disease (pt-VWD), which is characterized by autosomal dominant gain-of-function *missense* mutations occurring within the LRR region of GPIbα (encoded by the *GP1BA* gene) (**Figure 8**), as well as one deletion outside the repeat region. These mutations result in an extremely high affinity of the GPIb-V-IX for the VWF, inducing a spontaneous binding of platelets to large VWF multimers[81]. As a result, the higher molecular weight multimers are decreased or absent in plasma, not being available during the primary hemostasia. Furthermore, clearance methods remove platelet-VWF aggregates, manifesting in macrothrombocytopenia and leading to bleeding phenotypes[51].

3.3. Clinical manifestations of BSS: Symptoms and characteristic features.

Patients with BSS have a clinical history characterized by signs such as epistaxis, frequent gingival and cutaneous bleeding, as well as severe bleeding associated with trauma and surgical interventions. Clinically, the bleeding episodes are prolonged, the platelet count is low, and the platelets are larger in comparison to healthy donors (**Figure 10**)[52,57].

Given the crucial role of GPIb-V-IX in hemostasis, which involves the localization of platelets at the site of vascular injury, a functional impairment in platelets exacerbates the bleeding tendency in biallelic BSS beyond what would be expected solely based on platelet count, contributing to thrombocytopenia.

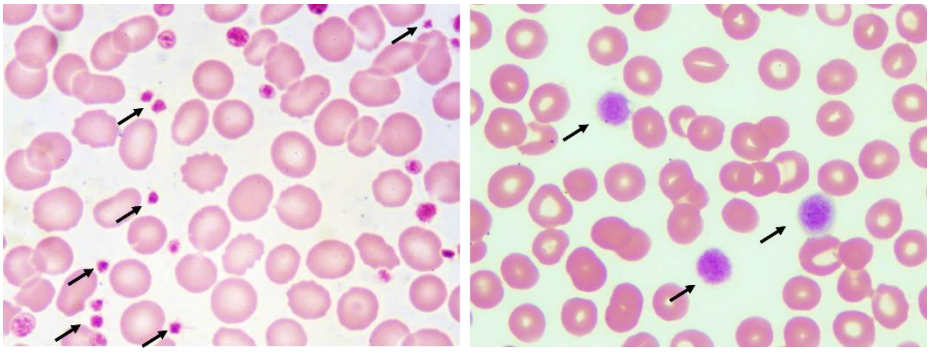

Figure 10. Comparative of blood smears from healthy donor and Bernard-Soulier Syndrome patient.

Blood smear from a healthy donor (left), with normal-size platelets and count. Bernard-Soulier Syndrome blood smear (right) with low count of giant platelets. Modified from *Nezir M, et al.*[164].

The resulting clinical and laboratory features make biallelic BSS a disorder that is easy to diagnose. The presence

on blood smears of very large platelets with some elements larger than red blood cells arouses suspicion of this disorder. Failure of platelets to aggregate *in vitro* after stimulation with ristocetin, which promotes VWF binding to GPIbα, supports the diagnostic hypothesis. Ristocetin promotes *ex vivo* interaction between VWF and platelets, by opening the unfolded VWF, exposing A1 domain and inducing a platelet agglutination response. In patients with BSS, the addition of ristocetin does not result in the characteristic platelet agglutination[82]. Then, undetectable or severely reduced amounts of GPIb-V-IX on platelet surfaces as determined by flow cytometry confirm the diagnosis of BSS.

When considering monoallelic BSS, the available data alone may not suffice to confirm the diagnosis of the syndrome. This is because certain those specific mutations affecting *GP1BA* and *GP1BB* that resulted in a milder variant of the disorder, characterized by macrothrombocytopenia and the presence of a pseudo-functional receptor that is externalized. So, to provide a clear diagnosis, it is necessary to sequence the responsible *loci*[57,58,64].

In the case of pt-VWD, the hyperreactivity that platelets suffer for VWF allows to distinguish this disorder with BSS. However, it remains essential to sequence the *GP1BA* locus to differentiate this disease from Von Willebrand Disease type 2B. In this particular case, the mutation affects the A1 domain of VWF, resulting in a significantly increased affinity for the GPIbα subunit. These diseases share similar characteristics,

making the sequencing of the *GP1BA* locus crucial for accurate differentiation [83–85].

3.4. Clinical management: Overview of current treatment options for managing BSS.

Patients with IPDs, such as GT or BSS, require treatment to control spontaneous mucocutaneous bleeding and, primarily, to minimize bleeding after trauma or surgical interventions[44].

One of the strategies implemented to manage these diseases is preventive care. Patients should have an understanding of the disease's characteristics to minimize the risk of bleeding. Consequently, they should avoid contact sports, receive hepatitis B vaccination, maintain dental hygiene to minimize gingival bleeding, and take other measures[44,52].

On the other hand, there are palliative treatments aimed at reducing the duration of bleeding episodes. For example, the use of antifibrinolytic agents is recommended to control bleeding caused by menorrhagia, gingival bleeding, or epistaxis[44,45]. Additionally, women with the syndrome experience bleeding problems during menstruation that can be alleviated with hormonal treatments[45,86]. Desmopressin, a synthetic analogue of antidiuretic hormone, is also used to treat BSS and other hereditary platelet disorders[2]. Desmopressin increases the plasma concentration of both VWF and factor VIII, reducing the clotting time needed to stop bleeding[45,86]. Desmopressin enhances platelet adhesiveness to the subendothelium due to an increased number of VWF molecules. However, in patients with BSS who lack the VWF

receptor, desmopressin may have an additional effect during hemostasis [86].

Another highly effective treatment to arrest bleeding is platelet transfusion from healthy donors. It is mainly used during surgeries and trauma to counteract severe bleeding. However, this treatment can lead to the development of alloantibodies against HLA molecules of non-compatible donors (platelet refractoriness) or against glycoproteins absent in the patients' platelets but present on the surface of healthy platelets (e.g., GPIb-V-IX receptor in BSS)[44,45,86]. To reduce the risk of platelet refractoriness, transfusions should be performed using leukodepleted platelets from a single HLA and AB0-compatible donor, rather than a pool of donors, which is the usual practice[45,46].

While many inherited platelet disorders can be considered benign to some extent, as they can be managed with supportive therapies, there are instances where bleeding or other complications become extremely severe, even life-threatening. Unfortunately, finding a definitive cure for IPDs remains challenging.

One potential treatment approach to reverse IPDs is the transplantation of allogeneic HSCs from HLA compatible donor[44,45,86]. HSCs are self-renewing cells found in the bone marrow responsible for generating all the different types of blood cells through the process of differentiation[87]. In severe cases, HSC transplants are performed, preferably using HLA-

identical siblings as donors. However, this scenario is relatively rare, so related or unrelated donors with compatible HLA are also utilized [44,86]. This procedure, known as allogeneic HSC transplantation, has proven to be an effective and curative treatment for various diseases, including certain cases of BSS [87–89].

Despite its effectiveness, the limited availability of fully compatible donors poses a significant challenge. Consequently, many patients undergoing this type of intervention are unable to find a completely compatible donor, increasing the risk of immune rejection or graft-versus-host disease [87,90].

Consequently, the need for alternative treatment options becomes imperative to address this limitation and offer a curative approach for IPDs. In this context, gene therapy has emerged as a highly promising avenue. By targeting and rectifying the genetic abnormalities responsible for IPDs, gene therapy presents the potential for a personalized and curative treatment strategy. While still in the preclinical research phase for numerous IPDs, it has already advanced to approved clinical trials for managing Whiskott-Aldrich Syndrome, among other diseases with base on HSCs. These trials involve the utilization of self-inactivating lentiviral vectors to drive the expression of therapeutic transgenes[91,92].

Therefore, gene therapy holds great promise as a curative option for IPDs, offering hope to patients who face

challenges in finding fully compatible donors for conventional treatments like allogeneic HSC transplantation, like could be severe bleeding disorders like GT or BSS[93–96].

4. Gene therapy.

Gene therapy emerged as a concept in 1972 when Friedman and Roblin proposed the use of healthy exogenous (therapeutic) DNA to replace its mutated version and responsible for causing a pathology[97,98] In fact, many discoveries have been achieved throughout the last decades. Now, the European Medicines Agency (EMA) has redefined gene therapy as a "biological medicinal product that contains an active substance which contains or consists of a recombinant nucleic acid used in or administered to humans to regulate, repair, replace, add or delete genetic sequences and its therapeutic, prophylactic or diagnostic effect relates directly to the recombinant nucleic acid sequence it contains, or to the product of genetic expression of this sequence"[99].

4.1. Gene therapy classifications according to target cells and delivery methodology.

Gene therapy allows the delivery of therapeutic genetic material to any specific cell-tissue-organ of the body for treatment. According to the cellular type and the objective of the therapy, we can distinguish two different modalities:

4.1.1. Germline and Somatic gene therapy.

Germline cells: This gene therapy involves the genetic modification of reproductive cells, such as sperm, ovules and eggs, to introduce heritable changes. The feasibility of germline therapy has been demonstrated successfully in various animal species, including mice, rats, rabbits, sheep,

cattle, goats, and pigs. However, its application in humans has been prohibited due to ethical concerns, limited advanced tools, and the absence of societal consensus[99,100].

Somatic cells: This is the predominant approach used in clinical settings. It focuses on treating the specific patient and does not result in inheritable changes that affect future generations. This targeted approach ensures that the benefits of gene therapy are confined to the individual undergoing treatment, without any long-term implications for their offspring[100,101]. When applying gene therapy to somatic cells, we have to determine whether the nucleic acids delivery will be *in vivo* or *ex vivo*.

4.1.2. *In vivo* and *Ex vivo* gene therapy.

We refer to *in vivo* gene therapy when the delivery or manipulation of cells is performed within the patient's body, using local or systemic delivery methods (**Figure 11**). Adeno-associated virus (AAV) vectors are commonly utilized in this therapy due to their non-integrating profile. This reduces the risk of insertional mutagenesis in non-desired target cells, a concern primarily associated with retroviruses and lentiviruses. However, AAV vectors have limited long-term expression, which poses a restriction. *In vivo* gene therapy-based treatments have already gained approval from the Food and Drug Administration (FDA) for diseases such as familial lipoprotein lipase deficiency (Glybera), retinal dystrophy (Luxturna), and spinal muscular atrophy (Zolgensma).

Additionally, non-viral vectors, naked DNA oligonucleotides, or siRNAs are also utilized in gene therapy when long-term expression of the delivered gene is not necessary. An example of this is the COVID-19 vaccines based on mRNA, which have been approved to combat the pandemic[99,102,103].

On the other hand, *ex vivo* gene therapy involves treating patient cells outside the body and then reintroducing them once they have been corrected. This approach requires collecting the patient's cells, culturing, modifying them, and subsequently transplanting them back into the patient (**Figure 11**). Compared to traditional allogenic transplantation, this cell-based gene therapy eliminates the need for a histocompatible donor and reduces the risk of graft-versus-host disease (GVHD). Retroviruses such as γ-retroviruses and lentiviruses are typically employed as vectors to deliver a normal copy of a specific defective gene into the genome of transplanted cells. *Ex vivo* gene therapy-based treatments have already received FDA approval for diseases like adenosine deaminase-associated severe combined immunodeficiencies (Strimvelis), β-thalassemia (Zynteglo), and large B-cell lymphoma (Yescarta and Kymriah), offering curative treatments for these conditions[99,102,104].

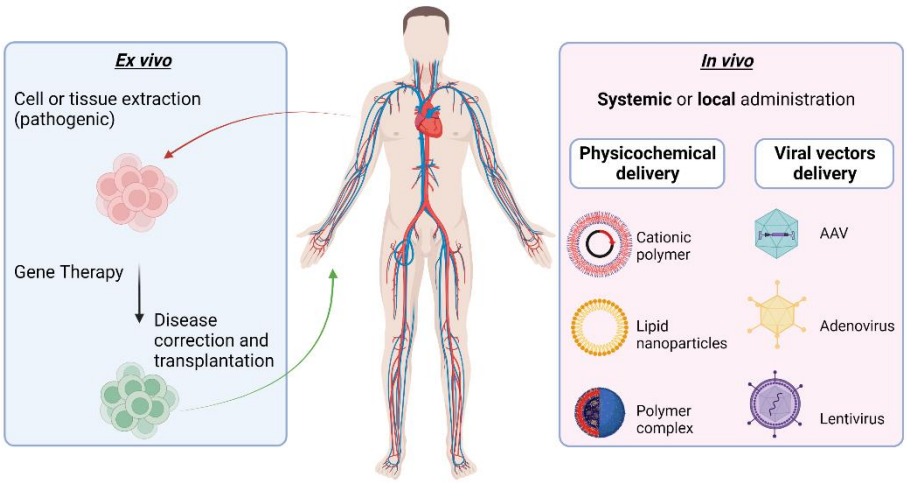

Figure 11. *Ex vivo* vs. *In vivo* gene therapy.
Schematic view of both modalities of gene therapy according to where the correction takes place. Image created by Martínez-Navajas, G. -Author (inspired in *Maestro, S. et al.*[110])

4.2. Most used delivery methodologies.

4.2.1. Physicochemical deliveries.

Physicochemical delivery methods in gene therapy encompass a range of techniques that utilize physical and/or chemical approaches to transport nucleic acids, such as DNA or RNA, into target cells. These methods play a crucial role in facilitating the effective delivery of nucleic acids for therapeutic purposes. Some widely used physicochemical delivery methods in gene therapy can be consulted in **Table 2**-**Table 3**[100,103,105–107]:

Table 2. Common physical methods for nucleic acid deliveries. Modified from N, Sayed et al. 2022 [103].

Nature of the method	Method	Description	Advantages	Limitations
Physical methods	Electroporation	This method utilizes controlled short electric impulses to enhance membrane permeability and deliver our cargo of interest.	It can be used for both in vivo and in vitro gene delivery. Cost effective, quick and reliable method.	Optimization of the method is laborious; reduced viability of the cells after electroporation. In vivo application is limited to the area of electric field and thermal damage.
	Microinjection	Microinjection is a direct approach for gene delivery with the use of microneedles to inject DNA into the cells.	This is a better and safer option than electroporation.	The process is laborious and has limited applicability for in vivo use, primarily restricted to dermal delivery.
	Particle Bombardment (Gene Gun)	Small gold or tungsten particles coated with DNA are propelled at high velocities into the target cells, allowing the DNA to enter the cells through the perforated cell membrane.	Transfection is independent of cell surface receptor interaction and fragment size; it is highly reproducible and less toxic to the cells.	The expression of transgene is low and transient.
	Sonoporation	Ultrasound causes cavitation that induces the growth and collapse of microbubbles creating enhanced cell permeation and delivery of genetic material.	Can be used for both in vivo and in vitro gene transfer, easy, reliable and safe.	Low transfection efficiency and causes injury to cells, ER stress and apoptosis.
	Magnetofection	Magnetic particles are mixed with DNA and introduced into the cells by using the magnetic field.	Can be used in vitro to deliver genes to cells that are difficult to transfect.	Agglomeration of the magnetofection reagents after the removal of magnetic field.
	Optoporation	Cells are directly irradiated using the laser beam. The cell permeability is governed by the pulse energy.	High survival rate.	Low throughput hence cannot be used on bulk samples.

Table 3. Common chemical methods for nucleic acid deliveries. Modified from N, Sayed et al. 2022[103].

Chemical methods	Calcium Phosphate	DNA, CaCl2 and phosphate buffer are mixed to form co-precipitate that is endocytosed by the cells. Mainly for in vitro transfections.	Easy Production. Storage stability.	Low transfection efficiency.
	Lipoplexes (Lipid based)	Liposomes are charged or neutral colloidal drug delivery systems prepared in the form of unilamellar or multilamellar vesicles.	Simple to formulate and is nonimmunogenic.	Transfection efficiency is low.
	Cationic Lipids	The lipids used for transfection comprise of a hydrophilic cationic head and a hydrophobic tail. These lipids form a unilamellar structure and their interaction is governed by the negative charge present on the nucleic acid and the relatively positive charge present on the lipids.	Simple to synthesize, reliable, low immunogenicity.	Heterogeneity of the formulation, structural instability, toxicity, inactivation in blood.
	Polymers	These polymers are positively charged and interact electrostatically with the phosphate backbone of DNA and generate the complexes that adhere over the cell membrane and enter inside the cell through endocytosis.	Can be used for in vitro and in vivo applications.	Cytotoxic.
	Nanoparticles (Gold, Silica, others)	These nanoparticles can be modified to enhance DNA binding, cellular uptake, endosomal escape, and target specific cells or tissues.	Protection of DNA from degradation, improved stability, controlled release, and potential for targeted delivery.	Low to medium transfection efficiencies.

4.2.2. Viral vector deliveries.

The use of viruses as delivery method for clinical purposes require the removal of the genes responsible of viral replication and pathogenicity. However, when the purpose is to treat cancer cells, maintaining their replicative capability could be useful. Typically, most employed viral vector used in gene therapy are AAVs, adenoviruses (AVs), Retroviruses (RVs)

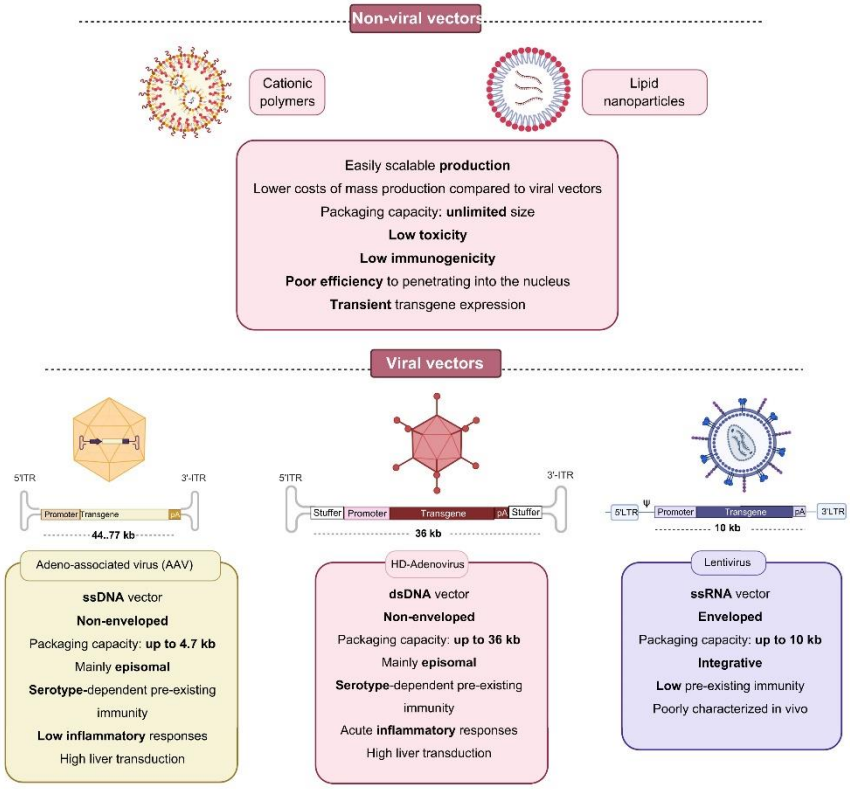

Figure 12. Comparison of non-viral and viral strategies to deliver nucleic acids into host cells.

Upper panel shows general characteristics for non-viral vectors while bottom panel compares the most commonly deliver strategies using viral vectors. Typically, AAVs and AVs are used for *in vivo* delivery while LVs are predominantly used for *ex vivo*, because their integrative profile. Modified from Maestro, S. *et al.*[110].

and Lentiviruses (LVs), according to the purpose of the therapy[107] which are summarized in the following **Figure 12**.

However, deeper explanation for each type continues as follows:

4.2.2.1. Adeno-associated viruses (AAVs)

Small, non-pathogenic single stranded DNA (ssDNA) viruses which requires a helper virus for replication and completion of their life cycle. The genome of these viruses is 4.7 kb in size and contains the *rep* genes (involved in replication) and the *cap* genes (which encode the viral capsid). Inverted terminal repeats (ITRs) are located at the ends of the genome. These ITRs form a secondary structure that harbors replication initiation and termination sequences, along with the packaging signal[103].

Recombinant AAVs are produced by removing both the *rep* and *cap* genes from the viral genome, creating space for the therapeutic gene (thus, 4.7 kb of space is available). These genes are provided separately for the generation of recombinant AAVs (in *trans)*. By eliminating these genes from the viral genome, the integration capability of the virus is lost. As a result, when the virus infects cells, it remains in episomal form within the nucleus. This characteristic reduces the risk of insertional mutagenesis. Additionally, there are different *cap* genes available, which promote specific tropism (preference for a particular cell type) and seroreactivity (different serotypes)[108,109].

Recombinant AAVs can infect both quiescent cells, where gene expression can be sustained for months to years, and dividing cells, where the therapeutic effect may be lost due to cell divisions[100,108,109].

4.2.2.2. Adenoviruses (AVs)

AVs are non-enveloped complex viruses with 36 kb linear double-stranded DNA (dsDNA) genome encoding various structural and non-structural genes. Therefore, these vectors provide ample space for insert our therapeutic cassette. Transduced cells maintain the DNA in episomal form and can reach stable therapeutic levels in absence of immune response, as reported for plasma proteins such us some coagulation factors, metabolic enzymes, erythropoietin, among others when delivered into quiescent tissues[99,100].

Adenoviruses possess highly desirable characteristics for liver gene delivery, making them an attractive option. They exhibit marked hepatotropism, enabling efficient targeting of liver cells, and they achieve high levels of gene expression in various cell types. Additionally, AVs are relatively easy to produce in large quantities with functional titers, have a large capacity for packaging genetic material, and show low genotoxicity[99].

The first-generation AV-based recombinant viruses initially lacked replication genes but retained a significant portion of the genome, allowing the introduction of exogenous genetic material of up to 8.5 kb. These vectors were effective

in transducing hepatocytes; however, attempts to prevent virus replication did not eliminate the expression of certain structural proteins, leading to a significant inflammatory and immune response. This immune reaction resulted in the elimination of infected cells within a relatively short time, resulting in only transient therapeutic effects. First-generation AV vectors have proven effective for developing vaccines and antitumoral treatments, including hepatic tumors, but have limitations for treating inherited diseases[99].

To achieve long-term gene expression, third-generation AV vectors, also known as helper-dependent adenoviruses (HDAVs), were developed. In HDAVs, all viral sequences, except for the terminal and packaging signal sequences, are removed. This design allows the delivery of large genetic sequences (up to 36 kb) and provides sustained transgene expression[99,107].

Despite their promising features, AV vectors still face challenges, primarily due to their immunogenicity, which limits their efficient and safe use in clinical trials. Furthermore, the lack of a suitable clinical-grade production platform remains a significant obstacle, particularly for HDAV vectors[107]. However, FDA approved few medicaments based on AVs for cancer treatment (Gendicine and Oncorine) [110].

4.2.2.3. Retroviruses (RVs) and lentiviruses (LVs)

Simple and complex RVs, such as the γ-retrovirus known as Moloney murine leukemia virus (M-MLV) and the

LVs called human immunodeficiency virus type 1 (HIV-1), offer significant advantages for gene therapy. One key reason is their ability, when engineered as vectors, to reliably integrate transgenic cargo into the chromosomes of host cells, establishing a strong foundation for long-lasting therapeutic gene expression[107,111–113].

Genetically, both types of viruses share similar characteristics. They are enveloped, single-stranded RNA (ssRNA) viruses that possess their own reverse transcriptase (RT), enabling the production of a double-stranded DNA provirus that integrates into the cell genome. The viral genome consists of the *env*, *gag*, and *pol* genes, which are flanked by long terminal repeats (LTRs). These LTRs contain enhancer/promoter elements necessary for integration. The *env* and *gag* genes encode structural viral proteins, while the *pol* gene encodes non-structural proteins, including the RT. LVs have two additional genes, *tat* and *rev*, responsible for encoding regulatory proteins. Moreover, LVs contain other crucial genetic elements, including *cis*-acting sequences. These include the RNA packaging signal (*ψ*), required for encapsidation of the viral genome into the virions, the polypurine tract (PPT), essential for the reverse transcription process, and the long-terminal repeats, which encompass the HIV promoter[107,112].

Biologically, there are distinctions between simple (γ-retroviral-based vectors) and complex (lentiviral-based vectors). Firstly, LVs demonstrate a preference for inserting

into gene coding regions, while γ-retroviral vectors show a preference for regulatory elements and transcription start sites, enriched in specific chromatin markers, thus disrupting host cell regulation upon vector integration. Another significant difference lies in their infection capabilities. γ-retroviral-based vectors selectively transduce dividing cells since they can only access the nucleus during mitosis when the nuclear envelope is unraveled. In contrast, LVs can infect both dividing and quiescent cells, as they can reach the nucleus without relying on the unravelling mechanism[107,110].

These findings have been motivating over the past years the use of LV vectors rather than γ-RV vectors, offering a better option due to their ability to integrate into non-dividing cells and their safer integration profile. LVs also offer a larger cargo capacity, lower likelihood of silencing once integrated, and various options for pseudotyping with alternative envelope proteins. These advantages have made LVs the primary choice for stable gene transfer into somatic stem cells[112].

- ***Recombinant lentiviral vector generation.***

During vector generation, the LTRs are maintained, while the viral genes are removed and replaced with the therapeutic sequence, which has a capacity of 8–9 kb. In addition to the transgene, the engineered RVs vectors maintain *cis*-acting elements which include the LTRs and the packaging signal (*ψ*)[103,107,110].

The universal strategy for viral vector production involves dividing the viral genome into multiple distinct DNA molecules (**Figure 13**), which are co-transfected into a virus-producing cell line. In the case of LVs, their production is achieved through co-transfection of the 293T cell line with the modified lentiviral transfer vector, along with two additional plasmids: the envelope vector and the packaging vector. These plasmids provide the genes that have been removed from the viral skeleton but are necessary for vector synthesis[114,115].

The packaging plasmid contains the genes required for virus assembly and replication. Vectors are classified into different generations based on the packaging vector used. In first-generation vectors, the plasmid contains the viral genes (*gag*, *pol*, *tat*, *rev*, and accessory genes *vif*, *vpr*, *vpu*, and *nef*) except for the envelope genes. In second-generation vectors, several replication genes (*vif*, *vpr*, *vpu*, and *nef*) are removed from the packaging vector to develop a safer vector. Subsequently, third-generation vectors eliminate the *tat* sequences, and the packaging vector is divided into one vector

with *gag-pol* genes and another vector with the *rev* gene (**Figure 13**)[107,112].

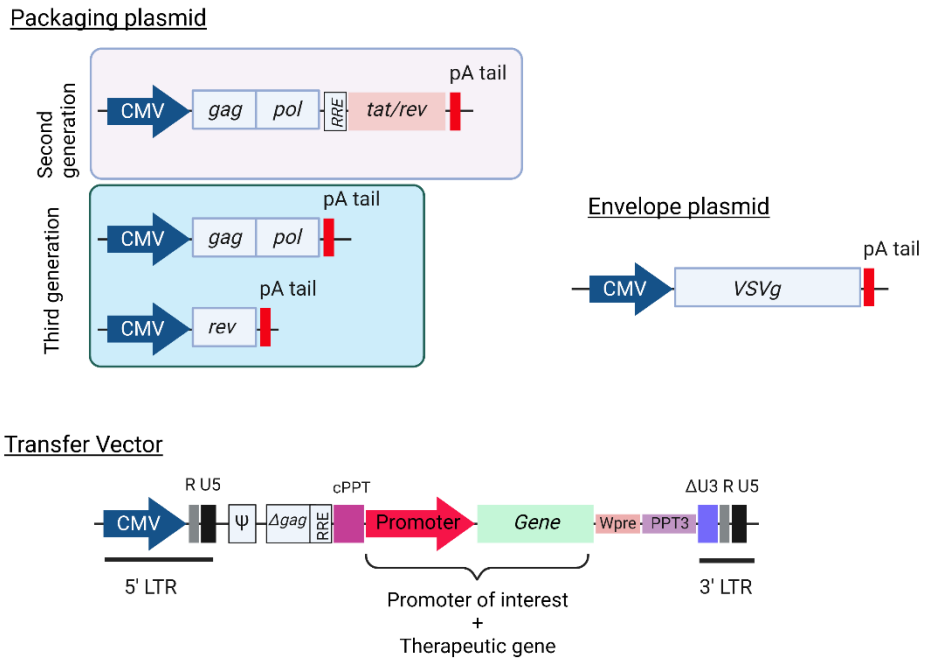

Figure 13. Transgenic SIN-LV production strategy.

Viral genome is divided into different plasmids (Packaging plasmid, Envelope plasmid and Transfer vector) and provided in *trans* to packaging cells which encapsulate our transgene into lentiviral vector particles. It is also specified the plasmid used to produce second and third generation of SIN-LVs. Image created by Martínez-Navajas, G. -Author.

The envelope plasmid (**Figure 13**) contains genes encoding envelope proteins. In vector optimization, wild-type (WT) envelope proteins can be replaced with other proteins through a process called "pseudotyping." Among the most used is the glycoprotein G of the vesicular stomatitis virus (*VSVg*). This envelope is more stable, allowing to produce high viral titers and efficient transduction of $CD34^+$ hematopoietic stem cells[112,114].

Finally, the transfer vector (**Figure 13**) contains the therapeutic gene along with *cis*-acting viral regulatory sequences (LTRs, *Δgag*, packaging signal *ψ,* and att sites) required for viral genome packaging, reverse transcription and integration, not containing viral proteins. The LV skeleton has been modified to include elements that optimize vector production and transduction. These include the cPPT/CTS sequences (central polypurine tract/central terminal sequence) and the RRE element (Rev response element), which increase transduction efficiency by facilitating transport of the viral RNA to the nucleus. Another *cis*-acting element used to improve transgene expression in the target cell is the WPRE sequence (post-transcriptional element from the woodchuck hepatitis B virus), which encodes a truncated form of the X protein involved in hepatocarcinomas[114,115].

In addition to improving vector efficiency, research efforts have also focused on reducing associated genotoxicity. Since LTRs contain enhancer and promoter sequences, their integration into the genome can activate adjacent genes, leading to insertional oncogenesis. Therefore, self-inactivating (SIN) vectors have been developed.

SIN lentiviruses have a deletion in the U3 region of the 3' LTR. During LTR duplication in the retro-transcription process, the truncated U3 region of the 3' LTR is copied into the 5' LTR, resulting in transcriptional inactivation of the viral genome. To maintain transgene expression in SIN vectors, an internal promoter determined by the researcher needs to be

included. Depending on the specificity and level of transgene expression required, a strong or moderate promoter, or a cell-specific or inducible promoter, can be incorporated into the vector[110,115].

- ***Recombinant lentiviral vector transduction.***

Once produced, SIN-LV particles are capable of only a single round of infection (transduction) once they encounter target cells. Reached the cellular cytoplasm, the LV vector genome transcripts undergo reverse transcription, converting them into double-stranded complementary DNA (cDNA) copies. These cDNA copies then integrate into the chromosomes of the target cells, leading to stable genetic

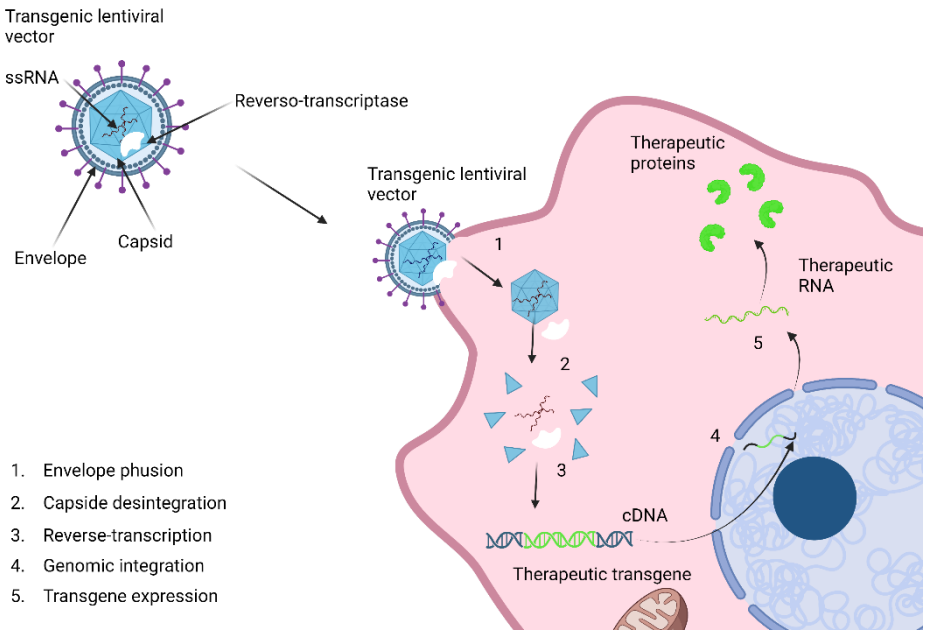

Figure 14. Integration of SIN-LV into the genome of the host cell.

Schematic view of the whole process since the LV reach the cell till cDNA is integrated into the chromatin. Image created by Martínez-Navajas, G. -Author.

modification. The reverse transcription process and subsequent chromosomal integration, which are essential for the long-lasting genetic modification of transduced cells, are facilitated by the reverse transcriptase and integrase proteins associated with the vector particles (**Figure 14**)[110,112,114,115].

These LV vector particles are highly advantageous for modifying stem cells. These vectors not only ensure the stable maintenance of the integrated viral vector genome within the stem cells but also enable its transmission to all subsequent generations of daughter and posterior differentiated cells.

4.3. Gene-therapy approaches according to the final goal.

Knowing the different typologies of gene therapy and delivery strategies, we can differentiate different approaches of gene-therapy application based on our final goal, and it commonly involves utilizing genetic materials such as DNA, mRNA, siRNA, miRNA, and anti-sense oligonucleotides combined with any of the previous delivery system. Among the different strategies, we can highlight (i) altering gene expression through RNA targeting, (ii) adding new genetic material into the host genome, (iii) modifying genes *in situ* or (iv) replacing mutated genes with healthy copies.

4.3.1. Gene expression alteration targeting RNA.

RNA exhibits a range of functions in biology and disease, acting as an intermediate (e.g., messenger RNA (mRNA)) or a final product (e.g., microRNA (miRNA)) of genes. Given the extensive involvement of RNA molecules in regulating gene expression, gene therapy strategies tailored to target RNA or generate effector RNA molecules warrant careful consideration. In this summary, we provide a concise overview of two frequently employed gene therapy strategies rooted in RNA biology[116].

4.3.1.1. Genetic Knockdown by interference RNA.

Typically, this strategy is valid for gain-of-function pathogenic variants that cause an excess of protein or an alternative protein which provokes toxicity. The use of RNA interference (RNAi) let us to target the pathological mRNA, impeding its translation, thus, diminishing and alleviating the pathological effects of the pathogenic variation[117].

On one hand, an approach to alleviate an excess of gene expression is the use of an effector small interfering RNA (siRNA), which is approximately 22 nucleotides long and single-stranded, can initially be expressed in the form of short hairpin RNA (shRNA). This shRNA is then processed into siRNA, which represses gene expression by triggering RNA degradation and/or inhibiting protein synthesis[118]. Additionally, the design of artificial miRNAs it is also employed to diminish aberrant gene expression (Graphical explanation on **Figure 15**)[99,116].

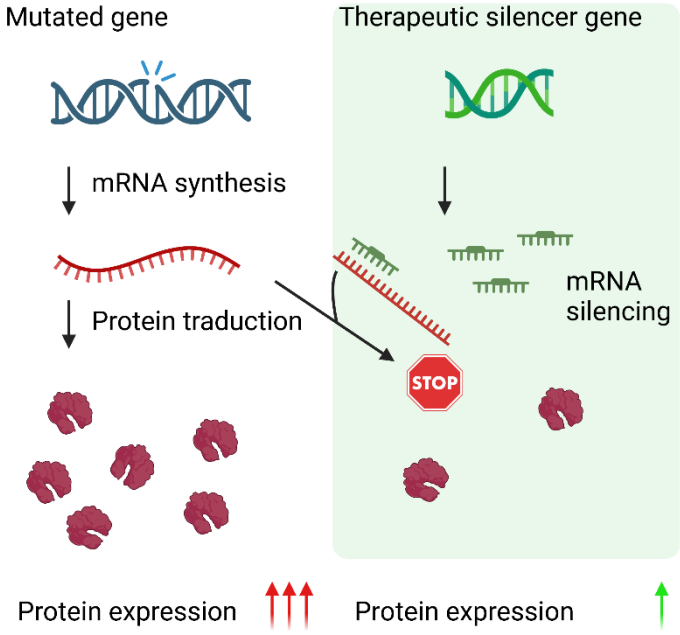

Figure 15. RNAi based strategy for gene therapy.

A pathogenic variant on a gene provokes a gain-of-function mutation which produces an excess of mature protein and/or an aberrant functional protein. RNAi strategies target this mRNA, diminishing the number of mRNA copies to be translated. Image created by Martínez-Navajas, G. -Author. (Inspired in Wang D & Gao G[119].

On the other hand, RNAi is also employed for disease generated by expression of toxic proteins resulting from gain-of-function pathogenic variants[119]. The problematic in these cases resides in that RNAi usually indiscriminately reduces the toxic mutant protein and the normal counterpart (the latter being expressed from the second gene copy in a diploid human genome), which can impair the gene's normal function. To overcome it, it is necessary to develop a smart RNAi design to target specifically the aberrant allele[116–118].

4.3.1.2. Reprogramming messenger RNA splicing by antisense oligonucleotides.

Most newly transcribed pre-mRNAs (in eukaryotes) undergo splicing to produce mature mRNAs that consist of exons responsible for directing protein synthesis. As a result, mRNA splicing plays a crucial role in regulating gene expression by determining which specific pre-mRNA sequences are included or excluded during translation.

Many diseases are caused by pathogenic variants that introduce premature stop codons. In cases where the affected coding DNA is too large to be replaced (such as Duchenne Muscular Dystrophy (DMD)), DNA or vector-derived RNA antisense oligonucleotides (AONs) are designed to induce exon skipping. This approach helps restore the correct reading frame instead of replacing the entire gene. By promoting exon skipping, this strategy allows to produce smaller functional proteins, thereby reducing the severity of the disease[116]. An example of this therapy is illustrated in **Figure 16**, which demonstrates the application of AON therapy to treat DMD (Duchenne muscular dystrophy). In this case, a mutation in exon 50 leads to the production of mRNA without this exon. Consequently, exon 51 now contains a premature stop codon. AON therapy assists in skipping exon 51 during the splicing

process, resulting in the production of a smaller yet functional protein[116–118].

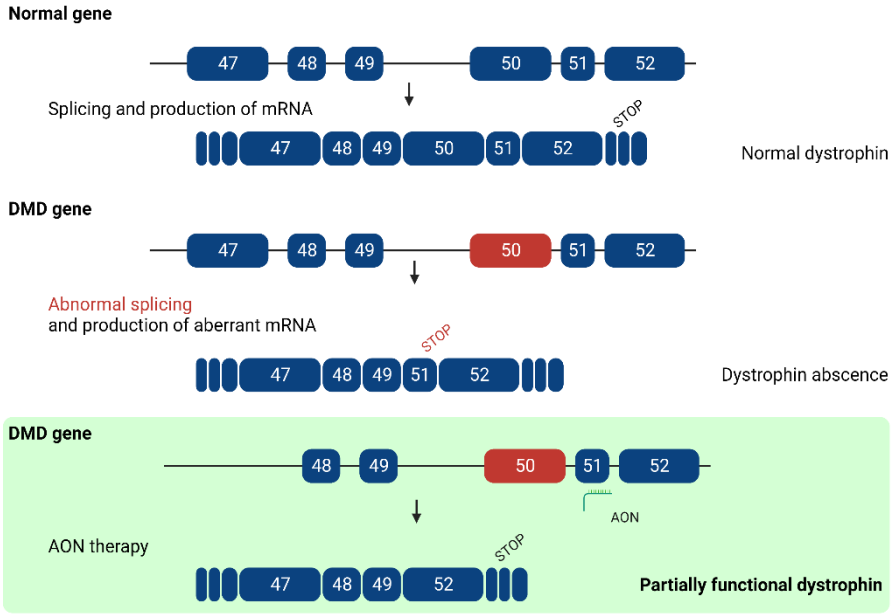

Figure 16. DMD treatment with AON therapy.

The regular splicing process of DMD pre-mRNA produces mature mRNA containing all exons necessary for the synthesis of complete dystrophin. However, in DMD, mutations in exon 50 lead to abnormal splicing, causing the exclusion of exon 50 from mature mRNA. This alteration shifts the reading frame and prevents the production of dystrophin. By binding to the splicing signal in exon 51, AON prevents its inclusion, resulting in the exclusion of both exon 51 and exon 50. As a result, the original reading frame is restored, and partially functional, albeit shorter, dystrophin is produced. Image created by Martínez-Navajas, G. -Author. (Inspired in Wang D & Gao G[119].

4.3.2. Gene Addition.

Complex disorders like cancer and heart diseases result from the combined effects of multiple genes and environmental factors, making gene replacement therapies unfeasible. These disorders are prevalent and urgent medical needs. Expression of external genes could aid to mitigate the effect of

multifactorial diseases. An example could be the heart failure because of low levels of non-mutated Ca^{2+}-ATPase and its compensation by overexpression of *SERCA2A* gene)[103,116]

Additionally, the emergence of new infectious diseases necessitates prompt treatment to prevent the economic and health consequences seen during the COVID-19 pandemic. Consequently, significant efforts have focused on gene therapy development, exemplified by COVID vaccines.

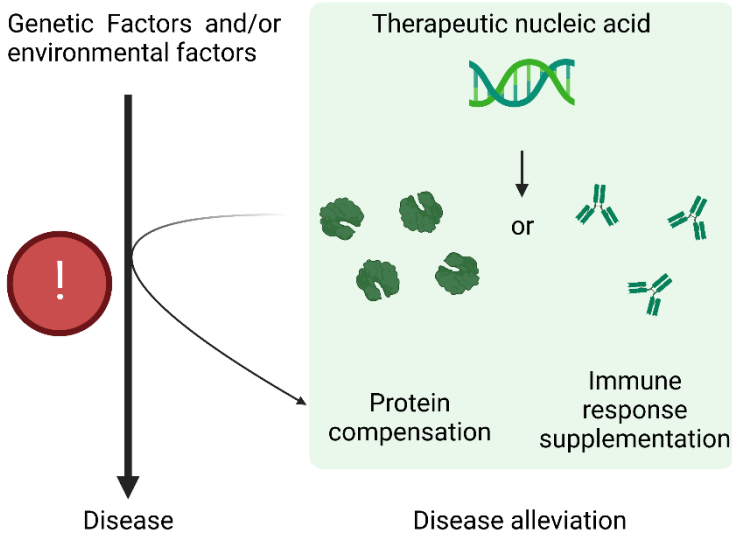

Figure 17. Gene addition strategies.

A complex disease cascade can be triggered by multiple genetic factors and/or environmental factors. However, the introduction of therapeutic genes through gene addition offers relief by complementing specific aspects of the disease mechanism. Image created by Martínez-Navajas, G. -Author. (Inspired in Wang D & Gao G[119].

By incorporating the gene therapy addition approach (**Error! Reference source not found.**), COVID vaccines aim t o stimulate an immune response by utilizing viral vectors or mRNA technology to deliver genetic instructions for producing the spike protein of SARS-CoV-2 and provide protection

against it. This strategy leverages the understanding of the disease mechanism and utilizes gene addition to supplement the immune response. While the vaccines do not directly replace or alter specific genes, they work to enhance the body's natural defenses by providing the necessary genetic instructions. Through widespread vaccination, the goal is to prevent the spread of the virus, mitigate its impact on public health, and ultimately bring an end to the global pandemic[120–122].

4.3.3. Gene Editing Technology.

Target-specific nucleases have emerged as a powerful toolkit for genome engineering. These nucleases, composed of a customizable DNA recognition module and a DNA cleavage domain, offer precise control over the places where we want to introduce genetic modifications. Zinc-finger nucleases (ZFNs) and transcription activator-like effector nucleases (TALENs) achieve sequence specificity by utilizing DNA-binding proteins. On the other hand, the clustered regularly interspaced short palindromic repeats (CRISPR-Cas9) system, based on RNA-guided DNA recognition, enables targeted modifications[123,124]. Although the specific mechanisms may vary, these designer nucleases initiate double-strand breaks (DSBs) at the desired DNA sequences. Subsequently, they facilitate various DNA modifications by employing two distinct DNA repair mechanisms: non-homologous end joining (NHEJ) and homologous directed repair (HDR) [123–129].

The utilization of these nucleases enables genome editing in viable cells for therapeutic purposes. This breakthrough technology facilitates the elimination or correction of harmful mutations and enables the insertion of beneficial mutations. Moreover, it has diverse applications, including the precise integration of transgenes at specific *loci*, the creation of cell lines as disease models through gene knockouts (KO) or knock-ins, and numerous other potential applications[123,124,126,127].

Despite the importance of all these engineered nucleases, we are going to focus in CRISPR-Cas9 systems, which has been widely developed and has evolved over the last years.

4.3.3.1. CRISPR-Cas9 as gene editing tool.

CRISPR-Cas9 is an adaptive prokaryotic immune system employed by numerous bacteria and archaea to defend against exogenous nucleic acids. This complex recognizes and cleaves invasive DNA, providing prokaryotes with a defense system against viral and plasmid attacks, as well as conferring acquired immunity to these microorganisms against future assaults. Currently, this system has been adapted for use in both *in vitro* and *in vivo* eukaryotic cells, serving as a highly specific genomic editing tool. It enables the generation of targeted insertions, deletions, or modifications at specific *loci*. The simplicity, cost-effectiveness, efficiency, and

specificity of the CRISPR-Cas9 system provide it with a competitive advantage over other nucleases[123,124,126].

This specificity is governed by a single-stranded guide RNA (sgRNA) containing 20-22 nucleotides. Through base-pair complementarity, the sgRNA directs the nuclease to a precise genomic *locus*[124,126]. In the CRISPR-Cas9 system derived from *Streptococcus pyogenes* (applied in this study), a 5'-NGG-3' sequence, known as the protospacer adjacent motif (PAM), must immediately follow the target DNA sequence where the sgRNA binds (refer to **Figure 19** for details) (5'-X20-NGG-3')[130]. Cas9 recognizes the PAM sequence and induces a DSB three nucleotides upstream of the NGG trinucleotide[131]. As previously mentioned, cellular machinery is responsible for repairing this DSB, utilizing two distinct mechanisms (**Figure 18**):

- The primary repair pathway is NHEJ, which rejoins the disrupted DNA strands at the break site. During repair, small insertions or deletions of nucleotides (*indel* mutations) can occur. This repair pathway is widely employed in research for generating gene knockouts since the insertion or deletion of a nucleotide within a coding region disrupts the reading frame, potentially leading to premature stop codons and loss of the coding sequence (refer to **Figure 18**). This mechanism is widely used to develop genetic KO to model genetic diseases, correct genetic diseases, among other uses[127,131,132].

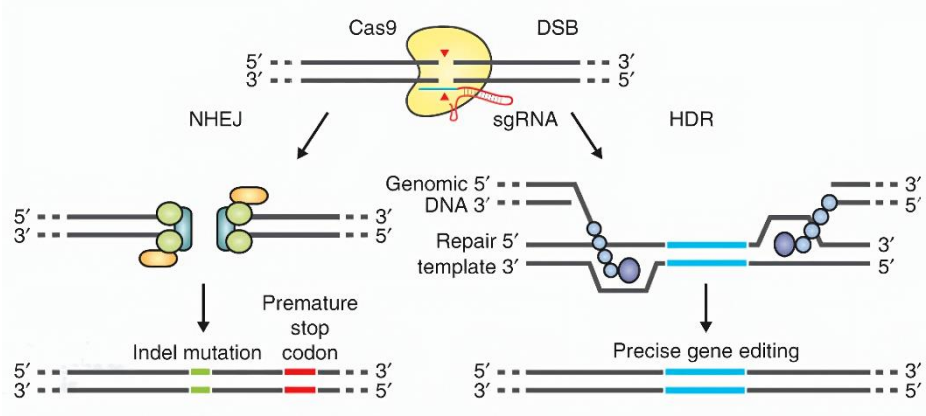

Figure 18. Repair mechanism of DSB for the gene editing strategy.

DSB induced by CRISPR-Cas9. Non-homologous end-joining mechanism (NHEJ, right) and Homology Directed Repair (HDR, left). Modified from Ran et al., 2013[165].

- An alternative to NHEJ is HDR. This secondary repair pathway is less efficient and requires the presence of a DNA template (or donor) for homologous recombination to take place. From a gene editing standpoint, HDR is particularly intriguing as it enables the introduction of specific mutations carried by the donor DNA, which can be incorporated into the genome through homologous recombination. By designing a tailored donor DNA, this mechanism allows for the reversal of mutations causing monogenic diseases, induce precise mutations (as disease modelling), among many others (**Figure 18**)[127,131,132].

Despite all the advantages of CRISPR-Cas9 system, its main limitation resides in the occurrence of off-target effects. Within the CRISPR-Cas9 system, up to 5 mismatches in the distal region from the PAM sequence can be tolerated,

potentially leading to off-target effects. In contrast, the proximal region is more conserved (**Figure 19**). If a mismatch occurs in this proximal region, it results in a reduction in enzyme cleavage efficiency, and in some cases, complete loss of cleavage at that specific *locus*[129,132–134]. While controversy exists regarding the seed region of the sgRNA, several studies support the notion that the conserved region includes the first 2-5 nucleotides adjacent to the PAM sequence (proximal region of the guide), which play a crucial role in determining the specificity of Cas9 [133,135].

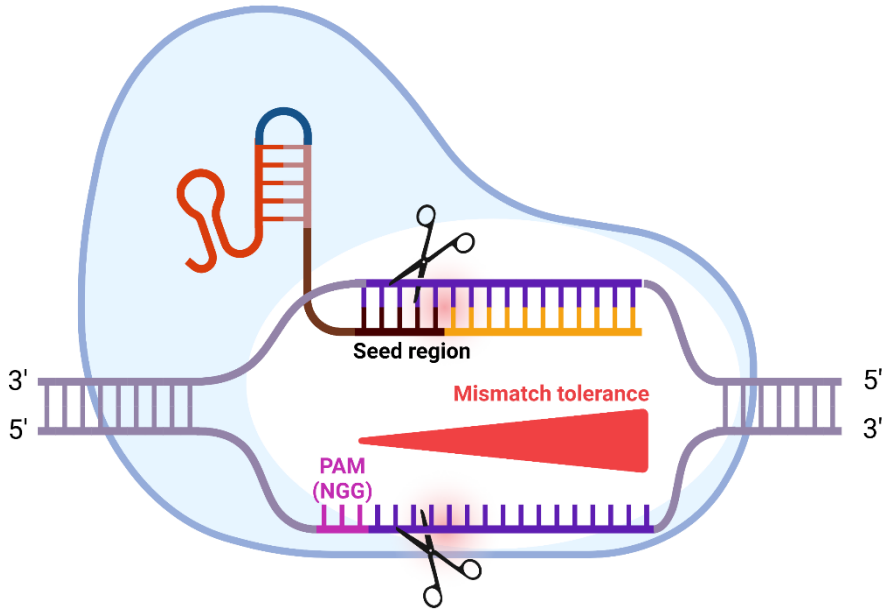

Figure 19. Schematic of CRISPR-Cas9 nuclease and mismatch tolerance.
Image created by Martínez-Navajas, G. -Author.

Although CRISPR technology holds immense potential in gene editing, concerns regarding off-target safety persist. However, the development of new technologies that modified CRISPR-Cas9 system, avoiding the generation of DSB

together with Cas9 fusion to new functional domains hold great promise for the future of clinical gene editing.

4.3.4. Gene Replacement.

Many human genetic diseases are clearly defined by a single gene defect, these are the monogenic diseases, and gene replacement is a straightforward approach to treat them (**Figure 20**). Not surprisingly, the majority of the most advanced clinical gene therapy development falls into the category of gene replacement. This is primarily because its simpler origin greatly facilitates research in this field. In addition, animal models that mimic monogenic human diseases are more easily obtained by naturally occurring mutation or genetic manipulation, which provides a valuable platform for pre-clinical testing[99,103,116].

To date, there are over 3000 ongoing clinical trials employing gene therapy replacement strategies (**Figure 20**)[99]. **Table 4** provides a comprehensive overview of registered viral vector-based therapy products that have been approved for commercialization[110]. This table clearly demonstrates the utility of gene therapy in treating various monogenic diseases, and the number of approved therapies continues to grow as research progresses.

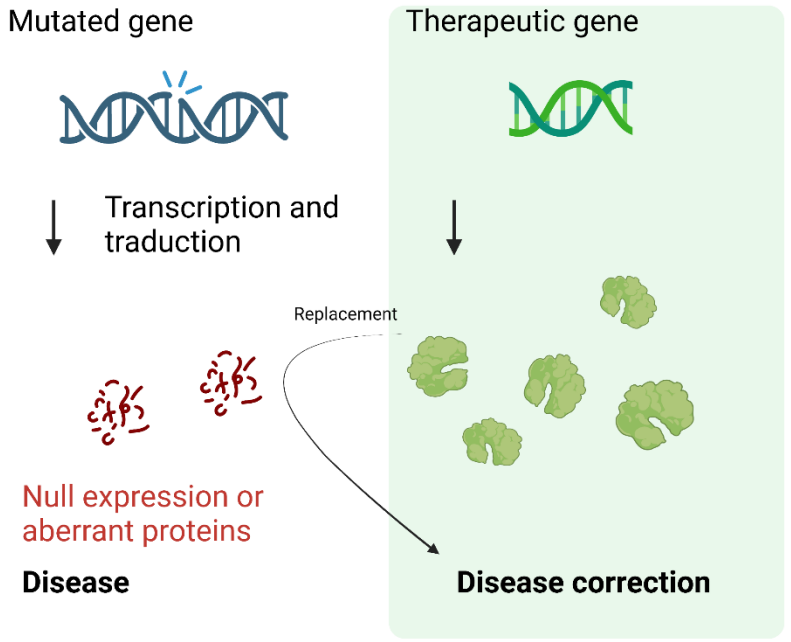

Figure 20. Gene replacement strategy.

A gene mutation disrupts protein synthesis (indicated by a red non-folded structures), resulting in the development of a disease. However, gene replacement offers a solution by providing a functional copy of the gene (represented by a green helix) that enables the production of normal proteins (depicted as green folded proteins), thus correcting the disease. Image created by Martínez-Navajas, G. -Author. (Inspired in Wang D & Gao G[119]).

These are just a few examples of how the importance of gene therapy is increasing for monogenic diseases, providing curative treatments instead of lifelong dependence on palliative measures in the past. As mentioned, ongoing advancements in this field are enabling the initiation of clinical trials for numerous diseases, including bleeding disorders such as Hemophilia A and B, Fanconi Anemia and many others.

Table 4. Gene Therapy treatments based on viral vectors, which involve gene therapy replacement, approved for marketing authorization.

Product name	Target disease	Parental virus	Transgene	Replication status
Rexin-G	Solid tumors	Gamma-retrovirus	Cyclin G1	Replication defective
Strimvelis	ADA-SCID	Gamma-retrovirus	ADA	Replication defective
Zalmoxis	Leukemia	Gamma-retrovirus	HSV-thymidine kinase	Replication defective
Yescarta	Diffuse large B-cell lymphoma	Gamma-retrovirus	Chimeric T cell receptor	Replication defective
Invossa [a]	Osteoarthritis	Gamma-retrovirus	TGF-β1	Replication defective
Kymriah	B-cell acute lymphoblastic leukemia	Lentivirus	Chimeric T-cell receptor	Replication defective
Zynteglo	Transfusion-dependent beta-thalassemia	Lentivirus	β-globin	Replication defective
Gendicine	Head and neck squamous cell carcinoma	Adenovirus 5	p53	Replication defective
Oncorine (H101)	Nasopharyngeal carcinoma	Adenovirus 5	None	Replication competent
Imlygic	Unresectable melanoma	Herpes simplex virus	GM-CSF	Replication competent
Glybera [b]	Lipoprotein lipase deficiency	AAV1	Lipoprotein lipase	Replication defective
Luxturna	Leber's congenital amaurosis	AAV2	RPE65	Replication defective
Zolgensma	Spinal muscular atrophy type I	AAV9	SMN1	Replication defective

[a] **Permission revoked May 2019**

[b] **Product discontinued in 2017**

4.4. Gene Therapy for monogenic diseases in the hematology field.

Gene therapy is a promising field that holds the potential to provide curative treatments for patients with monogenic diseases. While these diseases may not be as severe or dramatic as cancer, the associated symptoms can significantly impact the quality of life of affected individuals. The lack of a definitive cure and the reliance on specific medications or constant vigilance can have a profound effect not only on their physical health but also on their mental health, cognitive function, and overall sense of well-being[136].

It is important to recognize that according to the monogenic disease, different gene therapy approaches and gene delivery methods are required. It is necessary to identify the underlying cause of the disease and determine the target cell to develop an effective curative treatment. Based on this information, the appropriate gene therapy tool can be selected and delivered in the most suitable manner to achieve a therapeutic treatment or a curative outcome.

One example can be seen in bleeding disorders, where the deficiency of certain coagulation factors affects proper blood functionality. In these cases, the root cause lies within the hepatocytes, which are responsible for releasing some of these factors into the plasma to carry out their functions. Understanding the nature of the target cell is essential in selecting an appropriate delivery strategy, whether *in vivo* or

ex vivo, and determining the most suitable viral vector for that specific cell type. For instance, hepatocytes are known to have a non-dividing profile, making AVs or AAVs excellent strategies as they can provide long-lasting therapeutic effects.

In the context of inherited platelet disorders, similar to clotting factor deficiencies, these conditions directly impact the impaired hemostasis[1]. However, unlike clotting factor deficiencies that originate from hepatocytes, IPDs are primarily associated with abnormalities in platelets[86]. As discussed in previous sections, the target cells involved in IPDs are HSCs which resides in the bone marrow. HSCs serve as the primary source for platelet production through a differentiation process[5], and any dysfunction or aberrations in these cells can lead to the manifestation of IPDs, so targeting them is essential to correct IPDs.

Other deficiencies affecting diverse cellular types, with HSCs as the source of aberrant cells, are studied and under clinical trials. To date, primary immunodeficiencies (PID), red blood cell diseases and metabolic diseases are the target of these studies. Respect PIDs, just one affecting platelet is under clinical trials, this is Wiskott-Aldrich Syndrome (**Table 1**), showing very promising data. In addition, different PIDs affecting other hematopoietic linages are also being investigated, like SCID-X1 or ADA-SCID (**Figure 21**)[136]. Notably, in 2022, two medicaments based on LV vector technology counts with FDA approval for the treatment of severe β-Thalassemia (bluebird bio's betibeglogene

autotemcel) and of Cerebral Adrenoleukodistrophy (elivaldogene autotemcel).

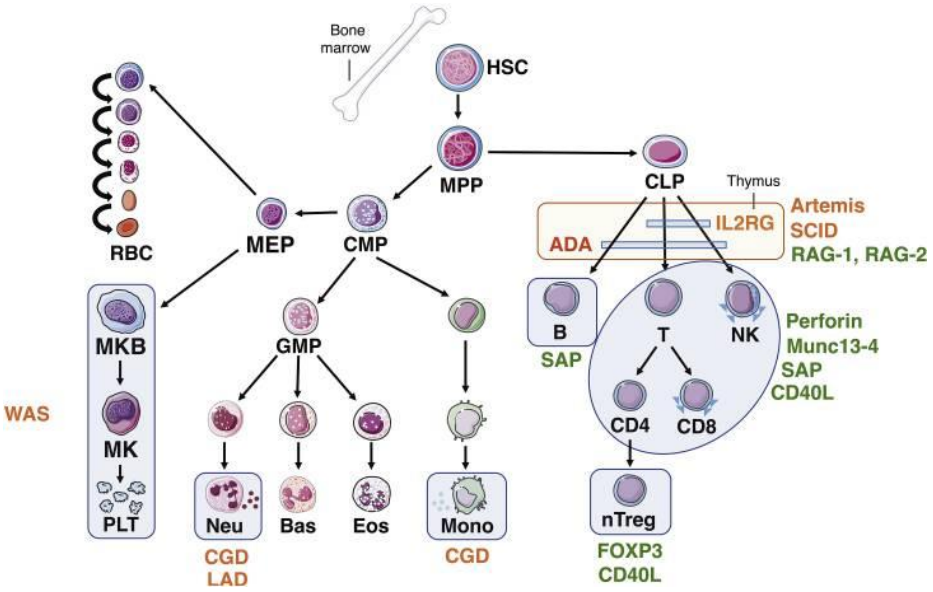

Figure 21. Gene therapy for primary immunodeficiencies.

Each hematopoietic cell lineage is depicted in schematic representations. The primary immunodeficiencies, indicated by blue boxes, primarily impact specific cell type(s). The color-coded genes represent different stages of development, with approved gene products shown in red, products under clinical trial in orange, and products in preclinical studies in green. Figure from Tucci, F, et al; 2021[139].

In all cases, the workflow comprises the *ex vivo* treatment of $CD34^+$ HSCs with SIN-LVs which integrates the therapeutic gene. These cells are then reinfused into myeloablative patients with busulfan treatment to favor the posterior engraftment. Integrated transgene would be inherited by daughter and differentiated cells, where it would be expressed, thus, correcting the disease[137,138].

Indeed, patients who have undergone this type of treatment have shown significant disease correction, indicating the sustained engraftment of gene-corrected hematopoietic stem and progenitor cells (HSPCs). Decades of preclinical and clinical research have played a crucial role in advancing vector engineering, transduction procedures, and the conditioning regimen used prior to transplantation. These advancements aim to deplete hematopoietic progenitors, facilitate the homing and engraftment of gene-corrected HSCs in the bone marrow. Notably, the introduction of third-generation self-inactivating LVs has enhanced the transduction efficiency of long-term engrafting HSPCs, leading to improved immune recovery and a significant reduction in the risk of insertional mutagenesis[136].

However, there are still several challenges that need to be addressed in the field of gene therapy. One of these challenges is the long-term monitoring of the efficiency and safety of RV and LV based gene therapy products in patients. There is a potential risk of insertional mutagenesis, where the integrated vector DNA may disrupt the normal functioning of the genome. Additionally, there is a need to expand HSPC gene therapy to new diseases, beyond the current applications. In fact, it is only a matter of time before other IPDs begin to develop their own curative gene therapy treatments[113]

5. Disease modeling for Bernard-Soulier Syndrome and preclinical approaches.

Since the first reported case of BSS in 1948 by hematologists Bernard and Soulier[139], significant efforts have been made to uncover the underlying basis of the disease. As previously mentioned, prolonged bleeding times, thrombocytopenia, and the presence of giant platelets were the typical signs used to diagnose the syndrome.

Prior to the advent of gene therapy, researchers investigated the syndrome by observing its typical signs and analyzing various laboratory parameters. These parameters included studying platelet aggregation in response to different stimuli such as ristocetin and VWF, as well as assessing levels of fibrinogen and other factors. This analysis involved examining samples from multiple patients, allowing for comparisons to identify similarities and differences[140,141].

It was from 1978 onwards that several researchers identified the GPIb-V-IX receptor as the responsible glycoprotein for the syndrome. Subsequently, the identification of different subunits comprising the entire receptor shed light on the pathogenic variants found in all of them except for GPV. These variants resulted in a dysfunctional receptor assembly or its complete absence from the platelet surface, giving rise to distinct phenotypes according to the specific mutation that each gene exhibited.

5.1. Cellular models to investigate the receptor biology.

Since 1992, coinciding with the emergence of the gene therapy field, there has been an increasing interest in the assembly of receptors with specific mutations[142]. However, due to the scarcity of patients and their varying bleeding tendencies, obtaining samples that could provide a comprehensive understanding of the biological basis of the disease has been challenging. To address this, researchers began investigating the GPIb-V-IX receptor by inducing exogenous overexpression in different cell lines. The mammalian Chinese Hamster Ovary cells (CHO) have traditionally been used due to their ability to amplify genes in a non-human background [143]. Less frequently, HEK-293, K562 human cells and other lines were also used to analyze specific mutations[142]. In all cases, the study of specific mutations involved achieving stable expression of the receptor by co-transfecting expression plasmids that separately encode the coding sequences (CDS) of the WT subunits and the remaining mutated subunit, then comparing it with the coexpressed WT receptor. This approach allowed authors to mimic specific missense or nonsense variants and assess their effects on the assembly of the entire receptor.

5.2. Models to study the differentiation process: Induced Pluripotent Stem cells.

Those cellular models where ectopic expression of the receptor is achieved are useful for studying how these mutations specifically impact on its assembly and functionality *per se*. However, they do not provide insights into the effects of these mutations on the differentiation of HSCs or the specific cell types affected (such as MKs and platelets).

This limitation could be overcome by utilizing another revolutionary development in gene therapy field. The generation of induced pluripotent stem cells (iPSCs) through the reprogramming of animal or human differentiated cells. This is achieved by overexpressing four key genes, which can transform somatic cells into a state resembling embryonic stem cells (ESCs). iPSCs offer several advantages over human ES cells, including addressing ethical concerns and overcoming biological differences between humans and mice[144].

Currently, iPSC technology is playing a crucial role in advancing biological research. It facilitates disease modeling, drug screening, and cell replacement therapy. Patient-derived iPSCs can be maintained *in vitro* for long periods time and differentiated into specific cell types, including MKs, allowing for the study of disease mechanisms and the testing of new treatments *in vitro*[145,146]. However, despite its clear advantages, this procedure sometimes faces limitations when it comes to replicating the differentiation process and obtaining

a sufficient quantity and quality of the desired target cells[147–149].

This technology has been applied to model BSS, patient-derived iPSCs has served to provide new disease models able to mimic the differentiation that HSC suffer through MKs and platelets for *GP1BA (Type A1-BSS)* and *GP1BB (Type B-BSS)* genes[150], reproducing the characteristics giant platelets in a epigenetic human background. Platelets derived from BSS-iPSCs were larger than their WT counterparts. Importantly, LV correction restored GPIb-V-IX expression, improved platelet production and reduced platelet size in both BSS-iPSCs models.

Additionally, our laboratory successfully reprogrammed peripheral mononuclear blood cells to iPSCs from Type C BSS patients carrying different mutations, p.Asn45Ser, p.Phe55Ser and p.Trp71Arg[151–153]. As a proof of concept, we could perform a genetic rescue of these cells using LV under non-physiological promoters, achieving overexpression of GPIX in MKs (**Figure 22**). However, these cells experienced a dramatical reduction in viability throughout the differentiation process of HSCs into MKs and platelets, resulting in a low-quality outcome (not published data).

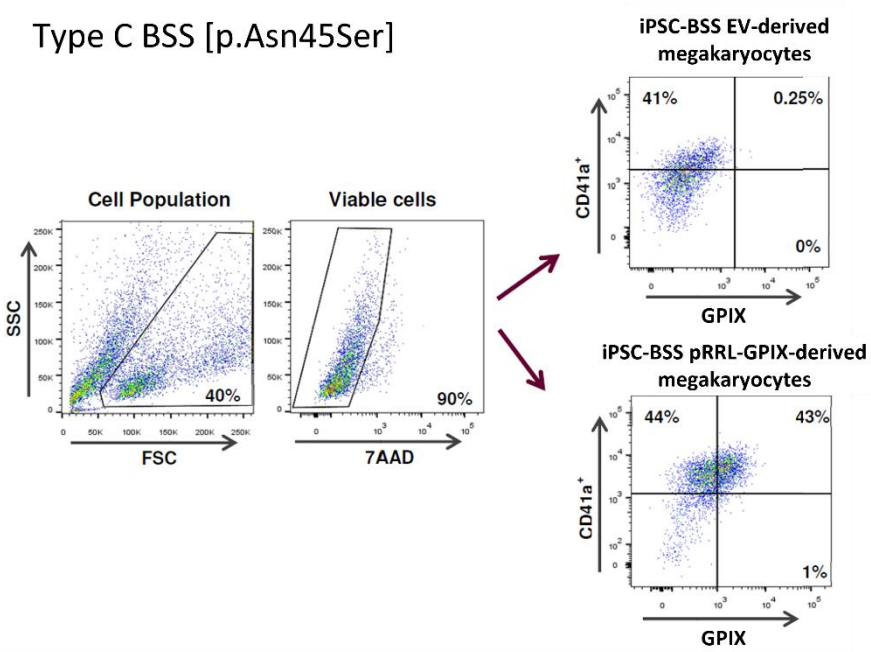

Figure 22. Genetic rescue of iPSC-BSS-GPIX-p.Asn45Ser-derived MKs.

GPIX genetic rescue on megakaryocytes differentiated from iPSCs derived from peripheral blood mononuclear cells. Modified from PhD Thesis Bonillo-Lamolda, M.

5.3. Murine and zebrafish animal models of Bernard-Soulier Syndrome.

Finally, disease models using cell lines fail to capture the full extent of hemostasis disruption within the organism or accurately mimic thrombopoiesis. This limitation arises primarily from the fact that platelets, as anucleate cytoplasmic fragments, cannot be experimentally manipulated using the same strategies commonly employed for cultured cells *in vitro*. The release of platelets from mature MKs and their response to vascular injury are specialized cellular processes exclusive to platelets themselves. Moreover, these processes occur within a multifactorial environment that is challenging to reproduce accurately *in vitro*.

To investigate these characteristics, new murine models (*Mus musculus*) were developed for *mGp1ba*[154], *mGp1bb*[155,156] and *mGp9*[157], being this last one the least explored. These models mirrored the human phenotype by exhibiting a reduced number of giant platelets with impaired assembly of the VWF receptor. Additionally, these abnormalities affected to thrombin response among other processes that cannot be studied through cell experiments. Furthermore, various researchers have developed murine models with *Gp5*-KO to examine its role in relation to the GPIb-V-IX complex and its involvement in pathophysiology.

Recently, researchers have also developed animal models based on zebrafish (*Danio rerio*) for *Gp1ba*[158] and

Gp9[159], which instead of platelets carry its homologous cell type, thrombocytes. These models found similar findings regarding impaired bleeding tendencies achieving a similar phenotype to BSS.

Interestingly, it has been reported that LV-mediated transduction of *hGP1BA* and *hGP1BB* in *mGp1ba* [96] and *mGp1bb* [160] HSCs KO, respectively, followed by their reinfusion into the corresponding murine model, resulted in the alleviation of the macrothrombocytopenia and the reversion prolonged bleeding times. However, no studies have been conducted for *mGp9*-KO. These findings reinforce the perspective that BSS should be considered as a potential disorder to be managed through the implementation of gene therapy approaches.

CHAPTER II

HYPOTHESIS

The continuous evolution of the gene therapy field has resulted in the FDA approval of two treatments based on self-inactivating LV vectors, with several others currently being investigated in clinical trials. In all cases, the objective is to introduce *ex vivo* a therapeutic transgene into HSCs, the source of abnormal cells. Once these cells are corrected, they are reinfused through an autologous transplantation, effectively reversing the disease and avoiding the immunological challenges associated with allogeneic transplants.

Regarding BSS, successful correction using LV-mediated approaches has been achieved for *GP1BA* (BSS Type A1) and *GP1BB* (BSS Type B) disease models in both murine and human iPSCs. However, such correction has not yet been tested for *hGP9* (BSS Type C), despite it being associated with a greater number of variants.

Our study hypothesis aims to explore the potential of SIN LVs expressing human GPIX as a curative treatment for BSS Type C, given its monogenic cause and relatively small gene size.

To achieve stable and tissue-specific expression of GPIX, it is essential to integrate our therapeutic cassette into the patient's HSCs, which give rise to abnormal MKs and platelets. However, due to the limited availability of patients and their unique bleeding characteristics, it may not be feasible to isolate HSCs for testing our gene therapy tools. Therefore,

alternative preclinical models are necessary to evaluate the efficacy of these gene replacement strategies.

Taking advantage of the revolutionary CRISPR-Cas9 technology, we aim to establish BSS disease models in human megakaryoblastic cell lines by individually knocking out each subunit, including GPV. These novel models will enable us to investigate the specific contribution of each subunit in the assembly of GPIb-V-IX and will help us understand the diverse phenotypes observed in clinical settings.

Additionally, in order to mirror the differentiation phase and the generation of aberrant MKs and giant platelets, we will develop a human BSS Type C model using iPSCs as the closest alternative to HSCs.

The subsequent step involves developing self-inactivating LV vectors that express GPIX under physiological promoters to achieve tissue-specific expression suitable for clinical application. The previously established *GP9*-KO disease models will serve as preclinical tools to assess the functionality of our LVs in restoring GPIX expression, facilitating GPIb-V-IX reassembly, preserving binding capacity to VWF and producing normal-sized platelets.

Once optimized our GPIX-expressing LVs, confirming their functionality in HSCs from BSS patients harboring different *GP9* mutations is essential to validate this gene replacement tool. Through isolation from peripheral blood, transduction and differentiation into MKs and platelets, we will

validate the reversal of the phenotype, confirming the therapeutic potential of our gene therapy approach.

Lastly, the development of a novel murine model, designed specifically to evaluate the efficacy of our LVs in restoring normal physiological functions such as bleeding time, holds huge relevance as the definitive preclinical study preceding the progression to the clinical phase of the disease. This *in vivo* model will serve in future projects to further evaluate the efficacy of our GPIX-expressing LVs.

CHAPTER III

OBJECTIVES

Therefore, to carry out this research project, the work has been structured into the following objectives:

Objective 1: Investigate the assembly of GPIb-V-IX through CRISPR-Cas9 knockout generation and disease modeling: Exploring the roles of *GP1BA*, *GP1BB*, *GP9* *and* *GP5*.

1.1 Generation and characterization of megakaryoblastic Bernard-Soulier Syndrome models and *GP5*-KO, studying the contribution of each subunit to the assemblage of the GPIb-V-IX receptor.

1.2 Generation and validation of Bernard-Soulier Syndrome Type C model in induced Pluripotent Stem Cells.

Objective 2: Design and development of reporter and therapeutic GPIX-lentiviral vectors able to rescue GPIX expression and complex functionality in megakaryoblastic KO models.

2.1 Design and development of GPIX lentiviral vectors.

2.2 Genetic rescue of *GP9*-KO cellular models by GPIX-lentiviral transduction.

2.3 Analysis of GPIb-V-IX complex functionality in WT, *GP9*-KO and *GP9*-KO megakaryoblastic transduced cells.

Objective 3: GPIX-Lentiviral correction of Bernard-Soulier Syndrome Type C induced Pluripotent Stem Cells and posterior differentiation to megakaryocytes and platelets.

3.1 Analysis of GPIX reversion in megakaryocytes and platelets produced from transduced *GP9*-KO induced pluripotent stem cells.

3.2 Size determination in genetically rescued platelets produced from iPSCs *GP9*-KO.

Objective 4. Genetic-Rescue of isolated hematopoietic stem cells from Bernard-Soulier Syndrome patients carrying different pathogenic variations and posterior differentiation to megakaryocytes and platelets.

4.1 Corroboration of pathogenic variants from two unrelated Bernard-Soulier Syndrome Type C patients.

4.2 Genetic rescue in megakaryocytes and platelets produced from transduced non-mobilized HSCs from these Bernard-Soulier Syndrome patients.

Objective 5. Generation and characterization of Bernard-Soulier Syndrome *GP9*^{null} murine model.

5.1 Analysis and comparison of h*GP9* and m*Gp9* genes and their amino acidic sequences.

5.2 Development of a *GP9*^{null} murine model.

5.3 Hemogram analysis from *Gp9*^{null} murine model and its comparison with WT hematological parameters.

CHAPTER IV

MATHERIAL & METHODS

Objective 1: Investigate the assembly of GPIb-V-IX through CRISPR-Cas9 knockout generation and disease modeling: Exploring the roles of GP1BA, GP1BB, GP9 and GP5.

1.1. Cell Culture.

1.1.1. Megakaryoblastic cell lines.

-DAMI cells were acquired from the American Type Culture Collection (ATCC): Megakaryoblast cell line that constitutively expresses the GPIb-V-IX receptor[161] and its origin is unknown.

-MEG-01 (ATCC): Megakaryoblast cell line that expresses GPIb-V-IX receptor constitutively[162,163]. It was isolated in 1983 from the marrow of a 55-year-old, male patient with Chronic Myelogenous Leukemia (CML).

- ***Maintenance*:** Both megakaryoblastic cell lines grown in suspension and were cultured in RPMI 1640 medium (Biowest) supplemented with 10% Fetal Bovine Serum (FBS) (Biowest) and 1X Penicillin/Streptomycin (Sigma-Aldrich). Respect the culture conditions, cells were grown at 37ºC and 5% CO_2 in a humid incubator.
- ***Passages:*** Cells were passaged twice a week, seeding $1x10^5$ cells/mL in a T25 flask with 6 mL supplemented media. As culture conditions, cells were grown at 37ºC and 5% CO_2 in a humid incubator.
- ***Cryopreservation:*** The cells were collected when they reached a confluence of 90%, centrifuged at 300xG for

5 minutes. After the aspiration of the supernatant, cells were resuspended in 1 mL FBS supplemented with 10% of dimethyl sulfoxide (DMSO) and transferred into a cryotube. The cryotubes were stored in isopropanol containers (Mr. Frosty, ThermoFisher Scientific), in a freezer at -80ºC. After 24 hours, the vials were transferred to a liquid nitrogen tank at -196ºC.

1.1.2. Induced Pluripotent Stem Cells.

iPSC line was obtained from Cambridge Biomedical Research Centre Core Facility. This iPSC line was derived from adult dermal fibroblast using integrative murine retroviral vectors and has been previously reported by Moreau *et al.* to produce efficiently MKs and platelets *in vitro*[164].

- ***Maintenance*:** During the maintenance of the cell line, the cells were cultured in T25 coated with matrigel (BD Biosciences). We used E8[165] as culture medium (E4 (1X), ddH2O, FGF (100 µg/L) (PEPROTECH), TFGβ (1.8 µg/L) (PEPROTECH), Holo-transferrin (10.6 mg/L) (Sigma-Aldrich), Insulin (20 mg/L) (Sigma-Aldrich)). This medium was replaced every 24-48 hours depending on the cell confluence. To do this, the culture medium was aspirated and replaced with tempered E8 medium. As culture conditions, cells were grown at 37ºC and 5% CO_2 in a humid incubator.

- ***Passages:*** The cells were passaged twice a week when they reached a confluence between 80 and 90%. To do this, the culture medium was aspirated. Then, the cells were washed with 0.5 mM PBS-EDTA and after aspiration, they were incubated again with 0.5 mM PBS-EDTA for 4-7 minutes in an incubator at 37ºC. The use of PBS-EDTA dissociates the cells into small clusters, increasing their cell viability. After the incubation period, they were lifted with a scraper. The cells were diluted between 1:8 and 1:12 and added to a new T25 coated with Matrigel (Corning) and with E8 medium supplemented with Y-27632 2HCl 10 µM (Deltaclon). Each new T25 used required coating its surface with Matrigel (Dilution 1:20 in KnockOut DMEM (Fisher Scientific)) and incubating it at room temperature for at least 30 minutes. After this time, it was aspirated and replaced with E8 medium supplemented with Y-27632 10 µM. When single cells were required, and not small clusters, TrypLE was used instead of PBS-EDTA, and the same procedure was followed.
- ***Cryopreservation:*** The cells were detached when they reached a confluence between 80-90%, following the same procedure as in the previous paragraph. Once the scraper was used, the entire cell volume was collected and added to a 15 mL tube, diluted in PBS to neutralize the effect of EDTA. Subsequently, the cells were centrifuged for 4 minutes at 1200 RPM, the medium was

aspirated, and the cells were resuspended in 500 µL of E8 medium supplemented with Y-27632 10 µM and transferred to a labeled cryovial. Finally, 500 µL of E8 medium supplemented with 20% DMSO was added to each cryovial, reaching a final DMSO concentration in the cryovial of 10%. Then, cryovials were stored into liquid nitrogen tanks as previously described.

1.2. Knockout generation in megakaryoblastic cell lines with CRISPR-Cas9 system: GP1BA, GP1BB, GP9 and GP5 genes.

As described in the Chapter I, CRISPR-Cas9 is a system that creates DSB in specific and desired positions within the genome. This DNA specificity is given by a single guide RNA (sgRNA), that identifies the region of interest and anneals with it, allowing the endonuclease Cas9 to create a DSB. It will be repaired by the endogenous machinery by NHEJ, introducing *indels*. This impaired correction mechanism will create frameshift mutations when occurring within the CDS[166,167].

We used this technology to create a KO for each single gene encoding the different subunits of the GPIb-V-IX receptor. These genes include *GP1BA*, *GP1BB*, *GP9* (identified as driver genes for Type A1, Type B, and Type C, respectively), and *GP5* (which does not possess any pathogenic variants associated with BSS development).

1.2.1. Design of sgRNAs for each GPIb-V-IX receptor coding gene.

Two different software programs were utilized to design the sgRNAs. The predictions generated by both programs were compared, and the most favorable sgRNAs were selected. The software programs employed for this purpose were Breaking-Cas[168] and CRISPR Design (Integrated DNA Technologies). The coding sequence corresponding to each

locus was inputted into both programs to identify potential sgRNAs. The programs provided a list of potential sgRNAs, which were then sorted based on a scoring system that classified them.

For *GP1BA*, *GP1BB*, and *GP9* genes, our selection criteria were two: (i) First, we selected those that had fewer potential off-targets, and (ii) we aimed the maximum proximity of the Cas9 cleavage site to the 5'-ATG, favoring the introduction of *indels* as close to the beginning of the protein as possible, facilitating the generation of truncated subunits.

In the case of *GP5*, as mentioned, to our knowledge, there are no pathogenic mutations that affect GPIb-V-IX receptor assembly. This fact increases the difficulty of detecting the *GP5*-KO by flow cytometry. For this reason, we utilized two different sgRNAs to create a deletion of 200 base pairs (bp). This region would contain the start of the CDS, including the start codon (ATG). Consequently, we could generate the KO and detect it by conventional PCR. **Figure 23** represents a schematic view of the CRISPR-Cas9 designing

process, together with each genetic structure of the four genes that encode GPIb-V-IX receptor.

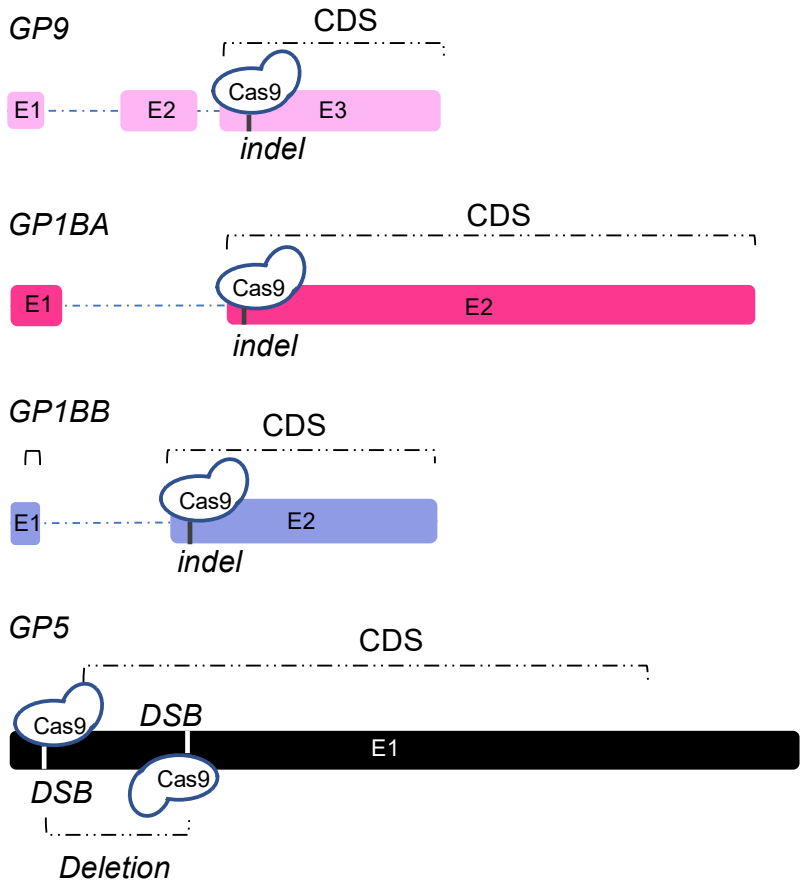

Figure 23. Schematic representation of the 5'-3' genetic structure of the genes *GP9*, *GP1BA*, *GP1BB*, and *GP5*.

Each genetic structure depicts the introns, exons, and coding sequences of every subunit, along with the cutting site where CRISPR-Cas9 is designed to target and the position where the *indel* should be introduced. Additionally, gene sizes are representative of each case. Image created by Martínez-Navajas, G. -Author.

Objective 1: Investigate the assembly of GPIb-V-IX through CRISPR-Cas9 knockout generation and disease modeling: Exploring the roles of GP1BA, GP1BB, GP9 and GP5.

Taking these criteria into account, we selected the *in silico* predicted sgRNAs (**Table 5. Selected sgRNAs to target *GP1BA*, *GP1BB*, *GP9* and *GP5*.**

DNA sequences for each sgRNA, indicating the targeted gene, the directional sequence (5'-3'), the score, off-targets in the genome and in genes, cutting site respect the ATG and total size of the CDS.

GENE	Guide Sequence (5'-3')	Score (BreakingCas)	Off-targets	Off-Targets (in genes)	CDS Cutting Site (From ATG)	CDS Length (bp)
GP9	CTCCCGGGGGCACGGACTGA (AGG)	88.3	105	93	191-192	534
GP1BA	GCCGGTTGAAGGAGACGTCC (AGG)	90.7	43	40	365-366	1959
GP1BB	TAGCTGCGCGGGGACGCTCG (TGG)	94.9	39	48	106-107	621
GP5_G1	GTGGCGCGCATCTCCGCGCT (AGG)	97.1	37	0	134-135	1683
GP5_G2	TTCGCGCCTGTACTGAACCC (TGG)	90.2	32	3	(-62)-(-61)	1683

***GP1BA*, *GP1BB*, *GP9* and *GP5*.Table 5**).

1.2.2. sgRNAs cloning into the PX-458 plasmid.

1.2.2.1. Plasmid description.

To develop our targeted CRISPR-Cas9 systems, we used CRISPR-Cas9 expressing plasmid, pSpCas9BB-2A-GFP (PX-458) (https://www.addgene.org/48138/, AddGene). This plasmid harbors an ampicillin resistance gene that facilitates the cloning process of sgRNA in bacteria, as well as a bacterial replication origin. It encodes the Cas9 protein and contains a region for cloning sgRNAs flanked by two *BbsI* restriction sites. The arrangement of these restriction sites results in their destruction upon digestion, preventing plasmid religation during cloning. Additionally, the plasmid contains a selection marker, the enhanced Green Fluorescent Protein (eGFP), which enables identification of eukaryotic cells that have incorporated the plasmid and are expressing Cas9 (see **Figure 24** for detailed information of the plasmid).

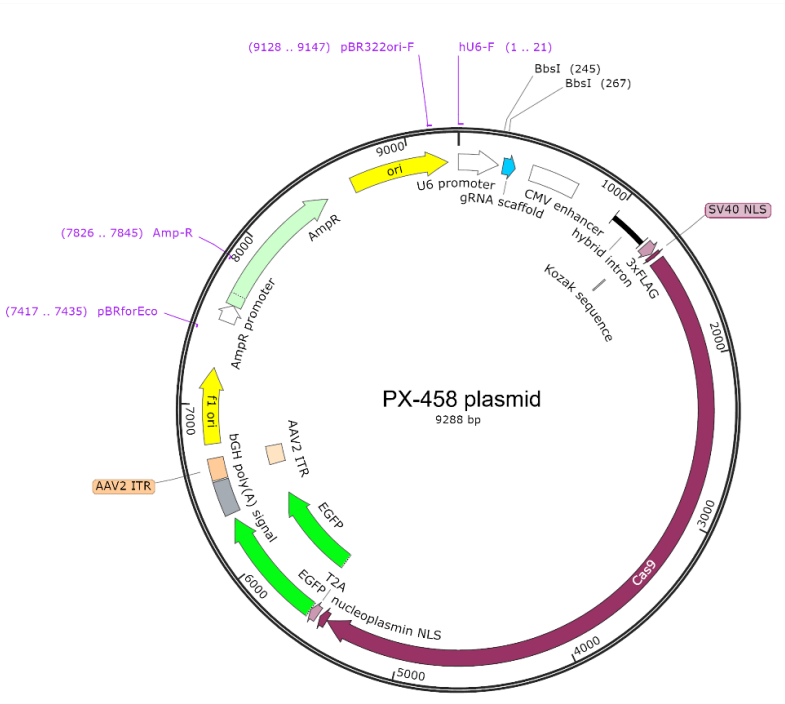

Figure 24. Schematic view of the PX-458 plasmid (9288 bp).

It contains a bacterial replication origin (ori), a bacterial resistance marker (ampicillin), two BbsI cloning sites to digest the plasmid and introduce the sgRNAs of interest, the Cas9 and eGFP CDS. Also indicated the hU6-FW primer for sequencing.

1.2.2.2. Plasmid digestion with *BbsI*.

To clone the sgRNAs into the plasmid, we digested 3 µg of plasmid with *BbsI* restriction enzyme (RE) for 1 hour at 37ºC (**Table 6**). The digested plasmid was separated in 1% ultrapure agarose gel (Invitrogen). The band was cut and purified using the NucleoSpin® Gel and PCR Clean-up kit (MACHERY-NAGEL), following the manufacturer's instructions.

Table 6. Required reagents and amounts to digest the PX-458 plasmid.

Reagent	*Volume*
BbsI (NEB)	2 µL
NebBuffer™ 2.1 (10X)	3 µL
PX-458 plasmid	3 µg
ddH_2O	To 30 µL

1.2.2.3. sgRNA and PX-458 plasmid ligation.

To clone the sgRNAs into the PX-458 plasmid, sgRNAs were synthesized flanked by overhanging ends that could hybridize by base complementarity with the protruding ends generated during the digestion (**Figure 25**). Furthermore, highlighted in red, we included a modification to improve the transcription of the sgRNA regulated under the *hU6* promoter.

5'- CACCGGNNNNNNNNNNNNNNNNNN -3'
3'- CCNNNNNNNNNNNNNNNNNNCAAA -5'

Figure 25. Schematic design of the sgRNAs.
The overhanging ends (highlighted in blue) are complementary to the overhanging ends generated by digesting PX-458. In red, a modification that favors the transcription of the sgRNA.

The sgRNAs were designed and ordered from the commercial supplier (Sigma-Aldrich) in a single-stranded format. Subsequently, the oligonucleotides were annealed and phosphorylated to form the oligoduplex, using the reagents detailed in **Table 7**. These oligoduplexes were then placed into

a thermocycler and incubated at 37°C for 30 minutes, followed by 95°C for 5 minutes, with a temperature gradient set to decrease at a rate of 5°C per minute to 25°C.

Table 7. Components and required volumes that are necessary to anneal and phosphorylate the sgRNAs.

Reagent	***Volume***
Oligo 1 (100 µM)	1 µL
Oligo 2 (100 µM)	1 µL
10X T4 Ligation Buffer (NEB)	1 µL
ddH_2O	6,5 µL
T4 PNK (NEB)	0,5 µL
Total	10 µL

The digestion of the PX-458 plasmid with the *BbsI* enzyme resulted in overhanging and cohesive ends that match those incorporated in the sgRNAs. After digesting the plasmid and hybridizing phosphorylated oligonucleotides, a ligation reaction was performed at 16 ºC overnight. The reaction conditions are specified in **Table 8**.

In addition, a negative ligation control was established in which the oligoduplex was not added to the ligation reaction. This control enabled us to detect the frequency of religation when the constructs were transformed. The ligation product was then transformed into competent *E. coli* DH5α bacteria the following morning.

Table 8. Required reagents and amounts to perform the ligation reaction between sgRNAs and the digested plasmid.

Reagent	***Volume***
Digested plasmid	1 µL
Oligoduplex (Dilution 1:200)	1 µL
2X T4 Ligation Buffer (NEB)	5 µL
ddH2O	4 µL
Ligase T4 (NEB)	1 µL
Total	11 µL

1.2.2.4. Bacterial heat shock transformation of the ligation products.

Bacterial transformation is a laboratory technique that permits the introduction of foreign DNA, such as plasmids, into **bacterial cells.** Competent cells are mixed with the foreign DNA and incubated for a brief period to allow for the uptake of the DNA. The transformed bacteria are then selected and cultured on a selective medium containing antibiotics or other compounds that only support the growth of bacteria that have taken up the foreign DNA.

To perform the transformation, we started with a 100 µL aliquot of competent *E. coli* DH5α bacteria to which 5 µL of the ligation product was added. The mixture was incubated on ice for 30 minutes. Then, a thermal shock was applied in a 42ºC water bath for 30 seconds, and finally, the bacteria were reintroduced to ice for 2 minutes. After this time, the bacteria were resuspended in 250 µL of SOC medium (ThermoFisher

Scientific) and incubated with agitation at 37ºC for 30 minutes. Then, for each transformation, two plates of LB-Agar (Sigma-Aldrich) supplemented with 100 µg/mL of ampicillin (ThermoFisher Scientific) were seeded with 100 µL bacteria and 250 µL. This facilitated the obtention of colonies that were spaced enough to be picked the next morning. The volume was spread over the surface of the plate with a sterile glass spatula. Once seeded, the plates were incubated in a 37ºC incubator for 16 hours (overnight).

The next morning, colonies were picked with inoculation loops and inoculated into 5 mL of liquid LB supplemented with ampicillin. The inoculum was incubated with agitation (200 RPM) in a 37ºC incubator for 16 hours (overnight).

1.2.2.5. Plasmid DNA extraction.

To extract plasmid DNA from *E. coli*, the bacteria were collected by centrifugation, and a miniprep was performed following the instructions provided by the NucleoSpin® Plasmid kit (MACHERY-NAGEL). After extraction, the DNA was quantified using NanoDrop spectrophotometry.

1.2.2.6. Confirmation digestions.

The ligation products underwent confirmation digestions. 300 ng of the plasmids were digested in a final volume of 10 µL, using *BbsI* enzyme (See details in **Table 9**). The plasmids that have incorporated the sgRNA could not be

digested by this enzyme, thus migrating in circular conformation when analyzed in an agarose gel.

Table 9. Required reagents and amounts to perform the confirmation digests.

Reagent	***Volume***
BbsI (NEB)	0.2 µL
NebBuffer™ 2.1 (10X)	1 µL
PX-458 plasmid	300 µg
ddH_2O	To 10 µL

1.2.2.7. Sanger sequencing of plasmid DNA and preparation of CRISPR-Cas9 plasmid working solutions.

The constructions that showed expected digestion patterns were sequenced in Stab Vida laboratories, verifying that the cloned sgRNAs did not present any mutations in their DNA sequence. Sanger sequencing required 3 µL of 10 µM stock hU6 sequencing primer (**Table 10**) and 10 µL of each plasmid sample at a concentration of 100 ng/µL.

Table 10. Chosen primers to sequence sgRNAs inserted into PX-458 plasmid.

Name	**Sanger Sequencing primers (5'-3')**
*U6*_promoter	GAGGGCCTATTTCCCATGATTCC

After sequencing, those constructions that did not contain mutations in their sequence were transformed into *E. coli* Stbl3. The following morning, a colony was picked and

inoculated into a tube with 5 mL of LB supplemented with ampicillin. A preculture was carried out for 8 hours at 37°C with shaking (200 RPM). After this time, 300 µL were inoculated into 300 mL of LB supplemented with ampicillin in a 1000 mL flask. The flasks were grown with shaking at 37°C overnight. The following morning, the bacteria were collected by centrifugation and their plasmid DNA were extracted using the NucleoBond® XtraMaxi kit (MACHERY-NAGEL). The extracted plasmid DNA was then eluted in water for embryo transfer (EMD Millipore) for 24 hours and quantified using Nanodrop.

1.2.3. Lipofection into DAMI and MEG-01 cells.

Transfection allows the introduction of exogenous nucleic acids into the interior of **eukaryotic** cells. Lipofection is a type of transfection in which nucleic acids are transported inside cationic liposomes, facilitating cellular entry by endocytosis[169]. This technique was used to introduce our constructs into the cytoplasm of megakaryoblastic cell lines (DAMI and MEG-01), performing the gene editing of each of the genes encoding the GPIb-V-IX complex

For lipofection, LipoD293™ Transfection Reagent (Sinagen) was used following these instructions:

-Day 0: Cells were plated in a 6-well plate at a density of 500.000 cells/well. Each well would be transformed with a different construct. Cell counting was performed using the trypan blue viability assessment method.

-Day 1: When the cells reached 60-80% confluence, the lipofection protocol was initiated. 30 minutes before starting the protocol, the cells were collected, washed, centrifuged, and resuspended in 1 mL of warm medium.

Two cocktails were prepared in two separate Eppendorf tubes for each construct:

• **Cocktail 1**: 50 µL of serum-free DMEM-HG, 2 µg of plasmid DNA.

• **Cocktail 2:** 50 µL of serum-free DMEM-HG, 6 µL of LipoD293.

Once the cocktails were prepared, the content of cocktail 2 was added to cocktail 1 and left to incubate at room temperature for 12 minutes. Finally, the mixture was added dropwise to its corresponding well using a fine capillary Pasteur pipette. After 8 hours, the medium was replaced, and the cells were eluted in a final volume of 3 mL.

-Day 2: Medium change.

-Day 3: Cells were collected and transferred to a sterile flow cytometry tube. Then, cells were separated by $eGFP^+$ fluorescence using a flow cytometer sorter (BD FACS Aria). To enrich the KO frequency, we established several pools with reduced number of initiating cells (~100-300). These cells were seeded on 96 well plates, expanded and screened for the highest KO frequency in each case.

1.2.4. Single cell cloning and clone screening.

To isolate the KO model for each GPIb-V-IX receptor coding gene, we estimated the KO frequency of each single pool started from reduced cell number. We used the most enriched one to establish single cell clones. Once expanded, we would be able to detect the KO. As explained in the previous section "**1.2.1"**, we followed two different methodologies for KO detection, according to the availability of commercial antibodies.

1.2.4.1. Flow cytometry technique to detect the knockouts for Bernard-Soulier Syndrome driver genes (*GP1BA*, *GP1BB* and *GP9*).

Regarding GPIX, GPIbα, and GPIbβ, it was possible to determine their expression by flow cytometry, due to the availability of antibodies specific to each human subunit..

- ***Flow cytometry to determine GPIbα, GPIbβ and GPIX KO frequency.***

As previously described, cells expressing CRISPR-Cas9 were sorted based on eGFP^{+} into several pools, resulting in a reduced number of cells seeded. This approach allowed us to achieve varying KO enrichment frequencies based on the number of founder-edited cells compared to founder non-edited cells in the pools.

Table 11. Antibodies panel to detect GPIX (CD42a), GPIbα (CD42b) and GPIbβ (CD42C).

Antibody	Fluorophore	Commercial Brand	Purpose
Anti-human CD42a	APC	Miltenyi Biotec	Detect GPIX-KO frequency from *GP9*-KO gene edited pools.
Anti-human CD42b	APC	Miltenyi Biotec	Detect GPIbα-KO frequency from *GP1BA*-KO gene edited pools.
Rat anti-human CD42c-RAM.1	Secondary antibody required conjugated with goat anti-rat AlexaFluor 488 (Invitrogen),	Kindly provided by Françoise Lanza	Detect GPIbβ-KO frequency from *GP1BB*-KO gene edited pools.

The pools were grown and expanded until they reached the 6-well plate format. Then, 500 µL aliquots of WT and edited cell pools were transferred into flow cytometry tubes. These cells were washed with PBS and centrifuged, and a pre-mix of PBS and the respective antibody was prepared (as indicated in **Table 11**). The pre-mix was added to the corresponding gene-edited pellet and incubated for 20 minutes for CD42a and CD42b. After washing and centrifugation, the cells were ready for flow cytometry analysis. In the case of cells incubated with RAM.1, another incubation with a secondary antibody goat anti-Rat AlexaFluor 488 (Invitrogen) was required. In addition, 7-Amino Actinomycin D (*7AAD)*, a viability solution to identify

dead cells, was added. Stained samples were then analyzed using FACS Canto II or FACS Verse flow cytometers from BD Biosciences.

- ***Flow cytometry analysis and gating strategy.***

Flow cytometry files were analyzed using Cytobank software[170]. First, cell population was identified facing FSC *vs.* SSC parameters. Once the population is visible, we established the primary population (**R1**). Then, R1 cells were analyzed for *7AAD* staining, therefore, the negative fraction (viable cells) was gated again, establishing the secondary population (**R2**). This population was now analyzed for APC (GPIX or GPIbα) or FITC (GPIbβ) staining. Two well identifiable populations should be observed in pools where gene-edited cells were incorporated. A part of the population expressed the WT protein, while CRISPR-Cas9 edited cells lost their expression (**Figure 26**).

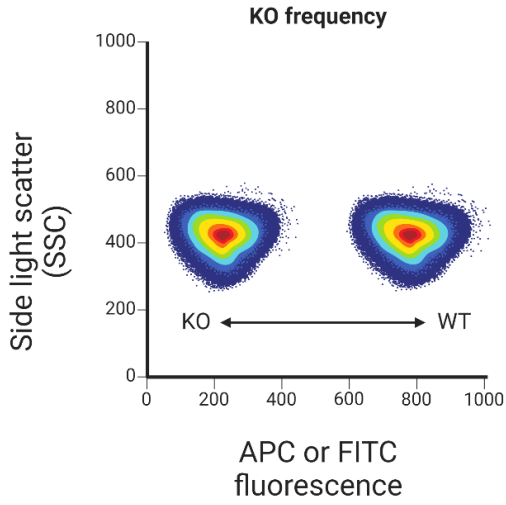

Figure 26. Schematic of flow cytometry dotplot exemplifying a typical screening for KOs.

Image created by Martínez-Navajas, G. -Author.

Then, the most enriched cellular pools were used to establish single cell clones, and, therefore, single-cell KO clonal populations for each subunit (GPIX, GPIbα or GPIbβ) were isolated.

1.2.4.2. PCR-based method to detect *GP5*-KO.

In the case of *GP5* gene, no commercial antibodies were available to detect GPV expression by flow cytometry. So, we decided to detect the KO by conventional PCR.

To facilitate the KO detection, we used two different *sgRNAs*, in order to create a 200 bp microdeletion. Therefore, we designed a primer pair to amplify ~1000 bp of the WT *GP5* genomic region containing the microdeletion. In this way, the observation of two different PCR-amplified bands (1000 bp (WT) and 800 bp (edited)) would indicate the presence of both alleles, (**Figure 27**).

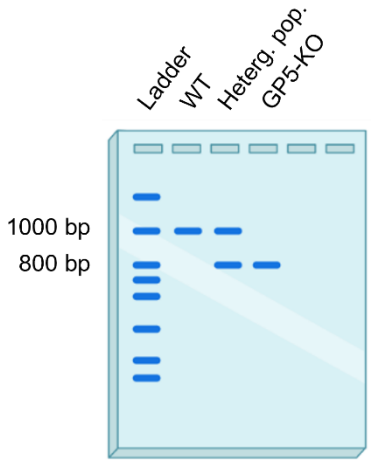

Figure 27. Schematic of the different possibilities when screening for *GP5* KO enriched pools or expanded single cell clones.
Image created by Martínez-Navajas, G. -Author.

To amplify the *GP5 locus* we carried out the following steps:

- ***Genomic DNA extraction.***

High-throughput screening was performed using QuickExtract (Lucigen) to lyse a reduced number of cells in 96-well plates. Half of the 96-well plate was reserved to expand the population, while the other half was resuspended in lysis

buffer, heated to 65ºC for 6 minutes, vortexed, and heated to 98ºC for 2 minutes. When high-quality gDNA was desired, an alternative gDNA isolation kit, NucleoSpin Tissue (Macherey-Nagel), was used following the manufacturer's instructions.

- ***PCR-primer design for GP5.***

To determine the presence of the 200 bp deletion induced by the CRISPR-Cas9 system in the *GP5* gene, it was necessary to design a specific primer pair (short DNA sequences that bind to specific locations on the DNA) for this gene that could amplify a sequence which contains the deleted region, so a differential migration could be observed in a PCR depending on the presence of the genetically edited alleles. Primer 3.0[171] and PrimerBLAST[172] software were used to design the primers, and their sequences are detailed in **Table 12**.

Table 12. Selected primer pairs (5'-3') to amplify GP5 from genomic DNA. It is also indicated PCR product size.

Name	*PCR primers (5'-3')*	*PCR size (bp)*
PCR_gDNA_GP5_FW	*GGATGTGATTTCGGTGGAAC*	*1051 bp*
PCR_gDNA_GP5_RV	*AGCAGAGCCGTTTTCACAAT*	*1051 bp*

- ***PCR reaction of GP5 and visualization on agarose gels***

To amplify the *GP5 locus* we utilized the GoTaq® kit (Promega). The reagents used to perform a single PCR reaction are determined in the **Table 13**.

Table 13. PCR reagents used to set up a single reaction of 25 µL.

Reagent	***Volume (Vf=25 µL)***
5X green GoTaq® flexi buffer (Promega)	5 µL
$MgCl_2$ 25 mM (Promega)	1.5 µL
Primer Mix (Stock 5 µM)	1.3 µL
dNTPs 10 mM (Invitrogen)	0.5 µL
GoTaq® G2 flexi DNA polymerase (Promega)	0.125 µL
ddH_2O	14.575 µL
DNA (20-200 ng µL)	2 µL

To determine the optimal temperature for amplifying the 1000 bp region, we established a gradient ranging from 54.4-60.6ºC to facilitate primer annealing to the template. The optimal PCR amplification was achieved at 54.4ºC. The detailed PCR steps, time, and conditions can be found in **Table 14**.

Next, 5 µL of the PCR product was mixed with 6X loading buffer (NEB) and loaded onto a 1% agarose gel with an appropriate DNA ladder. The mixture was then separated through electrophoresis at 100V for 30 minutes and visualized.

Table 14. Optimized PCR steps to amplify *GP5* gene. Cycles, step length and temperatures are also indicated for each phase.

PCR Conditions [Temperature (ºC) / Time (mm:ss)]				
Denaturalization	**Amplification (38 cycles)**			**Elongation**
	Denaturalization	*Hibridation*	*Elongation*	
95.0ºC/ 05:00 min	95.0ºC/ 00:30 s	54.4ºC/ 00:30 s	72.0ºC/ 01:00 min	72.0ºC/ 10:00 min

1.2.4.3. Limiting dilution technique for the isolation of single cell clones from the pools with the highest knock-out frequency.

We established single cell clones from the most-enriched population for each KO (*GP9*, *GP1BA*, *GP1BB* and *GP5*). To ensure single cell isolation, we restricted the seeding density to 0.5 cells per well in a 96-well plate format, using 100 µL of culture media per well. This corresponded to a working concentration of 5 cells/mL.

To prepare the cells for seeding, we washed, centrifuged, and resuspended each expanded enriched pool in prewarmed culture media. The cell concentration was determined using the trypan blue method. Subsequently, each sample was diluted three times at a 1:10 ratio, resulting in a 1:1000 dilution. The most diluted population was then used to pipette the necessary volume to achieve a working

concentration of 5 cells/mL for single cell cloning, following the formula below:

$$Co\ (\frac{1}{1000}) * Vo = Cf * Vf$$

We determined the required volume of our 1:1000 diluted cell concentration needed to achieve the working concentration of 5 cells/mL for a 96-well plate, which was 10 mL (V_f). An example of this process and the serial dilution protocol is detailed in **Figure 28**, using a starting cell concentration of $1.2x10^5$ cells/mL.

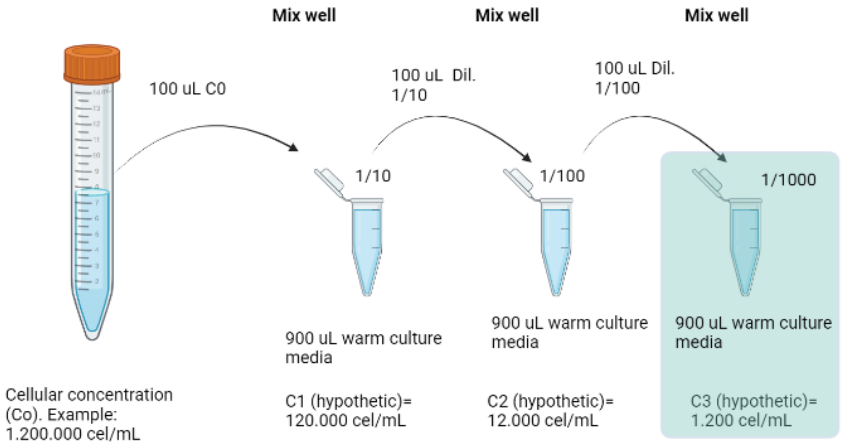

Figure 28. Schematic for the serial dilution protocol to achieve single cell clones.

C_o means initial concentration while diluted concentrations are expressed as C1-C3 (1:10, 1:100 and 1:1000, respectively). Image created by Martínez-Navajas, G. -Author.

Calculated the required volume, it was added to 10 mL of prewarmed media, mixed well and seeded 100 µL/well. Over

the following days, we monitored the plates to identify wells containing a single cell that had successfully grown into a clone. After 12-15 days, we analyzed half of the cells in each well, while the other half was passage into 24-well plates and subsequently into 6-well plates for further expansion.

To confirm that we had successfully generated KO clones for each target gene (*GP9*, *GP1BA*, *GP1BB* and *GP5*), we analyzed them by flow cytometry (*GP9*, *GP1BA* and *GP1BB*) or by PCR (*GP5*) to confirm the phenotype. For *GP9*, *GP1BA* and *GP1BB*, total absence of GPIX, GPIbα or GPIbβ surface expression indicated us the clone isolation, respectively. For *GP5*, PCR amplification of only one 800 bp band indicated us the KO presence.

Then, we characterized these confirmed KO amplifying their respective gene *locus* by PCR and sequencing them to detect CRISPR-Cas9 induced mutations.

1.2.5. PCR amplification and Sanger sequencing.

To analyze the CRISPR-Cas9 induced mutations generated in *GP9*, *GP1BA*, *GP1BB* and *GP5* for our megakaryoblastic cell lines, we had to amplify these genes and compare with their WT sequence.

1.2.5.1. PCR amplification of *GP5*.

In the case of *GP5* gene, we used the previously designed primer pair and optimized PCR conditions to amplify

both WT and *GP5*-KO alleles. gDNA was isolated from WT and *GP5*-KO selected clones and PCR was performed.

1.2.5.2 PCR amplification of BSS driver genes: *GP1BA*, *GP1BB* and *GP9*.

On the other hand, we needed to design primer pairs and optimize PCR conditions for BSS driver genes. We followed the same procedure as we did previously for the design of *GP5* primers and optimization of PCR conditions. The following sections will provide more details on this process.

- ***PCR-primer pairs design for GP1BA, GP1BB and GP9.***

To determine the genotype of mutations generated on the GPIb-V-IX receptor, clones of *GP1BA*, *GP1BB*, and *GP9* were sequenced. we sequenced clones of *GP1BA*, *GP1BB*, and *GP9*. Specifically, we sequenced the genomic region where Cas9 induced a DSB. To accomplish this, we designed a set of gene-specific primers for each target gene, which encompassed the region containing the sgRNA sequences. The design of primer pairs was facilitated using Primers 3.0 and the NCBI primer design tool The primer sequences are detailed in **Table 15. Selected primer pairs (5'-3') to amplify *GP1BA*, *GP1BB* and *GP9* from genomic DNA.**

Table 15. Selected primer pairs (5'-3') to amplify *GP1BA*, *GP1BB* and *GP9* from genomic DNA.

PCR product size it is also indicated.

Name	*PCR primers (5'-3')*	*PCR size (bp)*
PCR_gDNA_GP1BA_FW	*GCCTTACACTCGCCTCACTC*	*703*
PCR_gDNA_GP1BA_RV	*GCCCTCAGTGTCCTCTTCTG*	*703*
PCR_gDNA_GP1BB_FW	*CTCCGGCGATAGTGTGCTA*	*966*
PCR_gDNA_GP1BB_RV	*AGCAGCACCAGCAGCAAC*	*966*
PCR_gDNA_GP9_FW	*GATGGGGTCTCTGCTAAGGG*	*1078*
PCR_gDNA_GP9_RV	*AGCCCCAACTGATGTCTGGT*	*1078*

- ***PCR optimization for GP1BA, GP1BB and GP9.***

As previously detailed in *GP5* case, to optimize the PCR for these primer pairs, firstly, we established a temperature gradient ranging from 54.4 to 60.8ºC. The PCR reactive were the same as used for *GP5*, detailed in the **Table 13**.

GP1BA and *GP1BB* required an additional optimization step, due to the apparition of unspecific PCR products for both reactions. In the literature is described that the addition of Dimethyl Sulfoxide (DMSO) at low concentrations can enhance the specificity of PCR by reducing secondary structures that can form within DNA templates or primers, particularly at higher annealing temperatures. It can also help to denature DNA by breaking the hydrogen bonds that hold the double helix together, making the DNA more accessible to the PCR reaction components[173].

In this case, required reagents to develop the PCR were slightly modified as follows **Table 16**:

Table 16. PCR reagents used to set up a single reaction of 25 µL, including the addition of 10% DMSO to favors specific annealing.

Reagent	***Volume (Vf=25 µL)***
5X green GoTaq® flexi buffer (Promega)	5 µL
DMSO 10% (Fisher Scientific)	2.5 µL
$MgCl_2$ 25 mM (Promega)	1.5 µL
Primer Mix (Stock 5 µM)	1.3 µL
dNTPs 10 mM (Invitrogen)	0.5 µL
GoTaq® G2 flexi DNA polymerase (Promega)	0.125 µL
ddH_2O	12.075 µL
DNA (20-200 ng µL)	2 µL

Optimized PCR conditions to obtain single and specific PCR bands can be found in the following **Table 17**:

Table 17. Optimized PCR steps to amplify *GP1BA*, *GP1BB* and *GP9* genes.

Furthermore, DMSO addition is indicated when required to obtain unique specific bands. Cycles, step length and temperatures are also indicated for each phase.

	PCR Conditions [Temperature (ºC) / Time (mm:ss)]				
Target	**Denaturalization**	**Amplification (38 cycles)**			**Elongation**
		Denaturalization	*Hibridation*	*Elongation*	
GP1BA (10% DMSO)	95.0ºC/ 05:00 min	95.0ºC/ 00:30 s	54.4ºC/ 00:30 s	72.0ºC/ 01:00 min	72.0ºC/ 10:00 min
GP1BB (10% DMSO)	95.0ºC/ 05:00 min	95.0ºC/ 00:30 s	54.4ºC/ 00:30 s	72.0ºC/ 01:00 min	72.0ºC/ 10:00 min
GP9	95.0ºC/ 05:00 min	95.0ºC/ 00:30 s	60.0ºC/ 00:30 s	72.0ºC/ 01:00 min	72.0ºC/ 10:00 min

- ***Sanger sequencing of purified PCR products.***

The PCR products for *GP1BA*, *GP1BB*, *GP9* and *GP5* WT and CRISPR-Cas9 edited genes were separated on 1% agarose gels, producing single bands. PCR reactions were purified using the NucleoSpin® Gel and PCR Clean-up kit, following the manufacturer's instructions. The purified DNA was eluted in a final volume of 15 µL to concentrate the amplicons and remove any non-desired reagents from the PCR.

10 µL of purified PCR product were mixed with 3 µL of 10 µM sequencing primer, in our case, we used the forward primer of each primer pair employed to develop the PCR. This mixture was then sequenced in Stab Vida laboratories.

Then, ".ab1" files from Sanger sequencing were visualized using SnapGene Viewer software. The electropherograms were analyzed to identify unique and well-defined sequences, which indicated the reading of only one homozygous allele, as shown in **Figure 29**, **panel A**. Then, we extracted the sequence and compared with their WT counterparts, using the ClustalW multiple alignment software to favor the identification of the induced mutation.

However, when the electropherograms did not show unique sequences, it was a sign of the existence of a compound heterozygous mutation induced by CRISPR-Cas9 (**Figure 29**, **B**). Consequently, individual allelic sequences

could not be determined by conventional methods, and PCR product cloning in pGEM®-T was required to isolate and sequence single alleles.

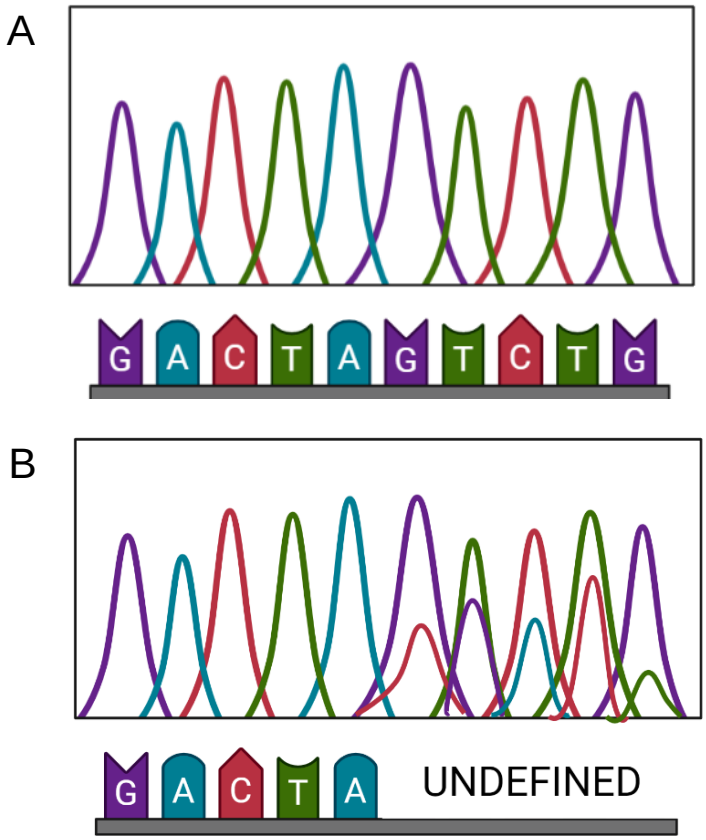

Figure 29. Schematic of electropherograms obtained from sequencing files.
A. Unique and well-defined sequence from homozygous alleles B. Overlapped and not-well defined sequence from heterozygous alleles. Image created by Martínez-Navajas, G. -Author.

- ***pGEM®-T technique to determine allelic sequences for compound heterozygous mutations.***

To discriminate and isolate single alleles from a heterozygous gene, we have used the pGEM®-T (Promega)

cloning vector (**Figure 30**). This vector is commercialized in linearized conformation with a single 3´-terminal thymidine (T) at both ends, interrupting the LacZ gene. It also harbors all the required sequences to facilitate its replication in bacteria and an ampicillin resistance gene, together with a multicloning site (MCS). To sequence this plasmid, it is typically used the SP6 and T7 primers, which flanks the MCS (**Table 18**).

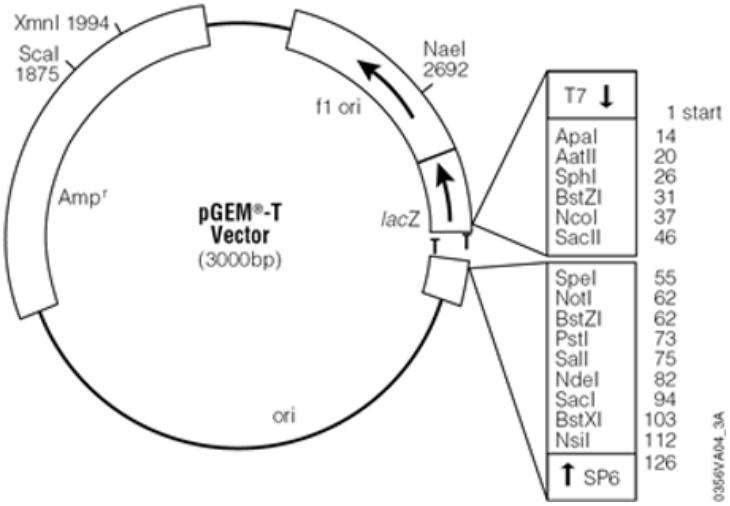

Figure 30. Schematic of the pGEM®-T plasmid indicating all the regions of interest.

Ampicillin resistance gene, *LacZ* gene, multicloning site flanking the protruding thymidine. Obtained from Promega Corporation.

IPTG (β-D-1-thiogalactopyranoside) is a chemical inducer used to mimic lactose and promote the expression of genes downstream of the *lac* operon in *E. coli*. X-gal (5-bromo-4-chloro-3-indolyl-β-D-galactopyranoside) is a substrate that is cleaved by β-galactosidase encoded by the *lacZ* gene, so when added to a bacterial culture, it produces a blue compound that can be visualized.

Table 18. Sequencing primers for pGEM®-T plasmid.

Name	Sanger Sequencing primers (5'-3')
T7	TAATACGACTCACTATAGGG
SP6	ATTTAGGTGACACTATAG

PCR amplicons typically have protruding adenines that are compatible with the protruding thymidine of the plasmid. Therefore, we cloned our heterozygous gene of interest into this plasmid and transformed it into *E. coli*. In this way, transformed bacteria incorporated only one plasmid harboring just one allele. Then, we cultured the bacteria on LB agar plates supplemented with ampicillin (100 µg/mL), IPTG (0.5mM), and X-Gal (80 µg/mL). This allows us to visually detect bacteria that have incorporated our cloned alleles, as white colonies that interrupt the *LacZ* gene. Conversely, blue colonies indicated the presence of recircularized plasmids. Therefore, white colonies should have incorporated each allele.

We picked at least 10 different white bacterial colonies for each heterozygous gene and cultured them in 5 mL of media for 16 hours at 37ºC and 220 RPM in a shaker incubator. The following morning, we isolated the pGEM-T plasmids as previously described. The plasmids were sequenced using SP6 and T7 primers (as listed in **Table 18**), identifying single alleles for each heterozygous gene in proportions close to 1:1 of sequenced alleles. Then, single allele sequences were

aligned with WT sequences to identify CRISPR-Cas9 induced mutations.

1.3. Contribution of each subunit to the assembly of GPIb-V-IX receptor.

To determine the role that each subunit play in the transport to the outer membrane of the remaining GPIb-V-IX complex subunits, we analyzed GPIbα, GPIbβ and GPIX expression by flow cytometry in each KO (*GP1BA*, *GP1BB*, *GP9* and *GP5*). Then, we focused our attention into GPIX subunit, and analyzed GPIX expression and distribution over the cell surface by ImageStream for all our knockouts.

1.3.1. Determination of GPIbα, GPIbβ and GPIX expression levels on the cell surface by flow cytometry in all our WT and knockout cell lines.

The *GP1BA*-KO, *GP1BB*-KO, *GP9*-KO, *GP5*-KO and WT megakaryoblastic cell lines were cultured, and single aliquots were taken from each cell line to be stained with antibodies against GPIbα, GPIbβ, and GPIX. Flow cytometry staining was performed in triplicate for each cell line, following the same instructions described in the section *"**1.2.4.1***".

In this case, flow cytometry data were interpreted and translated into a graph, taking into consideration the mean fluorescence intensities (MFI) and percentage of positive cells for each antibody.

- ***Statistical analysis***

Statistical analyses were performed using GraphPad Prism v9.4. MFI values and percentage of positive cells were

represented as mean values ± Standard Deviation (SD) for 3 independent experiments. Statistical significance was assessed with ANOVA two-way plus Tukey Multiple Comparison test comparing individual mean values among the samples for the same antibody (ns = non-significant, * $p < 0.05$; ** $p < 0.01$; *** $p<0.001$ and **** $p < 0.0001$).

1.3.2. GPIX-imaged expression analysis: ImageStream for WT and knockout cell lines.

The ImageStream platform, combines the features of flow cytometry and microscopy to generate high-resolution images of individual cells and analyze multiple parameters quantitatively.

Cells were collected and stained with GPIX (-APC) and CD41 (-PE) antibodies (BD Biosciences) for 20 minutes at room temperature. Stained cells were washed, centrifuged and fixed with 4% paraformaldehyde (PFA) (Merck Life Sciences) in PBS for 12 minutes, washed and permeabilized with 0,1%Triton X-100 detergent (Thermo Scientific) in PBS for 20 minutes. Then, cells were washed again and incubated with 1 µM Hoechst (Merck Life Sciences) for 3 minutes, washed and resuspended in FACS buffer. Lastly, data were acquired in an ImageStream® Mark II imaging Flow Cytometer (Amnis) and analyzed with IDEAS software (Amnis).

1.3.3. Functional validation of GPIb-V-IX receptor in absence of GPV subunit.

Our objective was to evaluate the functionality of the GPIb-V-IX receptor in the absence of the GPV subunit. The GPIb-V-IX complex is the primary receptor for VWF, with the GPIbα subunit containing the binding domain. Flow cytometry analysis of GPIbα expression was performed for each KO, leading us to consider this analysis for the *GP5* subunit, the only one that maintained consistent GPIbα expression. Firstly, we evaluated GPIbα binding capability to soluble VWF and compared to WT in presence of ristocetin. Secondly, we evaluated GPIbα adhesion capability to coated VWF in presence of botrocetin.

1.3.3.1. Analysis of the interaction between GPIb-V-IX receptor and soluble von Willebrand factor by flow cytometry.

To evaluate the GPIbα binding capability to soluble VWF, cells were collected and washed. Then, cells were incubated under 4 different conditions at 37ºC for 30 minutes: Ristocetin (1 mg/mL, ABP) plus VWF (Haematologic Technologies) (10 µg/mL); only VWF, only ristocetin and nothing. Following incubation, cells were washed and stained with anti-human VWF (Dako, 1:500) in a primary incubation (20 minutes), washed and then with the secondary antibody anti-rabbit-AlexaFluor 647 (Biolegend). Then, cells were incubated for 30 minutes at room temperature, washed with PBS, centrifuged, resuspended in FACS Buffer (PBS supplemented

with 5% FBS and EDTA 2 mM) and stained with 7AAD cell viability solution (BD Biosciences).

Finally, data was acquired using FACS Verse flow cytometry and interpreted.

- ***Gating strategy.***

To gate VWF^+ cells, firstly we established the negative population using the cells incubated with ristocetin. Then, we analyzed the cells incubated with VWF and with the mixture of VWF+ristocetin. *GP5*-KO percentage of VWF positive cells was relativized to WT.

- ***Statistical analysis***

Statistical significance was assessed with a two-tailed unpaired T-test comparing individual mean values (ns = non-significant, * $p < 0.05$; ** $p < 0.01$; *** $p<0.001$ and **** $p < 0.0001$).

1.3.3.2. Determination of GPIb-V-IX receptor binding capability to coated von Willebrand factor.

We assessed the quantity of cells that adhered to VWF-coated surfaces in this study. We adjusted the cell concentration to $3.5X10^5$ cells/mL and added 100 µL to 96-well plates coated with VWF (10 µg/mL) in PBS overnight at 4ºC. For each cell line, we established three conditions: Botrocetin (0.1 µg/mL), PBS-EDTA (10 mM), and Botrocetin + PBS-EDTA. Additionally, for the Botrocetin + PBS-EDTA condition,

we preincubated cells with 6B4[174] antibody (10 µg/mL) for 30 minutes before the 90-minute incubation at 37ºC. We then washed the cells three times with PBS, fixed, permeabilized, and stained them with DAPI (4′,6-diamidino-2-phenylindole, ThermoFisher Scientific) at a concentration of 1 µg/mL and Phalloidin-tetramethylrhodamine B isothiocyanate (TRITC, Santa Cruz Animal Health) at a concentration of 2 µg/mL for 30 minutes at room temperature. Finally, we used an Axio Observer Z1 inverted fluorescence microscope (Zeiss) to capture immunofluorescence images, and we determined cell number using Fiji free software [175].

- ***Statistical analysis***

Statistical significance was assessed with an ordinary one-way ANOVA plus Tukey's multiple comparison test for comparing individual adhered cell number mean values (ns = non-significant; * $p < 0.05$; ** $p < 0.01$; *** $p<0.001$ and **** $p < 0.0001$).

1.4. Creation and validation of Bernard-Soulier Syndrome Type C model in induced pluripotent stem cells.

iPSCs are an ideal model to study BSS because their capacity to differentiate into mature MKs and platelets. We utilized an iPSC line derived from adult dermal fibroblasts using integrative murine retroviral vectors, which has been previously reported by Moreau *et al*., which efficiently produce MKs and platelets *in vitro* [164].

1.4.1. Development of *GP9*-knockout in induced pluripotent stem cells.

To create the *GP9*-KO model from iPSCs, we utilized a similar methodology as we did for generating KOs in megakaryoblastic cells. However, due to the difficulty in incorporating exogenous DNA into iPSCs, we employed an alternative transformation technique called nucleofection. The KO enrichment strategy was similar, but we estimated the frequency of successful KO using *in silico* method based on sanger sequencing of PCR amplified gene-edited locus *GP9*. Finally, we confirmed the BSS Type C typical phenotype by differentiating the iPSCs after isolating the KO.

1.4.1.1. Nucleofection.

We used nucleofection to introduce our PX-458-*GP9*-sgRNAs construct into iPSCs, which are primary cells considered as difficult to transfect using traditional methods.

Nucleofection involves the use of voltage and specific reagents to introduce exogenous DNA into the cell. We used the Human Stem Cell Nucleofector® Kit 1 (Lonza) to perform the nucleofection. The protocol included the following steps:

Day 0: iPSCs were nucleofected when they reached 80-90% confluency in a T25 flask. One hour before starting the protocol, the culture medium was replaced with E8 supplemented with 10 µM Y27632. The cells were dissociated using TrypLE, neutralized, and centrifuged before adding 2 µg of the construct to the cell pellet. The pellet was resuspended with the nucleofection solution, collected, and introduced into the nucleofection cuvette. The cuvette was placed in the nucleofector and the pre-established program A-023 was applied. After the process was completed, the cells were collected with fresh culture medium, deposited in an Eppendorf tube, and incubated inside the incubator for 15 minutes at 37°C. After the incubation period, the cells were collected and transferred to a new T25 flask coated with Matrigel and supplemented with E8 medium with 10 µM Y27632. After 8 hours, the culture medium was replaced.

Day 1: The culture medium was replaced, and the efficiency of the process was observed using an EVOS fluorescence microscope.

Day 2: The cells were dissociated with TrypLE, filtered and sorted, selecting only $eGFP^+$ cells. Several pools of 500 cells/well were seeded in a 96-well plate that had previously

been coated with Matrigel to enrich the KO frequency. When the cells reached 80-90% confluency, they were passaged to 24-well plates and then to 6-well plates.

1.4.1.2. Synthego bioinformatic tool to detect the knock-out enrichment of cellular pools and single cell clones.

Due to the pluripotent epigenetic background, GPIX expression could not be detected by flow cytometry at this stage, which necessitated cell differentiation. To detect the KO frequency and overcome this limitation, we used the ICE CRISPR analysis tool from Synthego (Synthego Performance Analysis, ICE Analysis. 2019. v3.0). This bioinformatic software is optimized to detect the frequency of different reads in a Sanger sequencing file by comparing it with the reads of a WT sequence, offering NGS-quality results. The software estimates the KO frequency based on the type of mutation generated and the number of reads in comparison to the WT allelic sequence.

To analyze the KO enrichment, we extracted gDNA from expanded pools of WT and CRISPR-Cas9 edited cells, amplified their *GP9* locus by PCR, and sequenced the resulting products. The sequencing files were then compared using ICE analysis, and the data were plotted on graphs. We identified the most enriched pool for *GP9*-KO alleles based on the analysis and established several clones using the limiting dilution procedure. Single cell clones were seeded over Matrigel coated plates in E8-Y27632 culture medium. After 12-

15 days, 96 well plates were screened for individual colonies growing in adherence. Then, colonies were detached using PBS-EDTA 0.5 mM, half of the cells were used for analysis and the other half for expanding the clone.

To analyze single cell clones, we also used Synthego to compare the *GP9*-KO sequences with the WT sequence and detect full KOs for *GP9* by following the same procedure.

1.4.1.3. Characterization of the Bernard-Soulier Syndrome Type C disease model by Sanger sequencing and aminoacidic predictions.

To distinguish the different mutations affecting individual alleles (compound heterozygous), we expanded the predicted KOs and sequenced individual alleles using the pGEM®-T methodology. We compared these sequences with the WT using ClustalW to determine the CRISPR-Cas9-induced mutations. We then translated the mutated sequences into amino acid sequences to observe whether these mutations were producing truncated or aberrant proteins and to determine which GPIX functional domains were being affected. We used UniProt to identify these functional domains.

1.4.2. Differentiation of induced pluripotent stem cells WT and *GP9*-KO to megakaryocytes and platelets and functional validation.

We utilized a serum-free and animal component-free protocol that is more current and efficient than the previous

methods. This protocol, recently described by Moreau *et al,.*[164] involves the differentiation of hiPSCs to MKs through ectopic expression of GATA1, FLI1, and TAL1, which are essential transcription factors in the process of megakaryopoiesis, regulating both the formation and maturation of MKs.

1.4.2.1. Megakaryocytic differentiation.

The iPSC WT and *GP9*-KO lines were cultured in E8 medium, and when they reached 80% confluency, they were dissociated using TrypLE and collected by centrifugation at 150xG for 5 minutes. The general protocol can be followed through the **Figure 31**.

- ***Differentiation Phase 0: Seeding of pluripotent stem cells.***

On Day -1, we determined the number of cells using a Neubauer chamber and seeded 45,000 cells/well in 12-well cell culture plates (Corning) that were coated with Matrigel. The cells were then cultured in E8 medium at 37°C with 10µM Y27632.

- ***Differentiation Phase I: Pluripotent-to-mesoderm differentiation.***

From Day 0 to Day 2, we transduced the cells with a LV (Flash Therapeutics) that expresses GATA1, FLI1, and TAL1 together at MOI 80 for viral transduction. The cells were cultured in E6 medium, which is E4 supplemented with Holo-transferrin (10.6 mg/L) (Sigma-Aldrich) and Insulin (20 mg/L)

(Sigma-Aldrich) and supplemented with 20 ng/mL FGF2 (Peprotech), 10 ng/mL BMP4 (Peprotech), and 10 ng/mL protamine sulfate (Sigma Aldrich) to increase lentiviral transduction efficiency.

On **D1**, the LVs were washed away, and the cells were cultured in E6 medium supplemented with 20 ng/mL FGF2 and 10 ng/mL BMP4 to induce mesoderm differentiation.

- ***Differentiation Phase II: Megakaryocytic Maturation and Differentiation:***

From **Day 2 to Day 9**, megakaryocytic lineage differentiation was induced by changing the medium to CellGRO SCGM supplemented with 20 ng/mL TPO and 25 ng/mL SCF. The cell culture medium was supplemented with 40 ng/mL TPO and 50 ng/mL SCF on day 5, and on day 8, half of the medium was changed with CellGRO medium supplemented with 40 ng/mL TPO and 50 ng/mL SCF. On day 9, part of the cell culture was dissociated with TrypLE to analyze specific hematopoietic and MK lineage surface markers by staining with anti-CD34 (PECy7, BD Bioscience), anti-CD41 (PE), and anti-CD42a (APC) antibodies. The resulting cell populations were washed, stained for viability solution (*7AAD*) and analyzed with a BD FACS Canto II or Verse flow cytometer and Community Cytobank software. The remaining cell culture was transferred to 6-well cell culture plates without matrigel coating, in CellGRO medium supplemented with 20 ng/mL TPO and 25 ng/mL SCF.

- ***Differentiation Phase III: Megakaryocytic Maintenance:***

From **Day 9** onwards, every two days, half of the medium was changed with fresh CellGRO medium supplemented with 40 ng/mL TPO and 50 ng/mL SCF. The cell culture was maintained at a concentration of 0.5-2x10^6 cells/mL. On day 16 and 21, the cells were collected by centrifugation and stained again with the cellular markers CD34, CD41, GPIX and the viability solution of *7AAD* for flow cytometry analysis. The remaining cell culture was refreshed

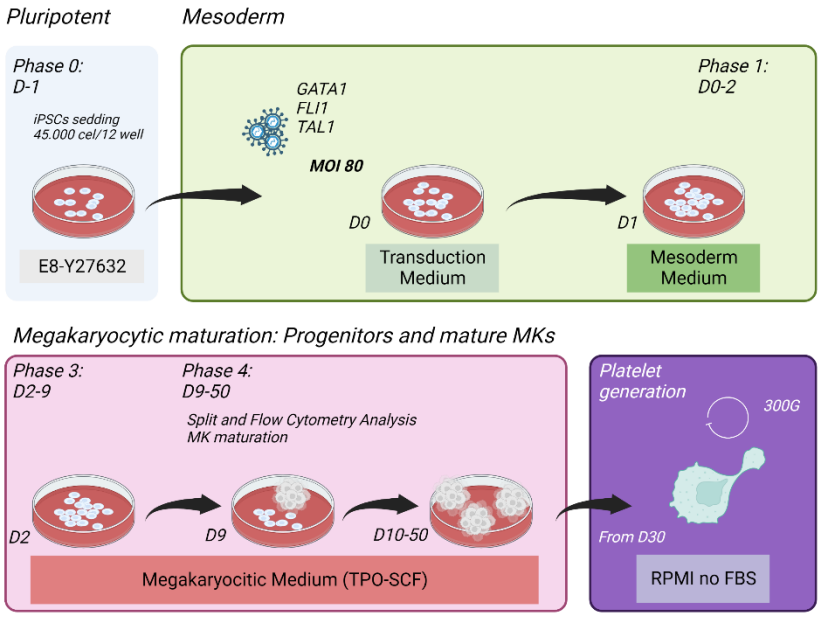

Figure 31. Schematic of megakaryocytic production protocol from induced pluripotent stem cells.

It is indicated the different phases that cells undergo throughout the differentiation, culture medium, involved cytokines and analysis days. Image created by Martínez-Navajas, G. -Author.

with complete medium and maintained until day 50 with half-medium changes every 2 days.

- ***Platelet generation from iPSCs-derived megakaryocytes and staining.***

From **Day 30** onwards, the cells were centrifuged at 300xG for 5 minutes and resuspended in RPMI 1640 without FBS. Next day, the entire supernatant was collected and centrifuged twice to isolate the platelets (first 150xG, 5 minutes, to separate cells, and secondly 350xG, 10 minutes, to isolate platelets Accel,5, Brake, 3). These were stained for flow cytometry analysis, as previously described.

- ***Platelet gating strategy in flow cytometry***

In this case, platelet population was identified by gating small particles of SSC. *vs.* CD41 expressing events. $CD41^+$ events were then gated and analyzed for GPIX expression in both populations.

- ***Cryopreservation***

Alternatively, from day 9 onwards, cells could be cryopreserved by pelleting them and resuspending in FBS supplemented with 10% DMSO.

- ***Statistical Analysis***

Statistical significance was assessed with a two-tailed unpaired T-test comparing individual mean values (ns = non-

significant, * $p < 0.05$; ** $p < 0.01$; *** $p<0.001$ and **** $p < 0.0001$).

1.4.2.2. ImageStream observation of platelet produced from induced pluripotent stem cells.

Platelet population was separated as described previously by sequential centrifugation. Then, was stained for CD41 and GPIX, fixed, acquired in ImageStream and analyzed with IDEAS software.

In this case, due to the differences between ImageStream and conventional cytometers, the gating strategy was slightly different, being unable to use SSC parameter. However, we used the most similar parameter available in this platform, “Area”. Then, we faced Area. *vs.* CD41 intensity fluorescence, establishing the first population (R1). Then, this population was assessed for GPIX expression, establishing the R2 population. From this population, an additional parameter to select those images that were in focus was applied (RMS gradient >**0.6).**

2. *Objective 2: Design and development of reporter and therapeutic GPIX-lentiviral vectors able to rescue GPIX expression and complex functionality in megakaryoblastic Knock-out models.*

2.1. Cell Cultures.

In addition to the culture of megakaryoblastic cell lines, in this objective we have also employed cell lines from different origins that would be utilized with different purposes in the following sections:

2.1.1. HEK 293T (ATCC).

The 293T cell line, which was formerly known as 293tsA1609neo, is a variant of human embryonic kidney 293 cells that has a high ability to be transfected and harbors the SV40 T-antigen. Typically, it is used to produce LV particles.

- ***Maintenance*:** This cell line grew in adherence and was cultured in DMEM-High Glucose (Biowest) supplemented with 10% Fetal Bovine Serum (FBS) (Biowest) and 1X Penicillin/Streptomycin (Sigma-Aldrich). Respect the culture conditions, cells were grown at 37ºC and 5% CO_2 in a humid incubator.
- ***Passages:*** The cells were regularly maintained by passaging them twice a week in a T25 flask with 6 mL of supplemented media and seeding $1x10^5$ cells/mL. To passage, the adherent layer of cells was washed with PBS and then treated with a 0.75X diluted TrypLE

solution in PBS for 5 minutes at 37ºC to dissociate them. The cells were then washed, counted and split as needed. The cells were cultured at 37ºC and 5% CO_2 in a humidified incubator to provide optimal growth conditions.

- ***Cryopreservation:*** The cells were collected when they reached a confluence of 90%, dissociated with TrypLE and centrifuged at 300xG for 5 minutes. After the aspiration of the supernatant, cells were resuspended in 1 mL FBS supplemented with 10% of dimethyl sulfoxide (DMSO) and transferred into a cryotube and stored as mentioned in the first objective.

2.1.2. Jurkat and THP-1 cell lines (ATCC)

Jurkat and THP-1 cell lines have a lymphocytic and monocyte origin, respectively. These lines were cultured, passaged and cryopreserved in the same conditions as the megakaryoblastic cell lines, described in the section 1.1.

2.2. Design and development of GPIX lentiviral vectors.

In order to develop functional LVs able to restore GPIX expression in BSS Type C disease models, we carried out the following steps:

2.2.1. Selection of a tissue-specific promoter for megakaryocytic gene expression.

In collaboration with Dr. Ute Moldich (Paul-Ehrlich Institut, Langen, Germany) we analyzed the behavior of various LVs that were expressing eGFP under different megakaryocytic specific promoters (**Figure 32**). As control, we used an empty vector pRRL-Neo. To analyze the specificity and functionality of these promoters regulating eGFP expression we transduced DAMI cells, due to its megakaryoblastic background.

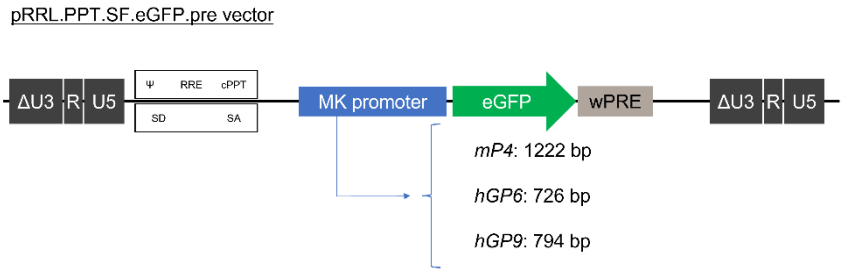

Figure 32. Schematic of pRRL vectors used to assess the specificity and functionality of the megakaryocytic promoters regulating the expression of eGFP.

Image created by Martínez-Navajas, G. -Author.

- ***Cell transduction of pRRL vectors.***

For cell transduction we applied the term MOI that refers to Multiplicity of Infection. MOI is a measure of the number of viral particles (or virions) used to infect a given number of cells in a culture. In virology, MOI is used to describe the ratio of the number of infectious viral particles to the number of target cells in a culture. For these experiments, $5x10^5$ DAMI cells were transduced with MOI 5. To assess the volume of ultracentrifuged LVs required, for this experiment and for all experiments in general, we followed the next formula:

$$Volume\ lentiviral\ vector\ (\mu L) = \frac{cell\ number\ x\ MOI}{vector\ titer\ (\frac{TU}{mL})}\ x\ 1000$$

2.2.2. Generation of the therapeutic cassette h*GP6*(p)-*GP9*.

2.2.2.1. Primer design and PCR reaction.

The reference sequences for both the h*GP6* promoter (h*GP6*(p)) and the CDS of the *GP9* gene were obtained from the NCBI and verified using *Ensembl*. From this information, we designed primers for the amplification of these regions through bioinformatics programs. The selected primer pairs were modified to incorporate a *PvuI* restriction site (**Table 19**) in the Reverse primer of the h*GP6* promoter and in the forward primer of the h*GP9* CDS. Therefore, after amplifying these regions, it would be possible to digest, ligate and reamplify the transgene. In the **Table 20** are detailed the PCR condition required to amplify both sequences.

Table 19. Selected primer pairs to amplify both h*GP6* promoter and hGP9 coding sequence.
Highlighted in red are the *PvuI* restriction sites introduced to favor the posterior ligation step.

Name	***PCR primers (5'-3')***	***PCR size (bp)***
PCR_promoter_GP6_FW	TTGAATTAGCAATGCACGCGCAGT	726
PCR_promoter_GP6_RV	TTCGATCGTGGTTCCTCAGCCCTGTC	*726*
PCR_CDS_GP9_FW	AACGATCGATGCCTGCCTGGGGAG	534
PCR_CDS_GP9_RV	AAGCATCTCAATCCAGGGCCTCTGT	*534*

Table 20. Optimized PCR conditions to amplify both promoter and CDS sequences.

	PCR Conditions [Temperature (ºC) / Time (mm:ss)]				
Target	**Denaturalization**	**Amplification (38 cycles)**			**Elongation**
		Denaturalization	*Hibridation*	*Elongation*	
PCR_promoter_GP6	95.0ºC/ 05:00 min	95.0ºC/ 00:30 s	60.0ºC/ 00:30 s	72.0ºC/ 01:00 min	72.0ºC/ 10:00 min
PCR_CDS_GP9	95.0ºC/ 05:00 min	95.0ºC/ 00:30 s	60.0ºC/ 00:30 s	72.0ºC/ 00:30 s	72.0ºC/ 10:00 min

2.2.2.2. PCR product digestion with *PvuI*.

After the amplification of both DNA sequences, we performed a digestion reaction with *PvuI* (NEB) at 37ºC for 1 hour in a heating block. Then, the digestion reaction was heat-inactivated at 65ºC for 20 minutes and used to perform the ligation between the protuberant and cohesive ends of the promoter and CDS. Ligation reaction was performed as indicated in the **Table 21**.

Table 21. Required reactive to set up the ligation reaction.

Reagent	***Volume (Vf= 10 µL)***
Digested hGP6 DNA (10 ng/ µL)	1 µL
Digested hGP9 DNA(10 ng/ µL)	1 µL
T4 Ligase buffer 10X (NEB)	1 µL
T4 Ligase (NEB)	1 µL
ddH_2O	6 µL

After the ligation of the promoter and CDS, a PCR amplification of the constructs was performed using the FW primer of the promoter and the RV primer of the CDS. The Phusion High-Fidelity DNA Polymerase (Thermo Scientific) was used for this purpose, which has a lower error rate. The protocol followed was the same as for conventional PCR. Single bands were detected in an agarose gel (1%) and purified.

2.2.2.3. Clonation of h*GP6*-h*GP9* into the intermediate cloning vector pCR®2.1

The cloning of constructions obtained by joining both promoter and CDS sequences was carried out using the TA Cloning® Kit (Invitrogen™, Life Technologies) which is constituted by the pCR®2.1 vector and the ExpressLink™ T4 DNA Ligase. The reaction was carried out overnight in a final volume of 10 µL, with 1 µL of Ligase and 1 µL of 10x Ligase Buffer, and the rest of the volume was filled with the pCR™2.1 vector, amplicon, and water if necessary.

The amplicon: pCR™2.1 vector ratios ranged from 7:1 to 3:1 depending on the concentration of the obtained amplicon. Once cloned, these plasmids were transformed into *E. coli DH5α* bacteria and seeded over LB agar plates supplemented with ampicillin, X-Gal and IPTG. After the incubation, the presence of white colonies indicated us that our transgene was successfully cloned into the intermediate vector (similar methodology as pGEM-T). Colonies were then processed, and the plasmid was purified and isolated.

Objective 2: Design and development of reporter and therapeutic GPIX-lentiviral vectors able to rescue GPIX expression and complex functionality in megakaryoblastic Knock-out models.

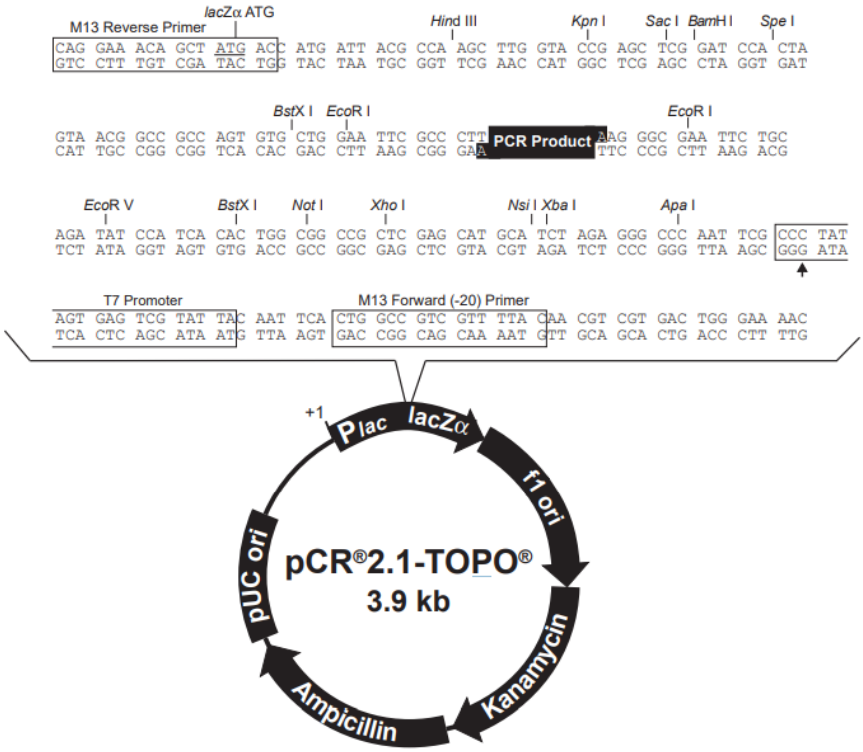

Figure 33. Schematic of pCR®2.1 plasmid.

Ampicillin and kanamycin resistance genes and all those sequences required to amplify plasmid DNA into bacteria are also highlighted. Image obtained from Invitrogen, Life Technologies.

As shown in the **Figure 33**, the transgene would be introduced in the middle of the MCS, flanked by *EcoRI* among others restriction sites. Confirmation digestion using *EcoRI* was performed to further validate the cloning of the transgene into the vector, using the reactive detailed in the **Table 22**. This would result in the release of a DNA fragment with the same size as the transgenic PCR product (promoter + CDS). In addition, we sequenced the plasmid to confirm the absence of mutations (T7 primer) in the transgene.

Table 22. Required reactive to digest pCR2.1-*GP6*(p)-GP9 plasmids.

Reagent	*Volume (Vf= 10 µL)*
Plasmid DNA	300 ng
NEBuffer™ EcoRI/SspI	1 µL
EcoRI	1 µL
ddH_2O	To 10 µL

2.2.3. Development and construction of diverse designs for therapeutic and reporter vectors.

2.2.3.1. Lentiviral vector backbones.

We used SE-IS2 LV as backbone to produce our constructs (**Figure 34**-A). This is a self-inactivated LV that expresses the eGFP under the control of the spleen focus-forming virus (SFFV) promoter and includes an insulator formed by a chimeric sequence composed by SAR2 and HS4-650 elements (IS2 insulator)[176]. We utilized this vector as a Reporter Empty Vector (R-EV) and as the backbone for constructing our Reporter Vector-GPIX (R-GPIX). To optimize the expression of the therapeutic gene, we tested several configurations by altering the position and orientation of the therapeutic cassette relative to the reporter cassette (SFFV-eGFP) (**Figure 34**-A).

Moreover, we modified the R-EV backbone by removing the SFFV-eGFP cassette, creating the Therapeutic Empty

Objective 2: Design and development of reporter and therapeutic GPIX-lentiviral vectors able to rescue GPIX expression and complex functionality in megakaryoblastic Knock-out models.

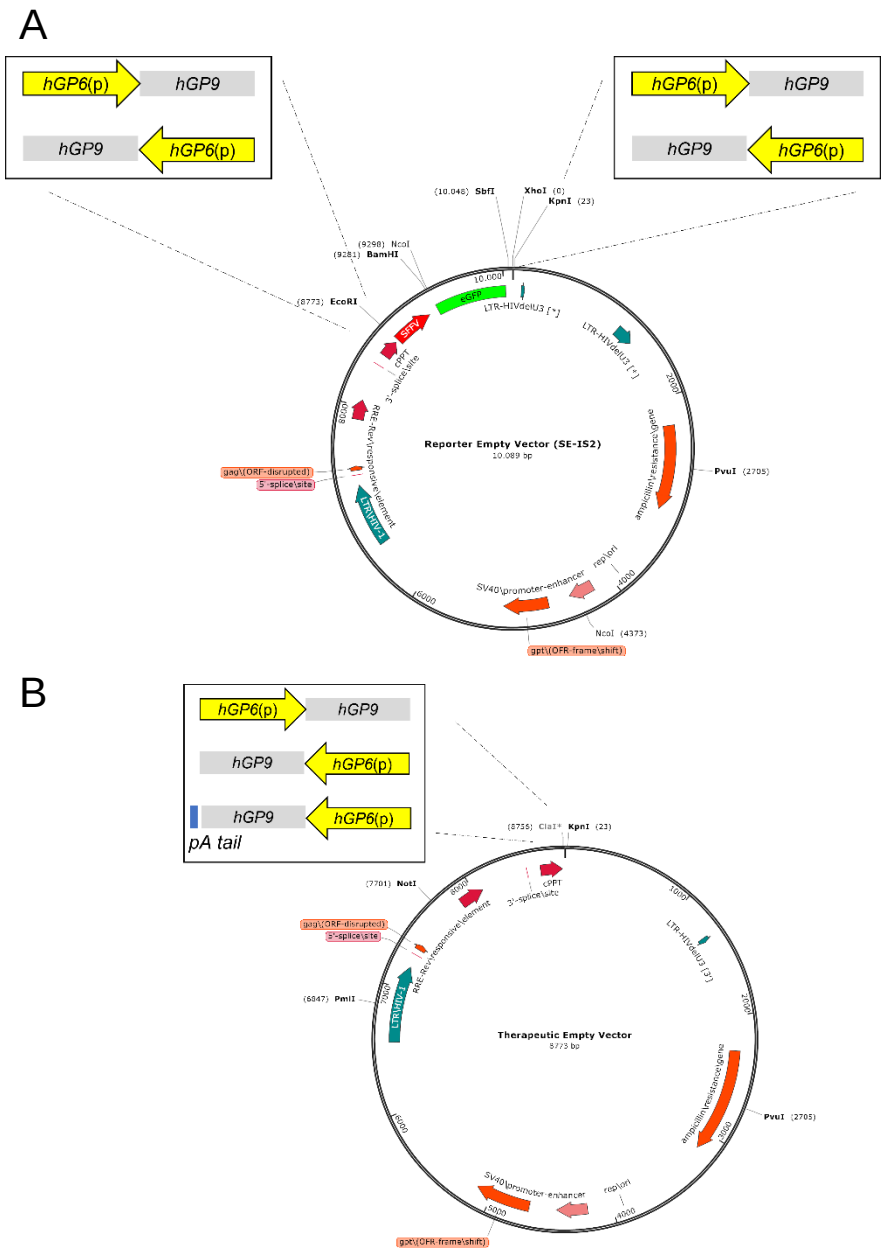

Figure 34. Lentiviral vector backbones used to produce our Reporter (A) and Therapeutic vectors (B).

It is also indicated the cloning strategy to evaluate the orientation and the position effect on GPIX expression.

Vector (T-EV) (**Figure 34-B**), which served as the backbone for constructing the Therapeutic Vector-GPIX (T-GPIX). In this case, we evaluated only the orientation of the therapeutic cassette. Additionally, we tested an improved version that incorporated an antisense polyA tail (**Figure 34-B).**

- ***Creation of the Therapeutic Empty Vector (T-EV).***

For this purpose, we digested the R-EV with EcoRI and XhoI unique sites (view restriction sites of **Figure 34-A**), sequentially due to the incompatibilities among both RE buffers, purifying the digested plasmid to remove residual components of the previous digestion reaction. Due to the large size of the plasmid involved in the cloning procedure and to have enough purified digested DNA, we always started from high DNA amounts ranging from 3 to 5 µg, in this way, we could minimize the loss of DNA during the purification steps.

Digested products were then loaded into a 1% agarose gel and separated to discriminate and purify the digested band corresponding to the LV that we would use as backbone for the therapeutic construct.

Then, overhanging ends were removed with Quick Blunting Kit (NEB) following its indications. This kit is utilized for the conversion of DNA that possesses incompatible 5´ or 3´ overhangs into 5´ phosphorylated, blunt-ended DNA. The blunting process of DNA is achieved through the use of T4 DNA Polymerase (NEB #M0203), which exhibits both 3´→5´ exonuclease activity and 5´→3´ polymerase activity. The

enzyme mix also includes T4 Polynucleotide Kinase (NEB #M0201) for the subsequent phosphorylation of the 5´ ends of blunt-ended DNA to facilitate the subsequent ligation that was carried out overnight at 16ºC. Usually, 27 femtomoles of vector are required to perform a successful ligation, therefore, to calculate the necessary amount of DNA we used the NEBBioCalculator® module (NEB).

Ligation products were then transformed into *E. coli DH5α*, to produce enough amount of plasmid for subsequent digestion confirmations and Sanger sequencing.

- ***Extraction and blunting of the therapeutic cassette hGP6(p)-GP9:***

EcoRI (NEB) was used to remove h*GP6*(p)-h*GP9* sequence from the intermediate vector pCR-2.1 and to clone it into both empty vector backbones described previously (R-EV and T-EV). Digested cassette was then blunted to remove *EcoRI* overhanging ends and phosphorylated.

- ***Digestion and blunting of lentiviral backbones R-EV and T-EV***

To evaluate the effect of GPIX expression orientation in the R-GPIX design, we utilized *KpnI* (NEB) or *EcoRI* (NEB) REs to linearize the R-EV LV backbones. This digestion allowed us to determine whether the insertion of the therapeutic cassette occurred before or after the reporter cassette. *KpnI* RE was used for T-GPIX design.

In all cases, we performed a blunting process to remove the overhanging ends. To avoid recircularization of empty vectors during the ligation step, blunt ends were not phosphorylated at 5'. Ligation reaction of blunt end-fragment generate a non-directional insertion, therefore, we could analyze the effect on GPIX expression of both possible orientations.

- ***Ligation reaction and generation of GPIX-expressing lentiviral vectors.***

Non-phosphorylated backbones were non-directional ligated with 5'-phosphorilated therapeutic cassettes. To calculate the required amount of purified vectors and inserts, we utilized NebBioCalculator module. Mixed all the required components (T4 DNA ligase, T4 DNA ligase buffer, purified vector, purified insert and H_2O), it was incubated overnight and transformed into competent bacteria. Positive LV constructs were detected by identification of predicted digestion pattern result of the confirmation digest using PvuI and NcoI REs. Then, positive constructs were sequenced.

2.2.3.2. Lentiviral vectors production.

Once validated the LV sequence, we produced LV particles for each construct. To achieve it, LVs were produced by 293T cells co-transfection of (1) plasmid vector (R-EV, R-GPIX, T-EV or T-GPIX), (2) pCMVDR8.91 packaging plasmid and (3) VSV-G (pMD2.G) plasmids. LV particles were produced in 293T cells using LipoD293T as follows:

- ***Day -1: Seeding.***

For each LV, we used five 100 mm tissue-culture treated culture dishes (Corning). From a T175 previously seeded to reach 70-80% confluency on day -1, 293T cells were dissociated using TrypLE 0,75X. Then, cell number was determined and each culture dish was seeded with $3.8x10^6$ cell/plate in a final volume of 9 mL 24 hours prior transfection.

- ***Day 0: Cell transfection.***

30 minutes prior lipofection, culture media was replaced. To minimize the surface area and force the interaction of the liposome with the cell, we added 5 mL of DMEM-HG supplemented with FBS and without antibiotics. Two different cocktails were then prepared for lipofection. Cocktail 1 consisted of a LV plasmid (10 µg), VSV-G envelope plasmid (3.2 µg), and pCMVDR8.91 packaging plasmid (6.4 µg), all resuspended in 500 µL of non-supplemented DMEM-HG per dish. Cocktail 2 consisted of 30 µL of LipoD293 resuspended in 500 µL of non-supplemented DMEM-HG per dish. Cocktail 2 was then added to Cocktail 1 and incubated for 15 minutes. The resulting mixture was added to the cell layer dropwise onto the culture dish while moving carefully using a capillary Pasteur pipette. Cells were incubated at 37ºC for 8 hours. Then, the culture medium was replaced with 7 mL of prewarmed DMEM-HG supplemented with FBS and without antibiotics.

- ***Day 2-3:***

Culture media was replaced and cell supernatants were collected, centrifuged to remove cell debris and ultracentrifuged at 25.000xG, 2 hours, 4ºC using SORVALL, WX ultra series centrifuge (Thermo Scientific) and resuspending viral pellet in 100-300 uL of non-supplemented RPMI. Single aliquots were then stored at -80ºC.

2.2.3.3. Lentiviral vectors titration.

Viral titers were determined by performing serial dilutions of the concentrated LVs over DAMI *GP9*-KO cells. GPIX positive cells were determined by flow cytometry seven days after transduction. Vector titration was calculated according to the following formula:

$$Titer = \frac{10^5\ plated\ cells * \%GPIX\ cells/100}{mL\ vector}$$

2.2.4. Flow cytometry evaluation of these different designs of lentiviral vectors.

2.2.4.1. Cell transduction.

DAMI, MEG-01 and non-megakaryoblastic cells were transduced with a MOI=10 (refer to previously detailed way to calculate the required volume). Required volume of LVs were added to culture media supplemented with 1 µg/mL protamine sulfate (Merck Life Sciences). Transduction was performed overnight, replacing culture media the following morning.

2.2.4.2. Flow cytometry evaluation in non-megakaryoblastic cells.

THP1, Jurkat and 293T transduced cells were analyzed by flow cytometry analyzing for 7AAD, GPIX and eGFP expression. These cells were monitored for one month period, setting day 7, day 21 and day 28 as analysis days.

2.2.4.3. Flow cytometry evaluation in Megakaryoblastic cells.

Flow cytometry was used to analyze transduced cells for the expression of 7AAD, GPIX, and eGFP. The cells were monitored and analyzed on day 7, day 21, and day 28 over a one-month period in DAMI WT, *GP9*-KO and *GP9*-KO transduced cells and end-point data was acquired on D28 for MEG-01 WT, *GP9*-KO and *GP9*-KO transduced cells.

Re-assembly of the receptor was then monitored on MEG-01 cell models by analyzing eGFP and GPIbα (CD42b) expression by flow cytometry and showing overlapped histograms.

ImageStream was also utilized to further validate flow cytometry results, showing most representative events for each cell line generated in both megakaryoblastic models.

- ***Statistical analysis***

For DAMI cell models, we used two-way ANOVA plus Holm-Šídák's multiple comparisons test to analyze the

evolution of GPIX expression over time by comparing mean fluorescence intensities and percentage of positive cells (eGFP and GPIX) at different time points. For MEG-01 cell models, we compared eGFP and GPIX end-point data to *GP9*-KO values using one-way ANOVA plus Dunnett's multiple comparisons test by calculating average ratios (relative to R-EV for eGFP and relative to WT expression for GPIX) of mean fluorescence intensities and percentage of positive cells. We used the following significance levels: ns = non-significant, * $p < 0.05$; ** $p < 0.01$; *** $p<0.001$ and **** $p < 0.0001$.

2.3. Analysis of GPIb-V-IX complex functionality in WT, GP9-KO and GP9-KO megakaryoblastic transduced cells.

Similar to the experiments performed in the section "1.4" we conducted analogous analysis to determine how functional was the rescued GPIb-V-IX receptor by GPIX-expressing LVs.

2.3.1. Analysis of genetically rescued GPIb-V-IX receptor binding capacity to soluble von Willebrand factor.

We evaluated the GPIbα binding capability to soluble VWF by flow cytometry. MEG-01 WT, *GP9*-KO and *GP9*-KO transduced cells were incubated with ristocetin and VWF as previously mentioned and analyzed by flow cytometry to evaluate the ratio of positive cells relativized to WT positive events and compared to *GP9*-KO signal.

Additionally, we also measured the agglutination capacity of all our cellular models in presence of ristocetin and VWF. For sedimentation experiments, $5x10^6$ cells/mL were resuspended in 250 µL PBS supplemented with 10 µg/mL VWF. After a pre-incubation period at 37ºC for 2 minutes under stirring conditions, ristocetin (1 mg/mL) was added to each single tube and light transmission was measured in a light-transmission aggregometer (Chrono-log) at 37ºC for 15 minutes. Measurements were made by pairs: WT *vs. GP9*-KO, R-EV *vs.* R-GPIX, T-EV *vs.* T-GPIX.

2.3.2. Analysis of adhesion capability in presence of botrocetin for genetically rescued GPIb-V-IX receptor.

In addition, we assessed the ability of GPIbα to adhere to immobilized VWF by immunofluorescence. We incubated MEG-01 WT, *GP9*-KO, and *GP9*-KO transduced cells with botrocetin and VWF, as described before, and analyzed them using immunofluorescence combined with ImageJ bioinformatic software. Our aim was to determine the ratio of positive cells in relation to WT positive events and to compare it to the *GP9*-KO signal.

2.3.3. Statistical analysis

Flow cytometry analyzed data of GPIbα binding capability to soluble VWF was compared respect *GP9*-KO samples and relativizing values to WT signal using one-way ANOVA plus Dunnett's multiple comparisons test.

For agglutination experiments, end point transmittance values of measured pair samples (R-EV *vs.* R-GPIX; T-EV *vs.* T-GPIX) were compared using one-way ANOVA plus Šídák's multiple comparisons test. Same statistical test was employed to analyze the relative number of adhered cells (respect WT). All comparison were analyzed by pairs (R-EV *vs.* R-GPIX; T-EV *vs.* T-GPIX).

We used the following significance levels: ns = non-significant, * $p < 0.05$; ** $p < 0.01$; *** $p<0.001$ and **** $p < 0.0001$.

3. Objective 3: GPIX-Lentiviral correction of Bernard-Soulier Syndrome Type C induced Pluripotent Stem Cells and posterior differentiation to megakaryocytes and platelets.

We measured the rescuing capability of our GPIX-expressing LVs in iPSCs by Immunocytofluorescence, flow cytometry and ImageStream to determine GPIX localization, expression levels and platelet size.

3.1. Analysis of GPIX reversion in megakaryocytes and platelets produced from transduced GP9-KO induced pluripotent stem cells.

3.1.1. Cell transduction.

$1.2x10^5$ *GP9*-KO iPSCs were seeded in E8 with 10 µM Y27632 over Matrigel coated 6 well plates. The following day, when the culture reached a confluence of 20-35%, media was replaced with E8 and iPSCs were transduced with a MOI of 50. Required volume of each LV were added to E8 media supplemented with 1 µg/mL protamine sulfate. Transduction was performed overnight, replacing culture media the following morning. After seven days of recovery, same cells were transduced again in same conditions, to enrich the number of transduced cells. After the two-hits transduction, cells were differentiated to MKs and platelets as previously described (refer to section 1.4.2).

3.1.2. Immunocytofluorescence of fibrinogen-adhered iPSCs.

To carry out the immunofluorescence, we used mature MKs produced from differentiated WT, *GP9*-KO, and *GP9*-KO transduced iPSCs on day 21. We prepared 8-well Nunc LabTek II chamber slides (Thermo Scientific) by coating them with fibrinogen (100 µg/mL) for 40 minutes at room temperature. Then, we aspirated the fibrinogen solution and seeded 45,000 cells per well in 150 µL E8. After incubating the cells for 60 minutes in the incubator, we aspirated the medium, washed the cells with PBS, and fixed them with 4% PFA solution for 10 minutes at room temperature. Next, we washed the cells three times and permeabilized them with 0.1% Triton X-100 detergent in 1X PBS for 15 minutes. We then washed the cells three more times and blocked them in 1% BSA in PBS for 1 hour. After blocking, we stained the cells with GPIX-APC and CD41-PE conjugated antibodies, which were diluted to 1:100 in 0.1% BSA in PBS and incubated them overnight at 4ºC.

The following morning, we washed the cells three times and incubated them with phalloidin-AlexaFluor405 (1:500) in 0.1% BSA in PBS for 1 hour at room temperature. After incubation, we washed the cells three times with 0.05% Tween 20 detergent in 1X PBS and once with PBS. Then, we removed the chamber and applied mounting media onto the surface. Finally, we placed a coverslip on top, avoiding air bubbles, and

cured the slide overnight at 4ºC. The pictures were taken the following morning in a Zeiss LSM 710 laser confocal microscope.

3.1.3. GPIX determination by flow cytometry and ImageStream.

To further validate GPIX expression in mature MKs and platelets produced from WT, *GP9*-KO, and *GP9*-KO transduced cells, the cells were differentiated for 21 days to produce MKs and 35 days to produce platelets, as described.

For the MKs, the cells were collected, washed, and stained with GPIX-APC, CD41-PE and *7AAD*. The stained cells were then analyzed using flow cytometry. In the case of platelets, a sequential centrifugation step of 150xG for 5 minutes was used to separate cells, followed by another centrifugation step of 300xG (Acceleration 3; Brake 3) for 5 minutes to isolate the platelet fraction.

The percentage of positive cells/platelets and MFI ratios (relativized to EV expression for eGFP and to WT expression for GPIX) were then plotted on a graph and statistically analyzed.

- ***Statistical analysis***

For this experiment, we used two-way ANOVA and Dunnett's multiple comparisons test to compare eGFP and GPIX data to *GP9*-KO values. We calculated the percentage of positive cells and the average ratios of mean fluorescence

intensities, relative to R-EV for eGFP and relative to WT expression for GPIX.

We set the following significance levels: ns for non-significant results, * for p-values less than 0.05, ** for p-values less than 0.01, *** for p-values less than 0.001, and **** for p-values less than 0.0001.

3.1.4. Size determination in genetically rescued *GP9*-KO platelets produced from induced pluripotent stem cells.

Same stained platelets were then analyzed by ImageStream platform, which allowed us to capture single pictures of the gated population and determine the average diameter of single events from this population. The IDEAS software was employed to measure the size of platelets through a series of steps. Initially, we identified the population of platelets expressing $CD41^+$ (**R1**). Subsequently, we applied two filters, one for circularity (**R2**) and another to select images in focus (**R3**). Afterwards, we identified each individual platelet and created a mask that encompassed the entire area of $CD41^+$ fluorescence signal from each platelet. Finally, using all the masks, the IDEAS software calculated the mean diameter ± SD of the selected single-platelet populations.

- ***Statistical Analysis***

Average mean diameter of platelets from differentiated iPSCs WT, *GP9*-KO and *GP9*-KO transduced cells were

compared using ordinary one-way ANOVA plus Dunnett's multiple comparisons test using the following significance levels: ns = non-significant, * $p < 0.05$; ** $p < 0.01$; *** $p<0.001$ and **** $p < 0.0001$.

4. *Objective 4. Genetic-Rescue of isolated hematopoietic stem cells from Bernard-Soulier Syndrome patients carrying different pathogenic variations and posterior differentiation to megakaryocytes and platelets.*

50 mL of fresh blood was collected in EDTA-tubes. Platelet-rich plasma (PRP) from BSS patients and healthy donors was separated by gravity-mediated decantation for 40 minutes. White blood cell fraction was isolated by centrifugation using Ficoll Paque™ PLUS (GE Healthcare), (400xG, 40 minutes, Accel 0, Brake 0) and extraction of the buffy coat. White blood cells were washed twice with PBS. Cell pellet was resuspended in 150 µL MACS Buffer and incubated with 50 µL anti-FCR and 50 µL anti-CD34 magnetic beads at 4ºC for 30 minutes (CD34MicroBead Kit UltraPure, Miltenyi Biotech). After a washing step, we performed an immunomagnetic selection of $CD34^+$ cells with MS columns (Miltenyi Biotech) (**Figure 35**).

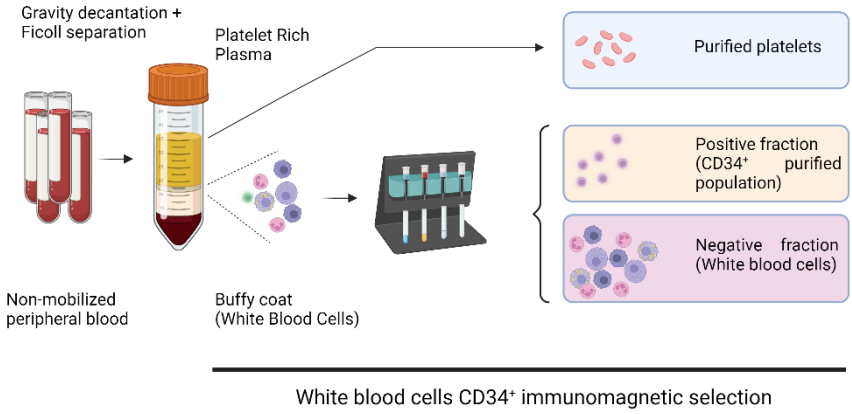

Figure 35. Schematic view of the followed procedure to isolate the different phases from our blood samples.

In our case, we were interested in the platelet population of the PRP and the buffy coat (white blood cells), which contain the population of circulating $CD34^+$ cells. Image created by Martínez-Navajas, G. -Author.

Objective 4. Genetic-Rescue of isolated hematopoietic stem cells from Bernard-Soulier Syndrome patients carrying different pathogenic variations and posterior differentiation to megakaryocytes and platelets.

4.1. Corroboration of pathogenic variants from two unrelated Bernard-Soulier Syndrome patients.

Negative fraction (white blood cells $CD34^-$) was used to isolate genomic DNA for *GP9 locus* PCR amplification and BSS patients' characterization by Sanger sequencing.

Our aim was to characterize the platelets of patients with BSS by determining their size and GPIX fluorescence using ImageStream. To this end, platelets were washed in PBS-EDTA 2 mM, centrifuged (300xG, 10 minutes, Accel 0, Brake 0), and stained with GPIX and CD41 for 30 minutes. The platelets were then washed again and analyzed using ImageStream. GPIX fluorescence was acquired, and platelet size was determined.

4.2. Genetic rescue in megakaryocytes and platelets produced from transduced non-mobilized hematopoietic stem cells from these Bernard-Soulier Syndrome patients.

To differentiate HSCs to MKs *in vitro*, cells were grown in StemSpam (StemCell Technologies) combined with different cocktails regarding to the differentiation stage as schematized in the **Figure 36**.

On **Day 0**, positive fraction was expanded in StemSpam 1X PS supplemented with cytokine cocktail 1: SCF (100 ng/mL) + FLT3L (100 ng/mL, Peprotech) + TPO (100 ng/mL) + SR1 (0,75 Um = 322,12 ng/mL, StemCell Technologies) + UM171 (35 nM = 15,87 ng/mL, StemCell Technologies) + IL-6 (100 ng/mL, Peprotech).

On **Day 2**, expanded HSCs were transduced with R-GPIX (MOI 50) and cultured with cytokine cocktail 2 (StemSpam + TPO (100 ng/mL) + FTL3 (100 ng/mL) + SCF (100 ng/mL) + 1% P/S).

On **Day 3** begins differentiation phase I, where megakaryoblast progenitor appearance occurs (Cytokine cocktail 3: TPO 100 ng/mL + SCF 100 ng/mL + IL-6 7.5 ng/mL). Finally, megakaryocytic maturation is achieved in differentiation phase II, where TPO 100 ng/mL is the unique supplementary cytokine administrated.

Objective 4. Genetic-Rescue of isolated hematopoietic stem cells from Bernard-Soulier Syndrome patients carrying different pathogenic variations and posterior differentiation to megakaryocytes and platelets.

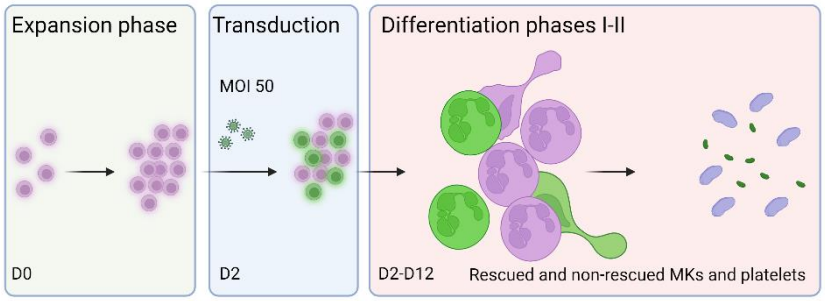

Figure 36. Schematic view of the megakaryocytic differentiation process.
Purified CD34 positive cells (HSCs) from non-mobilized peripheral blood from BSS patients were differentiated *in vitro* to megakaryocytes and platelets. Image created by Martínez-Navajas, G. -Author.

Megakaryocytes and platelets were collected and separated as previously described. Megakaryocytes were stained with GPIX-APC and CD41-PE, fixed and permeabilized with 4% PFA solution and 0.1X Triton X-100, respectively. Then, nuclear DNA from MKs was stained with Hoechst, washed and analyzed. Platelets were stained, fixed and analyzed. Data was adquired with ImageStream, including eGFP in the analysis and analyzed with IDEAS software to determine protein expression and platelet size.

- ***Statistical analysis***

We performed a size analysis comparison between healthy donor, BSS patients and transduced and non-transduced *in vitro* produced platelets. Average mean diameters of platelets were compared using ordinary one-way ANOVA plus Dunnett's multiple comparisons test using the

following significance levels: ns = non-significant, * $p < 0.05$; ** $p < 0.01$; *** $p<0.001$ and **** $p < 0.0001$.

5. Objective 5. Generation and characterization of Bernard-Soulier Syndrome GP9^{null} murine model.

5.1. Analysis and comparison of hGP9 and mGp9 genes and their amino acidic sequences.

To compare both gene sequences, *mGp9* (murine) and *hGP9* (human), we consulted *Ensembl* data base and obtained their CDS sequences and compared using ClustalW multiple alignment tool. Furthermore, their aminoacidic sequences were compared too and represented.

5.2. Development of a GP9^{null} murine model.

The design of the sgRNAs and ssODN to generate the *Gp9*^{null} murine model with CRISPR-Cas9 technology was carried out by Dr. Manuel Sanchez Martin, head of the transgenic facility at the University of Salamanca.

Briefly, *Gp9* KO mice were generated by deleting the complete Gp9 consensus coding sequence (CCDS20328) on chromosome 6. Two complementary CRISPR RNAs (crRNAs) Gp9 guide1 (5'-CTGTACCCAACACGCTGCTG-3') and Gp9 guide2 (5'-CCATGCCATCAAAAGCCCAC-3') flanking the coding sequence were designed with the Spanish National Biotechnology Centre (CNB)-CSIC web tool (http://bioinfogp.cnb.csic.es/tools/breakingcas/). A 200nt ssDNA (Gp9 ssODN) was designed as a template for producing a precise 710bp deletion. The crRNAs, the tracrRNA (trans-activating CRISPR RNA), and the ssODN were

produced by chemical synthesis at Integrated DNA Technologies. The crRNA and tracrRNA were annealed to obtain the mature sgRNAs. A mixture containing the sgRNAs, recombinant Cas9 protein (IDT), ssODN [Cas9 (30 ng/µl), annealed sgRNA (20 ng/µl each), and ssODN (10 ng/µ)] were microinjected into C57BL6/J zygotes at the Transgenic Facility (NUCLEUS, platform for research supporting) of the University of Salamanca. Edited founders were identified by polymerase chain reaction (PCR) amplification (Taq polymerase, NZYTech) with primers flanking the *Gp9* CCDS (primer FW 5'-ACATTTCCTGTTCTCTGTGG-3' and RV 5′-TGTGGAGGTGAGATTTAGGTC-3′).

***Gp9* ssODN:**

5'-
CCCTGTTTCCCTATCTGAGCAGAGGCTTGGATCTCTGCCAGAGACCA
AGAAGGCCCTGCTCCTCTCTACCACTCTTCCTGGGCTGTACCCAACA
CGCTGCACAGGGGGCAGGCTGAGGCCGCCTCATGGGCAAAGACAC
TTGCTGTCCAGTCTAAAGACCTGGGTTTTATCCCCAGGAGAGACCTA
AATCTCACCTCCAC-3'

The expansion of the mice colony and its maintenance is being carried out by the authorized personnel from the animal facilities of the "Centro de Instrumentación Científica-Centro de Investigación Biomédica", of the University of Granada.

5.3. Hemogram analysis from Gp9^{null} murine model and its comparison with WT hematological parameters.

Blood samples were collected from animal of 6-months age. To extract the blood, 1 mL syringes (25-27G) were used to puncture the lateral saphenous vein and 80-100 µL of blood were collected and transferred into EDTA collection tubes, mixing to avoid the coagulation. Then, blood samples were measured in a hematologic cell counter (Mythic 22CT; Orphee S.A.).

- ***Statistical analysis***

To compare mean hematological parameter values, we used the ordinary two-way ANOVA plus Šídák's multiple comparisons test, comparing males values and females values (ns = non-significant, * $p < 0.05$; ** $p < 0.01$; *** $p<0.001$ and **** $p < 0.0001$).

CHAPTER V

RESULTS

1. Objective 1: Investigate the assembly of GPIb-V-IX through CRISPR-Cas9 knockout generation and disease modeling: Exploring the roles of GP1BA, GP1BB, GP9 and GP5.

GPIb-V-IX receptor is localized on MKs and platelets surface membrane and is assembled by 4 subunits: GPIbα, GPIbβ, GPIX and GPV in 2:4:2:1 stoichiometry[60]. As previously mentioned, pathogenic variants affecting *GP9*, *GP1BA* or *GP1BB* genes impede the correct receptor assembly leading to absent, incomplete or dysfunctional receptor, promoting the different phenotypes of BSS described in the literature. However, up to date there are not mutations associated to *GP5* that could originate the BSS. To investigate the contribution of each subunit to the GPIb-V-IX assemblage, we decided to knockout *GP9*, *GP1BA, GP1BB* or *GP5* genes using CRISPR-Cas9 technology.

1.1. Generation and characterization of megakaryoblastic Bernard-Soulier Syndrome models and GP5-KO, studying the contribution of each subunit to the assemblage of the GPIb-V-IX receptor.

For this reason, we selected MEG-01 and DAMI cell lines, which are megakaryoblastic cells known to express the GPIb-V-IX receptor constitutively. This fact, together with the presence of two-well defined alleles for each gene, would allow

us to observe the migration behavior of each subunit in the absence of each other in a physiological manner.

Therefore, these cell lines would enable us to develop models of BSS Type A1, Type B, and Type C, by knocking out *GP1BA*, *GP1BB*, and *GP9*, respectively. Furthermore, by knocking out *GP5*, we would be able to investigate how the absence of this subunit affects the assembly of GPIb-V-IX and its contribution to the receptor's functionality.

1.1.1. sgRNAs design for Bernard-Soulier Syndrome driver genes (*GP1BA*, *GP1BB* and *GP9*) and *GP5*.

First, we designed specific sgRNAs considering maximal score and minimal off-targets criteria. Cutting site positions were calculated respect to ATG (**Table 5**). sgRNAs were designed to incorporate a protruding sequence complementary to *BbsI* overhang ends from digested plasmid.

To assess the ligation, sgRNA-PX-458 cloned plasmids were digested with *BbsI*. The two adjacent *BbsI* RE sites of the plasmid are self-destroyed in those constructs that had incorporated the sgRNA thus, impeding the posterior *BbsI* digestion. Therefore, constructs that incorporated the sgRNA should migrate similarly to undigested PX-458 plasmid (**Figure 37**).

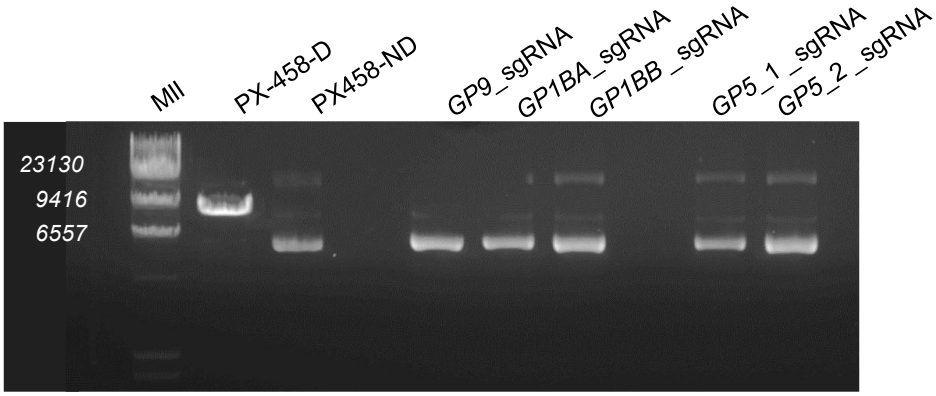

Figure 37. Agarose gel exhibiting BbsI digestion of PX-458 plasmids containing each single sgRNA.

Lane (L) 1 contains DNA molecular weight marker II. Lanes 2 and 3 contain BbsI-digested (D) and non-digested (ND) PX-458 plasmids, respectively. Lanes 4-8 represent pX-458 plasmids including *GP9*, *GP1BA*, *GP1BB*, and both *GP5* sgRNAs, respectively.

Once confirmed the cloning into PX-458 by *BbsI*-digestion and Sanger Sequencing, all the constructions were purified by maxiprep.

1.1.2. Generation of megakaryoblastic knockouts.

Once created the gene-editing tools to develop the KOs, our goal was to introduce them into the WT cells and screen for the highest KO frequencies to isolate the clone.

We first introduced CRISPR-Cas9 systems with sgRNAs targeting *GP1BA*, *GP1BB*, *GP9* and *GP5* into MEG-01 and DAMI WT cell lines to perform gene editing. However, we observed a reduced transfection rate in our megakaryoblastic cell lines due to the limited success of lipofection as a delivery method (**Figure 38**). The transfection

of the PX-458 plasmid, which includes eGFP as a reporter gene, allowed us to identify and sorter CRISPR-Cas9-expressing cells based on FITC fluorescence, what let us to enrich our gene edited population.

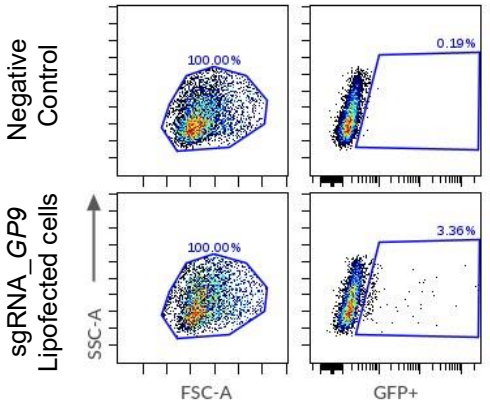

Figure 38. Representative flow cytometry dot plots for *GP9*-PX-458 sgRNA lipofected cells.

A reduced frequency of transfected cells is visible compared to the negative control. The transfected cells are identifiable by eGFP positive events. Similar outcomes were observed for the other constructions.

Then, we stablished several pools for each transfected sgRNA. These pools were initiated with reduced starting cells, consequently, based on the count of non-edited cells and KO-edited cells, we were able to induce various levels of KO enrichment. To identify these most enriched, we had to follow two different strategies motivated by the absence of functional commercial antibodies to recognize GPV expression.

1.1.2.1. *GP1BA*, *GP1BB* and *GP9* knockouts generation and isolation.

After expanding the eGFP$^+$ cell population, we measured GPIbα (in *GP1BA*-KO pool), GPIbβ (in *GP1BB*-KO pool) and GPIX (in *GP9*-KO pool) surface expression, identifying these different KO frequencies (data not shown). From these edited pools, we isolated single-cell clones, re-expanded them to establish new populations and identified several samples in which surface expression of GPIbα, GPIbβ or GPIX was completely absent, respectively (**Figure 39**).

In addition, we observed that MEG-01 WT cells have higher MFI levels than DAMI WT cells for all the components of the GPIb-V-IX complex.

1.1.2.2. *GP5* knockout generation and isolation.

In this case, the unavailability of functional commercial antibody against GPV impeded us to detect the KO by conventional flow cytometry. As mentioned, in this case we used two different sgRNAs to generate a DNA microdeletion. that were co-transfected into DAMI and MEG-01 cells. In this case, eGFP$^+$ cells were sorted and seeded following the same strategy and most enriched pools were detected by conventional PCR.

Objective 1: Investigate the assembly of GPIb-V-IX through CRISPR-Cas9 knockout generation and disease modeling: Exploring the roles of GP1BA, GP1BB, GP9 and GP5.

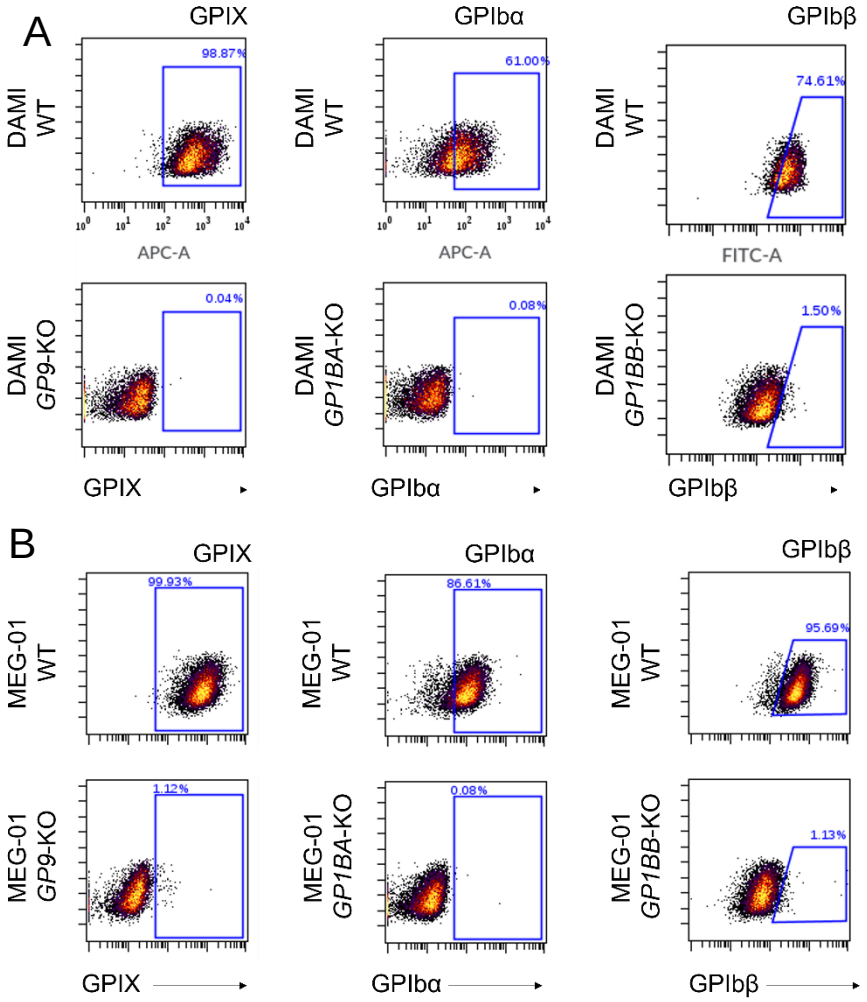

Figure 39. Isolation of clonal populations for GP1BA, GP1BB and GP9 KOs. Flow cytometry dot plots that show the expression levels of GPIX (column 1), GPIbα (column 2), and GPIbβ (column 3) in WT cells and their associated KO in both DAMI cells (panel A) and MEG-01 cells (panel B).

So, we designed a set of *GP5* primers that amplified a PCR product of 1000 bp of WT *GP5 locus* (**Figure 40**, **red arrows**). The two different sgRNAs were supposed to generate a microdeletion of 200 bp containing the 5'- ATG -3'

and consequently abolishing GPV expression. Thus, heterogenous edited populations should amplify both: WT original alleles (1000 bp) and *GP5*-KO edited alleles (800 bp), while pure homozygous KO populations should amplify only 800 bp region as a result of *GP5* microdeletion (**Figure 40**, **agarose gel schematic**).

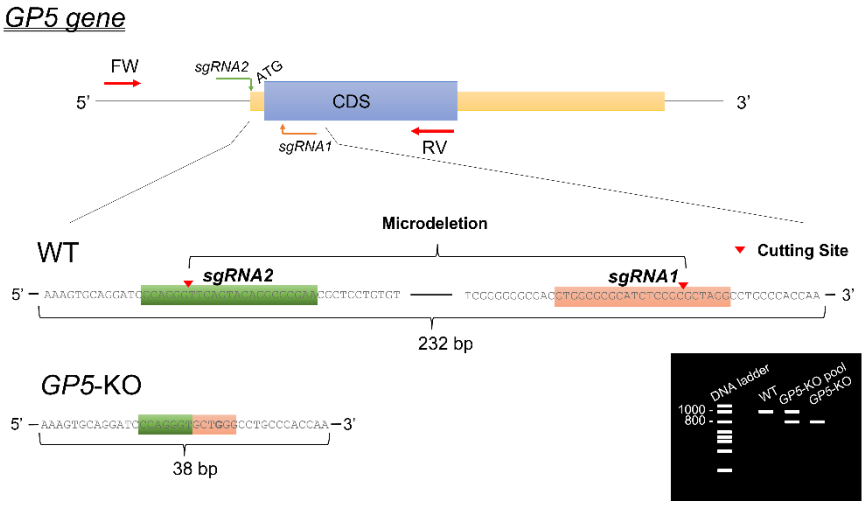

Figure 40. Schematic of *GP5*-KO strategy.

The gene structure of *GP5 locus* is illustrated from 5' to 3', with the coding sequence (CDS) indicated. The cutting sites for the sgRNAs, along with their respective sequences, are shown over the WT allele. Red arrows indicate the forward (FW) and reverse (RV) designed primers to amplify both WT and *GP5*-KO alleles. At the bottom, the resulting *GP5*-KO allele is depicted, along with an illustrative agarose gel. The gel displays the different outcomes that result from Cas9 editing, including the PCR amplification of the WT allele, a heterogeneous pool of gene-edited cells, and an isolated clone.

We carried out the workflow in both megakaryoblastic cell lines and obtained single-cell clones from the most enriched pool that contained our allele of interest (800 bp). **Figure 41** depicts our screening strategy for *GP5-KO* using

conventional PCR. We established several clonal populations from these pools.

In DAMI cells, the c5 clonal population was homozygous for the deletion, while the other clones were non-edited populations (**Figure 41**). In MEG-01, c10 was homozygous for the deletion, and most clones were heterozygous, with only one allele carrying the microdeletion. Clones c1 to c4 had aberrant deletions in *GP5 locus* caused by CRISPR-Cas9 tools (**Figure 41**).

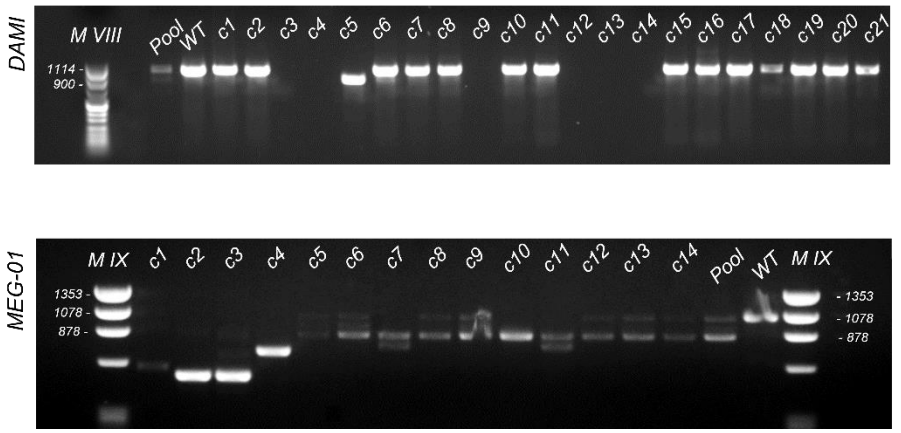

Figure 41. PCR-screening strategy for single-cell clones ("c") established from an enriched GP5-KO pool. DAMI (top) and MEG-01 (Bottom).

The positive control was obtained by PCR amplification of the wild-type (WT) allele. M VIII and M IX refer to different molecular weight DNA markers.

1.1.3. Characterization of megakaryoblastic knockouts.

Following the isolation and identification of each KO model by flow cytometry (BSS driver genes) and conventional

PCR (*GP5*-KO), the next step was to characterize the genetic mutations induced by CRISPR-Cas9 system in these *loci*. We first needed to amplify the affected genes (*GP1BA*, *GP1BB*, *GP9* and *GP5*) and then we sequenced them with Sanger sequencing. For this purpose, we designed primer pairs that centered the CRISPR-Cas9 cutting site in the middle of the amplicon, where the *indel* mutation would be introduced. In the case of *GP5*, we used the same primers previously optimized (**1.1.2.2**).

1.1.3.1. *GP1BA*, *GP1BB* AND *GP9* PCR conditions optimization.

The first step was to optimize the PCR reaction for each gene to obtain single bands using wild-type genomic DNA (gDNA) as the template. This was necessary because Sanger sequencing requires clean PCR products to generate clear reads of the sequence.

As a part of the optimization of PCR products, in **Figure 42**, we observed that the primer pairs designed for *GP1BA* and *GP1BB* genes were not sufficiently specific to amplify their target. To solve it, we optimized the PCR conditions, including a gradient of temperature and dimethyl sulfoxide (DMSO) addition **Figure 42; A-B**). After optimization, we realized that the best amplification conditions for *GP1BA* and *GP1BB* genes were achieved at 54.4°C with 10% DMSO. In contrast, the PCR reaction for the *GP9* gene was simpler to optimize: 60.8°C in absence of DMSO (**Figure 42; C**).

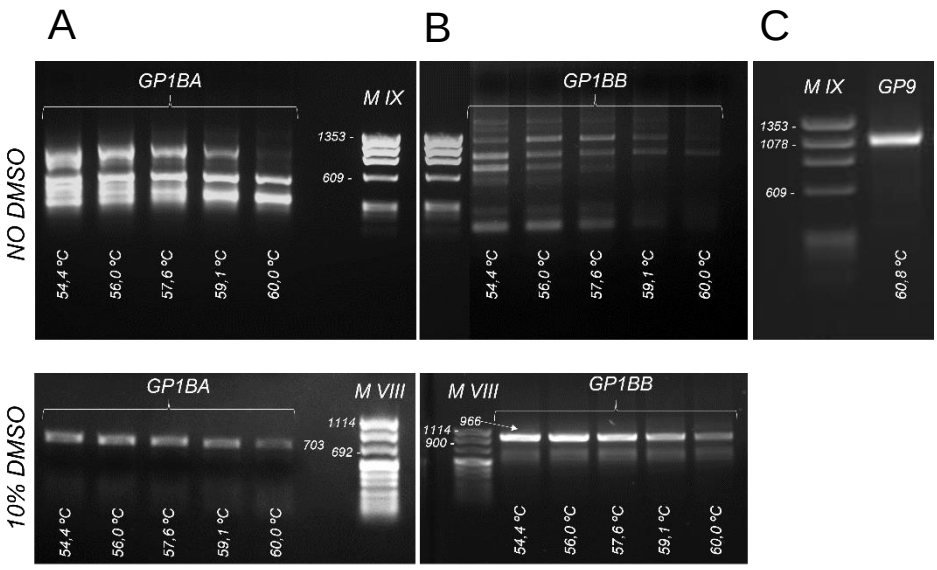

Figure 42. PCR optimization of *GP9*, *GP1BA*, and *GP1BB* PCR products.

A. Optimization of *GP1BA* PCR by establishing a temperature gradient (54.4-60.0°C) (top) and by adding 10% dimethyl sulfoxide (DMSO) to the gradient (bottom). **B**. Optimization of *GP1BB* PCR by establishing a temperature gradient (54.4-60.0°C) (top) and by adding 10% DMSO to the gradient (bottom). C. *GP9* PCR amplification at 60.8°C. (M IX: DNA marker IX; M VII: DNA marker VII).

1.1.3.2. Characterization of CRISPR-Cas9 induced mutations for each individual gene.

Once determined the optimal PCR, gDNA from edited *GP1BA*-KO, *GP1BB*-KO and *GP9*-KO cells was amplified by PCR using their respective primer pairs. Then, PCR products were purified and sequenced by Sanger Sequencing.

In the case of homozygous mutated alleles, only a clear spectropherogram could be observed. When observed overlapping sequences in the spectropherogram, it was an indicator of heterozygous mutations. To obtain the specific sequence of each mutated allele, it was necessary to clone the

PCR product carrying the heterozygous mutation into the pGEM-T plasmid (**pGEM®-T technique to determine allelic sequences for compound heterozygous mutations.**). Sequencing at least 10 colonies allowed the determination of the individual sequences for both alleles.

Notably, in all cases, CRISPR-Cas9 induced the appearance of *indel* mutations in the CDS of each gene. The mutated sequences for each KO were aligned with their WT counterparts, so we were able to characterize the pathogenic variants generated. These variations shifted the reading pattern and disrupted the original protein sequence, thus originating aberrant proteins, and explaining the phenotype previously observed (**Figure 39**). Specifically, detailed description can be found above:

- ***DAMI***

***GP9* gene:** Homozygous mutation.

-A homozygous mutation resulting from a duplication of a nucleotide at position 191 (A), leading to a frameshift mutation. This substitution replaces serine (Ser) with valine (Val) at position 65 out of 177 and introduces a premature termination codon 8 amino acids downstream.

GP1BA gene: Compound heterozygous mutation.

-Allele 1 has a deletion of a nucleotide at position 366 (C), leading to a frameshift mutation that replaces aspartic acid (Asp) with glutamic acid (Glu) at position 122 out of 652. This

results in a premature termination codon 7 amino acids downstream.

-Allele 2 has a point mutation at position 553, where adenine (A) is replaced with guanine (G) in the coding sequence, leading to a missense mutation that replaces asparagine (Asn) with aspartic acid (Asp) at position 165 out of 652.

GP1BB gene: Compound heterozygous mutation.

-Allele 1 has a duplication of a nucleotide at position 106 (C), leading to a frameshift mutation that replaces leucine (Leu) with proline (Pro) at position 36 out of 206. This introduces a premature termination codon 273 amino acids downstream.

-Allele 2 has multiple mutations: a substitution of adenine (A) with thymine (T) at position 91, replacing serine (Ser) with cysteine (Cys) at position 31 out of 206; a duplication of cytosine (C) at position 93; a substitution of thymine (T) with cytosine (C) at position 94; and a microdeletion of the sequence between positions 99 and 124. These mutations result in a missense mutation that replaces cysteine (Cys) with proline (Pro) at position 32 out of 206, and introduce a frameshift mutation that creates an aberrant protein with a stop codon placed 269 amino acids downstream.

- ***MEG-01.***

***GP9* gene:** Homozygous mutation

A frameshift mutation occurred due to the insertion of tetranucleotide [CGTC] between residues 191 and 192 of the coding sequence. This resulted in the replacement of a glutamine (Gln) residue with a histidine (His) residue (position 64 out of 177), and a premature termination codon occurred 10 amino acids downstream.

GP1BA gene: Homozygous mutation

A frameshift mutation occurred due to the deletion of the nucleotide sequence between nucleotides 363 and 373 of the coding sequence. This resulted in the replacement of an aspartic acid (Asp) residue with a glutamine (Gln) residue (position 122 out of 652), and a premature termination codon occurred 26 amino acids downstream.

GP1BB gene: Homozygous mutation

A frameshift mutation occurred due to the insertion of guanine (G) nucleotide between nucleotides 106 and 107 of the coding sequence. This resulted in the replacement of a leucine (Leu) residue with an arginine (Arg) residue (position 36 out of 206), and an aberrant protein was formed with a termination codon occurring 276 amino acids downstream.

To summarize, their abbreviated descriptions adapted to the Human Genome Variation Society (HGVS) nomenclature are listed in the **Table 23** (MEG) and the **Table 24** (DAMI).

Table 23. Detailed description of CRISPR-Cas9 generated mutations in MEG-01 cell lines according to Human Genome Variation Society (HGSV) nomenclature.

Mutations have been referred to CDS and aminoacidic sequences for both alleles.

(HGNC symbol)	cDNA sequence change	Amino acid change (Three letter code)
GP9	NM_000174.5:c.[191dup];[191dup]	NP_000165.1:p.[Ser65ValfsTer8];[Ser65ValfsTer8]
GP1BA	NM_000173.7:c.[366delC];[553A>G]	NP_000164.5:p.[Asp122GlufsTer7];[Asn185Asp]
GP1BB	NM_000407.5:c.[106dup];[91A>T; 93dup; 94T>C; 99_122del]	NP_000398.1:p.[Leu36ProfsTer273];[Ser31Cys;Cys32ProfsTer269]

Table 24. Detailed description of CRISPR-Cas9 generated mutations in DAMI cell lines according to Human Genome Variation Society (HGSV) nomenclature.

Mutations have been referred to CDS and aminoacidic sequences for both alleles.

(HGNC symbol)	cDNA sequence change	Amino acid change (Three letter code)
GP9	NM_000174.5:c.[191_192insCGTC];[191_192insCGTC]	NP_000165.1:p.[Gln64HisfsTer10];[Gln64HisfsTer10]
GP1BA	NM_000173.7:c.[363_373del];[363_373del]	NP_000164.5:p.[Asp122GlnfsTer26];[Asp122GlnfsTer26]
GP1BB	NM_000407.5:c.[106_107insG];[106_107insG]	NP_000398.1:p.[Leu36ArgfsTer273];p.[Leu36ArgfsTer273]

GP5 gene:

As anticipated, the use of two sgRNAs resulted in the creation of a microdeletion, with both sgRNA cleavage sites coinciding at the merge point (**Figure 43**). The deletion of the beginning of the CDS, including the 5'-ATG, generated a complete *GP5*-KO for both megakaryoblastic cell lines.

These novel models would allow us to study the role of this subunit in the assembly and functionality of the GPIb-V-IX receptor.

Figure 43. Alignment of DAMI and MEG-01 *GP5*-KO alleles with the WT allele.

CDS origin is highlighted in orange and sgRNAs are shadowed in green and light orange on the WT allele sequence. The cutting sites for each sgRNA are marked with red triangles. An asterisk symbol (*) indicates the conservation of nucleotides at the same location.

1.1.4. Contribution of each subunit to the assembly of GPIb-V-IX receptor.

The literature describes that patients with BSS have platelets with an absent, incomplete, or dysfunctional GPIb-V-IX receptor. However, it remains unclear how each pathogenic variant leads to a specific receptor phenotype. For the first time, we report the creation of various models of BSS by knocking out each of the genes responsible for the syndrome

(*GP1BA*, *GP1BB*, *GP9 and GP5*). The availability of these models would shed light on the assembly of the GPIb-V-IX receptor, contributing to a better understanding of the role of each individual subunit in the final conformation of the receptor and, therefore, in the different BSS phenotypes.

To determine how each subunit removal affects to whole receptor assembly, we analyzed CD42A (GPIX), CD42B (GPIbα) and CD42C (GPIbβ) expression by flow cytometry in both MEG-01 and DAMI WT and KO cellular models (*GP9*, *GP1BA*, *GP1BB* and *GP5*) (**Figure 44** and **Figure 45**). However, we were unable to determine GPV expression levels because there are no commercial human antibodies available for flow cytometry.

1.1.4.1. Migration dynamics in BSS disease models.

To begin, we investigated the migration dynamics of our different BSS models (*GP1BA*-KO [Type A1], *GP1BB*-KO [Type B], and *GP9*-KO [Type C]). As expected, the expression of GPIX was not detectable in both *GP9*-KO cell line models (**Figure 44**: **A-B**). However, its expression varied in the other two KO models. While GPIX expression was completely absent in *GP1BB*-KO cells ($p<0.0001$), it was significantly reduced in *GP1BA*-KO, that decreased to around~230.0 units *vs.* ~2300.0 units (of WT) in terms of MFI and 60.0% of positive cells in MEG-01 ($p<0.0001$), while in DAMI cells decreased to 80.0 units *vs.* 876 units (of WT) and around 30% positive cells in DAMI ($p<0.0001$).

Objective 1: Investigate the assembly of GPIb-V-IX through CRISPR-Cas9 knockout generation and disease modeling: Exploring the roles of GP1BA, GP1BB, GP9 and GP5.

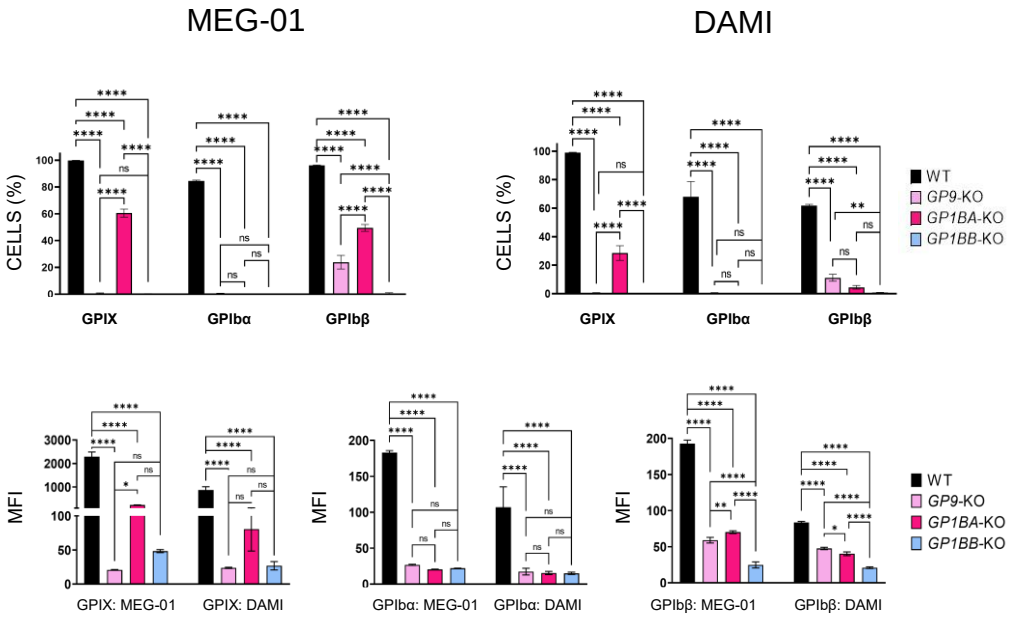

Figure 44. GPIb-V-IX expression analysis in terms of percentage and mean fluorescence intensity (MFI) in the different knock-out cellular models.

A. Flow cytometry analysis of GPIb-V-IX expression percentage for each subunit in MEG-01 (left) and DAMI (right) megakaryoblastic WT and KO cell lines. **B.** MFI comparison of GPIX (left panel), GPIbα (middle panel) and GPIbβ (right panel) subunits for MEG-01 and DAMI WT and KO cell lines. Black: WT, Pink: *GP9*-KO, Fuchsia: *GP1BA*-KO, Blue: *GP1BB*-KO. Statistical significance was assessed with ANOVA two-way plus Šídák's multiple comparisons test (ns: non-significant, ** $p < 0.01$ and **** $p < 0.0001$).

Importantly, the migration of GPIbα was completely absent in all three KO models (*GP9*-KO, *GP1BA*-KO, and *GP1BB*-KO) in both cell lines ($p<0.0001$) (**Figure 44**: **A-B**).

Regarding the GPIbβ subunit, it was not produced in both *GP1BB*-KO models, demonstrating the effectiveness of this gene-editing tool. However, as illustrated in both panels of the **Figure 44**, the GPIbβ subunit was able to migrate to the

cell membrane in *GP9*-KO (around 60.0 units vs 190.0 units and 20.0% of positive cells in MEG-01 cells and ~45.0 units vs ~85.0 units and 10% of positive cells in DAMI) and in *GP1BA*-KO (around 70.0 units vs 190.0 units and 50.0% of positive cells in MEG-01 cells and ~40.0 units vs 85.0 units and 5.0% of DAMI positive cells).

Our findings suggest that the absence of a single component of the GPIb-V-IX complex does not always prevent the other subunits from migrating to the cell membrane surface, thus confirming the varied receptor phenotypes that depend on the affected gene.

1.1.4.2. Influence of GPV to GPIbα, GPIbβ and GPIX trafficking to the outer membrane.

GPV is a component of the GPIb-V-IX receptor, which is not known to have any pathogenic variants in BSS. As a result, we turned our focus towards studying the effect of the absence of the GPV subunit in GPIb-V-IX assembly.

The data presented indicates that the absence of the GPV subunit affects the transport of GPIbβ towards the cell surface, but not GPIX or GPIbα, in both DAMI and MEG-01 cell models. In MEG-01 *GP5*-KO cells, the percentage of GPIbβ positive cells for reached 75%, while the analysis of MFI was of 462.13 units out of 733.52 units in WT, that represents 63% of GPIbβ expression levels compared to WT **Figure 45**, **A-B**. On the other hand, DAMI *GP5*-KO cells exhibited a 13% expression of GPIbβ, while MFI values reached 368.10 units

out of 609.81 units of the WT, 60% of GPIbβ expression compared to WT **Figure 45**, **A-B,** ($p<0.0001$ in all cases). In contrast, the percentage of expression and MFI values of GPIbα and GPIX were not affected by the lack of GPV (**Figure 45**, **A-B**). These results suggest that the GPV subunit exclusively participates in the migration of GPIbβ in megakaryoblastic cells, while its absence does not affect GPIbα nor GPIX migrations.

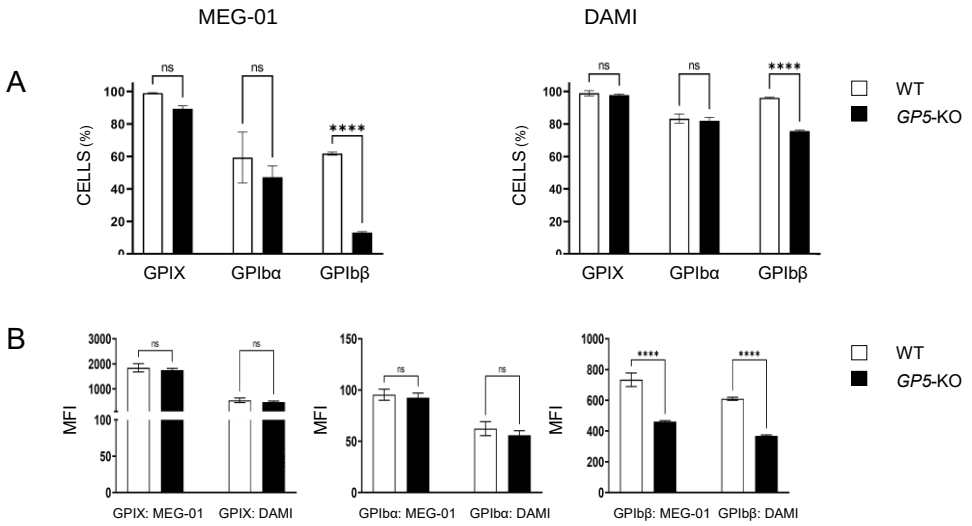

Figure 45. Surface expression comparison of GPIX, GPIbα, and GPIbβ subunits in MEG-01 and DAMI WT and GP5-KO cells.

A. Percentage of cells expressing each subunit on their surface. **B.** Mean fluorescence intensities (MFI) of cells expressing each subunit on their surface. Data represent mean ± SD for 3 independent experiments. Statistical significance was assessed with ANOVA two-way plus Šídák's multiple comparisons test (ns: non-significant and **** $p < 0.0001$).

1.1.5. Evaluation of GPIb-V-IX receptor functionality in absence of GPV.

Although there are not pathogenic variants associated to *GP5* gene in BSS, we decided to investigate GPIb-V-IX role when GPV is absent. We wondered whether the decrease of GPIbβ expression levels induced by GPV absence could affect the main role of the whole receptor recognizing and binding VWF, one of its main functions in platelets.

To evaluate it, we exposed the cells to a mixture of VWF and ristocetin. This molecule unfolds the A1 domain of VWF, transitioning to high-affinity binding for GPIbα. As shown in **Figure 46**, soluble VWF binding capacity is reduced by 28% in *GP5*-KO cells compared to WT cells ($p<0.01$). These results

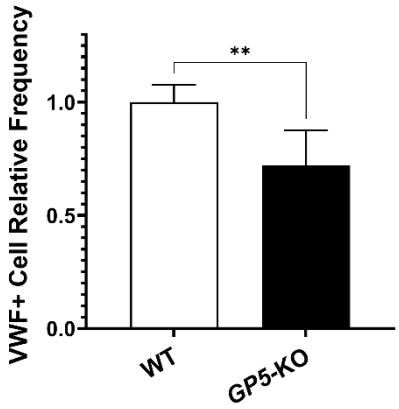

Figure 46. Binding capacity comparison to soluble VWF between WT and MEG-01 *GP5*-KO cells.

Data represent mean ± SD for 3 independent experiments. Statistical significance was assessed with two-tailed unpaired t-test to compare the means of the two groups (** $p < 0.01$).

suggest that the absence of *GP5* partially reduces the GPIb-V-IX binding capacity to VWF.

Furthermore, we also evaluated GPIbα adhesion capability to surface coated VWF. We performed VWF-coating assays in the presence of botrocetin (**Figure 47**). This molecule has been isolated from *Bothrops jararaca* snake venom and, similarly to ristocetin, induces a conformational change in VWF which promotes platelet agglutination[177].

MEG-01 WT cells, when incubated with EDTA to prevent adhesion of IIb-IIIa integrin to VWF, and botrocetin, were able to successfully attach to the well surface coated with VWF. (**Figure 47, A**). To demonstrate the specificity of this interaction, GPIbα-blocking antibody 6B4 was added[178]. In **Figure 47**- **A, left panels**, we can see that both WT and *GP5*-KO cells were able to recognize and bind to VWF, but WT cells bound more effectively than *GP5*-KO cells due to the presence of the GPV subunit. However, when these cells were incubated with a GPIbα-blocking antibody, they were unable to bind, demonstrating the specificity of the GPIbα-VWF interaction (**Figure 47**- **A, right panels)**.

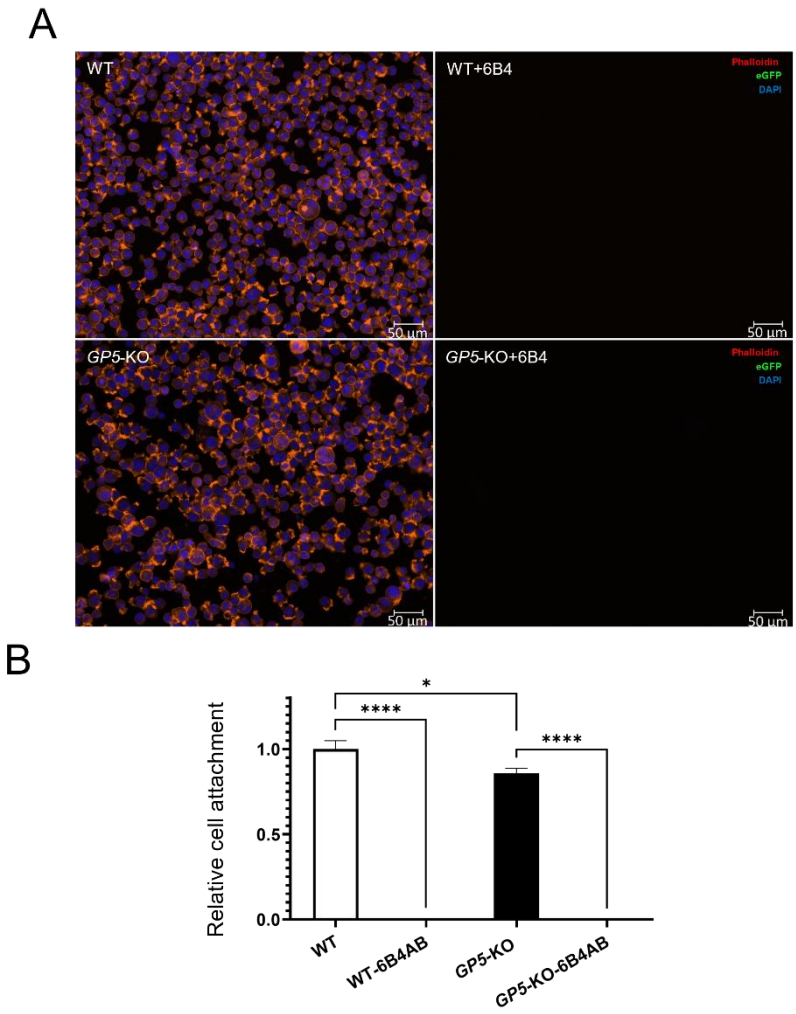

Figure 47. Evaluation of GP5-KO binding capability to surface coated VWF.

A. Immunofluorescence of cells incubated with botrocetin on a VWF coating. Merged channels of phalloidin (Red), DAPI (Blue) and eGFP (Green) can be observed when cells adhere to VWF. The first row shows the VWF-binding behavior of WT cells, WT cells incubated with 6B4, GPIbα-blocking antibody. The second row illustrates cells behavior when *GP5*-KO cells were exposed to same conditions. **B.** Binding representation. The bars represent the number of VWF-adherent cells relative to VWF-adherent WT cells. Data represent mean ± SD for 3 independent experiments. Statistical significance was assessed with ANOVA one-way plus Tukey's multiple comparisons test (ns: non-significant, * $p < 0.05$ and **** $p < 0.0001$).

In **Figure 47-panel B**, we compared the binding capabilities of the two cell lines and found statistically significant differences. Specifically, *GP5*-KO cells were less effective at binding to coated VWF than WT cells (with a binding capability of 85% compared to WT). In summary, the absence of the GPV subunit reduced the GPIb-V-IX adhesion to coated VWF. However, despite this decrease, *GP5*-KO cells still retained their binding capability.

1.1.5.1. GPIX localization in Bernard-Soulier Syndrome models and *GP5*-KO models.

Following our analysis of the migration patterns of each subunit in the absence of the others, we took a further step to determine the location of GPIX on the cell surface in all the KO models developed in this study. To achieve this goal, we employed the ImageStream platform, which allowed us to determine not only protein expression but also protein location at the single-cell level.

Accordingly, we analyzed GPIX expression in *GP5*-KO [Non-BSS phenotype], *GP1BA*-KO [BSS Type A1], *GP1BB*-KO [BSS Type B] and *GP9*-KO [BSS Type C] cell models. The results were consistent with the flow cytometry data described earlier, demonstrating that MEG-01 WT cells displayed higher levels of GPIX on the cell surface than DAMI WT cells (**Figure 48**). Additionally, GPIX expression was comparable between WT and *GP5*-KO cells. Notably, we observed a significant reduction in the transport of GPIX to the outer membrane in

GP1BA-KO cells, with only MEG-01 cells showing detectable levels. As expected, we could not observe GPIX in *GP1BB*-KO or *GP9*-KO cells, which aligns with the flow cytometry data. We also observed that CD41 was constitutively expressed on the outer membrane, indicating that the cells maintained their

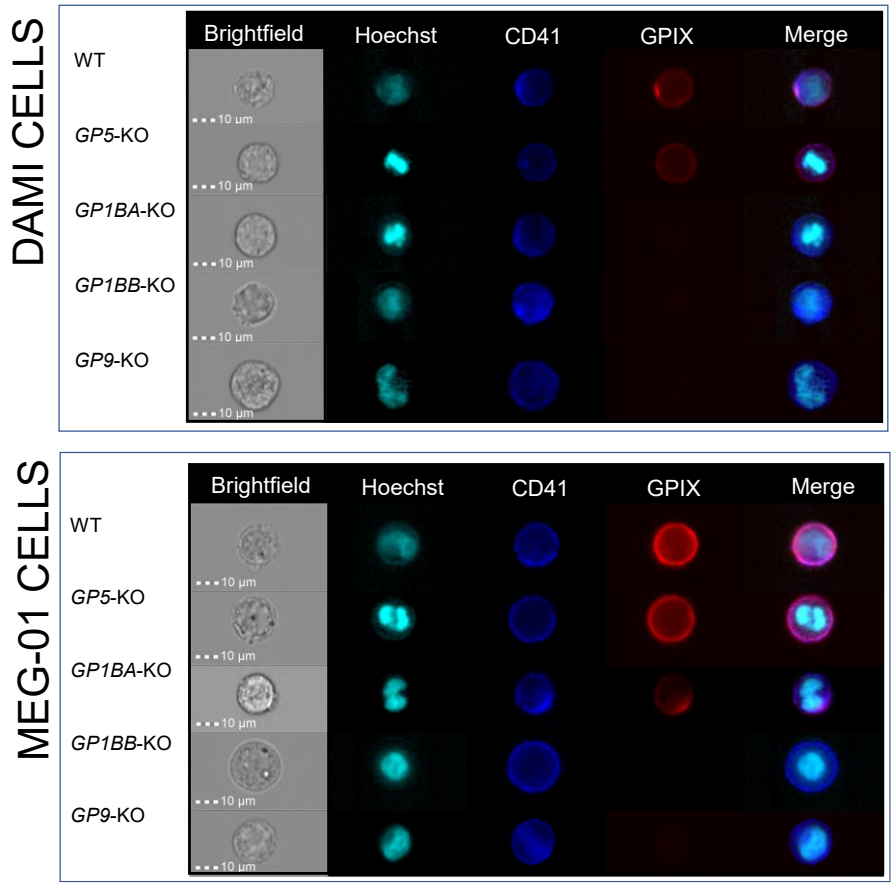

Figure 48. Representative ImageStream images of WT, GP5-KO, GP1BA-KO, GP1BB-KO and GP9-KO in both megakaryoblastic cell models.

DAMI (top) and MEG-01 (bottom) cells. Channels indicate the localization and expression levels for Hoechst (nucleic DNA, cyan), CD41 (Blue) and GPIX (Red). The last channel corresponds to the merged channels, except for the brightfield.

megakaryoblast nature despite the impairment of GPIb-V-IX complex migration (**Figure 48**).

Our investigation into BSS Type C highlighted the absence of GPIX expression on the cell membrane in both *GP9*-KO cell models (as it is shown in the **Figure 48** and **Figure 49**), resulting in a BSS-like phenotype. Consequently, these models are an excellent choice for evaluating gene therapy tools using LVs.

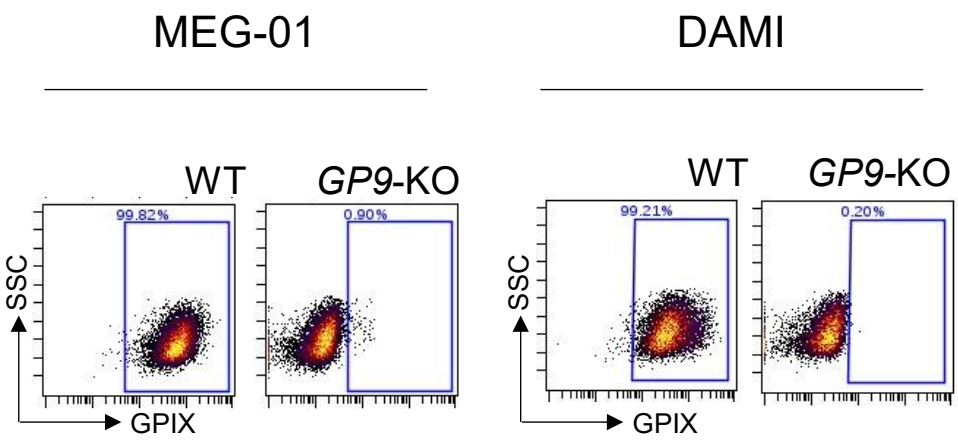

Figure 49. Absence of GPIX expression in GP9-KO cellular models.

Representative flow cytometry dot plots for GPIX expression of DAMI (top panel) and MEG-01 (bottom panel) WT and GP9-KO cells.

1.2. Generation and validation of Bernard-Soulier Syndrome Type C model in induced Pluripotent Stem Cells.

The constitutive expression of the GPIb-V-IX receptor in megakaryoblastic cells makes them a valuable tool for studying receptor biology. By creating genetic KOs, we have been able to replicate the behavior of specific mutations that affect the GPIb-V-IX receptor and simulate the characteristics of BSS. Although *GP9*-KO megakaryoblastic cells are a useful model for testing the efficacy of our gene therapy tools, which seek to restore GPIX expression and the entire receptor assembly, nevertheless, these models does not reproduce the origin of the disease.

Through a differentiation process, hematopoietic stem cells are the source of abnormal MKs and platelets, so treating them directly is essential. The reduced number of patients and the nature of the disease made it impossible to obtain bone marrow samples from which to isolate HSCs with experimental purposes. For this reason, to develop a curative and long-lasting treatment for BSS Type C, it was crucial to use an alternative model that reflects our target cells - the hematopoietic stem cells.

1.2.1. Evaluation of the effectiveness of human induced pluripotent stem cells as a tool for generating megakaryocytes and platelets.

As previously mentioned, human PSCs can differentiate from the pluripotent stage into any desired cellular type, including HSCs. In our case, we are interested in studying the manufacturing of MKs and platelets from the HSCs stage. Therefore, this cellular model can accurately mimic the entire biogenesis process, including all the epigenetic and gene-expression modifications that occur during maturation. As such, it provides a more realistic tool for studying the production of aberrant MKs and platelets, as well as the functionality of our gene-therapy tools throughout this process.

Several laboratories around the world have developed different *in vitro* megakaryocytic differentiation protocols where early mesodermal precursors, $CD34^+$ HSC, intermediate MK erythroid progenitors (MEP) ($CD34^+/CD41^+$), megakaryoblasts and fully mature MKs ($CD41^+/CD42^+$) are obtained from PSCs (as seen in the schematic view of the **Figure 50**)[164,179–181].

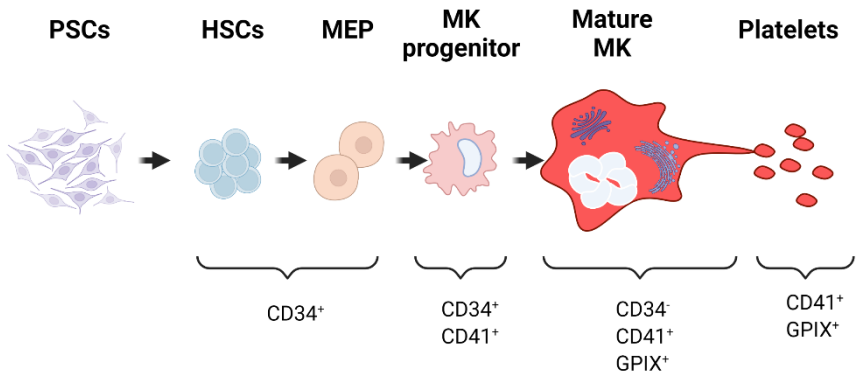

Figure 50. Schematic view of megakaryocytic differentiation process from Hematopoietic Stem Cells.

PSCs: Pluripotent Stem Cells; HSCs: hematopoietic stem Cells; MEP: megakaryocyte erythroid progenitor; MK: megakaryocyte.

In our case, the megakaryocytic differentiation of iPSCs was performed according to the protocol described by Moreau et al. [164], where pluripotent cells were differentiated towards megakaryocytic lineage by lentiviral overexpression of three essential transcription factors: *GATA1*, *FLI1*, and *TAL1*. The differentiation process was monitored by analyzing several differentiation markers during the 21-day period (**Figure 51**, **A-B**).

Throughout the differentiation process, the cells underwent dramatic morphological changes, beginning with adherent iPSCs that retained their pluripotent morphology from day 0 to day 2, and progressing to a typical mesodermal morphology from day 2 to day 7. Adherent mesodermal cells then released small suspension cells into the supernatant ($CD34^+$ HSCs), which increased in number and grew to form grape-like cell clusters from day 9 onwards. In our hands,

CD34^{+} HSC population increased from day 9 (65%) to day 15 (95%) and started to decrease as the culture aged. CD41^{+} cells emerged at day 9, firstly like CD34^{+}/CD41^{+} MEPs, that matured into megakaryoblast and mature MKs (CD41^{+}/GPIX^{+}) over

A

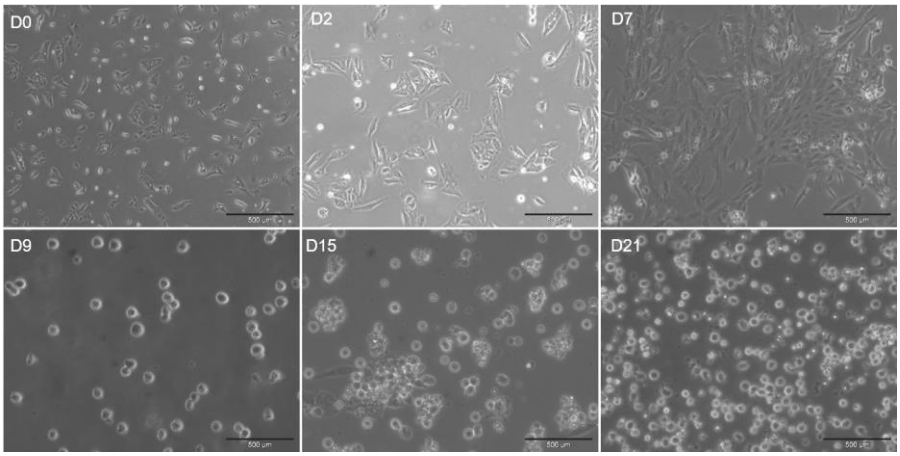

B

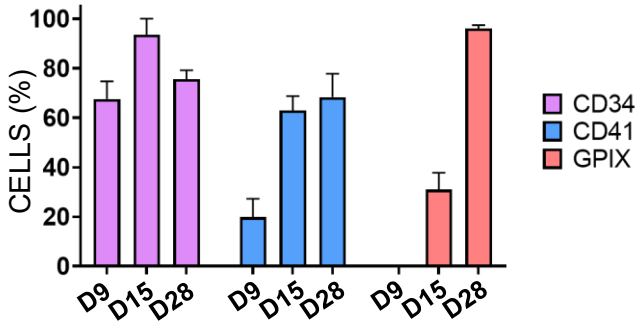

Figure 51. Morphological and phenotypical changes over the differentiation from induced pluripotent stem cells.

A. Morphological changes that cells suffer throughout 21 days *in vitro* differentiation: pluripotent morphology (D0), early mesoderm (D2), mature mesoderm (D7), primary hematopoietic stem cells (D9), megakaryocytic progenitors (D15) and mature megakaryocytes (D21). **B.** Flow cytometry analysis of CD34, CD41 and GPIX expression for 28 days differentiation from iPSCs WT.

time, reaching peak levels from day 21 onwards **(Figure 51, A-B)**. The culture could be maintained producing mature MKs and platelets for 2-3 weeks.

This iPSC model was capable of efficiently generating mature MKs and platelets, closely mimicking the differentiation process that hematopoietic stem cells undergo.

1.2.2. Creation and isolation of a Type C Bernard-Soulier Syndrome based on induced pluripotent stem cells technology.

Our next step was to create a disease model for BSS type C and assess whether it could replicate the main features of this disease: Impaired GPIX expression and giant platelets.

For this purpose, we used the CRISPR/Cas9 technology previously described. The scheme of work is illustrated in **Figure 52-A**. We introduced a CRISPR-Cas9 expressing vector, along with sgRNAs for *GP9*, into iPSCs WT by nucleofection. 48 hours later, we sorted eGFP^{+} iPSCs and cultured them in reduced cell number pools (~100 cells/pool), maintaining one with an elevated number of cells (10.000 cells), so we could estimate the efficacy of our enrichment strategy. The difficulty in this case lies in the fact that iPSCs do not express GPIX at the undifferentiated stage.

gDNA was isolated from the different pools and the *GP9* locus was amplified by PCR and sequenced to identify the pool with the highest frequency of KO alleles (**Figure 52-B**). From

a total of 14 pools of enriched eGFP^{+} cells [EP (Enrichment Pool) 1-14], the highest KO frequency was 62%, being highly superior to the general pool [GP (General Pool, 4%]. Then, we performed single cell cloning on this very enriched pool and isolated several clones.

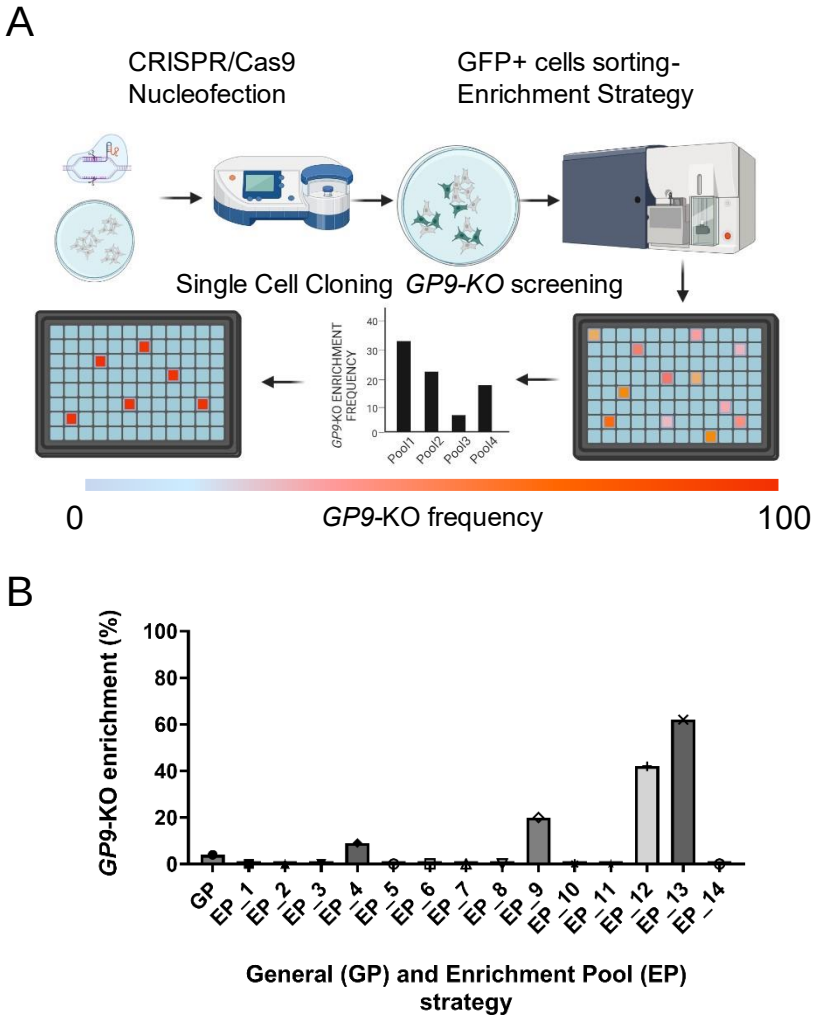

Figure 52. GP9-knockout generation and isolation from induced pluripotent stem cells.

A. Schematic view of the followed chronologic workflow to generate and isolate a *GP9*-KO clone in iPSCs. **B.** Experimental data where it is indicated the *GP9*-KO enrichment percentage that belongs to each gene-edited pool. Every column corresponds to an estimated KO percentage obtained by a bioinformatic analysis from *GP9* individual pool sanger sequencing files. GP: General Pool; EP: Enrichment Pool.

1.2.3. Characterization of the iPSC-Bernard-Soulier Syndrome Type C disease model.

To identify the *GP9*-KO clone, we performed *GP9* sanger sequencing on several clones, identifying those with frameshift mutations. We selected a *GP9*-KO case resulting from a compound heterozygous mutation affecting to the CRISPR-Cas9 cutting area. To determine single allele sequences, we used pGEM-T methodology (**pGEM®-T technique to determine allelic sequences for compound heterozygous mutations.**), which allowed us to verify single allele sequences and predict its final amino acid translation (**Figure 53, panel A**), resulting in the generation of a premature stop codon for both alleles. In detail:

-Allele 1 has two different mutations: A substitution of adenine (A) with cytosine (C) at position 191, replacing glutamine (Gln) with proline (Pro) at position 64 out of 206. A microdeletion of the sequence between positions 192 and 195, that results in a missense mutation that replaces serine (Ser) with cysteine (Cys) at position 65 out of 177 and introduce a frameshift mutation that creates a premature stop codon 17 amino acids downstream.

-Allele 2 carries a microdeletion of the sequence between positions 188 and 200, that results in a missense mutation that replaces leucine (Leu) with proline (Pro) at position 63 out of 177 and introduce a frameshift mutation that creates a premature stop codon 16 amino acids downstream.

From the original 177 amino acids full-length GPIX protein, we generated gene-edited alleles that codified for 66 and 80 amino acid-interrupted GPIX proteins, where the leucine-rich region associated with the extracellular domain

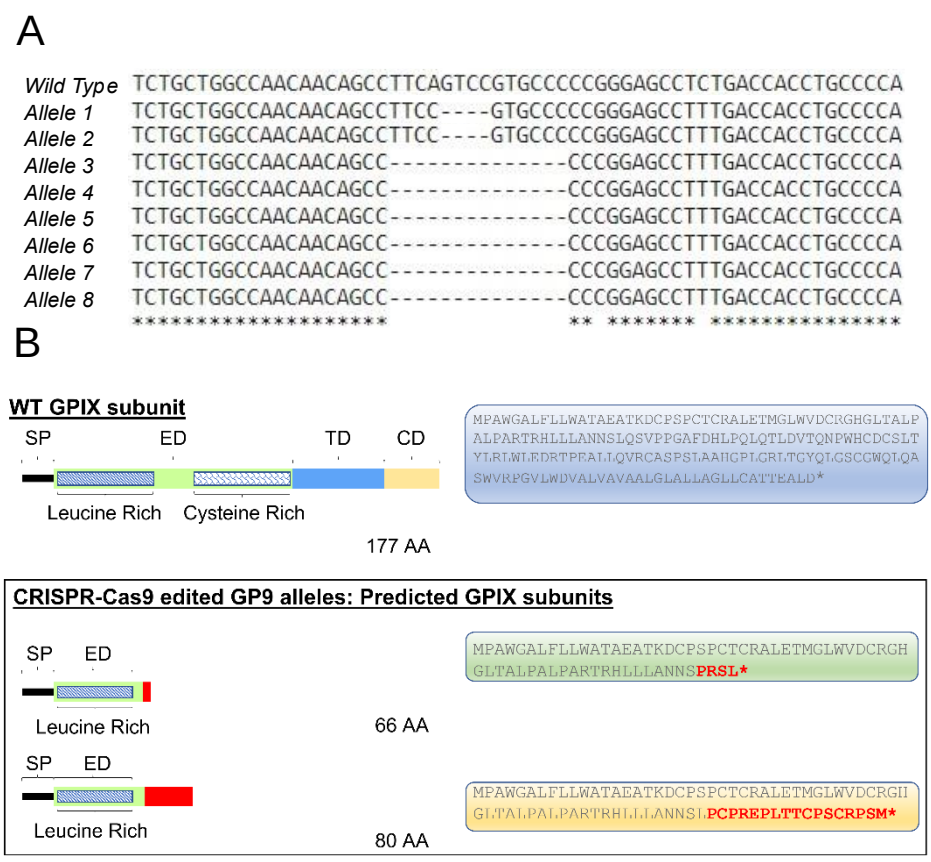

Figure 53. iPSCs *GP9*-KO clone characterization.

A. Local alignment (ClustalW) of *GP9* WT allele versus CRISPR-Cas9 heterozygous derived alleles. * means nucleotide conservation; - means nucleotide disruption. **B.** Comparison of GPIX-WT protein and *in silico* predicted proteins translated from each single edited allele. Protein length and structure is indicated (SP-signal peptide; ED-extracellular domain; TD-transmembrane domain; CD- cytosolic domain). * means stop codon. Non-conserved protein structure and amino acid sequences are highlighted in red.

was disrupted. Therefore, we predicted the generation of a KO *in silico* (**Figure 53, panel B**).

1.2.4. Functional validation of the Bernard-Soulier Syndrome Type C disease model.

After this *in silico* prediction, we had to confirm this phenotype *in vitro*. iPSCs were differentiated into MKs and platelets and analyzed by flow cytometry, demonstrating the lack of GPIX after 21 and 36 days for MKs (**Figure 54**, **panel A**) and platelets (**Figure 55**, **panel A**), respectively. GPIX^{+} populations were ~90% for WT and totally absent for *GP9*-KO iPSC derivatives (**Figure 54 & Figure 55, B panels**).

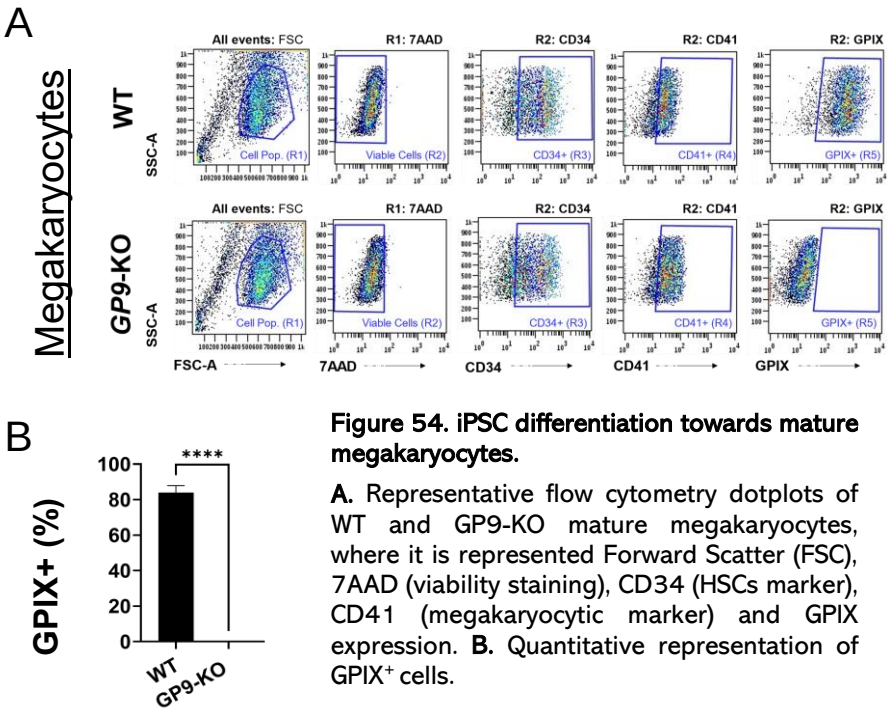

Figure 54. iPSC differentiation towards mature megakaryocytes.

A. Representative flow cytometry dotplots of WT and GP9-KO mature megakaryocytes, where it is represented Forward Scatter (FSC), 7AAD (viability staining), CD34 (HSCs marker), CD41 (megakaryocytic marker) and GPIX expression. **B.** Quantitative representation of GPIX^{+} cells.

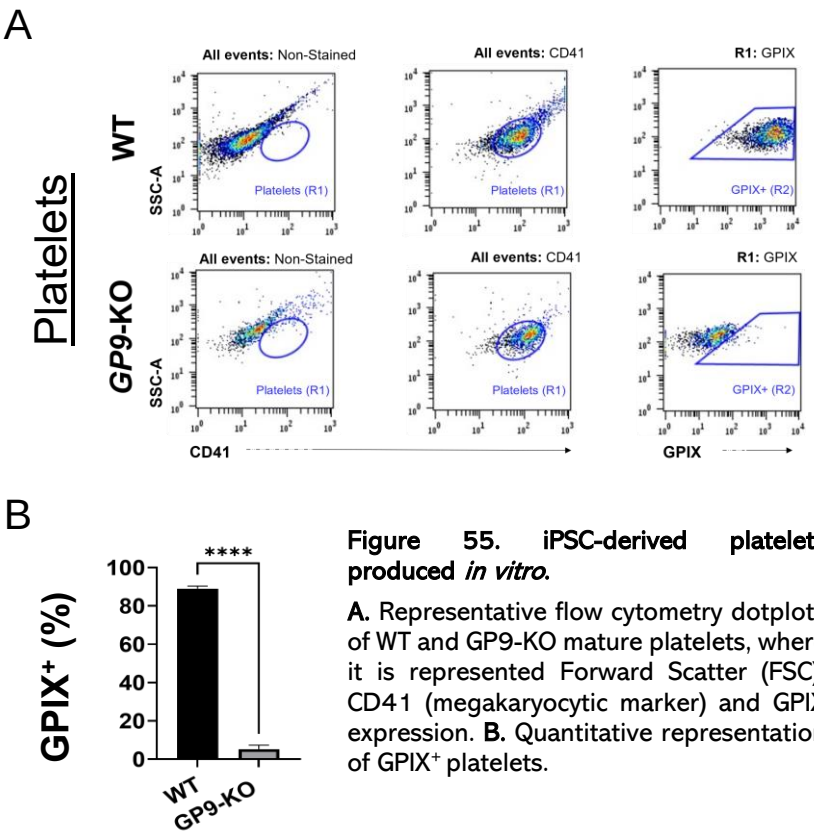

Figure 55. iPSC-derived platelets produced *in vitro*.

A. Representative flow cytometry dotplots of WT and GP9-KO mature platelets, where it is represented Forward Scatter (FSC), CD41 (megakaryocytic marker) and GPIX expression. **B.** Quantitative representation of GPIX$^+$ platelets.

One of the most typical signs of BSS is macrothrombocytopenia, which refers to a low platelet count but with large platelet size. We then analyzed platelets phenotype using ImageStream. This technique allowed us to capture an image of each individual event, so we were able to observe not only the fluorescence signal but also the platelet size.

Objective 1: Investigate the assembly of GPIb-V-IX through CRISPR-Cas9 knockout generation and disease modeling: Exploring the roles of GP1BA, GP1BB, GP9 and GP5.

The platelets generated from *in vitro* cultured iPSCs were slightly smaller than human platelets, but they co-expressed mature surface platelet markers, CD41 and GPIX (**Figure 56**). Interestingly, platelets generated from *GP9*-KO cells exhibited a larger size and the absence of GPIX, confirming the BSS phenotype and demonstrating the potential of iPSCs as a disease model to replicate the biological origin of BSS from HSCs. The creation of this disease model would allow us to evaluate how the expression of our lentiviral construct is affected throughout a differentiation process.

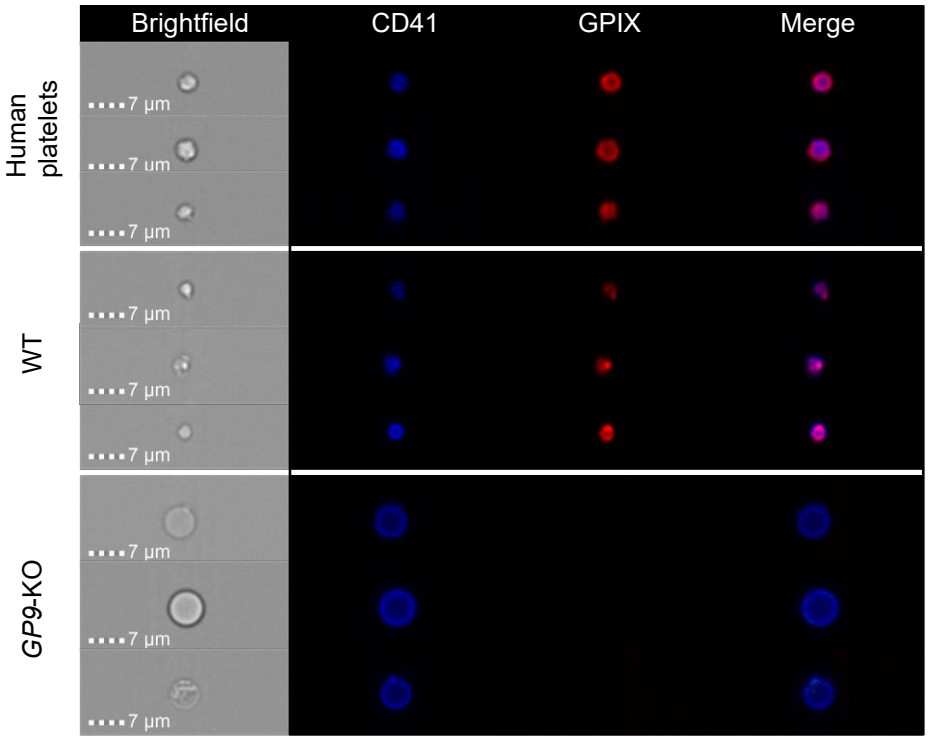

Figure 56. Representative ImageStream images of human platelets and platelets generated from iPSCs.

Platelets derived from WT and *GP9*-KO models showing their size, CD41 (Blue) and GPIX (Red) surface expression in each case and merged channel.

2. *Objective 2: Design and development of reporter and therapeutic GPIX-lentiviral vectors able to rescue GPIX expression and complex functionality in megakaryoblastic KO models.*

LVs are powerful tools for expressing an exogenous gene into the genome of a host cell. They are one of the most successful therapies among gene therapy treatments and are perfect candidates to treat different HSCs malignancies[115]. The aim of this study is to develop a curative treatment for BSS type C. According to its monogenic cause and *GP9* DNA length, this disease is a perfect candidate for LV-gene therapy curative treatment.

Consequently, our first aim was to develop LVs that correct GPIX deficiency by the overexpression of WT human *GP9*. In addition, restricting its expression to the megakaryocytic lineage was a prerequisite in order to approach our strategy to the clinical practice. For this reason, we studied the behavior of 3 different well-characterized MK-specific promoters: *mPf4*, *hGP6* and *hGP9*[182].

2.1. Design and development of GPIX lentiviral vectors.

2.1.1. Selection of a tissue-specific promoter for megakaryocytic gene expression.

To determine which tissue-specific promoters were most effective for our gene therapy strategy, we investigated the expression of eGFP in megakaryoblastic cellular model DAMI. Cells were transduced with pRRL-lentiviral vectors carrying these different promoters and found that eGFP expression under the *hGP9* promoter was the least functional, reaching low MFI levels (**Figure 57; A-B**). However, MFI levels were similar between the *mPf4* and *hGP6* promoters, with a much higher percentage of transduced cells under the *hGP6* promoter. Due to its human origin, smaller size, and higher percentage of transduced cells, we selected the *hGP6* promoter as our preferred promoter for the development of GPIX gene therapy tools.

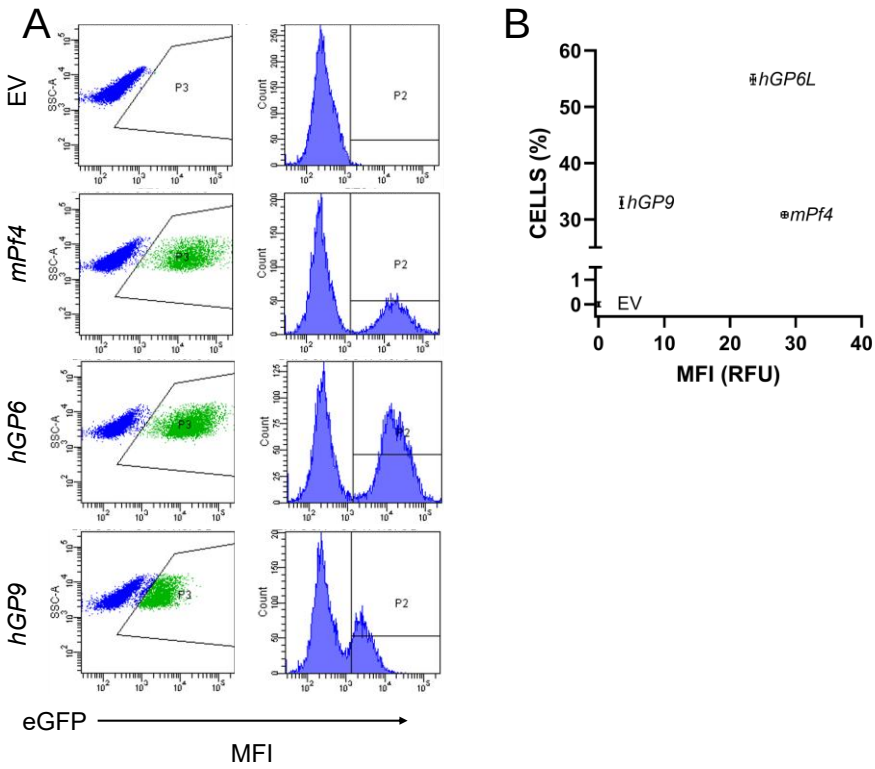

Figure 57. Comparison of megakaryocytic promoters.

A. Representative flow cytometry dot plot comparison of DAMI cells transduced with different LVs. Each LV express eGFP under the regulation of three different megakaryocytic (*mPF4*, *hGP6* and *hGP9*). Right dotplots indicate the percentage (%) of eGFP positive cells and left dotplots indicate Mean Fluorescence Intensities (MFI) of eGFP signal. **B.** % of positive cells *vs.* MFI representation of these three different promoters.

2.1.2. Generation of the therapeutic cassette *hGP6*(p)-*GP9*.

Therefore, we designed a therapeutic cassette consisting of *hGP6L*(p) followed by the complete WT CDS of human *GP9* (*hGP9*). Modified primers containing compatible RE sites were used to amplify both *hGP6L*(p) and h*GP9* sequences, as described in "**Primer design and PCR reaction."**. After RE digestion of the amplified sequences to create compatible ends and subsequent ligation, we performed a new PCR amplification of the fully ligated product. This new transgene was then cloned into an intermediate vector, increasing the number of RE sites flanking our transgene and facilitating the cloning process.

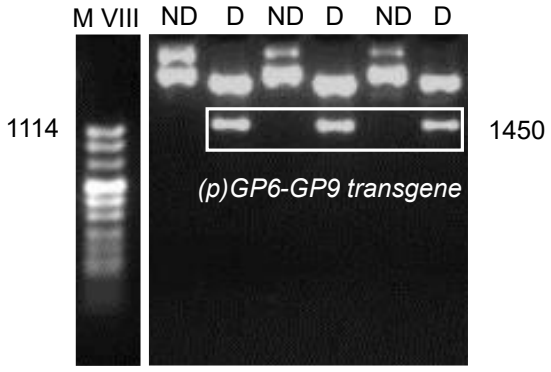

Figure 58. Colony analysis of intermediate vectors.

Agarose gel with non-digested (ND) and digested (D) plasmid harboring *hGP6*(p)-*GP9* transgene of 1450bp length. MVIII (DNA molecular weight marker VIII).

The product resulting from the digestion of the plasmid with transgene-flanking enzymes revealed that it had an approximate length of 1450 bp, which was the sum of both individual sequences (h*GP6*(p) and h*GP9*) (**Figure 58**). Then,

to confirm this result, the construct was validated by Sanger sequencing.

2.1.3. Development and construction of diverse designs for therapeutic and reporter vectors.

Looking into our final LV gene-therapy constructs, we designed two distinct LVs that we would employ with different purposes. On one hand, we created a Reporter Vector (R-GPIX), with final purpose of achieving a co-expression of eGFP together with GPIX, so we could evaluate how effective was the transduction according to eGFP levels. On the other hand, and with a clinical purpose, we designed a therapeutic vector (T-GPIX) that would correct GPIX deficiency without any reporter protein, something necessary for the clinical practice.

To create the R-GPIX vector, we used the SE-IS2-GFP^{+} LV as backbone [176]. As mentioned above, this LV harbors a SFFV(p)-eGFP cassette. In this case, we could check the cell transduction in megakaryocytic and non-megakaryocytic lineages due to its SFFV constitutive promoter. For the T-GPIX vector, the SFFV-eGFP cassette was removed from the R-GPIX. In both cases, our LV backbones included an insulator sequence (SAR2-HS 650) that prevents epigenetic silencing after genomic integration[176]. As shown in **Figure 59,** we used these backbones (Reporter Empty Vector harboring SFFV(p)-eGFP cassette (R-EV) and a Therapeutic Empty Vector (T-EV), respectively) as negative controls.

Objective 2: Design and development of reporter and therapeutic GPIX-lentiviral vectors able to rescue GPIX expression and complex functionality in megakaryoblastic KO models.

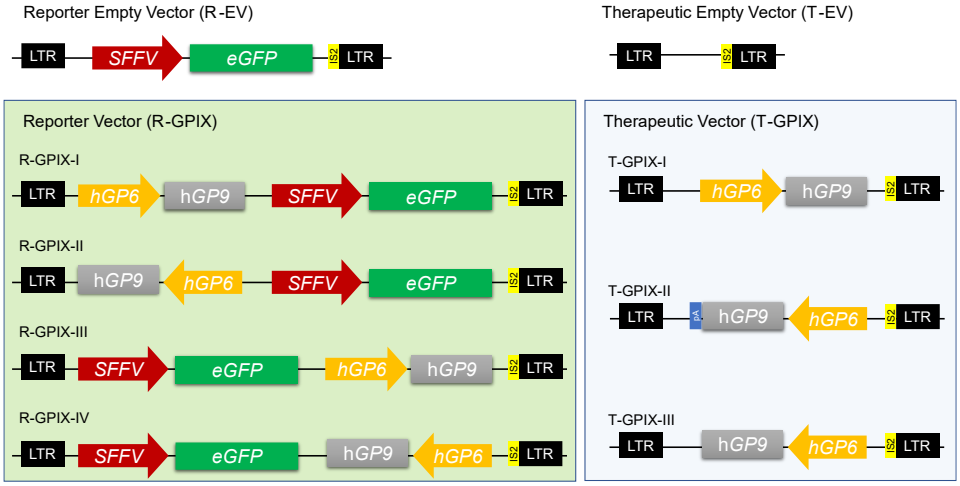

Figure 59. Schematic view of all lentiviral vector designs.

Left panel illustrates on the top the reporter empty vector (R-EV) , and all the designs based on the co-expression of GPIX and eGFP (R-GPIX), alternating the position and orientation of the therapeutic cassette (h*GP6*-GP9) respect the reporter cassette (SFFV-eGFP). Right panel shows the therapeutic empty vector (T-EV) and all the possible combinations based on the orientation of the therapeutic cassette. LTR: Long Terminal Repeat; SFFV: Spleen Forming Focus Virus; IS2: Insulator 2; eGFP: enhanced Green Fluorescent Protein; pA: polyA tail.

Several LV vectors were developed using these two backbones (R-EV and T-EV). Our objective was to assess the best GPIX expression in different designs based on the orientation and relative position of the therapeutic cassette in relation to the reporter cassette for R-GPIX (**Figure 59-Left**). In the case of the T-GPIX we designed both possible orientations of the cassette. Additionally, we also incorporated a polyA tail in the 3'-5' orientation to enhance its translation to protein. We avoided including this sequence in the 5'-3' orientation since the LTR already contains a polyA tail, and

adding an additional one would disrupt its function (**Figure 59-Right)**.

Then, we performed confirmation digestions using *PvuI* and *NcoI* REs (refer to **Figure 60**). These enzymes were chosen for their ability to generate different cuts within and outside of the therapeutic cassette. Depending on the location and orientation of the cassette with respect to the reporter cassette, different digestion patterns were observed, confirming each construction. The resulting digestion patterns confirmed the successful cloning, and we subsequently carried out Sanger sequencing and LV production for each construct.

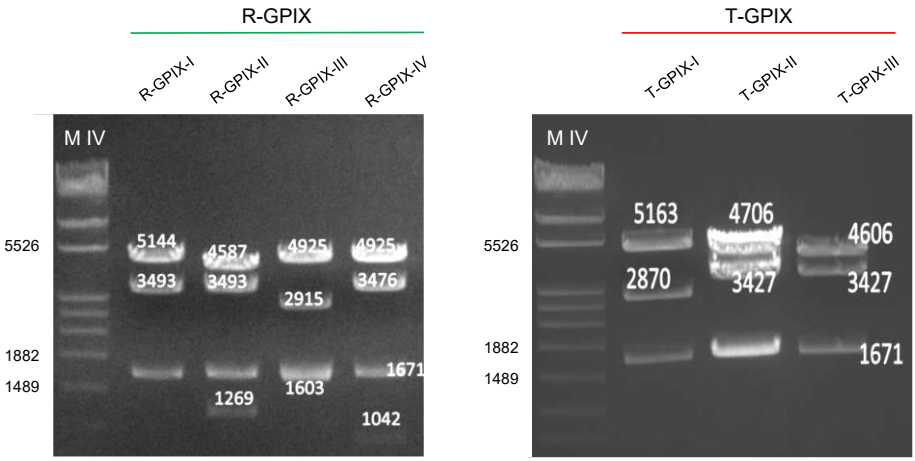

Figure 60. Digestion patterns of built LVs.

Agarose gels showing the resulting bands released from the confirmation digestions for each possible design, R-GPIX (left gel) and T-GPIX (right gel), using the *PvuI* and *NcoI* restriction enzymes.

2.1.4. Functional evaluation of the different lentiviral vector designs in a *GP9*-KO megakaryoblastic model.

We assessed the efficacy of GPIX recovery for each R-GPIX and T-GPIX construct by using DAMI *GP9*-KO cells, which lack GPIX expression. Megakaryocytic background of the cells allowed functional LVs to restore GPIX expression. Additionally, reporter vectors should co-express eGFP, demonstrating their suitability for co-expressing both proteins and enabling transduction tracking via eGFP.

Figure 61 illustrates the expression patterns for each construct. **For R-GPIX**, with same LV titer, all of our constructs expressed eGFP to a high percentage, but the MFI was higher in cases where the therapeutic cassette preceded the reporter cassette. Interestingly, we observed a clear position effect on GPIX expression. When the therapeutic cassette preceded the reporter cassette, GPIX expression was observable, but it was not detectable when the order was reversed. Furthermore, we noted that the orientation of the therapeutic cassette affected GPIX expression. When the cassette was in the positive strand, expression was lower, whereas when it was in the antisense orientation, GPIX expression was clearly superior (17.50% *vs.* 64.83%).

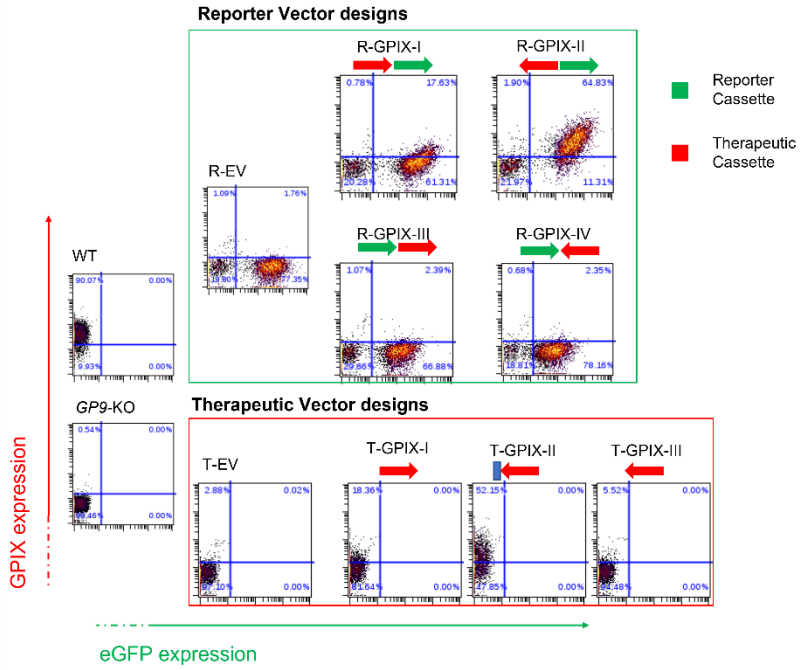

Figure 61. Analysis of the different lentiviral constructs by flow cytometry.

Representative flow cytometry dot plots whose belongs to DAMI WT, GP9-KO and GP9-KO cells transduced with all the designed lentiviral vectors. Top panel shows R-EV and the four R-GPIX designs. Bottom panel shows T-EV and the three-design tested. Flow cytometry dot plots show double positive populations for GPIX (Y-axis) and eGFP (X-axis).

For T-GPIX constructs, as expected, eGFP expression was not detectable. We observed different percentages of GPIX expression depending on the orientation of the therapeutic cassette (18.00% *vs.* 5.52% for positive and negative strands, respectively). However, to improve GPIX expression in our therapeutic design, we incorporated a poly-A tail sequence in the antisense orientation (T-GPIX-II), and we observed a clear improvement in GPIX expression, achieving levels similar to those of the best R-GPIX LV (R-GPIX-II).

Based on these data, we selected the lentiviral designs summarized in **Figure 62**, which produced the most effective GPIX expression when the therapeutic cassette was in the antisense orientation for both T-GPIX and R-GPIX constructs. In the case of R-GPIX LVs, the therapeutic cassette was more effective when positioned before the reporter cassette. In the case of our T-GPIX design, the incorporation of a polyA tail sequence improved GPIX expression. We continued our research with these sets of vectors.

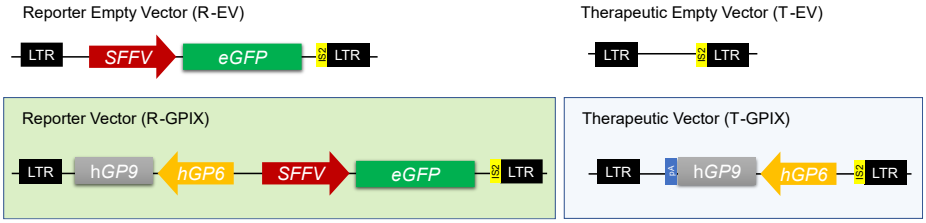

Figure 62. Schematic representation of selected lentiviral vectors.

The Reporter Empty Vector (R-EV), the Therapeutic Empty Vector (T-EV), and the chosen lentiviral vectors that can express GPIX therapeutically (T-GPIX; Therapeutic Vector) or co-express it with eGFP (R-GPIX; Reporter Vector).

2.1.5. Functional evaluation of selected designs in cell lines with non-megakaryoblastic background.

The next phase of our research involved investigating the specificity of LVs in various human cell lines that were not of megakaryocytic origin. We transduced 293-T (embryonic kidney cells), THP-1 (monocytic origin), and Jurkat (lymphocytic origin) cell lines with our four LV vectors (**Figure 63** for the Reporter LV and **Figure 64** for the Therapeutic LV).

We analyzed eGFP and GPIX expression in these cells using flow cytometry over a period of 28 days. As expected, eGFP expression was detected in all three cell lines transduced with R-EV or R-GPIX vectors due to the constitutive SFFV(p)-eGFP regulation, and it remained stable throughout the period of analysis. However, we observed no expression of GPIX on the cell membrane after transduction with R-GPIX or T-GPIX. This indicates that the synthesis, transport, and location of GPIX on the plasma membrane require recognition of the megakaryocytic-specific promoter *hGP6L* and/or the presence of the remaining subunits of the GPIb-V-IX complex.

Objective 2: Design and development of reporter and therapeutic GPIX-lentiviral vectors able to rescue GPIX expression and complex functionality in megakaryoblastic KO models.

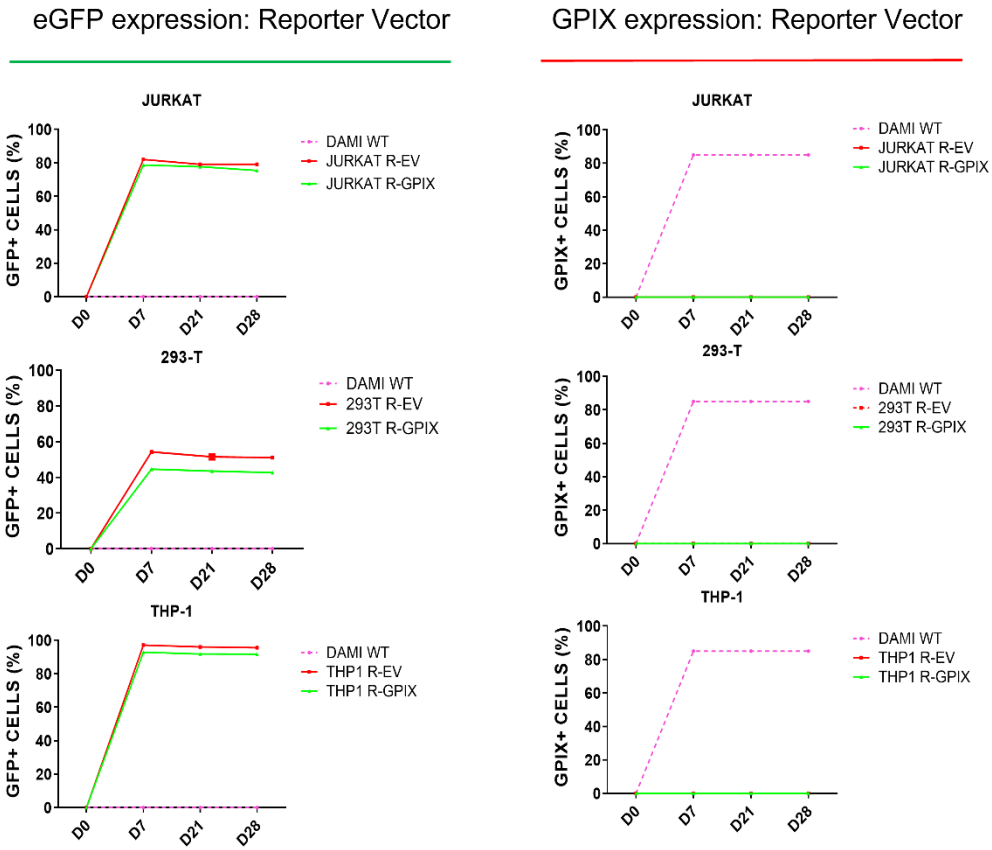

Figure 63. Analysis of tissue specific expression of GPIX after R-GPIX LVs transduction.

Evaluation of eGFP constitutive expression and GPIX tissue specific expression in four cell lines from different lineages transduced with R-EV and R-GPIX and compared with DAMI WT cells (pink). Cell lines analyzed: Jurkat (lymphocytic lineage), THP-1 (monocytic lineage) and 293-T cells (embryonic kidney).

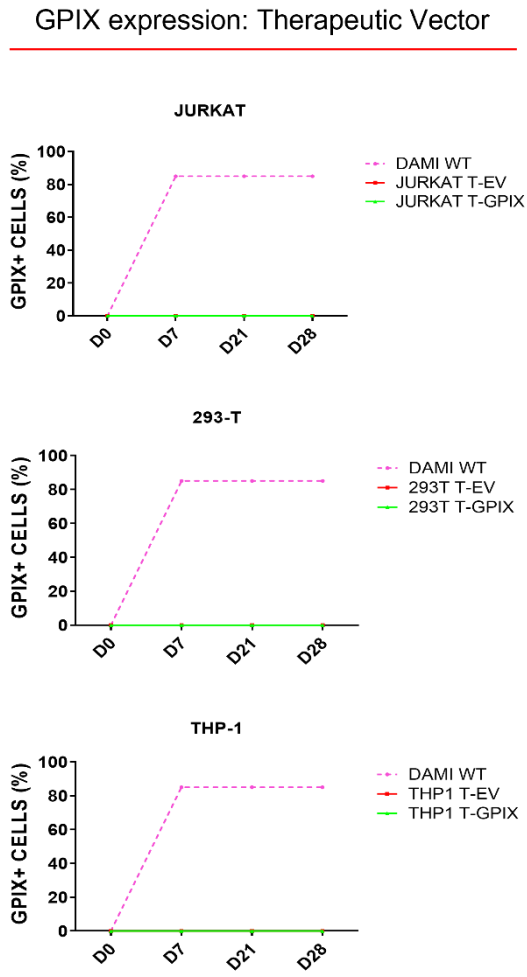

Figure 64. Analysis of tissue specific expression of GPIX after T-GPIX LV transduction.

Evaluation of GPIX tissue specific expression in four cell lines from different lineages transduced with T-EV and T-GPIX LVs and compared to DAMI WT cells (pink). Cell lines analyzed: Jurkat (lymphocytic lineage), THP-1 (monocytic lineage) and 293-T cells (embryonic kidney).

2.2. Genetic rescue of GP9-KO cellular models by GPIX-lentiviral transduction.

The development and identification of our GPIX-expressing LVs led us to test their functionality in *GP9*-KO disease models generated in the previous research objectives. Specifically, we assessed their ability to rescue GPIX expression in DAMI *GP9*-KO and MEG-01 *GP9*-KO cells, which are two different types of megakaryoblastic cell lines. The genetic correction of GPIX expression in both cellular models would confirm the suitability of our gene therapy tools for reversing GPIX expression in a megakaryoblastic background.

Moreover, if exogenous GPIX expression was achieved, we could confirm whether it can assemble with other components of the GPIb-V-IX receptor, and determine whether VWF-binding capability is regained, thus correcting the receptor functionality *in vitro*. This would represent a major step towards developing an effective gene therapy for BSS type C.

In addition, we have developed an iPSC-based disease model that accurately reproduces main BSS characteristics. Using our GPIX LVs to correct the *GP9*-KO mutation in this model would provide further evidence of the LVs suitability for reversing the disease characteristics, including the large size

and GPIX location, and ultimately addressing the underlying biology of the disease.

2.2.1. Analysis of GPIX expression in WT, *GP9*-KO and *GP9*-KO megakaryoblastic transduced cells.

2.2.1.1. Evaluation of GPIX stability over one month period post-transduction in DAMI *GP9*-KO cells.

As demonstrated, we utilized DAMI *GP9*-KO as a cellular tool to screen LVs expressing GPIX. However, we proceeded to analyze the genetic stability of GPIX expression over 28 days for all four LVs (**Figure 65**). Throughout the analysis (day 7 to day 28), we observed a relatively high and stable transduction of the reporter vectors, with approximately ~80% eGFP of positive cells and 750 units of MFI in both R-EV and R-GPIX (**Figure 65, panel A**).

Predictably, only R-GPIX successfully restored GPIX expression, reaching ~50% and ~170 units on day 7, and demonstrating a progressive increase in GPIX expression over time (~75% of positive cells and 830 units on day 28) (**Figure 65**, **A**). Likewise, the T-GPIX vector gradually restored GPIX expression, increasing from 40% to 52%, and finally to 73% ($p<0.05$) over time, with their correspondent MFI values of 130, 180 and 600 MFI units, respectively. In contrast, the T-EV did not recover GPIX expression (**Figure 65**, **B**). Furthermore, neither T-EV nor T-GPIX expressed eGFP.

Objective 2: Design and development of reporter and therapeutic GPIX-lentiviral vectors able to rescue GPIX expression and complex functionality in megakaryoblastic KO models.

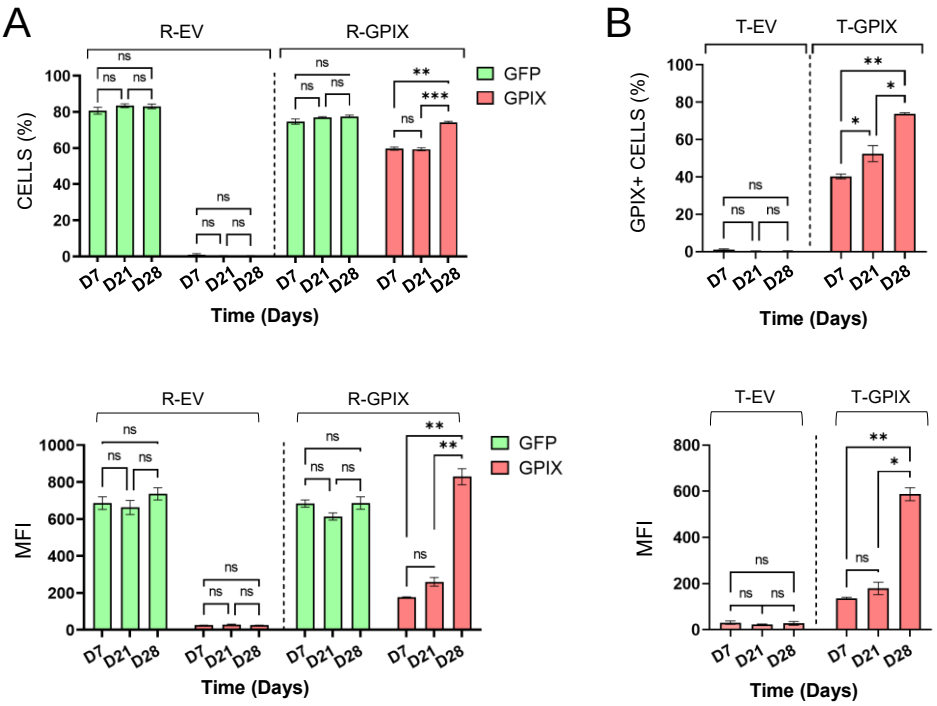

Figure 65. Evaluation of eGFP and GPIX expression and stability over 28 days.

A. Percentages of eGFP (Green bars) and GPIX (Red bars) positive cells and MFI values for DAMI *GP9*-KO transduced with R-EV and R-GPIX. **B.** Percentages of GPIX positive cells and MFI values for DAMI *GP9*-KO transduced with T-EV and T-GPIX. ns: non-significant; * p<0.05; **p<0.01; ***p<0.001.

2.2.1.2. Endpoint GPIX expression analysis in MEG-01 *GP9*-KO cells.

We also evaluated the effects of LVs in MEG-01 *GP9*-KO cells, as shown in **Figure 66**. After 28 days of analysis, we observed a high transduction efficiency (98% eGFP expression) for both R-GPIX and R-EV constructs. Interestingly, the MFI ratio value was higher for R-GPIX than R-EV, with values of 1.2 and 1.0, respectively (**Figure 66, A**).

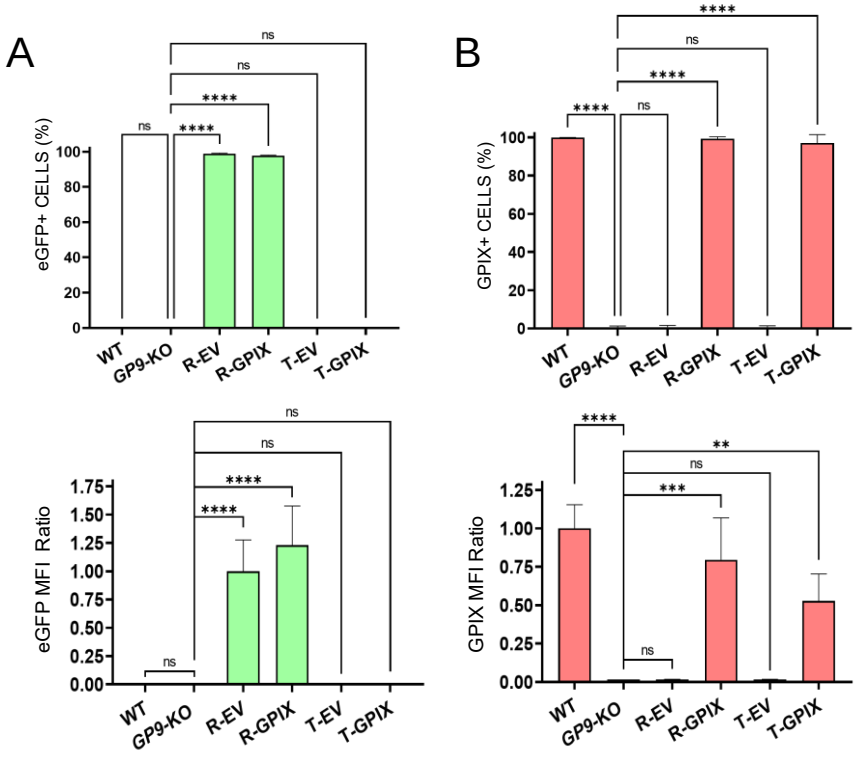

Figure 66. Evaluation of eGFP and GPIX expression levels in MEG-01 WT, *GP9*-KO and *GP9*-KO transduced with R-EV, R-GPIX, T-EV and T-GPIX.at day 28 post transduction.

A. Percentages (%) of eGFP (Green bars) positive cells and MFI ratio respect R-EV levels. **B.** Percentages (%) of GPIX (Red bars) positive cells and MFI ratio values respect MEG-WT. ns: non-significant; * p<0.05; **p<0.01; ***p<0.001; **** p<0.0001.

Moreover, we found that the GPIX expression rate was excellent in both R-GPIX and T-GPIX vectors, achieving about 98%. We calculated the ratios relativized to WT and obtained values of 0.75 and 0.55, respectively, demonstrating the effectiveness of these LVs. However, as expected, both R-EV and T-EV constructs did not recover GPIX expression, as shown in **Figure 66, B**.

2.2.1.3. Analysis of GPIbα externalization in the presence of exogenous GPIX: Reassembly of GPIb-V-IX.

Then, we investigated whether genetic rescue of GPIX in these BSS models restored the externalization of GPIbα, which contains the VWF domain, responsible for the receptor's binding capacity. **Figure 67** depicts GPIX (**left**) and GPIbα (**right**) protein levels for MEG-01 WT, *GP9*-KO and *GP9*-KO transduced with each LV. When *GP9*-KO cells were transduced with R-EV or T-EV, GPIX nor GPIbα could not be detected. However, when the BSS model was transduced with R-GPIX or T-GPIX, exogenous GPIX is expressed, and, consequently, GPIbα was restored to the surface, indicating that exogenous GPIX assembled with the other components of the receptor, and the full complex was repositioned on the surface, recovering its natural conformation.

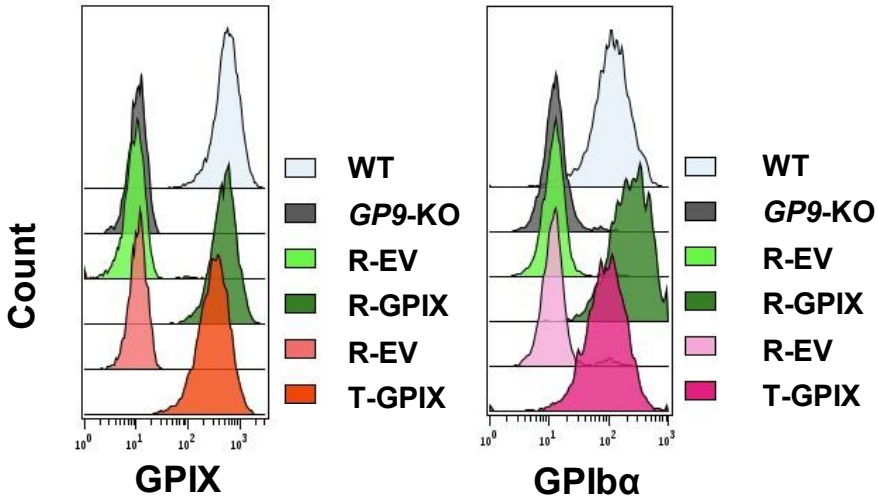

Figure 67. Overlapped histograms showing GPIX and GPIbα levels for MEG-01 WT, *GP9*-KO and *GP9*-KO transduced cells with R-EV, R-GPIX, T-EV and T-GPIX.

2.2.1.4. Determination of genetically rescued GPIX subunit localization in the plasma membrane.

Finally, we evaluated the expression and localization of GPIX in both *GP9*-KO cell models following lentiviral transduction using the ImageStream platform (**Figure 68; A-B**). DAMI and MEG-01 *GP9*-KO cells transduced with R-EV and R-GPIX constructs displayed a homogenous nuclear and cytosolic expression of eGFP. However, only the cells transduced with R-GPIX restored GPIX expression, which was localized in the plasmatic membrane like in DAMI and MEG-01 WT cells. Similarly, when DAMI and MEG-01 *GP9*-KO cells were transduced with T-GPIX, they regained the natural expression and distribution of GPIX all over the cell surface.

Objective 2: Design and development of reporter and therapeutic GPIX-lentiviral vectors able to rescue GPIX expression and complex functionality in megakaryoblastic KO models.

DAMI CELLS

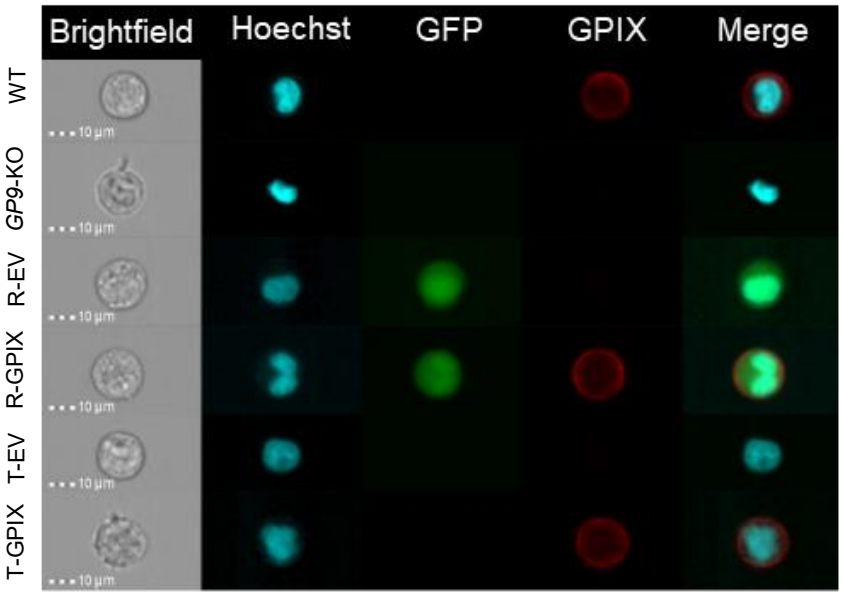

MEG-01 CELLS

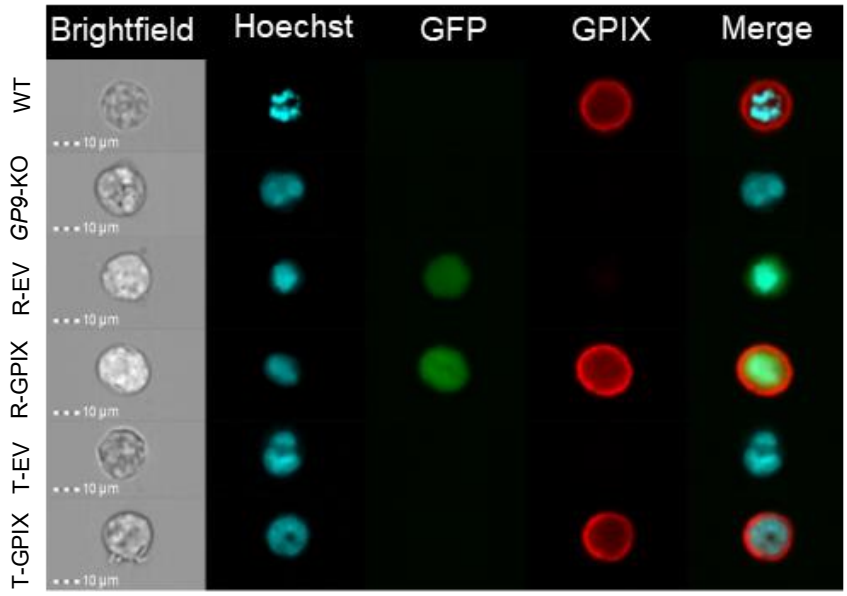

Figure 68. Lentiviral vectors restore GPIX expression in plasma membrane.

Representative single-cell images taken by ImageStream of WT, *GP9*-KO and *GP9*-KO cells transduced with R-EV, R-GPIX, T-EV and T-GPIX for DAMI (A) and MEG-01 (B). Channels indicate the localization and expression levels for Hoechst (nucleic DNA, cyan), eGFP (Green) and GPIX (Red). The last channel corresponds to the merged channels, except for the brightfield.

Taken together, our results demonstrate that our lentiviral constructs are tissue-specific, allowing GPIX expression in the megakaryocytic lineage. Furthermore, these gene therapy tools successfully restored the localization and WT expression levels of GPIX in *GP9*-KO megakaryoblastic BSS cellular models.

2.3. Analysis of GPIb-V-IX complex functionality in WT, GP9-KO and GP9-KO megakaryoblastic transduced cells.

As described before, it is well characterized that one of the most important GPIb-V-IX functions lies in its ability to bind VWF. GPIbα harbors an extracellular VWF-binding domain and is the responsible subunit to stablish the GPIb-V-IX/VWF interaction. The absence of GPIbβ or GPIX subunits lead to GPIbα disappearance from cell surface in DAMI and MEG-01 KO-models reproducing BSS phenotype.

In the previous subobjective "**2.2. Genetic rescue of *GP9-KO* cellular models by GPIX-lentiviral transduction.**", we demonstrated the significant impact of our LVs in rescuing GPIX expression in megakaryoblastic *GP9*-KO models. However, to provide conclusive evidence that this genetic rescue not only restores subunit expression, localization and proper assemblage with other components of the complex, it is essential to investigate whether the full receptor regains its functionality. For this reason, it is necessary to verify that our rescued GPIb-V-IX complex can recognize VWF in the same way than the original WT complex, so we would be recovering its natural functionality as well.

2.3.1. Comparison of GPIbα surface protein levels between MEG-01 and DAMI cells.

To assess the role of the GPIbα subunit in recognizing VWF, we analyzed GPIbα expression levels and localization in WT and *GP9*-KO cells using flow cytometry and ImageStream (**Figure 69** and **Figure 70**). Thus, we compared the MFI and cell percentage of GPIbα in DAMI and MEG-01 cellular models (**Figure 69**). Notably, MEG-01 WT cells displayed the highest MFI and percentage values via conventional flow cytometry, as well as a clear distribution of GPIbα in the plasma membrane by ImageStream compared to DAMI WT cells (**Figure 70**). In contrast, both *GP9*-KO BSS cellular models lacked GPIbα expression on their cell surface. Thus, due to the higher expression levels of GPIbα in MEG-01 cells, we considered them to be the optimal model for testing VWF binding capacity.

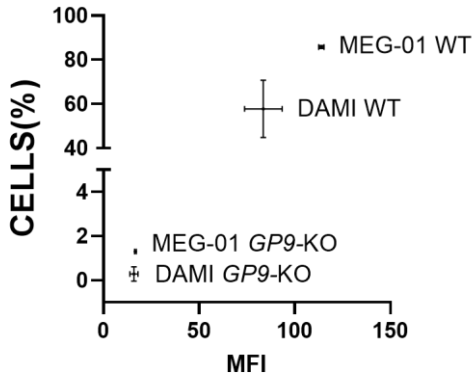

Figure 69. GPIbα subunit expression levels in DAMI *vs.* MEG-01.

Comparison of the percentage of positive cells *vs.* Mean Fluorescence Intensity (MFI) for GPIbα subunit expression in MEG-01 and DAMI WT and *GP9*-KO models.

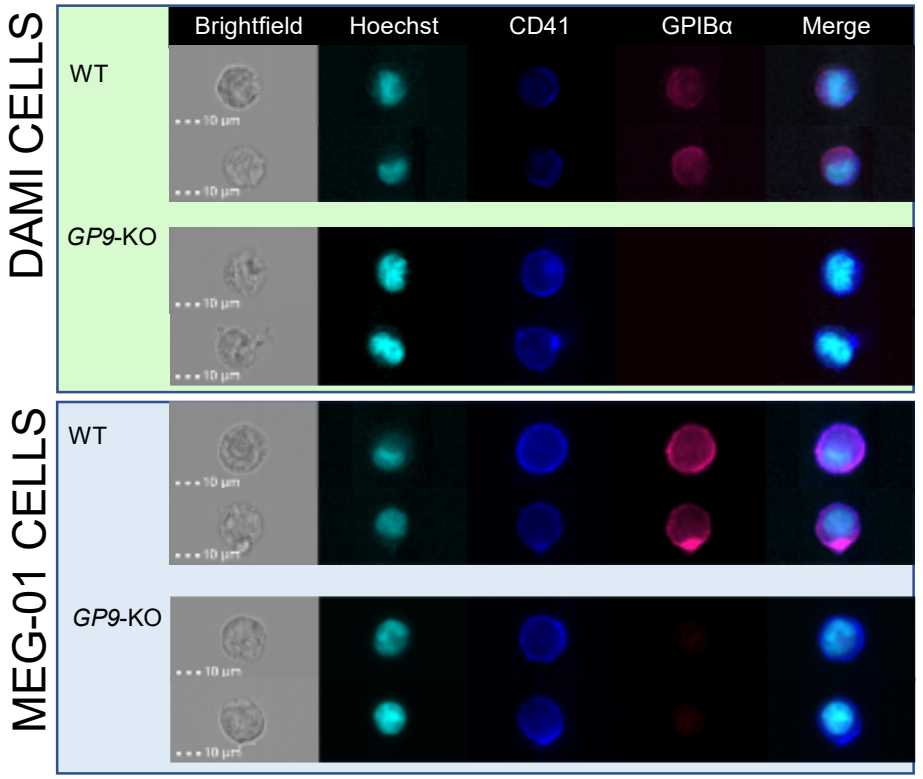

Figure 70. GPIbα subunit expression and localization in DAMI *vs.* MEG-01.

Representative ImageStream images for DAMI and MEG-01 individual cells indicating Hoechst (Cyan), CD41 (Blue) and GPIbα (Pink) expression levels. The last channel corresponds to the merge of the other channels, except for the brightfield.

2.3.2. Evaluation of genetically rescued GPIb-V-IX receptor functionality

2.3.2.1. Analysis of genetically rescued GPIb-V-IX receptor binding capacity to soluble von Willebrand factor.

Next, we evaluated cellular binding capacity to VWF by flow cytometry (**Figure 71**). We demonstrated that while MEG-01 WT cells bound VWF efficiently, we could not detect VWF binding for MEG-01 *GP9*-KO cells. Remarkably, MEG-01 *GP9*-KO cells transduced with LVs expressing GPIX (R-GPIX and T-GPIX) recovered their VWF binding capacity ($p<0.0001$), reaching similar levels than MEG-01 WT cells. In contrast, MEG-01 *GP9*-KO cells transduced with their empty vectors counterparts were not able to bind to VWF (**Figure 71**).

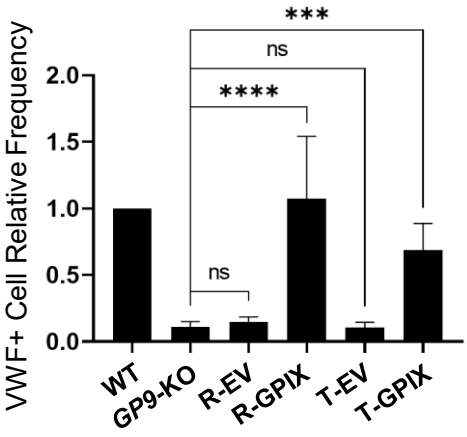

Figure 71. Flow cytometry VWF binding analysis.

Relative frequency of VWF^+ cells in WT, GP9-KO cells and GP9-KO cells transduced with R-EV, R-GPIX, T-EV and T-GPIX. Percentages were acquired by flow cytometry and relativized to WT percentage. ns: non-significant; ***$p<0.001$; ****$p<0.0001$.

These results indicates that exogenous GPIX constitutes functional GPIb-V-IX complexes capable to interact with VWF molecules *in vitro*.

2.3.2.2. Evaluation of ristocetin induced agglutination for genetically rescued GPIb-V-IX receptor.

Since ristocetin induces platelets agglutination in the presence of VWF via GPIbα[82], we aimed to test whether megakaryocytic cells expressing GPIb-V-IX complex exposed to ristocetin and VWF could agglutinate by bridging GPIbα-VWF-GPIbα **Figure 72**, **A**). However, due to the large size of the cells, the traditional RIPA assay does not work and therefore an adapted assay was developed.

Here, cells were incubated with ristocetin and VWF for 2 minutes under stirring conditions, followed by sedimentation under static conditions. We could observe a clear difference in the sedimentation curve between MEG-01 WT and *GP9*-KO cells using a light transmission aggregometer (**Figure 72, B, left panel**). MEG-01 WT cells sedimented faster due to the rapid formation of agglutinates, while MEG-01 *GP9*-KO cells showed higher transmittance percentage (less sedimentation rate) from minute 6 to the end of the analysis (15 minutes). Importantly, MEG-01 *GP9*-KO rescued with GPIX expressing LVs (R-GPIX and T-GPIX) showed similar or even higher agglutination properties than MEG-01 WT cells. End-point data for each lentiviral transduction is shown in **Figure 72, B, right panel**. Comparison of reporter vectors, R-EV vs R-GPIX, (80% *vs.* 60% transmittance, respectively), demonstrated a higher sedimentation rate after the genetic rescue. Similarly, MEG-01 *GP9*-KO transduced with the therapeutic vector (T-GPIX),

achieved percentages of transmittance identical to MEG-01 WT cells.

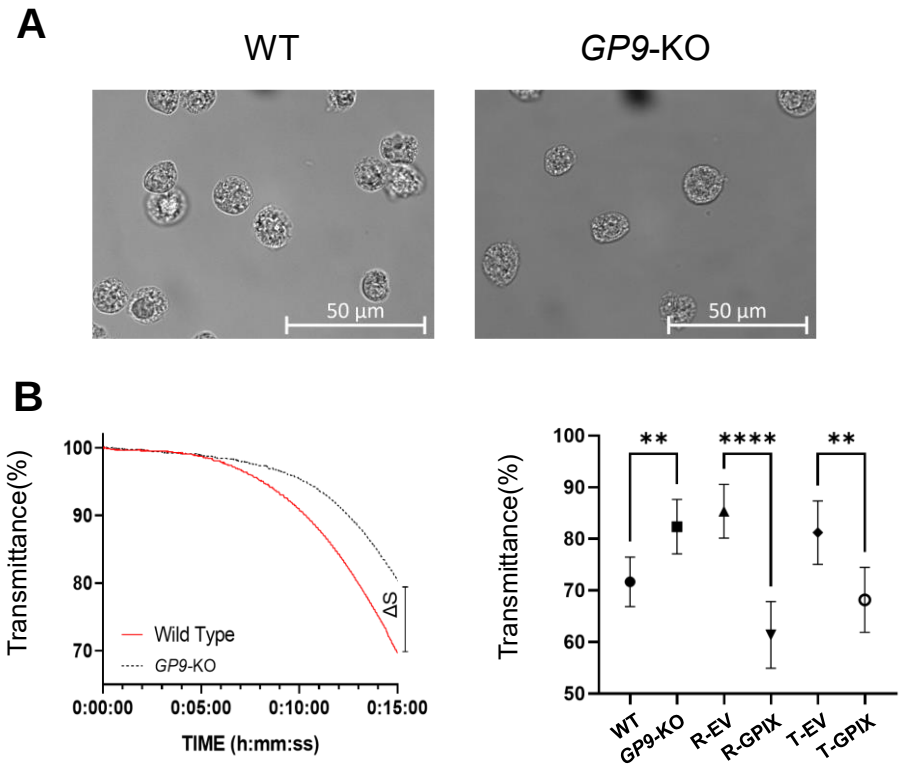

Figure 72. Ristocetin induced agglutination.

A. Example of a 100X image of WT and *GP9*-KO cells previously incubated with a VWF-Ristocetin mixture over a 15-minute period. **B.** Associated sedimentation curves showed as differential sedimentation rate (ΔS). End point data were transferred to right panel, where we indicated the differences for each pair: WT *vs. GP9*-KO; R-EV *vs.* R-GPIX and T-EV *vs.* T-GPIX. **p<0.01; **** p<0.0001.

Analysis of adhesion capability in presence of botrocetin for genetically rescued GPIb-V-IX receptor.

Then we investigated the adhesion capability to surface coated VWF using botrocetin as a promoter of the GPIbα-VWF interaction (previously described in Results **CHAPTER IV1.3.3.2**). MEG-01 WT cells incubated with EDTA and a mixture of VWF and botrocetin were able to bind to VWF-coated well surface (**Figure 73**, **top left panel**). In order to establish the specificity of this interaction, the addition of the GPIbα-blocking antibody 6B4 was performed[178].

In the presence of 6B4 blocking antibody, cells were unable to recognize and attach to VWF-coated surfaces, having the same behavior as MEG-01 *GP9*-KO cells lacking GPIbα (**Figure 73**, **top central and right panels**). MEG-01 *GP9*-KO cells transduced with GPIX expressing vectors (R-GPIX and T-GPIX) regained VWF binding capacity, while the specificity of the interaction was demonstrated with 6B4 blocking antibody (**Figure 73**, middle central and right panels for R-GPIX**;** bottom central and right panels for T-GPIX). In contrast, MEG-01 *GP9*-KO cells transduced with empty vectors (R-EV and T-EV) failed to bind to coated VWF (**Figure 73**, middle and bottom left panels). Furthermore, in these images, we can observe the agglutination pattern among cells, which tends to form clumps in the presence of botrocetin and VWF, exhibiting a similar effect to that which affects platelets.

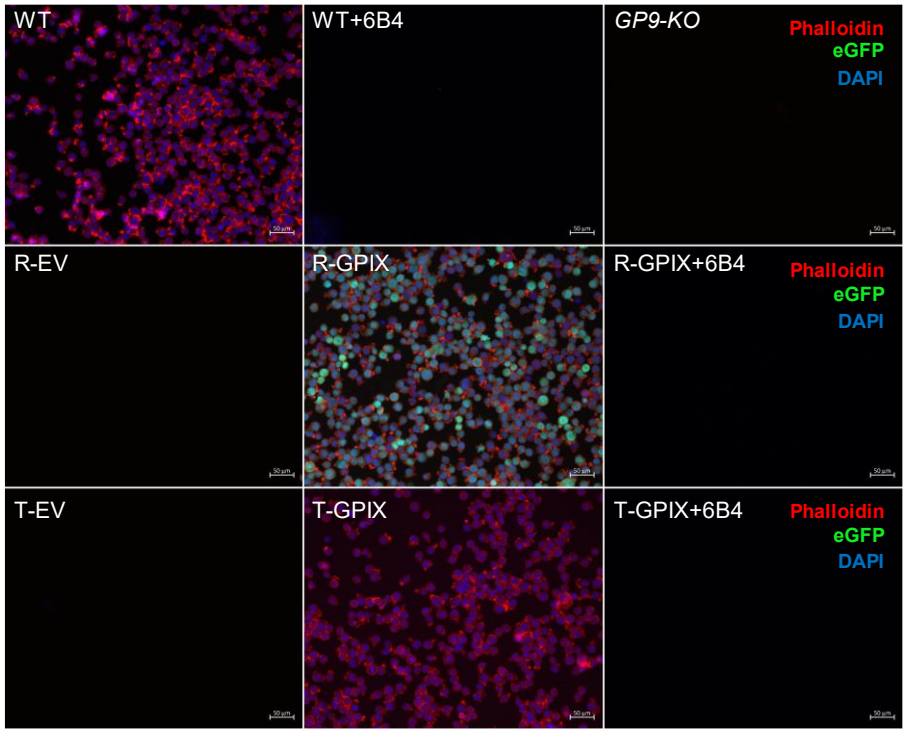

Figure 73. Immunocytofluorescence of cells incubated with botrocetin on a VWF coating.

Merged channels of phalloidin (Red), DAPI (Blue) and GFP (Green) can be observed when cells adhere to VWF. The first row shows the VWF-binding behavior of WT cells, WT cells incubated with 6B4, GPIbα-blocking antibody and *GP9*-KO cells. The second and third rows illustrate cells behavior when *GP9*-KO cells were transduced with R-EV, R-GPIX and R-GPIX+6B4 (second row) and T-EV, T-GPIX and T-GPIX+6B4 (third row).

To quantitatively analyze this cellular attachment to VWF-coated surfaces, we performed at least three independent replicates for every cellular model and experimental condition **(Figure 74)**.

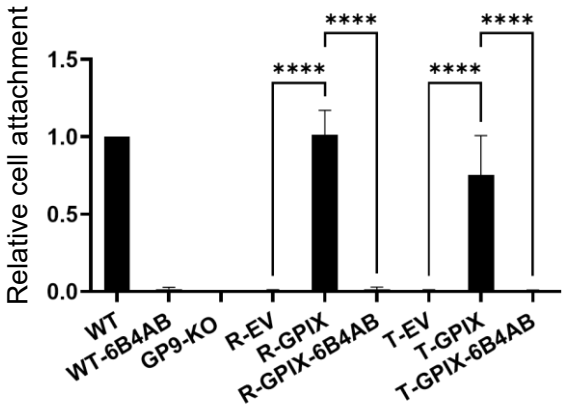

Figure 74. Relative cell attachment quantification.

The bars represent the number of VWF-adherent cells relative to VWF-adherent WT cells. Data represent mean ± SD for 3 independent experiments. Statistical significance was assessed ANOVA one-way and Holm-Šídák's Multiple Comparison test (**** $p < 0.0001$).

Altogether, we have demonstrated that lentiviral transduction of *GP9*-KO cells with exogenous GPIX restored a functional GPIb-V-IX able to interact through its GPIbα subunit with soluble or immobilized VWF.

3. Objective 3: GPIX-Lentiviral correction of Bernard-Soulier Syndrome Type C induced Pluripotent Stem Cells and posterior differentiation to megakaryocytes and platelets.

3.1. Analysis of GPIX reversion in megakaryocytes and platelets produced from transduced GP9-KO induced pluripotent stem cells.

As a first approach to analyze whether our LVs restores GPIX expression, WT, *GP9*-KO and *GP9*-KO cells transduced with R-EV, R-GPIX, T-EV and T-GPIX were differentiated to MKs. WT and *GP9*-KO rescued MKs started to express GPIX from D15 onwards, reaching maximum peak levels on D21, following exactly same expression patterns as exhibited the WT derived MKs (**Figure 51**). Then, we decided to study GPIX expression by confocal microscopy of mature MKs seeded over a fibrinogen coating, one of the main substrates of the αIIb-βIII integrin (CD41-CD61 heterodimer).

In the **Figure 75** we illustrate different magnifications of WT, *GP9*-KO and *GP9*-KO rescued MKs over a fibrinogen coating. Those MKs were capable of recognizing and expanding over the coating, indicating that these cells express functional CD41-CD61 heterodimers capable of binding to its substrate. We then observed the distribution of phalloidin, CD41, GPIX, and eGFP expression in the cells.

To achieve this, we stained permeabilized cells to observe both cytosolic and membrane expression. As shown, phalloidin staining is consistent among the different conditions, with stable expression and spreading over the coating as integrins recognize their substrate. CD41 expression is also stable and distributed over the cell surface and is easily identifiable inside of microvesicles or granules within the cytosol, as seen in brightfield.

It is important to note that R-GPIX and R-EV express eGFP, as they harbor the reporter cassette, which is mainly accumulated in the nucleus (as shown in **Figure 75-B**). Interestingly, despite the exclusion of Hoechst or DAPI for this experiment, cells with multiple nuclei are easily detectable in brightfield, a typical characteristic of mature MKs. The role of GPIX is significant, as WT cells express it in the same manner as CD41, distributed over the cell and stored in granules. Conversely, *GP9*-KO and *GP9*-KO transduced with EVs do not express GPIX, as expected (**Figure 75-A**). In contrast, T-GPIX and R-GPIX transduced cells recover the expression and distribution pattern of GPIX, indicating the functionality of the vectors (**Figure 75; B-C**).

Analysis of GPIX reversion in megakaryocytes and platelets produced from transduced GP9-KO induced pluripotent stem cells.

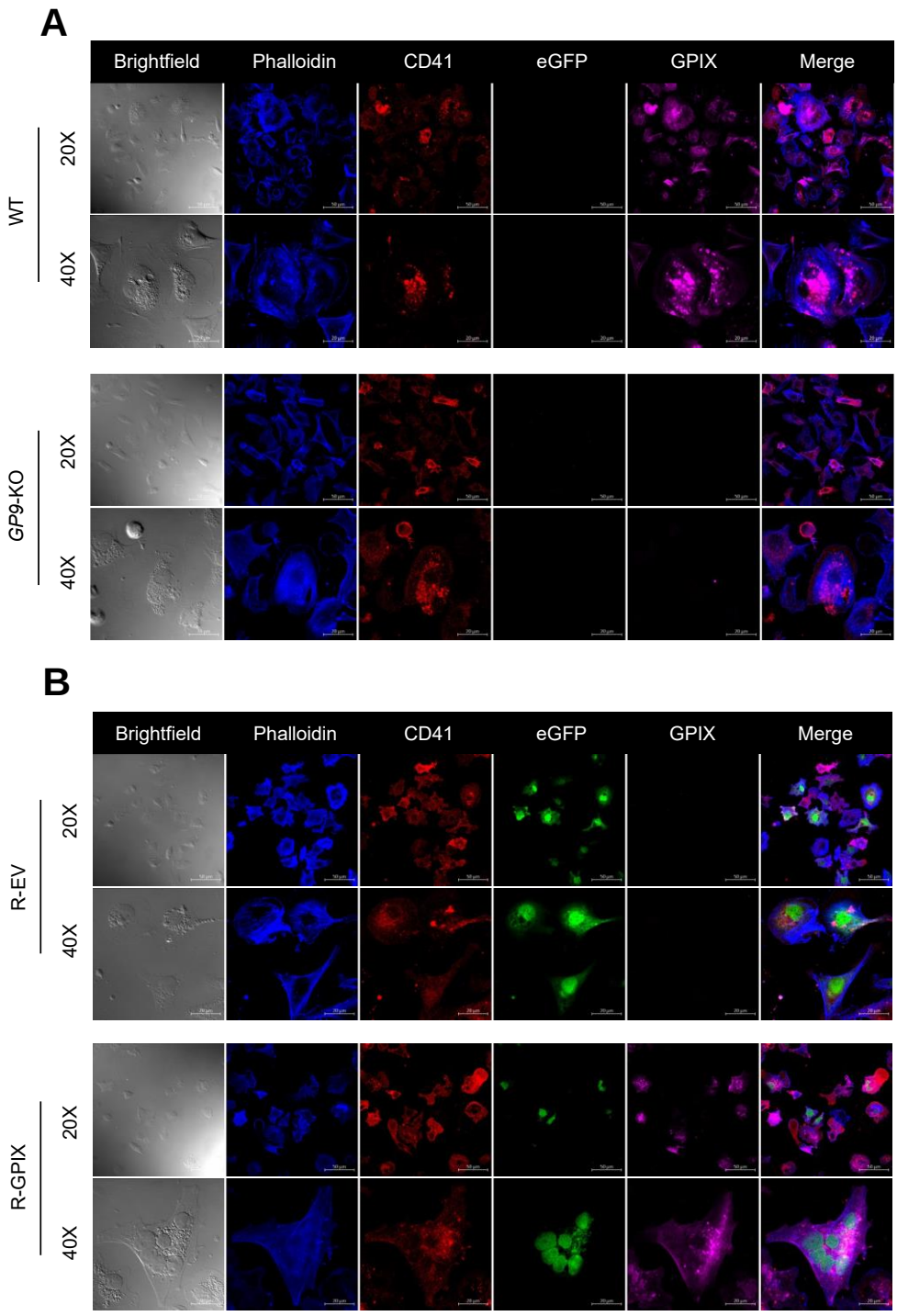

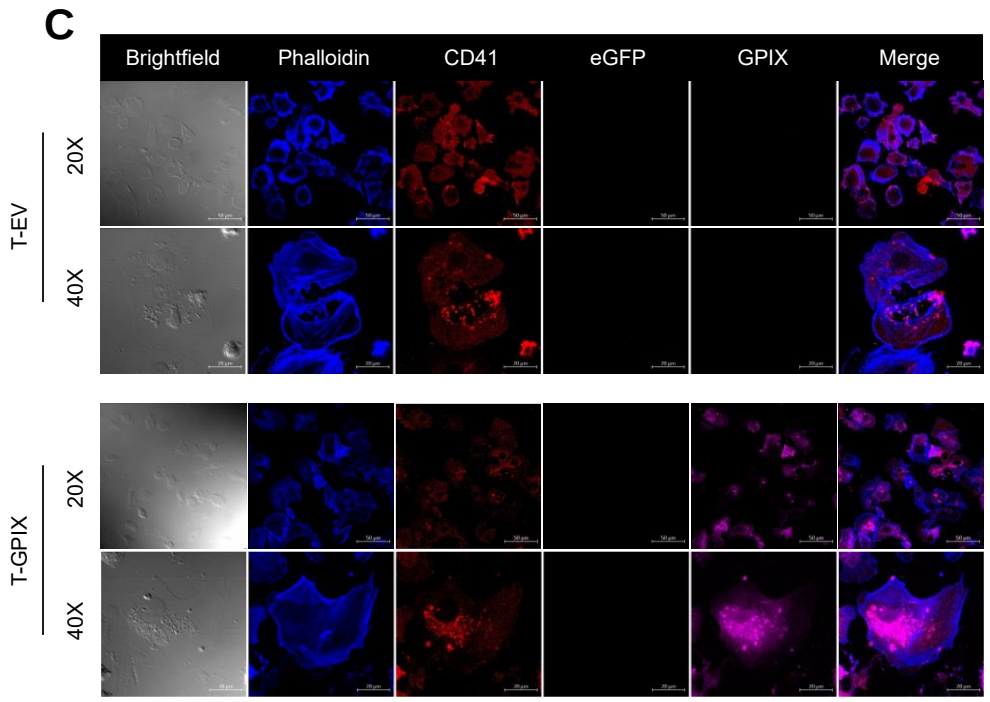

Figure 75. Immunocytofluorescence of mature megakaryocytes produced from differentiated iPSCs spread over a fibrinogen coating.

Each cell line is illustrated with 20X and 40X magnifications, showing brightfield, phalloidin staining (Blue), CD41 (Red), eGFP (Green), GPIX (Pink). Last channel is the result of all merged channels except for brightfield. A. Comparative of differentiated megakaryocytes produced from iPSCs WT vs *GP9*-KO. B. Comparative of differentiated megakaryocytes produced from iPSCs *GP9*-KO transduced with R-EV vs R-GPIX. C. Comparative of differentiated megakaryocytes produced from iPSCs *GP9*-KO transduced with T-EV vs T-GPIX.

Next, we evaluated the effectiveness of our GPIX-expressing LVs by flow cytometry. The cells were transduced with eGFP reporter (R-EV and R-GPIX) and therapeutic vectors (T-EV and T-GPIX). They were then differentiated into MKs and platelets (**Figure 76** and **Figure 77**) and analyzed.

The MKs generated from R-EV and R-GPIX transduced iPSCs expressed similar percentages of eGFP-positive cells (~60% for R-EV and ~70% for R-GPIX) (**Figure 76-A, green bars**). However, the eGFP-positive events in platelets generated from them were lower (~60% for R-EV and ~40% for R-GPIX) (**Figure 77-A, green bars**). Both R-GPIX and T-GPIX LVs were effective in restoring GPIX expression in both MKs and platelets (~70% and ~80%, respectively) ($p<0.0001$) (**Figure 76** and **Figure 77**, **A panels, red bars**). GPIX MFI ratio values were similar between MKs and their derived platelets for R-GPIX (0.64 *vs.* 0.71). Interestingly, while the rescued GPIX percentages were similar in the case of T-GPIX, their MFI ratios relative to WT were higher in rescued platelets than in rescued MKs (0.49 *vs.* 0.64 MFI ratio, for MKs and platelets, respectively) (**Figure 76** and **Figure 77, B, red bars**). In all cases, the percentages indicated us a good transduction efficiency, but the MFI ratios indicated that the protein levels were lower than WT (in both MKs and platelets).

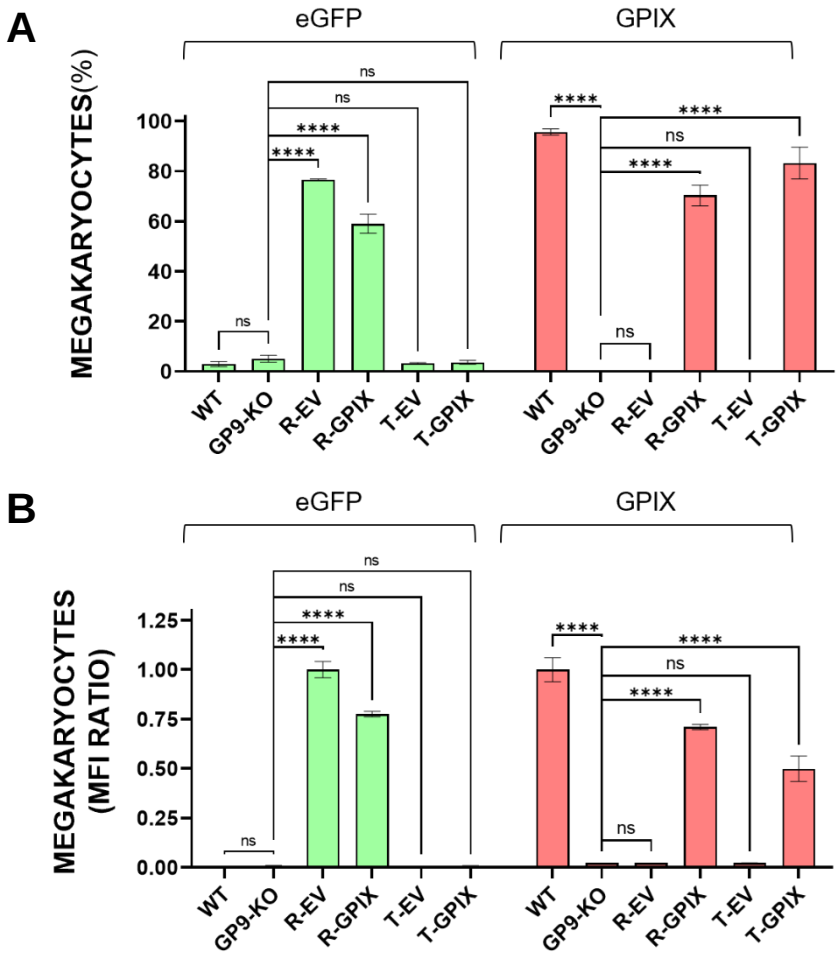

Figure 76. Rescued lentiviral GPIX expression in iPSC-*GP9*-KO-derived megakaryocytes.

Top panel shows the percentage of MKs (CD41+) expressing eGFP or GPIX on day 21, while the bottom panel displays the MFI ratio relativized to R-EV (eGFP) and WT (GPIX) values for WT, *GP9*-KO or *GP9*-KO cells transduced with LVs.

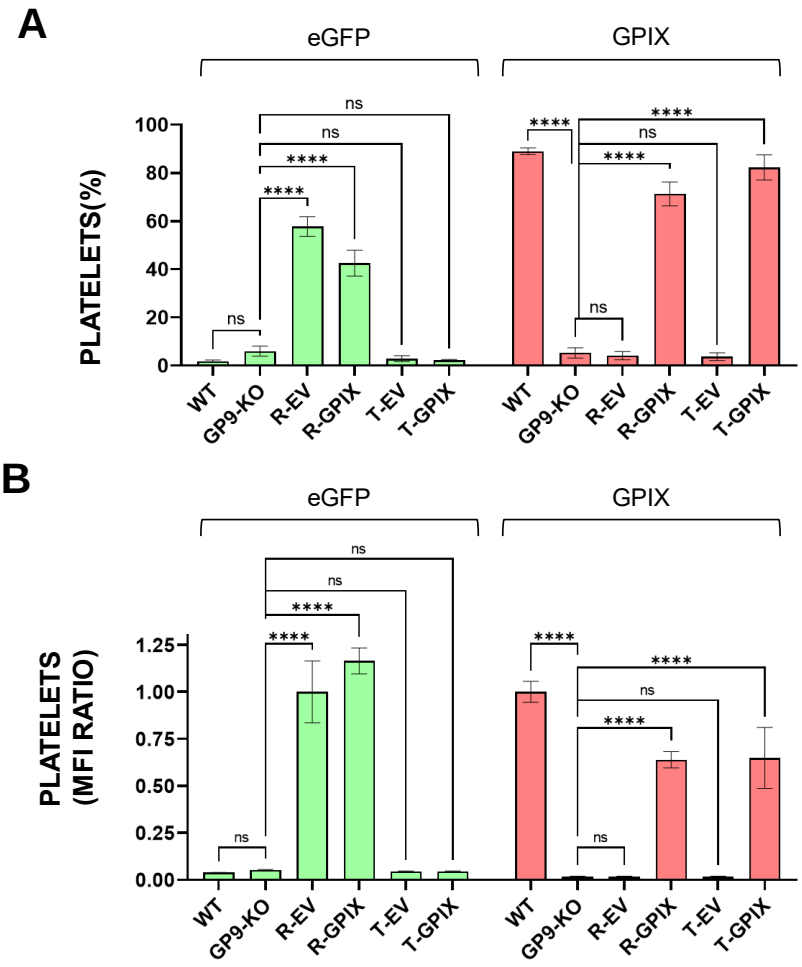

Figure 77. Rescued lentiviral GPIX expression in iPSC-*GP9*-KO-derived platelets.

Top panel shows the percentage of platelets ($CD41^{+}$) expressing eGFP or GPIX on day 21, while the bottom panel displays the MFI ratio relativized to R-EV (eGFP) and WT (GPIX) values for WT, *GP9*-KO or *GP9*-KO platelets produced from cells transduced with lentiviral vectors.

In all cases, the dynamics of megakaryocytic differentiation in GPIX rescued iPSCs *GP9*-KO were similar to iPSCs WT with GPIX expression appearing from day 15 onwards (**data not shown**).

3.2. Size determination in genetically rescued platelets produced from iPSCs GP9-KO.

Finally, we analyzed platelet size and GPIX expression and localization by ImageStream (**Figure 78**). As shown, human platelets isolated from healthy donors are slightly bigger than platelets produced from WT iPSCs (3.3 *vs.* 2.6 µm, $p<0.0001$, respectively). Notably, both of them co-express CD41 and GPIX on their surface, indicating their platelet nature. Interestingly, iPSC-*GP9*-KO-derived platelets reproduced not only GPIX absence, but also their larger size in comparison with WT counterparts (6.70 *vs.* 2.6 µm). iPSC *GP9*-KO transduced with reporter vectors generated eGFP positive platelets. R-EV maintained larger size and the absence of GPIX expression like non-transduced platelets from iPSCs *GP9*-KO. Very importantly, platelets derived from GPIX transduced iPSCs *GP9*-KO recovered GPIX expression in their surface and reduced their size reverting the main characteristics of platelets from BSS Type C patients (**Figure 78, A-B**).

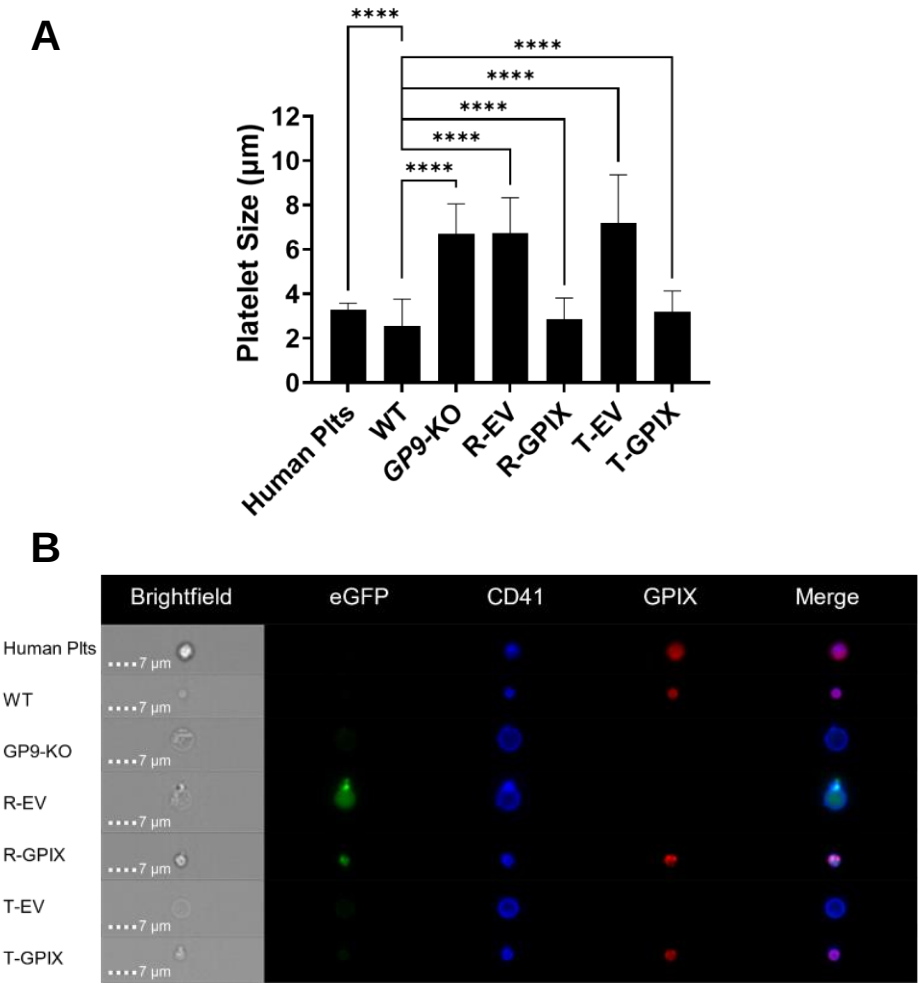

Figure 78. Analysis of the platelet size and protein expression in human platelets and platelets produced from iPSCs WT, *GP9*-KO and *GP9*-KO transduced with R-EV, R-GPIX, T-EV and T-GPIX.

A. Size expressed in µm for each platelet type. **B.** Representative ImageStream images of human platelets and platelets generated from all our iPSC models showing their size, cytosolic eGFP expression (Green), CD41 (Blue) and GPIX (Red) surface expression in each case. Data represent mean ± SD for at least 3 independent experiments. Statistical significance was assessed with ANOVA one-way plus Dunnett's Multiple Comparison test. (**** $p<0.0001$).

Objective 3: GPIX-Lentiviral correction of Bernard-Soulier Syndrome Type C induced Pluripotent Stem Cells and posterior differentiation to megakaryocytes and platelets.

Taken together, we have demonstrated that GPIX expressing LVs are very effective restoring GPIX expression and size of platelets generated *in vitro* from this novel BSS Type C cellular model.

4. Objective 4. Genetic-Rescue of isolated hematopoietic stem cells from Bernard-Soulier Syndrome patients carrying different pathogenic variations and posterior differentiation to megakaryocytes and platelets.

All the data presented clearly demonstrates that our GPIX-LVs are functional in terms of reversing GPIX expression, localizing on the cell surface, and assembling within the GPIb-V-IX receptor complex, allowing for its full exteriorization and functionality in recognizing VWF, one of its main roles. Furthermore, we have successfully reversed GPIX expression in MKs and platelets derived from iPSCs, resulting in the production of normal-sized platelets rather than the typical BSS giant platelets.

4.1. Corroboration of pathogenic variants from two unrelated Bernard-Soulier Syndrome Type C patients.

Our next aim was to evaluate these gene editing tools in HSCs from BSS Type C patients, our future target cells for *ex vivo* therapy. Because of the extremely small number of BSS patients available, we only had accessed to two different BSS Type C Spanish and Portuguese patients carrying p.W71S and p.F55S mutations, respectively. We sequenced *GP9* locus from DNA isolated from peripheral mononuclear blood cells and confirmed their mutations (**Figure 79**).

Objective 4. Genetic-Rescue of isolated hematopoietic stem cells from Bernard-Soulier Syndrome patients carrying different pathogenic variations and posterior differentiation to megakaryocytes and platelets.

Both patients carried different missense mutations associated with *GP9*. Specifically, one mutation involved a nucleotide change from TCT to TTT, resulting in the substitution of phenylalanine (F) with serine (S) at position 55 in the protein sequence. The other mutation involved a nucleotide change from TGG to CGG, resulting in the substitution of tryptophan (W) with arginine (R) at position 71 in the protein sequence. Both missense mutations may alter the protein's three-dimensional structure, affecting its stability,

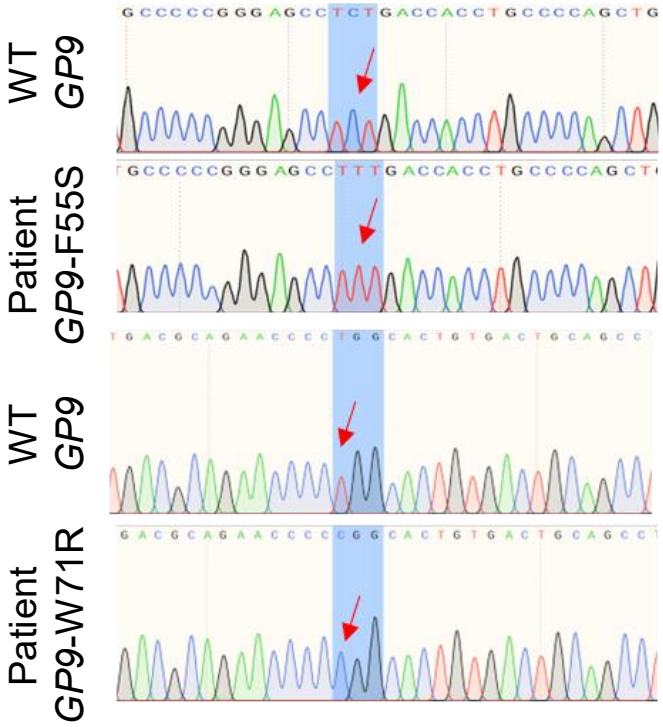

Figure 79. Sanger sequencing analysis of BSS Type C patients.
Electropherogram alignment of GP9 DNA sequences from two different Bernard-Soulier Syndrome patients carrying the pathogenic variants F55S and W71R against its WT sequence.

activity, and interaction with other subunits, and prevent GPIX migration to the cell surface.

4.1.1. Platelet analysis and phenotypical confirmation of Bernard-Soulier Syndrome.

Next, we examined the platelets of both BSS patients and confirmed the absence of GPIX on the membrane surface by ImageStream and flow cytometry (**Figure 80** and **Figure 81**; respectively). We also observed larger platelets than normal, consistent with previous findings in the literature[183–186].

Objective 4. Genetic-Rescue of isolated hematopoietic stem cells from Bernard-Soulier Syndrome patients carrying different pathogenic variations and posterior differentiation to megakaryocytes and platelets.

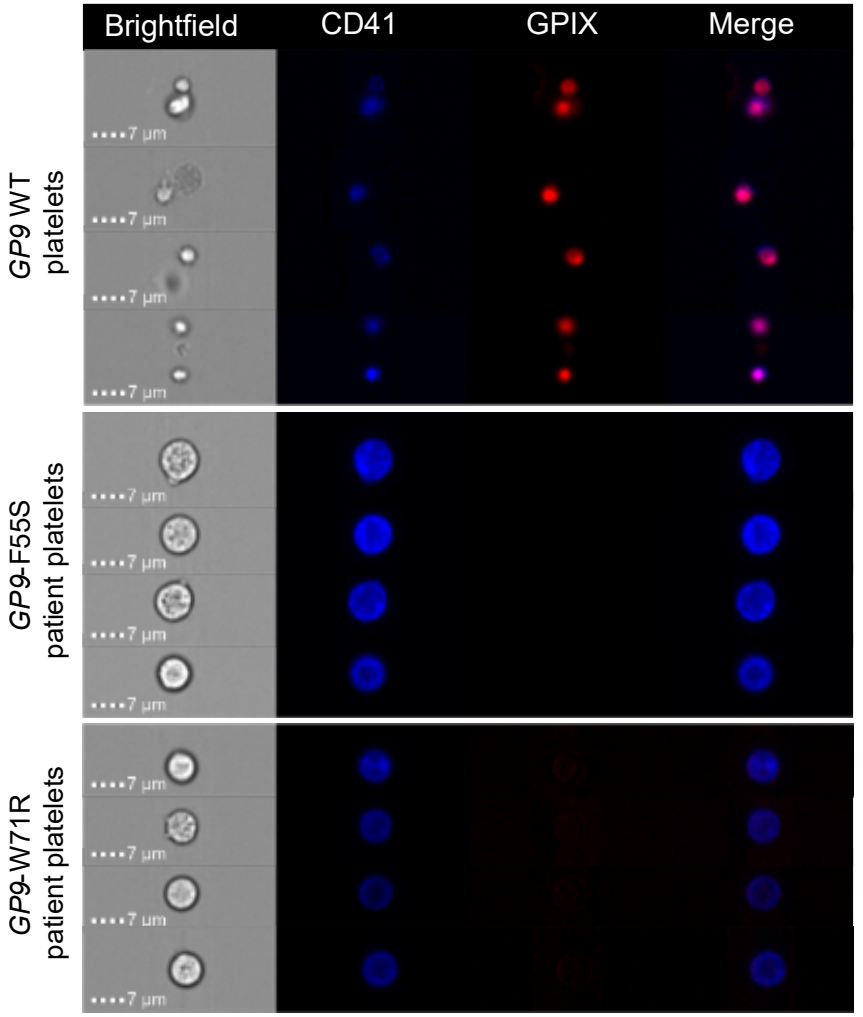

Figure 80. ImageStream platelets analysis from BSS Type C patients.

Representative ImageStream platelet images from donor and BSS patients indicating size and expression of CD41 (Blue) and GPIX (Red) surface markers. Last channel is the result of the merge of these channels except for brightfield.

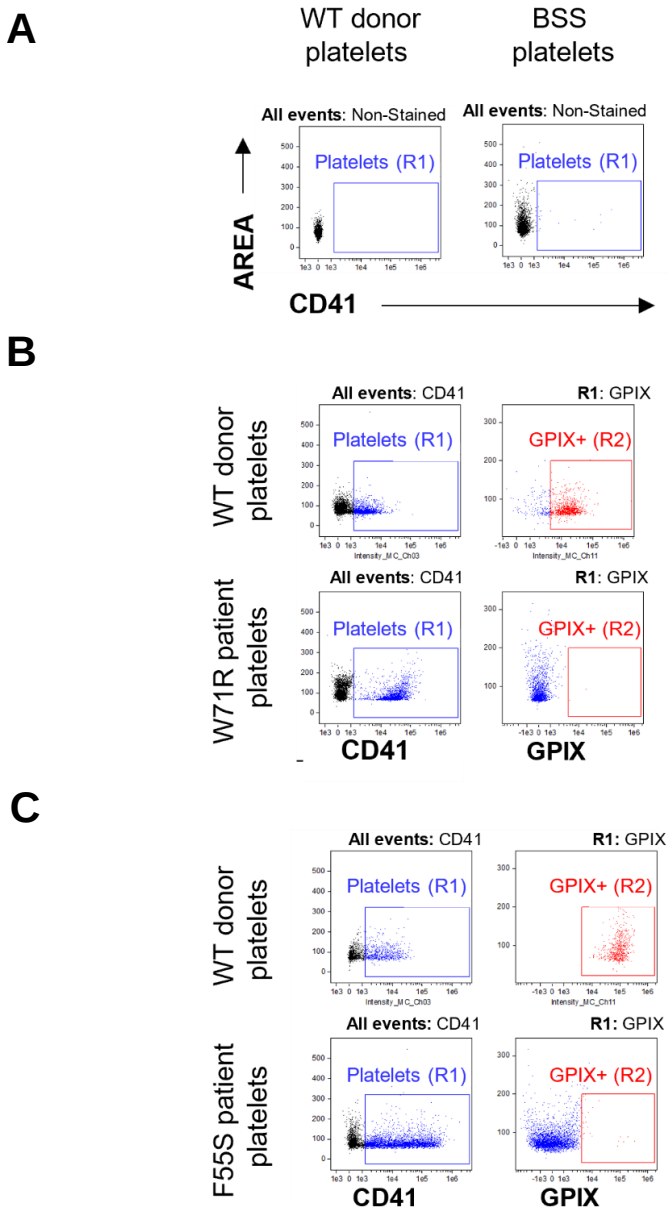

Figure 81. Flow cytometry dot plots obtained from BSS W71R, F55S patients and donor platelets showing CD41 expression profile and GPIX expressing platelets from this first population.

A. Non-stained donor and BSS platelets. **B.** Healthy vs. W71R platelets. **C.** Healthy vs. F55S platelets.

4.2. Genetic rescue in megakaryocytes and platelets produced from transduced non-mobilized HSCs from both Bernard-Soulier Syndrome Type C patients.

Considering the characteristics of the disease, we decided to isolate HSCs from non-mobilized peripheral blood samples rather than bone-marrow biopsies. The extremely reduced number of circulating $CD34^+$ cells purified (~50.000 cells/50 mL blood) forced us to focus our efforts on a single vector. R-GPIX was selected because allowed us to follow transduction efficiency and GPIX recovery by flow cytometry and ImageStream. $CD34^+$ isolated HSCs from both patients were expanded, transduced with R-GPIX and differentiated to MKs/platelets for 10 days.

Non-transduced MKs neither express eGFP nor GPIX, while transduced cells re-established GPIX expression/localization together with eGFP cytoplasmatic expression (**Figure 82, upper panel**). For platelets analysis, mature MK culture supernatants were collected, platelets were enriched by centrifugation, labeled with CD41 and GPIX and analyzed by Image Stream (**Figure 82, bottom**). In this case, platelets derived from non-rescued HSCs showed larger size and absence of GPIX, whereas platelets produced from transduced HSCs showed smaller size and expressed GPIX in the surface and eGFP in the cytosol.

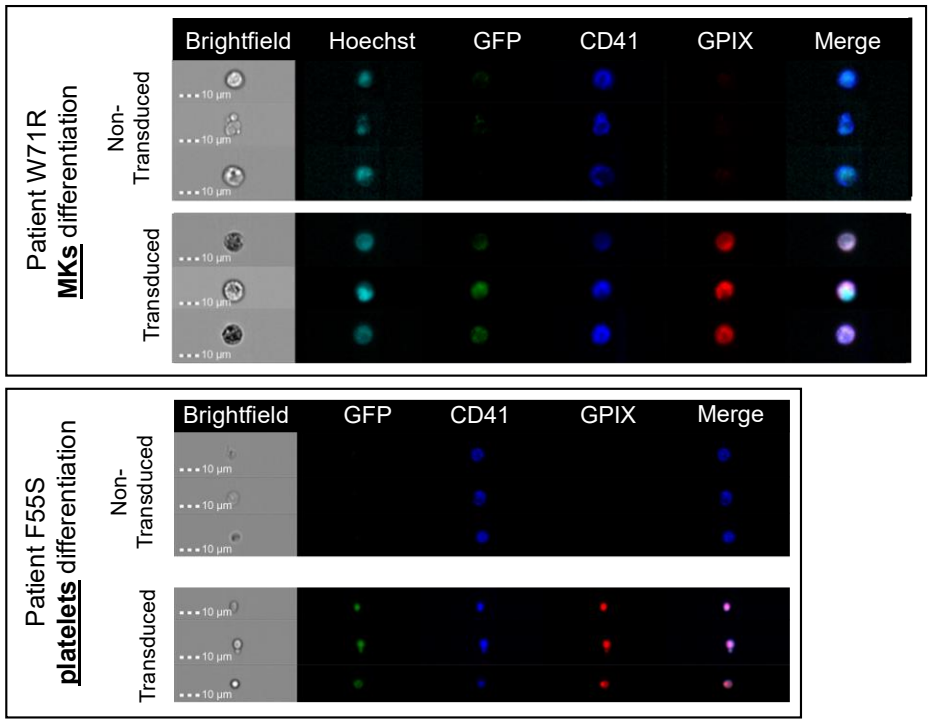

Figure 82. Rescued HSC-derived megakaryocytes and platelets derived from BSS Type C patients.

ImageStream events corresponding to differentiated megakaryocytes and platelets obtained from transduced and non-transduced W71R-BSS-HSCs and F55S-BSS-HSCs, respectively. Top panel shows MKs from W71R patient and bottom panel shows platelets from F55S. Channels indicate the localization and expression levels for Hoechst (nucleic DNA, cyan), eGFP (Green), CD41 (Blue) and GPIX (Red). The last channel corresponds to the merged channels, except for the brightfield.

We compared the average diameter of healthy patients' platelets with those from both BSS patients and matched them with platelets produced from non-transduced and transduced differentiated F55S HSCs. Consequently, a quantitative study was conducted, and remarkably, platelets produced from non-transduced HSCs exhibited the exact same size as those from the patients (both BSS patients). Moreover, what makes it even

more intriguing is that platelets derived from transduced HSCs not only reverted the giant phenotype but also produced platelets with the exact same size as those from healthy donors (**Figure 83**).

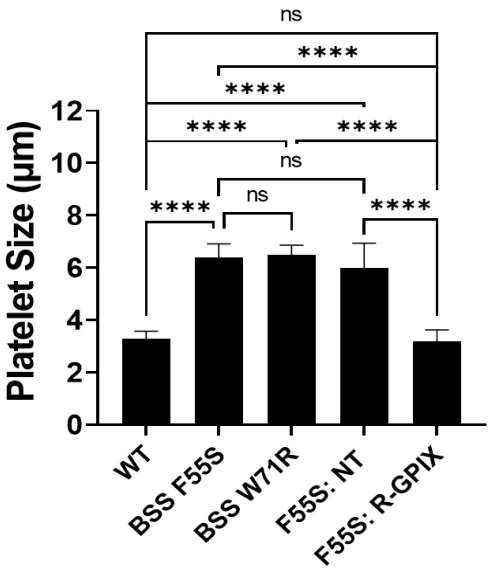

Figure 83. Comparison of platelet diameters from healthy donors, BSS patients and produced from transduced and non-transduced differentiated F55S-HSCs.

Representation of platelet size showed by their diameter (µm) belonging to platelets from a human healthy control, W71R and F55S both BSS patients, and those produced from non-transduced and R-GPIX transduced F55S isolated and differentiated CD34+.cells. Data represent mean ± SD. Statistical significance was assessed with ANOVA one-way plus Tukey Multiple Comparison test (ns = non-significant, **** $p < 0.0001$).

Our results collectively demonstrate that lentiviral-mediated therapy reinstates GPIX expression in MKs and platelets derived from primary HSCs isolated from patients with

BSS Type C. Furthermore, our R-GPIX also generates platelets of normal size, effectively reversing the giant phenotype. Consequently, these findings provide further confirmation of the therapeutic potential of this approach for treating Bernard-Soulier Syndrome Type C.

5. Objective 5. Generation and characterization of Bernard-Soulier Syndrome GP9 null murine model.

We have successfully demonstrated that our LVs are capable of restoring GPIX expression in megakaryoblastic cells, MKs, and platelets produced from iPSCs. Additionally, the lentiviral exogenous GPIX assembled with the other components of the receptor, allowing for its full conformation and restoring its functionality. Although these experiments validate our LVs as a successful gene therapy tool to reverse BSS Type C and serve as a preclinical model, we would like to reverse the disease *in vivo* to fully validate our gene therapy tools and complete our preclinical studies.

5.1. Analysis and comparison of hGP9 and mGp9 genes and their amino acidic sequences.

Firstly, we decided to compare *hGP9* with its murine version, *mGp9*, to assess their genetic structures and protein sequences to develop a BSS Type C model that could mirror the human version. As illustrated in **Figure 84**, although murine gene differ with the human version composed of three exons and the murine version composed of two exons, the CDS length is exactly the same in both cases.

When we aligned their amino acid sequences, we found that the proteins are 86% similar, with 72% identity (meaning that many amino acid residues are in the same location in both proteins) and most of the different amino acids maintained

highly similar properties to the original. However, if the GPIX subunits are too different, they may not be able to assemble with the murine GPIb-V-IX receptor subunits, which would prevent us from using this model to assess the functionality of our gene therapy tool.

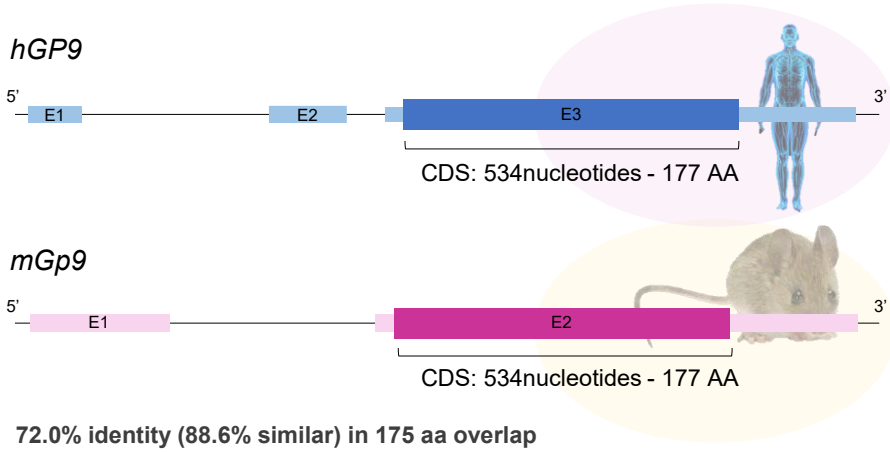

72.0% identity (88.6% similar) in 175 aa overlap

```
Homo_sapiens      MPAWGALFLLWATAEATKDCPSPCTCRALETMGLWVDCRGHGLTALPALPARTRHLLLAN  60
Mus_musculus      MTTWGLLFLLWPATTDTQACPRPCTCQSLETMGLKVNCEGQGLTALPVIPAHTRQLLLAN  60
                  * :** ***** ::  *: ** ****:******* *:*.*:******.:**:**:*****

Homo_sapiens      NSLQSVPPGAFDHLPQLQTLDVTQNPWHCDCSLTYLRLWLEDRTPEALLQVRCASPSLAA  120
Mus_musculus      NSLRSVPPGAFDHLPQLWDLDVTHNPWHCDCSLTYLRLWLEDHMPEALMHVYCASPDLAT  120
                  ***:**************  ****:******************: ****::* ****.**:

Homo_sapiens      HGPLGRLTGYQLGSCGWQLQASWVRPGVLWDVALVAVAALGLALLAGLLCATTEALD     177
Mus_musculus      RRPLGQLTGYELGSCGWKLPPSWAYPGVWWDVSLVAVAVLGLILLAGLLNTFTESRN     177
                  : ***:****:******:*  **. *** ***:*****.*** ****** : **: :
```

*** Amino acid conservation**
: Amino acid with strong similar properties
. Amino acid with weak similar properties

Figure 84. Comparative at genetic and amino acid levels between *hGP9* and *mGp9*.

Genetic structure and percentages of similarity and identity between amino acid sequences are indicated. * Amino acid conservation; : amino acid with strong similar properties; . amino acid with weak similar properties.

5.2. Development of a GP9^{null} murine model.

Based on these findings, we designed and developed a *Gp9*^{null} murine model to test the efficacy of our GPIX-LVs in restoring platelet function and syndrome reversal *in vivo*. Our KO strategy involved using two sgRNAs that targeted the upstream and downstream regions of the CDS, which allowed us to create a full deletion. Additionally, we provided a single-stranded oligodeoxynucleotide (ssODN) to facilitate the HDR, which included two homology arms that flanked the CDS (**Figure 85**, schematic design).

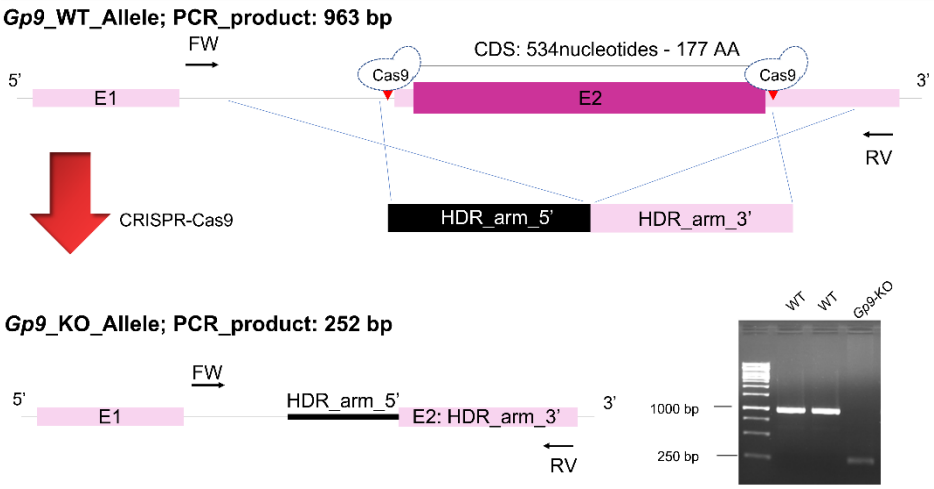

Figure 85. CRISPR-Cas9 deletion strategy for *mGp9*.

Usage of two sgRNAs to delete completely the *mGp9* coding exon 2. Positioned PCR primer pairs and agarose gel with resulting PCR products of WT and *Gp9*-KO specimens are shown. FW: Forward; RV: Reverse. HDR: Homology Directed Repair; CDS: Coding DNA sequence.

To create the murine knockout, we collaborated with Dr. Manuel Sanchez Martin, head of the transgenic facility at the University of Salamanca. Dr. Sanchez Martin microinjected the gene-editing tools over mouse zygotes and was easily achieved by conventional PCR, due to the chosen primer pair amplified 963 bp of the WT sequence, while it only amplified 252 bp when the mouse harbored both mutated alleles (homozygous mutation) (**Figure 85**, agarose gel).

5.3. Hemogram analysis from Gp9^{null} murine model and its comparison with WT hematological parameters.

The identification and isolation of the murine model has allowed us to expand our mouse colony to a sufficient number of individuals for conducting experiments. While awaiting further colony expansion, we conducted a preliminary study by analyzing the hemogram of several *Gp9*^{null} mice at 6 months age and compared it with reference values for the same WT murine model.

Our analysis has revealed that our murine model accurately reproduces the key characteristics of human Bleeding Severity Score (BSS), as summarized in **Figure 86**. The murine model exhibited a decrease in platelet count (~950,000 vs. ~180,000 platelets/µL in WT and *Gp9*^{null}, respectively) and demonstrated an increase in platelet size, as indicated by Mean Platelet Volume (MPV) in the hemogram.

The MPV values indicated that the platelets in the murine model were approximately 2.2 times larger in volume compared to the WT mice (~5.0 vs. ~11.2 fL). Notably, the *Gp9*^{null} murine model did not exhibit any sex-based differences in blood cell production, as the blood parameters were similar between male and female individuals.

Considering that the murine model accurately replicates

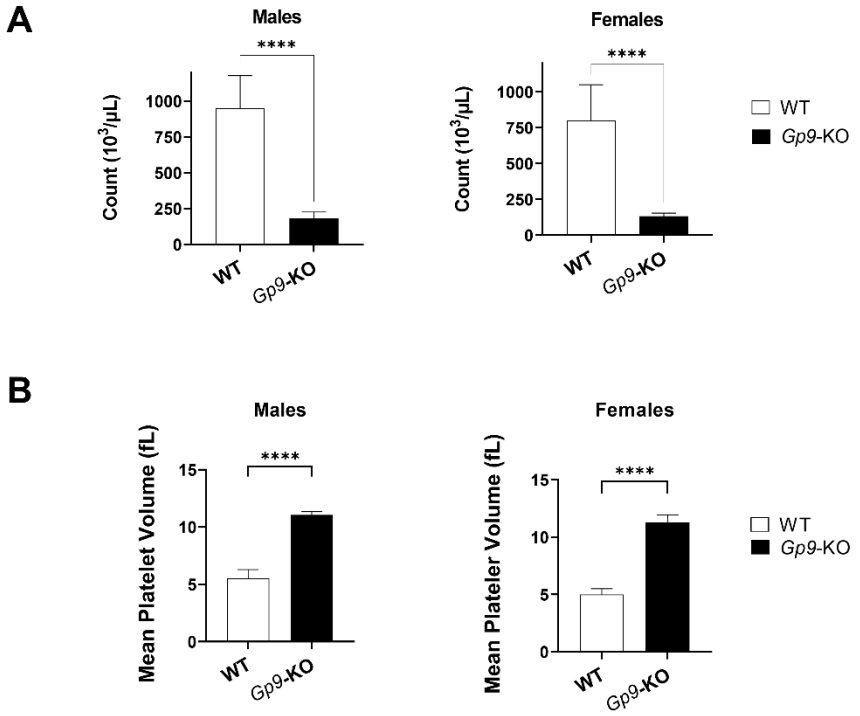

Figure 86. Platelet comparatives between WT and *Gp9*^{null} mice.

A. Comparative of platelet blood counts. B. Comparative of mean platelet volume

the BSS phenotype *in vivo*, we anticipate that these mice will develop disease symptoms similar to those observed in humans, including altered clotting capability.

Our next steps involve purifying and isolating HSCs from bone marrow extracted from the mouse tibia and femur, expanding and transducing these cells *in vitro*, and reinfusing the treated HSCs into recipient *Gp9*-KO mice. The disease will be reversed once the platelet count, size, location, and functionality of the GPIb-V-IX receptor are corrected in the mouse. Tail bleeding assays will help us confirm the disease reversal, and we will monitor these processes over time to assess the long-term stability of our therapeutic gene therapy tools. Achieving full reversion would serve as a comprehensive preclinical study for the treatment of BSS Type C and allow us to progress to the clinical phase for reversing this congenital disease in the next future.

CHAPTER VI

DISCUSSION

It is well known that GPIb-V-IX, localized on the plasma membrane of megakaryocytes and platelets, is the result of the assembly of 4 subunits: GPIbα, GPIbβ, GPIX and GPV. These subunits exhibit a stoichiometry of 2:4:2:1 and are stabilized through transmembrane domain interactions, disulfide bonds between GPIbα and 2-GPIbβ molecules and GPIbβ and GPIX also exhibit extracellular interactions[77,187]. Finally, GPV is weakly associated to GPIb-IX by transmembrane interaction with GPIbα[61].

Typically, BSS is described as an autosomal recessive disease, being necessary to have both alleles mutated to develop the syndrome (biallelic BSS). While no pathogenic variants have been associated to *GP5* to date, it is well reported that homozygous or compound heterozygous mutations affecting *GP1BA*, *GP1BB* or *GP9* originates BSS type A1, B or C, respectively. In these cases, the GPIb-V-IX receptor appears as truncated, dysfunctional, or absent at the outer membrane[57].

Historically, mammalian (CHO) and human cell lines (293T, K562, L cells…) have been utilized to replicate GPIb-V-IX receptor formation and biology. CHO cells have gained popularity in the biotechnology industry due to their ability to efficiently produce human cellular proteins containing posttranslational modifications, such as glycosylations[188]. As a result, they have emerged as the primary platform for analyzing GPIb-V-IX receptor assembly and the effects of diverse mutations identified in BSS patients. This has been

accomplished by transfecting all subunits or a subset of subunits along with the one containing the specific variant of interest[189–194].

However, it is important to note that the resulting expressions obtained through these cell lines may not accurately represent the physiological conditions. This is because the unknown number of plasmid copies of each subunit, driven by non-physiological promoters, are being investigated within a non-human environment and/or different epigenetic backgrounds.

By utilizing CRISPR-Cas9 editing tools, we successfully performed knockout experiments for each individual subunit coding gene (BSS driver genes and *GP5*) and observed the migration patterns of every subunit except for GPV, which we could not obtain specific antibody. In general terms, our data contrast with the information available in the literature.

Interestingly, we discovered that the expression of GPIbα is highly dependent on the presence of other subunits, as it is undetectable in both *GP1BB*-KO and *GP9*-KO cellular models. Consistent with our findings, *Dong et al.,* analyzed receptor stability in CHO cells, where co-transfection experiments of α, α/IX and α/β did not serve to detect GPIbα externalization, while α/β/IX allowed its transport[195]. The absence of either of these subunits results in the targeting and degradation of GPIbα in the lysosomes.

In line with these findings, GPIX and GPIbα were absent in MKs and platelets from a BSS type C patient carrying a homozygous deletion of the entire *GP9* gene[54]. In contrast, BSS patients carrying the W127X mutation in *GP9,* originally described in Japan[196], exhibit a deficiency of GPIX expression while displaying residual surface expression of GPIbα[197]. Subsequently, *Takata et al.* quantified GPIbα relative MFI expression compared to healthy controls, revealing that it ranged from 7-11% in this group of BSS patients[194]. Despite the reduced expression level of GPIbα, platelets from W127X patients were capable of binding to immobilized VWF under high-shear conditions *in vitro*. Furthermore, in a BSS type C patient carrying the p.Phe55Ser variant, *Noris et al.* confirmed reduced GPIbα expression using three different antibodies[198]. The percentage of GPIbα positive platelets ranged from 41.5% to 86.6%. However, when calculating the relative expression of GPIbα compared to WT using each antibody, we observed expression levels ranging from 8-11%. Consistent with our findings, several studies have reported reduced GPIbα expression, with less than 10% relative expression, in all analyzed BSS patients, regardless of the disease-causing variant[59,199,200]. In the case of our *GP1BA*-KO models, we observed relative GPIbα expression levels of 11-13%. It is important to consider this data because, in many cases, studies describe "decreased expression compared to WT" without acknowledging that the protein may be entirely absent,

as evident in our KO models, and what they are observing is residual and/or unspecific fluorescence.

According to our data, GPIbβ is indispensable for the assembly of the entire complex. In its absence, none of the remaining three subunits can be detectable at the outer membrane. In contrast, when the absent subunits are GPIX or GPIbα, GPIbβ can be visible to a greater or lesser extent in cell surface, ranging from 0.3-0.5 expression ratio relativized to WT for both KOs. In line with our results, in BSS type B patients the GPIb-V-IX complex is fully absent[53,193,201]. Identical surface expression data were obtained from a patient with Velocardial Syndrome (hemizygous microdeletion of 22q11.2 containing the GP1BB locus) carrying a p.Pro96Ser mutation in the other GP1BB allele[202].

Our data also indicates that GPIX can migrate to the outer membrane in absence of GPIbα (GP1BA-KO), nevertheless, its transport it is dramatically affected (ratio of 0.05 respect WT expression). However, it requires GPIbβ, in its absence it cannot be externalized. This fact is supported by *Minkov et al.,* who described two BSS patients who were siblings and carried a heterozygous compound mutation (frameshift (c.1601_1602delAT) and nonsense (c.1036C>T)) that affects *GP1BA*, abolishing its fully expression. Similarly, GPIX expression could be observed in some BSS type A1 patients containing homozygous or compound heterozygous variants in *GP1BA*[203,204]. Additionally, overexpression experiments in CHO cells show that co-transfection of mutant

GP1BA, with WT-*GP1BB* and WT-*GP9* leads to a decreased GPIX expression in comparison to CHO cells expressing WT-*GP1BA*. In contrast, when WT-*GP1BA*, WT-*GP9* and variant p.Asn64Thr *GP1BB* were co-transfected, none of the subunits could be detected[193], suggesting GPIbβ-GPIX co-migration[193,202,205].

It is important to note that our KO designs were specifically engineered to truncate the proteins in the extracellular N-terminal domain of GPIbα, GPIbβ, and GPIX. Consequently, only the primary section of the extracellular domains were conserved. This fact holds significant importance because our KO models replicate the assembly process in the absence of almost the entirely subunit. However, it should be noted that patient-specific assemblies may differ from our data due to the presence of *missense* or *nonsense* mutations occurring at various locations within the protein. These variants may not affect the domains that potentially play a crucial role in the interaction between subunits like could be transmembrane domains. Thus, this fact would explain the presence of aberrant GPIb-V-IX receptors.

As mentioned in the Introduction Chapter, thirteen pathogenic variants associated to *GP1BA* and fourteen in *GP1BB* can be found in dominant inheritance, characterized by pseudo-functional receptors and inducing mild or asymptomatic forms of BSS[206], however, the underlying basis of this mechanism is not understood. These variants are mainly associated with the LRR domains of both subunits, that in the

case of GPIbα coincides with the LBD, responsible for VWF binding. Interestingly, patients with Velocardiofacial Syndrome typically exhibit symptoms caused by a hemizygous microdeletion within human chromosome 22q11, specifically involving the *GP1BB* gene. This deletion commonly results in the manifestation of 50% functional receptors and, in some cases, intermediate platelet size[207]. Surprisingly, these patients do not exhibit clear bleeding tendencies. In such cases, the protein product is generated from a single healthy allele, leading to only a partial quantity available for receptor formation, which explains the reduced expression. Conversely, in the case of monoallelic forms of BSS, we hypothesize that the issue lies not in quantity but in quality. Depending on whether the monoallelic BSS affects GPIbα or GPIbβ, both healthy and aberrant subunits would be produced. As a result, the aberrant subunits would compete with their healthy counterparts during receptor assembly. Of particular interest is the case of GPIbβ, as its stoichiometry (2 molecules per receptor) could generate a wider range of phenotypes: $\alpha\beta^{H}\beta^{H}$IX (healthy), $\alpha\beta^{H}\beta^{A}$IX (potentially non-functional), and $\alpha\beta^{A}\beta^{A}$IX (non-functional) [β^{H}: healthy subunit; β^{A}: Aberrant subunit]. Indeed, supporting evidence for this hypothesis was obtained by *Kurowaka et al.* when they co-expressed various ratios of healthy and aberrant (p.Tyr88Cys) *GP1BB* genes with healthy copies of *GP9* and *GP1BA*, resulting in different receptor phenotypes[208]. Once again, our megakaryoblastic models would be way more suitable to study these hypotheses

due to its two-alleles well defined condition. If this would be confirmed, it may be necessary to take it into account for future gene-therapy treatments for *missense* subunits which could compete with the new synthesized and therapeutic ones.

Next, we have analyzed the enigmatic *GP5* subunit, which is one the most abundant glycoproteins on platelets surface, however its role is not fully understood. We decided to investigate its contribution to GPIb-IX assembly in a human megakaryoblastic background. To do that, we performed a *GP5*^{null} with CRISPR-Cas9, by deleting a fragment which harbored the ATG, that resulted in the obstruction of GPV protein translation. Flow cytometry expression analysis in MEG-01 and DAMI cells revealed that the absence of GPV did not affect the expression of GPIbα and GPIX, while the expression of GPIbβ was significantly reduced in terms of percentage. In terms of MFI, the reduction ratio was 0.60 compared to WT expression. This observation is controversial. Different authors who studied *Gp5*^{null} murine models did not observe any decrease in the expression of the GPIb-V-IX complex. However, it is important to note that they did not analyze the individual subunits; instead, they employed an antibody targeting the GPIb-IX complex as a whole. Consequently, if the epitope of the antibody was binding to either GPIX or GPIbα subunits, their data and our findings regarding receptor biology would align[209,210].

Concerning the assembly of GPV within the complex, it has been described that BSS patient platelets do not exhibit

externalization in the absence of other subunits[211,212]. However, while some authors have reported residual levels of GPV within the membrane through co-transfection experiments in CHO cells[213], other authors have failed to detect it independently, necessitating the presence of the remaining subunits for externalization[214]. Despite we were unable to analyze GPV expression due to the unavailability of the antibody, we consider that our cell models can provide more realistic information regarding the contribution of other subunits to GPV externalization and anchorage to the membrane.

Controversial data regarding the functionality of GPV murine models has also been reported. While *Kahn et al.* did not observe any alterations compared to WT mice in terms of thrombocytopenia, giant platelets, thrombin response, and VWF binding capacity [209], *Ramakrishan et al.* uniquely found differences in low-dose thrombin responses[210]. However, in both cases, VWF binding remained unaffected. In our experiments, the reduction of GPIbβ led us to focus on functional assays based on VWF binding, where we observed a decreased response with ratios of 0.72 and 0.85 for soluble and adhered binding experiments, respectively. These differences could be attributed to variances in the binding characteristics between murine GPIb-V-IX receptor and hVWF, as the authors employed a different assay while we measured hVWF-hGPIb-V-IX interactions. Despite the lack of correlation between these observations, the reduction we

observed may not be sufficient to be detectable or significantly impact platelet functionality in a clinical setting, potentially resulting in an asymptomatic condition. Therefore, it is reasonable to confirm that mutations in GPV do not manifest in BSS as reported by other authors[211,215,216]. However, these discrepancies in observations make the study of this glycoprotein, one of the most abundant on the platelet surface, particularly interesting as it is not well understood.

The development of disease models using human cell lines that constitutively express the receptor on their surface represents a significant advancement and may be a more widely accepted approach for analyzing the GPIb-V-IX receptor than traditional experiments performed in CHO mammalian cells or human cell lines. Our megakaryoblastic models offer several advantages in investigating receptor formation and specific pathogenic variants. These models possess the natural ratio of two alleles for each gene, maintain the regulation of their own promoter, and retain the epigenetic background of megakaryoblastic cells. Additionally, we can observe GPIb-V-IX complex localization, complete agglutination experiments or perform VWF-coating assays in the presence of ristocetin or botrocetin. By utilizing LVs, traditional CRISPR-Cas9 combined with HDR or new technologies based on CRISPR-Cas9 systems like prime or base editors, specific mutations can be introduced in specific localizations within the genes, thus, real effects could be explored. Therefore, we could study both biallelic and

monoallelic BSS specific mutations respectively. Similarly, WT DAMI, MEG-01 or iPSCs could be genetically edited becoming useful tools to study other diseases affecting megakaryocytes and platelets, such as Glanzmann Thrombasthenia, platelet-type von Willebrand disease or Scot Syndrome[217], among others.

Regarding BSS type C, it has been widely reported that mutations affecting *GP9* are the most common subtype of BSS[77,159]. Multiple studies have convincingly shown that lentiviral-based gene therapy represents a viable approach for correcting BSS type A1 and Type B. However, despite the significant frequency of pathogenic variants associated with this gene, no therapy has been explored for correcting BSS type C to date.

The initial investigation into the suitability of LVs as potential gene therapy tools for correcting BSS was conducted by *Shi et al*.[218]. They demonstrated that these vectors could be utilized to generate chimeric GPIb-V-IX receptors. In their study, they modified the *GP1BA* gene by incorporating a hemagglutinin tag (HA-Tag) and controlling its expression through a megakaryocytic promoter. The researchers transduced megakaryoblastic cells expressing GPIb-V-IX with these LVs. Flow cytometry and immunoprecipitation techniques were employed to detect HA-GPIb-V-IX, revealing that the transgenic HA-GPIbα could effectively compete with the WT GPIbα for integration into the assembled receptor. This discovery provided evidence that exogenously overexpressed

individual subunits could assemble and integrate within the receptor, thereby highlighting the potential of LVs for treating BSS type A1[218] .

Having confirmed its therapeutic power, same research group decided to transduce CD34^{+}-HSCs cells isolated from *Gp1ba*^{null} mice using these gene therapy tools. The transduced cells were then transplanted into lethally irradiated *Gp1ba*^{null} mice. Normal sized and functional circulating platelets expressing hGPIbα indicated the reversion of the BSS phenotype. This finding postulated lentiviral-based gene therapy as a promising approach for treating patients with mutations in *GP1BA*[96].

Similarly, *Strassel et al*. successfully reversed BSS type B in *Gp1bb*^{null} mice using the same *ex vivo* strategy[160]. In this instance, LVs were engineered to over-express *hGP1BB* under the constitutive *EF1α* promoter. The expression of GPIb-V-IX in the treated mice, along with the recovery of VWF binding, demonstrated the functional effectiveness of LV approaches in correcting BSS type B in a mouse model[45].

As observed, various authors have demonstrated the effectiveness of LVs as potent tools for restoring GPIb-V-IX expression in BSS type A1 and B. Given the length of *GP9* DNA, its monogenic etiology, and its higher frequency compared to other BSS types, it emerges as a prime candidate for correction using LVs and, consequently, gene therapy for the treatment of this disease.

In our research, we have developed a novel series of self-inactivated LVs specifically designed for reverting BSS type C. To achieve a durable and curative treatment with lifelong expression of GPIX, our approach targets the source of abnormal megakaryocytes and, subsequently, platelets, by focusing on HSCs. Targeting HSCs offers the advantage of ensuring a permanent and stable correction over time due to their ability to replenish the bone marrow[137,219].

LVs have also revolutionized the field of transgenic animals, increasing the creation efficacy through the integration of their cargo, reducing the time-consuming and laborious technology that characterizes the traditional pronucleus microinjection[220]. Nowadays it is employed to create transgenic mice, sheep, dogs, cow, among other mammals. For example, *Wang et al*. generated a eGFP transgenic mice who did not experience epigenetic silencing, having a linear correlation between gene expression and number of integrations[221].

However, that is not the common situation regarding transgene expression and stability in transgenic animals. It is reported that heterogenous expression and epigenetic silencing by promoter methylation can occur when transgenes were delivered by LVs. In these studies, it existed a negative correlation between CpG methylation levels and transgene expression. Extensive hypermethylation induces gene silencing by impeding the binding of the transcription machinery. For instance, *Liu et al*., generated eGFP transgenic

sheep where eGFP was regulated by CMV promoter, and methylations levels ranged from 34.7-83% in the tested tissues[222]. *Tian et al*., developed another transgenic sheep where they were expressing a tricistronic LV for three fluorescent proteins mediated by 2A peptide under the regulation of CMV promoter. In this case, both, CMV promoter and fluorescent protein sequences were highly methylated, thus, impeding their transcription. These authors attributed this extensive methylation pattern to 2A peptide viral origin[223]. *Hofmann, et al.*, also observed hypermethylation of both, promoter and CDS in transgenic pigs[224]. Similarly, Wen et al. experienced hypermethylation of the CDS in liver when creating a transgenic mouse for the *hTTR* gene[225].

These authors postulated that these differences might be influenced by the number of integrations and the position where this integration takes place. *Sauvain et al*. could demonstrate that LVs integration mechanism had affinity for actively transcribed regions of fertilized zygotes[226]. However, it is important to consider that the open chromatin regions found in a zygote may differ from those in a differentiated cell due to variations in transcription activities exhibited by different cell types.

Interestingly, *Herbst et al.*[227] observed significant hypermethylation in the SFFV promoter of transgenic mice expressing SET binding protein and eGFP. However, they found that the lack of transgene expression in mice was unlikely to be dependent on the integration site of the lentiviral

vector. This conclusion was supported by several findings. Firstly, in a study involving 15 different mice with individual lentiviral vector integrations at various genomic sites, as well as in the offspring of five selected mice, transgene expression was not detected. Secondly, the genomic regions surrounding the integration sites showed the ability to transcribe endogenous genes, which was observed in the offspring of three different transgenic mice. Lastly, they observed similar silencing of the promoter region in differentiating embryonic stem cells in vitro and adult hematopoietic stem cells in vivo when the lentiviral vector carried promoters derived from viruses. However, when internal promoters were utilized, this methylation did not occur, enabling successful transgene expression.

Thus, viral-derived promoters are susceptible to recognition by methylating defense mechanisms, resulting in their silencing, whereas endogenous promoter sequences remain mainly unsilenced and are more desired for achieving stable expression of the transgenes.

In order to avoid the epigenetic silencing phenomenon, a proposed approach for achieving long-term expression involves the combination of insulator elements with tissue-specific endogenous promoters to protect the transgene from the methyltransferases. *Zhang et al*., investigated the effects of different promoter sequences on the methylation levels of transduced P19 cells (stem carcinoma cells) using LVs expressing eGFP[228]. They compared the SFFV viral promoter,

EF1α human promoter, and A2UCOE sequence (containing dual divergently transcribed promoters within a methylation-free CpG island)[229]. After 44 days, SFFV showed extensive methylation on CpG islands, EF1α had intermediate levels, while A2UCOE effectively protected the transgene from methylation. The authors attributed the loss of expression to methylation rather than culture imbalances, comparing the ratio of integrations to eGFP expression. They found that although the ratio of vector copy numbers remained stable, the percentage of eGFP decreased. To confirm the protective role of A2UCOE, the authors inserted a shorter version of A2UCOE upstream of SFFV, which resulted in reduced methylation. This experiment further supported the protective function of A2UCOE. The same experiments were performed *in vivo* using transduced HSCs at 3 and 6 months post-engraftment, yielding similar results and indicating the protective role of the A2UCOE sequence.

Similarly, the chicken β-globin locus control region HS4 element, has been utilized to flank transgenes. However, the effectiveness of this approach has been limited, providing only partial protection and being dependent on the specific cell type. Moreover, incorporating the cHS4 insulator within lentiviral vectors can lead to a notable decrease in production efficiency, thereby reducing its usefulness for gene therapy applications[230,231]. Years later, *Benabdellah et al*., developed an improved version of this methylation blocking system that we have incorporated within our LVs, the HS4-SAR insulator

(SE-IS2 system)[232]. This is a chimeric insulator which comprises a SAR element, characterized by its binding properties to the nuclear matrix and defining independent chromatin domains, and a reduced version of the well-characterized HS4 insulator. This new system offered a less evident titer diminishment, maintained the barrier activity and protected the transgene expression. Importantly, this effect was maintained during the expansion and differentiation of hESCs.

Interestingly, our LVs demonstrated functionality by restoring GPIX expression in *GP9*-KO cells. In line with Benabdellah, we observed no reduction in the expression of the therapeutic cassette or the reporter cassette, this last including the SFFV -viral- promoter regulating eGFP production. These findings were also observed when LVs were utilized to rescue the same model based on iPSCs. Throughout the differentiation phase, which lasted for more than 36 days until platelet formation, we did not observe any potential epigenetic silencing of the T-GPIX nor R-GPIX construct, highlighting the suitability of this design. However, it is crucial to conduct long-term evaluations in an *in vivo* system to assess the functionality of our therapeutic vector (lacking a viral promoter) and understand the impact on the reporter vector, which incorporates a viral promoter.

Similar to our GP9-KO iPSC model, Mekchay et al. conducted a study where they reprogrammed peripheral blood mononuclear cells from BSS type A1 and type B patients (GP1BA and GP1BB) into induced pluripotent stem cells (iPSCs), representing specific pathogenic variants associated with the disease. The differentiated megakaryocytes (MKs) and platelets derived from these iPSCs exhibited the characteristic BSS phenotype. Upon transduction with GP1BA or GP1BB-pTREG-lentiviral vectors, the MKs were able to recover CD42B expression, with levels ranging from 18% to 42%, respectively [150]. It is worth noting the higher transduction efficiency achieved by our GPIX-LVs in reversing the BSS phenotype compared to pTREG-lentiviral vectors.

Proved the functionality of our gene therapy tools in all our disease models, the next step was to further validate our results in our target cells, HSCs from BSS patients. To do this, we localized two patients carrying different homozygous missense mutations associated to GPIX (p.Phe55Ser, p.Trp71Ser). It is reported that exist a small percentage of $CD34^+$ circulating cells in non-mobilized peripheral blood[233–235], so, we decided to isolate this population and transduce them with our LVs. The small number of circulating cells only let us to perform one experiment to assess if our LVs were capable to restore GPIX expression in patients carrying *GP9 missense* mutations.

Initially, we characterized *GP9* mutations by Sanger Sequencing. Then, we confirmed BSS type C phenotype by

ImageStream/Flow Cytometry *GPIX* absence. In our study we have measured accurately the average size of healthy (3.3 µm) controls and BSS patients (6.4 µm diameter). Despite BSS platelets having an almost double diameter compared to healthy platelets, it is necessary to calculate the area in order to explain the reported increase in MFI. The most appropriate approximation would be the area of a circle, considering their discoid morphology. Using the formula $A = \pi r^2$, which represents the surface area of a circle, we can estimate the surface area where antibodies would bind in the absence of permeabilization. These values would amount to 8.56 µm² for healthy platelets and 32.17 µm² for BSS platelets, resulting in a 3.75-fold increase in surface area, what correlates with the ratios previously reported. Interestingly, and similarly to what is reported from different authors [183–186,194], in platelets from BSS patients, CD41, as long as other platelet integrins, have higher MFI values than healthy controls, ranging between 3-4 times.

Then, we isolated $CD34^+$ cells from non-mobilized blood, transduced with R-GPIX to assess the transduction efficiency and differentiated to MKs and platelets. We could confirm that, despite the reduced number of starting cells and the complexity of the protocol, we could recover CD41-GPIX expression in MKs and platelets when these cells were transduced with the GPIX-LV. Non-transduced cells did not express GPIX neither their platelets, as expected. Furthermore, obtained platelets from non-transduced cells

exhibited giant size (BSS), while transduced cell produced normal sized GPIX^{+} platelets, similar to those from healthy donors.

The findings that this work yields for the usage of GPIX-LVs to revert BSS phenotype together with previous studies, also propose this disease as a potential candidate to be cured by *ex vivo* gene therapy treatments on hematopoietic stem cells.

However, despite our good result, proving its functionality in an *in vivo* model where to analyze the recovery of the physiological parameters would provide invaluable information regarding the suitability of this approach. Animal models provide valuable tools for studying platelet dysfunction. Platelets, being anucleate cytoplasmic fragments, cannot be easily manipulated using conventional *in vitro* strategies commonly employed for cultured cells [154].

One of our concerns would be the possibility that transplanted BSS patients could develop platelet refractoriness overtime, because of the continuous production of rescued platelets expressing functional and externalized GPIb-V-IX complex. Platelets refractoriness is a dramatic platelet count reduction that occurs after receiving platelet transfusions. It can be caused by immune or nonimmune factors (bleeding, splenic sequestration, etc.)[236].

Among the immune-mediated causes, antibodies against HLA class I, ABO, human platelets antigens (HPA) and

drug-dependent antibodies have been described[236]. These antibodies interact with antigens located on the outer membrane of transfused platelets. Consequently, these conjugated platelets are removed from circulation. HLA class I antibodies are the most frequently detected in multitransfused patients (23%) and the main cause for immune-mediated.

Our autologous transplantation proposal avoids the production of these kind of antibodies, however, we cannot discard the appearance of antibodies against GPIb-V-IX complex. So far, 35 HPA antibodies have been identified in multitransfused patients, in lower frequency than previous ones (2-8%)[236]. Among them, antibodies against GPIb-IX and GPV have been noted.

Unlike HLA class I antibodies, the presence of HPA antibodies has not been associated with platelet refractoriness[237,238]. HPA antibodies may only pre-exist in those BSS patients who previously received any platelet transfusions and the facility to develop them may be related to the grade of receptor impairment. Interestingly, in the case of Glanzmann Thrombastenia, severity of alloimmunization against IIb-IIIa integrin varies accordingly to the severity of the disease, distinguishing: Type I <5%; Type II, 5-20% and Type III >20% of non-functional integrin on the platelet membrane. The major severe alloimmune response is associated with less integrin externalization, thus Type I[239].

Then, a screening test to confirm the presence of all these antibodies should be recommendable before proposing autologous gene therapy approaches for BSS treatment. In addition, periodic screening tests, focused on antibodies against GPIb-V-IX complex, would allow us to monitor the generation of new antibodies after HSC autologous transplantation.

Immune-mediated refractoriness has been described in BSS type A1 animal model[96]. Lentiviral-based gene therapy expressing human GPIbα was effective to rescue BSS type A1 phenotype in *Gp1ba*^{null} mice. However, secondary transplantation experiments showed a transitory platelet refractoriness in 1 out of 8 transplanted animals. This animal developed antibodies against the human GPIbα at week 17, just during the platelet count drop. However, the animal progressively recovered normal platelet count and the antibodies were no longer detectable 4 weeks later. Preclinical experiments in BSS type C animal models will be required to evaluate our concern, due to the low number of clinical data about alloimmunization in BSS patients available. Additionally, they would provide important information regarding the specificity, effectiveness and biosafety of these gene therapy tools *in vivo*.

We have successfully developed a GP9^{null} murine model that accurately replicates the characteristic features of reduced platelet count and increased platelet volume (Giant platelets). Remarkably, these findings align with a previously reported

GP9^{null} murine model by the International Mouse Phenotyping Consortium [157], although it was primarily developed for research purposes and made available to the scientific community without in-depth analysis[157]. Similarly, murine models with *Gp1ba*^{null} and *Gp1bb*^{null} mutations have also been instrumental in recreating macrothrombocytopenia and the absence of the GPIb-V-IX receptor, faithfully reproducing key aspects of the human disease. It is presumed that our murine model will likewise exhibit impaired assembly of the GPIb-V-IX receptor.

In addition, conducted genetic rescue experiments in these models, which proved crucial in confirming the ability of human subunits to assemble within the murine GPIb-V-IX receptor[96,154,160]. The reversion of tail bleeding time and the alleviation of macrothrombocytopenia in both cases provided strong indications of disease reversion. Notably, a recently developed zebrafish *Gp9^{null}* model also displayed thrombocytopenia and bleeding tendencies, which were reversed upon microinjecting *hGP9 mRNA* into embryos of the knockout model[159]. Although no gene therapy approaches have been attempted in BSS type C models thus far, these findings offer promising data for our future experiments.

Our final goal is to go into the clinical trial phase after demonstrating the fully reversal or alleviation of the disease. Presumably, GPIX-expressing LVs would restore the assembly of the receptor GPIb-V-IX, despite of the subunit differences in species.

In summary, this research has provided insights into GPIb-V-IX assembly and has developed a novel gene therapy tool capable of correcting BSS type C for the first time. This approach involves expressing the native form of *hGP9* under the regulation of the megakaryocyte-specific promoter *hGP6L*. The LV designed in this study successfully restored GPIX expression in *GP9*-KO models, including megakaryoblast cell lines, induced pluripotent stem cells, and hematopoietic stem cells derived from two different BSS type C patients.

The genetic rescue achieved in this research resulted in the recovery of GPIX-WT expression levels, proper localization, complete receptor assembly, and functionality in terms of VWF recognition. Furthermore, experiments conducted with pluripotent stem cells and hematopoietic stem cells from patients demonstrated the reversal of platelet size abnormalities.

To further advance the research, a $Gp9^{null}$ murine model was developed to accurately replicate the macrothrombocytopenia phenotype and the absence of the receptor on the surface of megakaryocytes and platelets. Future experiments will focus on assessing the stable expression of our therapeutic cassette and evaluating the reversal of macrothrombocytopenia as well as the recovery of tail bleeding time. These crucial experiments will serve as a foundation for evaluating the clinical feasibility of these gene therapy tools.

CHAPTER VII

CONCLUSIONS

~**English**~

1. CRISPR-Cas9 system successfully induced mutations in DAMI and MEG-01 cells which interrupted the coding sequence of *GP1BA*, *GP1BB* and *GP9 genes*, or abolished the full translation of *GP5*, thus, creating knock-outs for each single subunit.
2. GPIbα is the most sensitive subunit, as it is unable to reach the membrane surface in the absence of GPIbβ or GPIX.
3. GPIbβ is indispensable for GPIb-V-IX assembly, and in its absence, none of the remaining subunits can be detected on the membrane. Furthermore, GPIbβ is the only subunit capable of partial externalization without the presence of the other subunits.
4. GPIX is only observed in association with GPIbβ, and its plasma membrane transport is significantly affected by the absence of GPIbα.
5. While GPV is not essential for GPIb-IX assembly, its absence leads to reduced externalization of GPIbβ and a slight impact on the overall receptor functionality in terms of binding and adherence to VWF.
6. Designed self-inactivating GPIX-Lentiviral vectors showed megakaryocytic-specificity in human cell lines.
7. Genetically rescued *GP9*-KO cells successfully reassembled the entire GPIb-V-IX receptor and

demonstrated functionality by binding VWF, in both its soluble and adhered form, and allowed cell aggregation.

8. *GP9*-KO induced pluripotent stem cells accurately mirrored the main features of Bernard-Soulier Syndrome-HSCs, including differentiation to megakaryocytes and platelets lacking GPIb-V-IX receptor and exhibited an enlarged size.
9. GPIX-Lentiviral vector transduction reversed the reassembly of GPIb-V-IX complexes and restored normal-sized platelets in *GP9*-KO induced pluripotent stem cells megakaryocytic derivatives.
10. *Ex vivo* differentiation of non-transduced $CD34^+$ HSCs from two unrelated Bernard-Soulier Syndrome type C patients generated megakaryocytes and giant platelets lacking GPIb-V-IX receptor on their surface.
11. *Ex vivo* differentiation of GPIX-transduced $CD34^+$ HSCs from two unrelated Bernard-Soulier Syndrome type C patients restored GPIX externalization in both megakaryocytes and platelets and normalized platelet size.
12. The $Gp9^{null}$ murine model reproduced the main features observed in Bernard-Soulier Syndrome patients, including reduced platelet count and giant platelets.

~**Castellano**~

1. El sistema CRISPR-Cas9 indujo mutaciones en las células DAMI y MEG-01, interrumpiendo la secuencia codificante de los genes *GP1BA*, *GP1BB* y *GP9*, o anulando la traducción completa de *GP5*, creando así knock-outs para cada subunidad.
2. GPIbα es la subunidad más sensible, ya que no puede llegar a la superficie de la membrana en ausencia de GPIbβ o GPIX.
3. GPIbβ es indispensable para el ensamblaje de GPIb-V-IX, y en su ausencia, ninguna de las subunidades restantes se puede detectar en la membrana. Además, GPIbβ es la única subunidad capaz de externalización parcial sin la presencia de las otras subunidades.
4. GPIX solo se observa en asociación con GPIbβ, y su transporte en la membrana plasmática se ve significativamente afectado por la ausencia de GPIbα.
5. Si bien GPV no es esencial para el ensamblaje de GPIb-IX, su ausencia conduce a una reducción en la externalización de GPIbβ y un ligero impacto en la funcionalidad general del receptor en términos de unión y adherencia al VWF.
6. Los vectores lentivirales autoinactivantes de GPIX lograron su expresión restringida al linaje megacariocítico.

7. Las células *GP9*-KO genéticamente rescatadas reensamblaron con éxito todo el receptor GPIb-V-IX y demostraron funcionalidad al unirse al VWF, tanto en su forma soluble como adherida, y permitieron la agregación celular.
8. Las células madre pluripotentes inducidas *GP9*-KO reflejaron con precisión las características principales del síndrome de Bernard-Soulier en células madre hematopoyéticas, incluyendo la diferenciación a megacariocitos y plaquetas que carecen del receptor GPIb-V-IX y presentan un mayor volumen plaquetario.
9. La transducción con el vector lentiviral GPIX permitió el reensamblaje del complejo GPIb-V-IX y recuperó el tamaño normal en las plaquetas producidas a partir de megacariocitos diferenciados procedentes de células madre pluripotentes inducidas *GP9*-KO.
10. La diferenciación *ex vivo* de células madre hematopoyéticas $CD34^+$ no transducidas de dos pacientes no emparentados con el síndrome de Bernard-Soulier tipo C generó megacariocitos y plaquetas gigantes que carecían del receptor GPIb-V-IX en su superficie.
11. La diferenciación *ex vivo* de células madre hematopoyéticas $CD34^+$ transducidas con GPIX de dos pacientes no emparentados con el síndrome de Bernard-Soulier tipo C restauró la externalización de

GPIX tanto en megacariocitos como en plaquetas, normalizando el volumen plaquetario.

12. El modelo murino *Gp9*^{null} reprodujo las características principales observadas en pacientes con el síndrome de Bernard-Soulier, incluyendo la reducción del recuento de plaquetas y el incremento del volumen plaquetario.

CHAPTER VIII

BIBLIOGRAPHY

1. Xu, X.R., Zhang, D., Oswald, B.E., Carrim, N., Wang, X., Hou, Y., Zhang, Q., Lavalle, C., McKeown, T., Marshall, A.H., et al. (2016). Platelets are versatile cells: New discoveries in hemostasis, thrombosis, immune responses, tumor metastasis and beyond. Crit Rev Clin Lab Sci *53*, 409–430. 10.1080/10408363.2016.1200008.

2. Diz-Küçükkaya, R. (2013). Inherited platelet disorders including Glanzmann thrombasthenia and Bernard-Soulier syndrome. Hematology Am Soc Hematol Educ Program *2013*, 268–275. 10.1182/asheducation-2013.1.268.

3. Menter, D.G., Kopetz, S., Hawk, E., Sood, A.K., Loree, J.M., Gresele, P., and Honn, K. V. (2017). Platelet “first responders” in wound response, cancer, and metastasis. Cancer and Metastasis Reviews. 10.1007/s10555-017-9682-0.

4. van der Meijden, P.E.J., and Heemskerk, J.W.M. (2019). Platelet biology and functions: new concepts and clinical perspectives. Nat Rev Cardiol *16*, 166–179. 10.1038/s41569-018-0110-0.

5. Stone, A.P., Nascimiento, T.F., and Barrachina, M.N. (2020). The bone marrow niche from the inside out: how megakaryocytes are shaped by and shape hematopoiesis. Blood *136*, 2125–2132. 10.1182/BLOOD.2019000962.

6. Boscher, J., Guinard, I., Eckly, A., Lanza, F., and Léon, C. (2020). Blood platelet formation at a glance. J Cell Sci *133*. 10.1242/jcs.244731.

7. Gremmel, T., Frelinger, A.L., and Michelson, A.D. (2016). Platelet physiology. Semin Thromb Hemost *42*, 191–204. 10.1055/s-0035-1564835.

8. Quach, M.E., Chen, W., and Li, R. (2018). Mechanisms of platelet clearance and translation to improve platelet storage.

9. Xu, X.R., Carrim, N., Neves, M.A.D., McKeown, T., Stratton, T.W., Coelho, R.M.P., Lei, X., Chen, P., Xu, J., Dai, X., et al. (2016). Platelets and platelet adhesion molecules: Novel mechanisms of thrombosis and anti-thrombotic therapies. Thromb J *14*. 10.1186/s12959-016-0100-6.

10. Marjoram, R.J., Li, Z., He, L., Tollefsen, D.M., Kunicki, T.J., Dickeson, S.K., Santoro, S.A., and Zutter, M.M. (2014). α2β1 integrin, gpvi receptor, and common fcrγ chain on mouse platelets mediate distinct responses to collagen in models of thrombosis. PLoS One *9*. 10.1371/journal.pone.0114035.

11. Madamanchi, A., Santoro, S.A., and Zutter, M.M. (2014). α2β1 Integrin. In, pp. 41–60. 10.1007/978-94-017-9153-3_3.

12. Nieswandt, B., Varga-Szabo, D., and Elvers, M. (2009). Integrins in platelet activation. Journal of Thrombosis and Haemostasis *7*, 206–209. 10.1111/j.1538-7836.2009.03370.x.

13. Purdy, M., Obi, A., Myers, D., and Wakefield, T. (2022). P- and E- selectin in venous thrombosis and non-venous pathologies. Journal of Thrombosis and Haemostasis *20*, 1056–1066. 10.1111/jth.15689.

14. André, P. (2004). P-selectin in haemostasis. Br J Haematol *126*, 298–306. 10.1111/j.1365-2141.2004.05032.x.

15. Repsold, L., and Joubert, A.M. (2021). Platelet function, role in thrombosis, inflammation, and consequences in chronic myeloproliferative disorders. Cells *10*. 10.3390/cells10113034.

16. Geraldo, R.B., Sathler, P.C., Lourenço, A.L., Saito, M.S., Cabral, L.M., Rampelotto, P.H., and Castro, H.C. (2014). Platelets: Still a therapeutical target for haemostatic disorders. Int J Mol Sci *15*, 17901–17919. 10.3390/ijms151017901.

17. Yadav, S., and Storrie, B. (2016). The cellular basis of platelet secretion: Emerging structure/function relationships. Platelets *28*, 108–118. 10.1080/09537104.2016.1257786.

18. Beavo, J.A., Barrett, S.J.E., Ganten, P.D., Geppetti, B.P., Michel, F.M.C., Page, I.C.P., and Rosenthal, L.W. Handbook of Experimental Pharmacology.

19. Jenne, C.N., and Kubes, P. (2015). Platelets in inflammation and infection. Platelets *26*, 286–292. 10.3109/09537104.2015.1010441.

20. Andrews, R.K., and Berndt, M.C. (2004). Platelet physiology and thrombosis. Thromb Res *114*, 447–453. 10.1016/j.thromres.2004.07.020.

21. Jackson, S.P., Mistry, N., and Yuan, Y. (2000). Platelets and the injured vessel wal l- 'Rolling into action.'Focus on glycoprotein Ib/V/IX and the platelet cytoskeleton. Trends Cardiovasc Med *10*, 192–197. 10.1016/S1050-1738(00)00062-1.

22. Rodrigues, M., Kosaric, N., Bonham, C.A., and Gurtner, G.C. (2019). Wound Healing: A Cellular Perspective. Physiol Rev *99*, 665–706. 10.1152/physrev.00067.2017.-Wound.

23. Bochenek, M.L., and Schäfer, K. (2019). Role of Endothelial Cells in Acute and Chronic Thrombosis. Hamostaseologie *39*, 128–139. 10.1055/s-0038-1675614.

24. Clemetson, K.J. (2012). Platelets and primary haemostasis. Thromb Res *129*, 220–224. 10.1016/j.thromres.2011.11.036.

25. Surin, W.R., Barthwal, M.K., and Dikshit, M. (2008). Platelet collagen receptors, signaling and antagonism: Emerging approaches for the prevention of intravascular thrombosis. Thromb Res *122*, 786–803. 10.1016/j.thromres.2007.10.005.

26. Ni, H., and Freedman, J. (2003). Platelets in hemostasis and thrombosis: Role of integrins and their ligands. Transfusion and Apheresis Science *28*, 257–264. 10.1016/S1473-0502(03)00044-2.

27. Scharf, R.E. (2018). Platelet Signaling in Primary Haemostasis and Arterial Thrombus Formation: Part 2. Hamostaseologie *38*, 211–222. 10.1055/s-0038-1675149.

28. Gale, A.J. (2011). Current understanding of hemostasis. Toxicol Pathol *39*, 273–280. 10.1177/0192623310389474.

29. Monagle, P., and Massicotte, P. (2011). Developmental haemostasis: Secondary haemostasis. Semin Fetal Neonatal Med *16*, 294–300. 10.1016/j.siny.2011.07.007.

30. Franco, A.T., Corken, A., and Ware, J. (2015). Platelets at the interface of thrombosis, inflammation, and cancer. Blood *126*, 582–588. 10.1182/BLOOD-2014-08-531582.

31. Kraemer, B.F., Borst, O., Gehring, E.M., Schoenberger, T., Urban, B., Ninci, E., Seizer, P., Schmidt, C., Bigalke, B., Koch, M., et al. (2010). PI3 kinase-dependent

stimulation of platelet migration by stromal cell-derived factor 1 (SDF-1). J Mol Med (Berl) *88*, 1277–1288. 10.1007/S00109-010-0680-8.

32. Gill, P., Jindal, N.L., Jagdis, A., and Vadas, P. (2015). Platelets in the immune response: Revisiting platelet-activating factor in anaphylaxis. J Allergy Clin Immunol *135*, 1424–1432. 10.1016/J.JACI.2015.04.019.

33. Iannacone, M. (2016). Platelet-mediated modulation of adaptive immunity. Semin Immunol *28*, 555–560. 10.1016/J.SMIM.2016.10.008.

34. Kral, J.B., Schrottmaier, W.C., Salzmann, M., and Assinger, A. (2016). Platelet Interaction with Innate Immune Cells. Transfus Med Hemother *43*, 78–88. 10.1159/000444807.

35. Carthy, J.M. (2018). TGFβ signaling and the control of myofibroblast differentiation: Implications for chronic inflammatory disorders. J Cell Physiol *233*, 98–106. 10.1002/JCP.25879.

36. Gaertner, F., and Massberg, S. (2019). Patrolling the vascular borders: platelets in immunity to infection and cancer. Nat Rev Immunol *19*, 747–760. 10.1038/s41577-019-0202-z.

37. Weis, S.M., and Cheresh, D.A. (2011). Tumor angiogenesis: molecular pathways and therapeutic targets. Nat Med *17*, 1359–1370. 10.1038/NM.2537.

38. Dongre, A., and Weinberg, R.A. (2019). New insights into the mechanisms of epithelial-mesenchymal transition and implications for cancer. Nat Rev Mol Cell Biol *20*, 69–84. 10.1038/S41580-018-0080-4.

39. Assinger, A. (2014). Platelets and infection - an emerging role of platelets in viral infection. Front Immunol *5*. 10.3389/FIMMU.2014.00649.

40. Shannon, O. (2015). Platelet interaction with bacterial toxins and secreted products. Platelets *26*, 302–308. 10.3109/09537104.2015.1014471.

41. Sivapalaratnam, S., Collins, J., and Gomez, K. (2017). Diagnosis of inherited bleeding disorders in the genomic era. Br J Haematol *179*, 363–376. 10.1111/bjh.14796.

42. Ver Donck, F., Downes, K., and Freson, K. (2020). Strengths and limitations of high-throughput sequencing for the diagnosis of inherited bleeding and platelet disorders. Journal of Thrombosis and Haemostasis *18*, 1839–1845. 10.1111/jth.14945.

43. Kumar, R., and Carcao, M. (2013). Inherited Abnormalities of Coagulation. Hemophilia, von Willebrand Disease, and Beyond. Pediatr Clin North Am *60*, 1419–1441. 10.1016/j.pcl.2013.09.002.

44. Balduini, C.L., Pecci, A., and Noris, P. (2013). Diagnosis and treatment of inherited thrombocytopenias. Semin

Thromb Hemost *39*, 161–171. 10.1055/s-0032-1333540.

45. Nurden, A.T., Freson, K., and Seligsohn, U. (2012). Inherited platelet disorders. Haemophilia *18*, 154–160. 10.1111/j.1365-2516.2012.02856.x.

46. Palma-barqueros, V., Revilla, N., Sánchez, A., Cánovas, A.Z., Rodriguez-alén, A., Marín-quílez, A., González-porras, J.R., Vicente, V., Lozano, M.L., Bastida, J.M., et al. (2021). Inherited platelet disorders: An updated overview. Int J Mol Sci *22*. 10.3390/ijms22094521.

47. Al-Huniti, A., and Kahr, W.H. (2020). Inherited Platelet Disorders: Diagnosis and Management. Transfus Med Rev *34*, 277–285. 10.1016/j.tmrv.2020.09.006.

48. Lentaigne, C., Freson, K., Laffan, M.A., Turro, E., and Ouwehand, W.H. (2016). Inherited platelet disorders: Toward DNA-based diagnosis. Blood *127*, 2814–2823. 10.1182/blood-2016-03-378588.

49. Jung, N., and Shim, Y.J. (2020). Current Knowledge on Inherited Platelet Function Disorders. Clinical Pediatric Hematology-Oncology *27*, 1–13. 10.15264/cpho.2020.27.1.1.

50. Shim, Y.J. (2020). Genetic classification and confirmation of inherited platelet disorders: Current status in korea. Clin Exp Pediatr *63*, 79–87. 10.3345/kjp.2019.00052.

51. Nurden, A.T., and Nurden, P. (2020). Inherited thrombocytopenias: history, advances and perspectives. Haematologica *105*, 2004–2019. 10.3324/haematol.2019.233197.

52. Lanza, F. (2006). Bernard-Soulier syndrome (hemorrhagiparous thrombocytic dystrophy). Orphanet J Rare Dis *1*, 46. 10.1186/1750-1172-1-46.

53. Boeckelmann, D., Hengartner, H., Greinacher, A., Nowak-Göttl, U., Sachs, U.J., Peter, K., Sandrock-Lang, K., and Zieger, B. (2017). Patients with Bernard-Soulier syndrome and different severity of the bleeding phenotype. Blood Cells Mol Dis *67*, 69–74. 10.1016/j.bcmd.2017.01.010.

54. Ghalloussi, D., Rousset-Rouvière, C., Popovici, C., Garaix, F., Saut, N., Saultier, P., Tsimaratos, M., Chambost, H., Alessi, M.C., and Baccini, V. (2020). Bernard–Soulier syndrome: first human case due to a homozygous deletion of GP9 gene. Br J Haematol *188*, e87–e90. 10.1111/bjh.16374.

55. Orsini, S., Noris, P., Bury, L., Heller, P.G., Santoro, C., Kadir, R.A., Butta, N.C., Falcinelli, E., Cid, A.R., Fabris, F., et al. (2017). Bleeding risk of surgery and its prevention in patients with inherited platelet disorders. The Surgery in Platelet disorders And Therapeutic Approach (SPATA) study. Haematologica *102*. https://doi.org/10.3324/haematol.2016.160754.

56. Sharma, P., Nicoli, E.R., Serra-Vinardell, J., Morimoto, M., Toro, C., Malicdan, M.C. V., and Introne, W.J. (2020). Chediak-Higashi syndrome: A review of the past, present, and future. Drug Discov Today Dis Models *31*, 31–36. 10.1016/j.ddmod.2019.10.008.

57. Andrews, R.K., and Berndt, M.C. (2013). Bernard – Soulier Syndrome : An Update. Semin Thromb Hemost *1*, 656–662.

58. Berndt, M.C., and Andrews, R.K. (2011). Bernard-Soulier Syndrome. Haematologica *96*, 355–359. 10.3324/haematol.2010.039883.

59. Savoia, A., Pastore, A., de Rocco, D., Civaschi, E., di Stazio, M., Bottega, R., Melazzini, F., Bozzi, V., Pecci, A., Magrin, S., et al. (2011). Clinical and genetic aspects of Bernard-Soulier syndrome: Searching for genotype/phenotype correlations. Haematologica *96*, 417–423. 10.3324/haematol.2010.032631.

60. Luo, S.Z., Mo, X., López, J.A., and Li, R. (2007). Role of the transmembrane domain of glycoprotein IX in assembly of the glycoprotein Ib-IX complex. Journal of Thrombosis and Haemostasis *5*, 2494–2502. 10.1111/j.1538-7836.2007.02785.x.

61. Mo, X., Liu, L., López, J.A., and Li, R. (2012). Transmembrane domains are critical to the interaction between platelet glycoprotein V and glycoprotein Ib-IX

complex. Journal of Thrombosis and Haemostasis *10*, 1875–1886. 10.1111/j.1538-7836.2012.04841.x.

62. Rijkers, M., van der Meer, P.F., Bontekoe, I.J., Daal, B.B., de Korte, D., Leebeek, F.W.G., Voorberg, J., and Jansen, A.J.G. (2016). Evaluation of the role of the GPIb-IX-V receptor complex in development of the platelet storage lesion. Vox Sang *111*, 247–256. 10.1111/vox.12416.

63. Bendas, G., and Schlesinger, M. (2022). The GPIb-IX complex on platelets: insight into its novel physiological functions affecting immune surveillance, hepatic thrombopoietin generation, platelet clearance and its relevance for cancer development and metastasis. Exp Hematol Oncol *11*. 10.1186/s40164-022-00273-2.

64. López, J.A., Andrews, R.K., Afshar-Kharghan, V., and Berndt, M.C. (1998). Bernard-Soulier Syndrome. Blood *91*, 4397–4418.

65. Bradford, H.N., Pixley, R.A., and Colman, R.W. (2000). Human factor XII binding to the glycoprotein Ib-IX-V complex inhibits thrombin-induced platelet aggregation. Journal of Biological Chemistry *275*, 22756–22763. 10.1074/jbc.M002591200.

66. Dong, J.-F., Li, C.Q., and L6pez, J.A. (1994). Tyrosine Sulfation of the Glycoprotein Ib-IX Complex: Identification of Sulfated Residues and Effect on Ligand Binding+.

67. Jurk, K., Clemetson, K.J., de Groot, P.G., Brodde, M.F., Steiner, M., Savion, N., Varon, D., Sixma, J.J., Van Aken, H., and Kehrel, B.E. (2003). Thrombospondin-1 mediates platelet adhesion at high shear via glycoprotein Ib (GPIb): an alternative/backup mechanism to von Willebrand factor. The FASEB journal : official publication of the Federation of American Societies for Experimental Biology *17*, 1490–1492. 10.1096/fj.02-0830fje.

68. Baglia, F.A., Shrimpton, C.N., Emsley, J., Kitagawa, K., Ruggeri, Z.M., López, J.A., and Walsh, P.N. (2004). Factor XI interacts with the leucine-rich repeats of glycoprotein Ibα on the activated platelet. Journal of Biological Chemistry *279*, 49323–49329. 10.1074/jbc.M407889200.

69. Marchese, P., Murata, M., Mazzucato, M., Pradella, P., De Marco, L., Ware, J., and Ruggeri, Z.M. (1995). Identification of Three Tyrosine Residues of Glycoprotein Ibα with distinct roles in von Willebrand Factor and α-Thrombin binding. J Biol Chem *270*, 9571–9578.

70. Huizinga, E., Tsuji, S., Romijn, R.A.P., Schiphorst, M., de Groot, P.G., Sixma, J.J., and Gros, P. (2002). Structures of Glycoprotein Ibα and Its Complex with von Willebrand Factor A1 Domain. Science (1979) *297*, 1176–1179. DOI: 10.1126/science.107355.

71. Zhang, W., Deng, W., Zhou, L., Xu, Y., Yang, W., Liang, X., Wang, Y., Kulman, J.D., Zhang, X.F., and Li, R. (2015). Identification of a juxtamembrane mechanosensitive domain in the platelet mechanosensor glycoprotein Ib-IX complex Key Points. Thrombosis and Hemostasis *125*, 562–569. 10.1182/blood-2014-07.

72. Andrews, R.K., Gardiner, E.E., Shen, Y., Whisstock, J.C., and Berndt, M.C. (2003). Glycoprotein Ib – IX – V. Int J Biochem Cell Biol *35*, 1170–1174.

73. Li, R., and Emsley, J. (2013). The organizing principle of the platelet glycoprotein Ib-IX-V complex. Journal of Thrombosis and Haemostasis *11*, 605–614. 10.1111/jth.12144.

74. Burkhart, J.M., Vaudel, M., Gambaryan, S., Radau, S., Walter, U., Martens, L., Geiger, J., Sickmann, A., and Zahedi, R.P. (2012). The first comprehensive and quantitative analysis of human platelet protein composition allows the comparative analysis of structural and functional pathways. Blood *120*. 10.1182/blood-2012-04-416594.

75. Deng, W., Xu, Y., Chen, W., Paul, D.S., Syed, A.K., Dragovich, M.A., Liang, X., Zakas, P., Berndt, M.C., Di Paola, J., et al. (2016). Platelet clearance via shear-induced unfolding of a membrane mechanoreceptor. Nat Commun *7*. 10.1038/ncomms12863.

76. Hoffmeister, K.M., Josefsson, E.C., Isaac, N.A., Clausen, H., Hartwig, J.H., and Stossel, T.P. (2003). Glycosylation Restores Survival of Chilled Blood Platelets.

77. Savoia, A., Kunishima, S., De Rocco, D., Zieger, B., Rand, M.L., Pujol-Moix, N., Caliskan, U., Tokgoz, H., Pecci, A., Noris, P., et al. (2014). Spectrum of the mutations in bernard-soulier syndrome. Hum Mutat *35*, 1033–1045. 10.1002/humu.22607.

78. OMIM Entry - # 231200 - BERNARD-SOULIER SYNDROME (2017). Omim.org. https://www.omim.org/entry/231200.

79. Balduini, C.L., Savoia, A., and Seri, M. (2013). Inherited thrombocytopenias frequently diagnosed in adults. Journal of Thrombosis and Haemostasis *11*, 1006–1019. 10.1111/jth.12196.

80. Skalníková, M., Staňo Kozubík, K., Trizuljak, J., Vrzalová, Z., Radová, L., Réblová, K., Holbová, R., Kurucová, T., Svozilová, H., Štika, J., et al. (2022). A GP1BA Variant in a Czech Family with Monoallelic Bernard-Soulier Syndrome. Int J Mol Sci *23*. 10.3390/ijms23020885.

81. Othman, M. (2011). Platelet-type Von Willebrand disease: Three decades in the life of a rare bleeding disorder. Blood Rev *25*, 147–153. 10.1016/j.blre.2011.03.003.

82. Coller, B.S. (1978). The effects of ristocetin and von Willebrand factor on platelet electrophoretic mobility. Journal of Clinical Investigation *61*, 1168–1175. 10.1172/JCI109032.

83. Othman, M., and Favaloro, E.J. (2021). 2B von Willebrand disease diagnosis: Considerations reflecting on 2021 multisociety guidelines. Res Pract Thromb Haemost *5*. 10.1002/rth2.12635.

84. Bury, L., Falcinelli, E., Mezzasoma, A.M., Guglielmini, G., Momi, S., and Gresele, P. (2022). Platelet dysfunction in platelet-type von Willebrand disease due to the constitutive triggering of the Lyn-PECAM1 inhibitory pathway. Haematologica *107*, 1643–1654. 10.3324/haematol.2021.278776.

85. Othman, M., and Gresele, P. (2020). Guidance on the diagnosis and management of platelet-type von Willebrand disease: A communication from the Platelet Physiology Subcommittee of the ISTH. Journal of Thrombosis and Haemostasis *18*, 1855–1858. 10.1111/jth.14827.

86. Seligsohn, U. (2012). Treatment of inherited platelet disorders. Haemophilia *18*, 161–165. 10.1111/j.1365-2516.2012.02842.x.

87. Hatzimichael, E., and Tuthill, M. (2010). Hematopoietic stem cell transplantation. Stem Cells Cloning *3*, 105–117. 10.2147/SCCAA.S6815.

88. Locatelli, F. (2003). Hematopoietic Stem-Cell Transplantation for the Bernard–Soulier Syndrome. Ann Intern Med *138*, 79. 10.7326/0003-4819-138-1-200301070-00028.

89. Rieger, C., Rank, A., Fiegl, M., Tischer, J., Schiel, X., Ostermann, H., and Kolb, H. (2006). Allogeneic stem cell transplantation as a new treatment option for patients with severe Bernard-Soulier Syndrome. Thromb Haemost *95*, 190–191.

90. Randolph, M.K., and Zhao, W. (2015). Genome editing and stem cell therapy pave the path for new treatment of sickle-cell disease. Stem Cell Investig *2*, 22. 10.3978/j.issn.2306-9759.2015.11.02.

91. Aiuti, A., Biasco, L., Scaramuzza, S., Ferrua, F., Cicalese, M.P., Baricordi, C., Dionisio, F., Calabria, A., Giannelli, S., Castiello, M.C., et al. (2013). Lentiviral hematopoietic stem cell gene therapy in patients with wiskott-aldrich syndrome. Science (1979) *341*. 10.1126/science.1233151.

92. Ferrua, F., Cicalese, M.P., Galimberti, S., Giannelli, S., Dionisio, F., Barzaghi, F., Migliavacca, M., Bernardo, M.E., Calbi, V., Assanelli, A.A., et al. (2019). Lentiviral haemopoietic stem/progenitor cell gene therapy for treatment of Wiskott-Aldrich syndrome: interim results of a non-randomised, open-label, phase 1/2 clinical study.

Lancet Haematol *6*, e239–e253. 10.1016/S2352-3026(19)30021-3.

93. Fang, J., Hodivala-Dilke, K., Johnson, B.D., Du, L.M., Hynes, R.O., White, G.C., and Wilcox, D.A. (2005). Therapeutic expression of the platelet-specific integrin, αIIbβ3, in a murine model for Glanzmann thrombasthenia. Blood *106*, 2671–2679. 10.1182/blood-2004-12-4619.

94. Fang, J., Jensen, E.S., Boudreaux, M.K., Du, L.M., Hawkins, T.B., Koukouritaki, S.B., Cornetta, K., and Wilcox, D.A. (2011). Platelet gene therapy improves hemostatic function for integrin αIIbβ3-deficient dogs. Proc Natl Acad Sci U S A *108*, 9583–9588. 10.1073/pnas.1016394108.

95. Wilcox, D.A., and White, G.C. (2003). Gene therapy for platelet disorders: Studies with Glanzmann's thrombasthenia. Journal of Thrombosis and Haemostasis *1*, 2300–2311. 10.1046/j.1538-7836.2003.00476.x.

96. Kanaji, S., Kuether, E.L., Fahs, S.A., Schroeder, J.A., Ware, J., Montgomery, R.R., and Shi, Q. (2012). Correction of murine bernard-soulier syndrome by lentivirus-mediated gene therapy. Molecular Therapy *20*, 625–632. 10.1038/mt.2011.231.

97. Friedmann, T., and Roblin, R. (1972). Gene Therapy for Human Genetic Disease? Science (1979) *175*, 949–955. 10.1126/science.175.4025.949.

98. Pushpendra, S., Arvind, P., and Anil, B. (2012). Nucleic Acids as Therapeutics. In From Nucleic Acids Sequences to Molecular Medicine, V. A. Erdmann and J. Barciszewski, eds. (Springer Berlin Heidelberg), pp. 19–45. 10.1007/978-3-642-27426-8_2.

99. Goswami, R., Subramanian, G., Silayeva, L., Newkirk, I., Doctor, D., Chawla, K., Chattopadhyay, S., Chandra, D., Chilukuri, N., and Betapudi, V. (2019). Gene therapy leaves a vicious cycle. Front Oncol *9*. 10.3389/fonc.2019.00297.

100. Sayed, N., Allawadhi, P., Khurana, A., Singh, V., Navik, U., Pasumarthi, S.K., Khurana, I., Banothu, A.K., Weiskirchen, R., and Bharani, K.K. (2022). Gene therapy: Comprehensive overview and therapeutic applications. Life Sci *294*. 10.1016/j.lfs.2022.120375.

101. Kumar, S.R., Markusic, D.M., Biswas, M., High, K.A., and Herzog, R.W. (2016). Clinical development of gene therapy: results and lessons from recent successes. Mol Ther Methods Clin Dev *3*, 16034. 10.1038/mtm.2016.34.

102. Tang, R., and Xu, Z. (2020). Gene therapy: a double-edged sword with great powers. Mol Cell Biochem *474*, 73–81. 10.1007/s11010-020-03834-3.

103. Kay, M.A. (2011). State-of-the-art gene-based therapies: The road ahead. Nat Rev Genet *12*, 316–328. 10.1038/nrg2971.

104. Siddiqui, M.A. (2004). Gene therapy: An overview. Journal International Medical Sciences Academy *17*, 53–54. 10.4103/0975-8844.124249.

105. Ramamoorth, M., and Narvekar, A. (2015). Non viral vectors in gene therapy - An overview. Journal of Clinical and Diagnostic Research *9*, GE01–GE06. 10.7860/JCDR/2015/10443.5394.

106. Du, X., Wang, J., Zhou, Q., Zhang, L., Wang, S., Zhang, Z., and Yao, C. (2018). Advanced physical techniques for gene delivery based on membrane perforation. Drug Deliv *25*, 1516–1525. 10.1080/10717544.2018.1480674.

107. Maestro, S., Weber, N.D., Zabaleta, N., Aldabe, R., and Gonzalez-Aseguinolaza, G. (2021). Novel vectors and approaches for gene therapy in liver diseases. JHEP Reports *3*. 10.1016/j.jhepr.2021.100300.

108. Li, C., and Samulski, R.J. (2020). Engineering adeno-associated virus vectors for gene therapy. Nat Rev Genet *21*, 255–272. 10.1038/s41576-019-0205-4.

109. Wang, D., Tai, P.W.L., and Gao, G. (2019). Adeno-associated virus vector as a platform for gene therapy

delivery. Nat Rev Drug Discov *18*, 358–378. 10.1038/s41573-019-0012-9.

110. Zittersteijn, H.A., Gonçalves, M.A.F.V., and Hoeben, R.C. (2021). A primer to gene therapy: Progress, prospects, and problems. J Inherit Metab Dis *44*, 54–71. 10.1002/jimd.12270.

111. Dufait, I., Liechtenstein, T., Lanna, A., Bricogne, C., Laranga, R., Padella, A., Breckpot, K., and Escors, D. (2012). Retroviral and Lentiviral Vectors for the Induction of Immunological Tolerance. Scientifica (Cairo) *2012*, 1–14. 10.6064/2012/694137.

112. Poletti, V., and Mavilio, F. (2021). Designing lentiviral vectors for gene therapy of genetic diseases. Viruses *13*. 10.3390/V13081526.

113. Arabi, F., Mansouri, V., and Ahmadbeigi, N. (2022). Gene therapy clinical trials, where do we go? An overview. Biomedicine and Pharmacotherapy *153*. 10.1016/j.biopha.2022.113324.

114. Sakuma, T., Barry, M.A., and Ikeda, Y. (2012). Lentiviral vectors: Basic to translational. Biochemical Journal *443*, 603–618. 10.1042/BJ20120146.

115. Milone, M.C., and O'Doherty, U. (2018). Clinical use of lentiviral vectors. Leukemia *32*, 1529–1541. 10.1038/s41375-018-0106-0.

116. Wang, D., and Gao, G. (2014). STATE-OF-THE-ART HUMAN GENE THERAPY: PART II. GENE THERAPY STRATEGIES AND APPLICATIONS. Discover Medicine *18*, 151–161.

117. Deng, Y., Wang, C.C., Choy, K.W., Du, Q., Chen, J., Wang, Q., Li, L., Chung, T.K.H., and Tang, T. (2014). Therapeutic potentials of gene silencing by RNA interference: Principles, challenges, and new strategies. Gene *538*, 217–227. 10.1016/j.gene.2013.12.019.

118. Borel, F., Kay, M.A., and Mueller, C. (2014). Recombinant AAV as a platform for translating the therapeutic potential of RNA interference. Molecular Therapy *22*, 692–701. 10.1038/mt.2013.285.

119. San Sebastian, W., Samaranch, L., Kells, A.P., Forsayeth, J., and Bankiewicz, K.S. (2013). Gene Therapy for Misfolding Protein Diseases of the Central Nervous System. Neurotherapeutics *10*, 498–510. 10.1007/s13311-013-0191-8.

120. Watanabe, M., Nishikawaji, Y., Kawakami, H., and Kosai, K.I. (2021). Adenovirus biology, recombinant adenovirus, and adenovirus usage in gene therapy. Viruses *13*. 10.3390/v13122502.

121. Nakagami, H. Development of COVID-19 vaccines utilizing gene therapy technology.

122. Abu Abed, O.S. (2021). Gene therapy avenues and COVID-19 vaccines. Genes Immun *22*, 120–124. 10.1038/s41435-021-00136-6.

123. Biagioni, A., Chillà, A., Andreucci, E., Laurenzana, A., Margheri, F., Peppicelli, S., Del Rosso, M., and Fibbi, G. (2017). Type II CRISPR/Cas9 approach in the oncological therapy. Journal of Experimental & Clinical Cancer Research *36*, 80. 10.1186/s13046-017-0550-0.

124. Cox Turitz, D.B., Platt, R.J., and Zhang, F. (2015). Therapeutic Genome Editing: Prospects and Challenges. Nat Med *21*, 121–131. 10.1038/nm.3793.

125. Ormond, K.E., Mortlock, D.P., Scholes, D.T., Bombard, Y., Brody, L.C., Faucett, W.A., Garrison, N.A., Hercher, L., and Isasi, R. (2017). Human Germline Genome Editing. The American Journal of Human Genetics *101*, 167–176. 10.1016/j.ajhg.2017.06.012.

126. Men, K., Duan, X., He, Z., Yang, Y., Yao, S., and Wei, Y. (2017). CRISPR/Cas9-mediated correction of human genetic disease. Sci China Life Sci *60*, 447–457. 10.1007/s11427-017-9032-4.

127. Pineda, M., Moghadam, F., Ebrahimkhani, M.R., and Kiani, S. (2017). Engineered CRISPR Systems for Next Generation Gene Therapies. ACS Synth Biol. 10.1021/acssynbio.7b00011.

128. Lucas, D., O'Leary, H.A., Ebert, B.L., Cowan, C.A., and Tremblay, C.S. (2017). Utility of CRISPR/Cas9 systems in hematology research. Exp Hematol. 10.1016/j.exphem.2017.06.006.

129. Gundry, M.C., Dever, D.P., Yudovich, D., Bauer, D.E., Haas, S., Wilkinson, A.C., and Singbrant, S. (2017). Technical Considerations for the use of CRISPR/Cas9 in hematology research. Exp Hematol. 10.1016/j.exphem.2017.07.006.

130. Ran, F.A., Hsu, P.D.P., Wright, J., Agarwala, V., Scott, D. a, and Zhang, F. (2013). Genome engineering using the CRISPR-Cas9 system. Nat Protoc *8*, 2281–2308. 10.1038/nprot.2013.143.Genome.

131. Wu, X., Kriz, A.J., and Sharp, P.A. (2014). Target specificity of the CRISPR-Cas9 system. Quantitative Biology *2*, 59–70. 10.1007/s40484-014-0030-x.

132. Cho, S.W., Kim, S., Kim, Y., Kweon, J., Kim, H.S., Bae, S., and Kim, J.-S. (2014). Analysis of off-target effects of CRISPR/Cas-derived RNA-guided endonucleases and nickases. Genome Res *24*, 132–141. 10.1101/gr.162339.113.

133. Zhang, X.-H., Tee, L.Y., Wang, X.-G., Huang, Q.-S., and Yang, S.-H. (2015). Off-target Effects in CRISPR/Cas9-mediated Genome Engineering. Mol Ther Nucleic Acids *4*, e264. 10.1038/mtna.2015.37.

134. Fu, B.X.H., St Onge, R.P., Fire, A.Z., and Smith, J.D. (2016). Distinct patterns of Cas9 mismatch tolerance in vitro and in vivo. Nucleic Acids Res *44*, 5365–5377. 10.1093/nar/gkw417.

135. Wang, S.W., Gao, C., Zheng, Y.M., Yi, L., Lu, J.C., Huang, X.Y., Cai, J. Bin, Zhang, P.F., Cui, Y.H., and Ke, A.W. (2022). Current applications and future perspective of CRISPR/Cas9 gene editing in cancer. Mol Cancer *21*. 10.1186/s12943-022-01518-8.

136. Tucci, F., Scaramuzza, S., Aiuti, A., and Mortellaro, A. (2021). Update on Clinical Ex Vivo Hematopoietic Stem Cell Gene Therapy for Inherited Monogenic Diseases. Molecular Therapy *29*, 489–504. 10.1016/j.ymthe.2020.11.020.

137. Biffi, A., Montini, E., Lorioli, L., Cesani, M., Fumagalli, F., Plati, T., Baldoli, C., Martino, S., Calabria, A., Canale, S., et al. (2013). Lentiviral hematopoietic stem cell gene therapy benefits metachromatic leukodystrophy. Science (1979) *341*. 10.1126/science.1233158.

138. Mussolino, C., Alzubi, J., Pennucci, V., Turchiano, G., and Cathomen, T. (2017). Genome and epigenome editing to treat disorders of the hematopoietic system. Hum Gene Ther, hum.2017.149. 10.1089/hum.2017.149.

139. BERNARD, J., and SOULIER, J.P. (1948). [On a new variety of congenital thrombocytary hemo-ragiparous dystrophy]. Sem Hop *24*, 3217–3223.

140. Bithell, T.C., Parekh, S.J., and Strong, R.R. (1972). PLATELET-FUNCTION STUDIES IN THE BERNARD-SOULIER SYNDROME*. Annals New York Academy of Sciences *201*, 141–160. doi: 10.1111/j.1749-6632.1972.tb16296.x.

141. Howard, M.A., Hardisty, R., and Hutton, A. (1973). Hereditary Giant Platelet Syndrome: A Disorder of a New Aspect of Platelet Function. Br Med J *4*, 586–588. DOI: 10.1136/bmj.2.5866.586.

142. Lopez, J.A., Leung, B., Reynolds, C.C., Li, C.Q., and Fox, J.E.B. (1992). Efficient plasma membrane expression of a functional platelet glycoprotein Ib-IX complex requires the presence of its three subunits. Journal of Biological Chemistry *267*, 12851–12859. 10.1016/s0021-9258(18)42354-x.

143. Dumont, J., Euwart, D., Mei, B., Estes, S., and Kshirsagar, R. (2016). Human cell lines for biopharmaceutical manufacturing: history, status, and future perspectives. Crit Rev Biotechnol *36*, 1110–1122. 10.3109/07388551.2015.1084266.

144. Hockemeyer, D., and Jaenisch, R. (2016). Induced pluripotent stem cells meet genome editing. Cell Stem Cell *18*, 573–586. 10.1016/j.stem.2016.04.013.

145. Choi, K.-D., Yu, J., Smuga-Otto, K., Salvagiotto, G., Rehrauer, W., Vodyanik, M., Thomson, J., and Slukvin, I. (2009). Hematopoietic and Endothelial Differentiation of Human Induced Pluripotent Stem Cells. Stem Cells *27*, 559–567. 10.1634/stemcells.2008-0922.

146. Dorn, I., Klich, K., Arauzo-Bravo, M.J., Radstaak, M., Santourlidis, S., Ghanjati, F., Radke, T.F., Psathaki, O.E., Hargus, G., Kramer, J., et al. (2014). Erythroid differentiation of human induced pluripotent stem cells is independent of donor cell type of origin. Haematologica *100*, 32–41.

147. Yasui, R., Sekine, K., and Taniguchi, H. (2021). Clever experimental designs: Shortcuts for better iPSC differentiation. Cells *10*. 10.3390/cells10123540.

148. Lee, J.H., Laronde, S., Collins, T.J., Shapovalova, Z., Tanasijevic, B., McNicol, J.D., Fiebig-Comyn, A., Benoit, Y.D., Lee, J.B., Mitchell, R.R., et al. (2017). Lineage-Specific Differentiation Is Influenced by State of Human Pluripotency. Cell Rep *19*, 20–35. 10.1016/j.celrep.2017.03.036.

149. Weinberger, L., Ayyash, M., Novershtern, N., and Hanna, J.H. (2016). Dynamic stem cell states: Naive to primed pluripotency in rodents and humans. Nat Rev Mol Cell Biol *17*, 155–169. 10.1038/nrm.2015.28.

150. Mekchay, P., Ingrungruanglert, P., Suphapeetiporn, K., Sosothikul, D., Ji-Au, W., Maneesri Le Grand, S.,

Israsena, N., and Rojnuckarin, P. (2019). Study of bernard-soulier syndrome megakaryocytes and platelets using patient-derived induced pluripotent stem cells. Thromb Haemost *119*, 1461–1470. 10.1055/s-0039-1693409.

151. Lopez-Onieva, L., Lamolda, M., Montes, R., Lozano, M.L., Vicente, V., Rivera, J., Ramos-Mejía, V., and Real, P.J. (2017). Induced pluripotent stem cells derived from Bernard-Soulier Syndrome patient's peripheral blood cells with a p.Phe55Ser mutation in the GPIX gene. Stem Cell Res *20*, 10–13. 10.1016/j.scr.2017.02.001.

152. Lopez-Onieva, L., Machuca, C., Lamolda, M., Montes, R., Lozano, M.L., Vicente, V., Rivera, J., Ramos-Mejía, V., and Real, P.J. (2016). Generation of a human induced pluripotent stem cell (iPSC) line from a Bernard-Soulier syndrome patient with the mutation p.Asn45Ser in the GPIX gene. Stem Cell Res *17*, 603–606. 10.1016/j.scr.2016.11.012.

153. Lopez-Onieva, L., Montes, R., Lamolda, M., Romero, T., Ayllon, V., Lozano, M.L., Vicente, V., Rivera, J., Ramos-Mejía, V., and Real, P.J. (2016). Generation of induced pluripotent stem cells (iPSCs) from a Bernard–Soulier syndrome patient carrying a W71R mutation in the GPIX gene. Stem Cell Res *16*, 692–695. 10.1016/j.scr.2016.04.013.

154. Ware, J., Russell, S., and Ruggeri, Z.M. (2000). Generation and rescue of a murine model of platelet dysfunction: The Bernard-Soulier syndrome. Proceedings of the National Academy of Sciences (PNAS) *97*, 2803–2808. doi: 10.1073/pnas.050582097.

155. Strassel, C., Nonne, C., Eckly, A., David, T., Leon, C., Freund, M., Cazenave, J.P., Gachet, C., and Lanza, F. (2007). Decreased thrombotic tendency in mouse models of the Bernard-Soulier syndrome. Arterioscler Thromb Vasc Biol *27*, 241–247. 10.1161/01.ATV.0000251992.47053.75.

156. Kato, K., Martinez, C., Russell, S., Nurden, P., Nurden, A., Fiering, S., and Ware, J. (2004). Genetic deletion of mouse platelet glycoprotein Ibβ produces a Bernard-Soulier phenotype with increased α-granule size. Blood *104*, 2339–2344. 10.1182/blood-2004-03-1127.

157. Meehan, T.F., Conte, N., West, D.B., Jacobsen, J.O., Mason, J., Warren, J., Chen, C.K., Tudose, I., Relac, M., Matthews, P., et al. (2017). Disease model discovery from 3,328 gene knockouts by the International Mouse Phenotyping Consortium. Nat Genet *49*, 1231–1238. 10.1038/ng.3901.

158. Dhinoja, S., Al Qaryoute, A., Fallatah, W., Demaria, A., and Jagadeeswaran, P. (2022). Characterization of zebrafish gp1ba mutant and modelling Bernard Soulier

syndrome. Blood Coagulation and Fibrinolysis *33*, 272–279. 10.1097/MBC.0000000000001135.

159. Lin, Q., Zhou, R., Meng, P., Wu, L., Yang, L., Liu, W., Wu, J., Cheng, Y., Shi, L., and Zhang, Y. (2022). Establishment of a Bernard-Soulier syndrome model in zebrafish. Haematologica *107*, 1655–1668. 10.3324/haematol.2021.278893.

160. Strassel, C., Bull, A., Moog, S., Receveur, N., Mallo, L., Mangin, P., Eckly, A., Freund, M., Dubart-Kupperschmitt, A., Gachet, C., et al. (2016). Lentiviral gene rescue of a Bernard–Soulier mouse model to study platelet glycoprotein Ibβ function. Journal of Thrombosis and Haemostasis *14*, 1470–1479. 10.1111/jth.13355.

161. Bagheri, P.M., Govaerts, I., and De Ley, M. (2011). Role of metallothionein in differentiation of leukemia cells. Mol Biol Rep *38*, 3017–3022. 10.1007/s11033-010-9967-7.

162. Schweinfurth, N., Hohmann, S., Deuschle, M., Lederbogen, F., and Schloss, P. (2010). Valproic acid and all trans retinoic acid differentially induce megakaryopoiesis and platelet-like particle formation from the megakaryoblastic cell line MEG-01. Platelets *21*, 648–657. 10.3109/09537104.2010.513748.

163. Vallance, T.M., Sheard, J.J., Meng, Y., Torre, E.C., Patel, K., Widera, D., and Vaiyapuri, S. (2021). Development and characterization of a novel, megakaryocyte NF-κB reporter cell line for investigating

inflammatory responses. Journal of Thrombosis and Haemostasis *19*, 107–120. 10.1111/jth.15118.

164. Moreau, T., Evans, A.L., Vasquez, L., Tijssen, M.R., Yan, Y., Trotter, M.W., Howard, D., Colzani, M., Arumugam, M., Wu, W.H., et al. (2016). Large-scale production of megakaryocytes from human pluripotent stem cells by chemically defined forward programming. Nat Commun *7*, 1–15. 10.1038/ncomms11208.

165. Chen, G., Gulbranson, D.R., Hou, Z., Bolin, J.M., Ruotti, V., Probasco, M.D., Smuga-Otto, K., Howden, S.E., Diol, N.R., Propson, N.E., et al. (2011). Chemically defined conditions for human iPSC derivation and culture. Nat Methods *8*, 424–429. 10.1038/nmeth.1593.

166. Barman, A., Deb, B., and Chakraborty, S. (2020). A glance at genome editing with CRISPR–Cas9 technology. Curr Genet *66*, 447–462. 10.1007/s00294-019-01040-3.

167. Zhang, J.H., Adikaram, P., Pandey, M., Genis, A., and Simonds, W.F. (2016). Optimization of genome editing through CRISPR-Cas9 engineering. Bioengineered *7*, 166–174. 10.1080/21655979.2016.1189039.

168. Oliveros, J.C., Franch, M., Tabas-Madrid, D., San-León, D., Montoliu, L., Cubas, P., and Pazos, F. (2016). Breaking-Cas-interactive design of guide RNAs for CRISPR-Cas experiments for ENSEMBL genomes.

Nucleic Acids Res *44*, W267–W271. 10.1093/NAR/GKW407.

169. Felgner, P.L., Gadek, T.R., Holm, M., Roman, R., Chan, H.W., Wenz, M., Northrop, J.P., Ringold, G.M., and Danielsen, M. (1987). Lipofection: a highly efficient, lipid-mediated DNA-transfection procedure. Proc Natl Acad Sci U S A *84*, 7413–7417. 10.1073/pnas.84.21.7413.

170. Kotecha, N., Krutzik, P.O., and Irish, J.M. (2010). Web-based analysis and publication of flow cytometry experiments. Curr Protoc Cytom. 10.1002/0471142956.cy1017s53.

171. Untergasser, A., Cutcutache, I., Koressaar, T., Ye, J., Faircloth, B.C., Remm, M., and Rozen, S.G. (2012). Primer3-new capabilities and interfaces. Nucleic Acids Res *40*. 10.1093/nar/gks596.

172. Ye, J., Coulouris, G., Zaretskaya, I., Cutcutache, I., Rozen, S., and Madden, T.L. (2012). Primer-BLAST: A tool to design target-specific primers for polymerase chain reaction.

173. Jensen, M.A., Fukushima, M., and Davis, R.W. (2010). DMSO and betaine greatly improve amplification of GC-rich constructs in de novo synthesis. PLoS One *5*, 1–5. 10.1371/journal.pone.0011024.

174. Fontayne, A., Vanhoorelbeke, K., Pareyn, I., Van Rompaey, I., Meiring, M., Lamprecht, S., Roodt, J.,

Desmet, J., and Deckmyn, H. (2006). Rational humanization of the powerful antithrombotic anti-GPIbα antibody: 6B4. Thromb Haemost *96*, 671–684. 10.1160/TH06-06-0297.

175. Schindelin, J., Arganda-Carreras, I., Frise, E., Kaynig, V., Longair, M., Pietzsch, T., Preibisch, S., Rueden, C., Saalfeld, S., Schmid, B., et al. (2012). Fiji: An open-source platform for biological-image analysis. Nat Methods *9*, 676–682. 10.1038/nmeth.2019.

176. Benabdellah, K., Gutierrez-Guerrero, A., Cobo, M., Muñoz, P., and Martín, F. (2014). A chimeric HS4-SAR insulator (IS2) that prevents silencing and enhances expression of lentiviral vectors in pluripotent stem cells. PLoS One *9*. 10.1371/journal.pone.0084268.

177. Dong, J.-F., Berndt, M.C., Schade, A., McIntire, L. V, Andrews, R.K., and López, J.A. (2001). Ristocetin-dependent, but not botrocetin-dependent, binding of von Willebrand factor to the platelet glycoprotein Ib-IX-V complex correlates with shear-dependent interactions.

178. Wu, D., Meiring, M., Kotze, H.F., Deckmyn, H., and Cauwenberghs, N. (2002). Inhibition of Platelet Glycoprotein Ib, Glycoprotein IIb/IIIa, or Both by Monoclonal Antibodies Prevents Arterial Thrombosis in Baboons. Arterioscler Thromb Vasc Biol *22*, 323–328. 10.1161/hq0202.102321.

179. Liu, H., Liu, J., Wang, L., and Zhu, F. (2021). In vitro Generation of Megakaryocytes and Platelets. Front Cell Dev Biol *9*. 10.3389/FCELL.2021.713434.

180. Sugimoto, N., and Eto, K. (2017). Platelet production from induced pluripotent stem cells. Journal of Thrombosis and Haemostasis *15*, 1717–1727. 10.1111/jth.13736.

181. Izady, E., Saltanatpour, Z., Liu, L.P., Alizadeh, A., and Hamidieh, A.A. (2022). Toward in Vitro Production of Platelet from Induced Pluripotent Stem Cells. Stem Cell Rev Rep *18*, 2376–2387. 10.1007/S12015-022-10366-4.

182. Latorre-Rey, L.J., Wintterle, S., Dütting, S., Kohlscheen, S., Abel, T., Schenk, F., Wingert, S., Rieger, M.A., Nieswandt, B., Heinz, N., et al. (2017). Targeting expression to megakaryocytes and platelets by lineage-specific lentiviral vectors. Journal of Thrombosis and Haemostasis *15*, 341–355. 10.1111/jth.13582.

183. Drouin, J., Carson, N.L., and Laneuville, O. (2005). Compound heterozygosity for a novel nine-nucleotide deletion and the Asn45Ser missense mutation in the glycoprotein IX gene in a patient with Bernard-Soulier syndrome. Am J Hematol *78*, 41–48. 10.1002/ajh.20236.

184. Lozano, M., Escolar, G., Díaz-Ricart, M., Mazzara, R., and Ordinas, A. (1995). Glycoprotein IIb-IIIa and

Glycoprotein IV Expression on Bernard-Soulier Syndrome Platelets. Blood *15*, 3763–3763.

185. Rivera, C.E., Villagra, J., Riordan, M., Williams, S., Lindstrom, K.J., and Rick, M.E. (2001). Identification of a new mutation in platelet glycoprotein IX (GPIX) in a patient with Bernard-Soulier syndrome. Br J Haematol *112*, 105–108. 10.1046/j.1365-2141.2001.02529.x.

186. Watanabe, R., Ishibashi, T., Saitoh, Y., Shichishima, T., Maruyama, Y., Enomoto, Y., Handa, M., Oda, A., Ambo, H., Murata, M., et al. (2003). Bernard-Soulier syndrome with a homozygous 13 base pair deletion in the signal peptide-coding region of the platelet glycoprotein Ibâ gene. Blood Coagulation and Fibrinolysis *14*, 387–394. 10.1097/01.mbc.0000061313.06975.55.

187. Quach, M.E., and Li, R. (2020). Structure-function of platelet glycoprotein Ib-IX. Journal of Thrombosis and Haemostasis *18*, 3131–3141. 10.1111/jth.15035.

188. Fischer, S., Handrick, R., and Otte, K. (2015). The art of CHO cell engineering: A comprehensive retrospect and future perspectives. Biotechnol Adv *33*, 1878–1896. 10.1016/j.biotechadv.2015.10.015.

189. Lanza, F., De La Salle, C., Baas, M.J., Schwartz, A., Boval, B., Cazenave, J.P., and Caen, J.P. (2002). A Leu7Pro mutation in the signal peptide of platelet glycoprotein (GP)IX in a case of Bernard-Soulier syndrome abolishes surface expression of the GPIb-V-

IX complex. Br J Haematol *118*, 260–266. 10.1046/j.1365-2141.2002.03544.x.

190. Strassel, C., David, T., Eckly, A., Baas, M.-J., Moog, S., Ravanat, C., Trzeciak, M.-C., Vinciguerra, C., Cazenave, J.-P., Gachet, C., et al. (2006). Synthesis of GPIbb with novel transmembrane and cytoplasmic sequences in a Bernard-Soulier patient resulting in GPIb-defective signaling in CHO cells. Journal of Thrombosis and Haemostasis *4*, 217–228.

191. Wang, Z., Zhao, X., Duan, W., Fu, J., Lu, M., Wang, G., Bai, X., and Ruan, C. (2004). A novel mutation in the transmembrane region of glycoprotein IX associated with Bernard-Soulier syndrome. Thromb Haemost *92*, 606–613. 10.1160/TH04-04-0240.

192. Suzuki, K., Hayashi, T., Akiba, J., Satoh, S., and Kato, T. (1999). Phenotypic Consequence of the Gene Abnormality in the Platelet Glycoprotein IX Gene Observed in a Patient with Bernard-Soulier Syndrome through Mammalian Cell Expression System.

193. Strassel, C., Pasquet, J.M., Alessi, M.C., Juhan-Vague, I., Chambost, H., Combrié, R., Nurden, P., Bas, M.J., La Salle, C. De, Cazenave, J.P., et al. (2003). A novel missense mutation shows that GPIbβ has a dual role in controlling the processing and stability of the platelet GPIb-IX adhesion receptor. Biochemistry *42*, 4452–4462. 10.1021/bi026213d.

194. Takata, Y., Kanaji, T., Moroi, M., Seki, R., Sano, M., Nakazato, S., Sueoka, E., Imamura, Y., and Okamura, T. (2012). Platelets with a W127X mutation in GPIX express sufficient residual amounts of GPIbα to support adhesion to von Willebrand factor and collagen. Int J Hematol *96*, 733–742. 10.1007/s12185-012-1216-5.

195. Dong, J.-F., Gao, S., and Ló Pez, J.A. (1998). Synthesis, Assembly, and Intracellular Transport of the Platelet Glycoprotein Ib-IX-V Complex* Downloaded from.

196. Noda, M., Fujimura, K., Takafuta, T., Shimomura, T., Fujlmoto, T., Yamamoto, N., Tanoue, K., Arai, M., Suehiro, A., Kakishita, E., et al. (1995). Heterogenous Expression of Glycoprotein lb, IX and V in Platelets from Two Patients with Bernard-Soulier Syndrome Caused by Different Genetic Abnormalities. Thromb Haemost *74*, 1411–1415. 10.1055/s-0038-1649956.

197. Kunishima, S., Yamada, T., Hamaguchi, M., and Saito, H. (2006). Bernard-Soulier Syndrome due to GPIX W127X Mutation in Japan Is Frequently Misdiagnosed as Idiopathic Thrombocytopenic Purpura. Int J Hematol *83*, 366–367. 10.1532/IJH97.06017.

198. Noris, P., Simsek, S., Stibbe, J., and Von Dem Borne, A.E.G.K. (1997). A phenylalanine-55 to serine amino-acid substitution in the human glycoprotein IX leucine-rich repeat is associated with Bernard-Soulier syndrome. Br J Haematol *97*, 312–320.

199. SUMITHA, E., JAYANDHARAN, G.R., DAVID, S., JACOB, R.R., SANKARI DEVI, G., BARGAVI, B., SHENBAGAPRIYA, S., NAIR, S.C., ABRAHAM, A., GEORGE, B., et al. (2011). Molecular basis of Bernard–Soulier syndrome in 27 patients from India. Journal of Thrombosis and Haemostasis *9*, 1590–1598. 10.1111/j.1538-7836.2011.04417.x.

200. Ali, S., Ghosh, K., and Shetty, S. (2014). Novel genetic abnormalities in Bernard-Soulier syndrome in India. Ann Hematol *93*, 381–384. 10.1007/s00277-013-1895-x.

201. Hadjkacem, B., Elleuch, H., Gargouri, J., and Gargouri, A. (2009). Bernard-Soulier syndrome: Novel nonsense mutation in GPIbβ gene affecting GPIb-IX complex expression. Ann Hematol *88*, 465–472. 10.1007/s00277-008-0611-8.

202. Tang, J., Stern-Nezer, S., Po-Ching, L., Matyakhina, L., Riordan, M., L. C. Luban, N., Steinbach, P.J., and Kaler, S.G. (2004). Mutation in the leucine-rich repeat C-flanking region of platelet glycoprotein Ib β impairs assembly of von Willebrand factor receptor. Thromb Haemost *92*, 75–88. DOI: 10.1160/TH-04-02-0071.

203. Bragadottir, G., Birgisdottir, E.R., Gudmundsdottir, B.R., Hilmarsdottir, B., Vidarsson, B., Magnusson, M.K., Larsen, O.H., Sorensen, B., Ingerslev, J., and Onundarson, P.T. (2015). Clinical phenotype in heterozygote and biallelic Bernard-Soulier syndrome-A

case control study. Am J Hematol *90*, 149–155. 10.1002/ajh.23891.

204. Özdemir, Z.C., Düzenli Kar, Y., Ceylaner, S., and Bör, Ö. (2020). A novel mutation in the GP1BA gene in Bernard-Soulier syndrome. Blood Coagulation and Fibrinolysis *31*, 83–86. 10.1097/MBC.0000000000000868.

205. McEwan, P.A., Yang, W., Carr, K.H., Mo, X., Zheng, X., Li, R., and Emsley, J. (2011). Quaternary organization of GPIb-IX complex and insights into Bernard-Soulier syndrome revealed by the structures of GPIβ and a GPIβ/GPIX chimera. Blood *118*, 5292–5301. 10.1182/blood-2011-05-356253.

206. Dib, F., Quéméner, A., Bayart, S., Boisseau, P., Babuty, A., Trossaërt, M., Sigaud, M., Ternisien, C., Drillaud, N., Eveillard, M., et al. (2022). Biological, clinical features and modelling of heterozygous variants of glycoprotein Ib platelet subunit alpha (GP1BA) and glycoprotein Ib platelet subunit beta (GP1BB) genes responsible for constitutional thrombocytopenia. Br J Haematol *199*, 744–753. 10.1111/bjh.18462.

207. Filho, J.T.D.S., Ribeiro, H.A.D.A., Fassbender, I.P.B., Ribeiro, J.M.M.C., Ferreira Júnior, W.D.S., and Figueiredo, L.C.S. (2019). Bernard-Soulier syndrome associated with 22q11.2 deletion and clinical features of DiGeorge/velocardiofacial syndrome. Blood Coagulation

and Fibrinolysis *30*, 423–425. 10.1097/MBC.0000000000000849.

208. Kurokawa, Y., Ishida, F., Kamijo, T., Kunishima, S., Kenny, D., Kitano, K., and Koike, K. (2001). A Missense Mutation (Tyr88 to Cys) in the Platelet Membrane Glycoprotein Ib Gene Affects GPIb/IX Complex Expression Bernard-Soulier Syndrome in the Homozygous Form and Giant Platelets in the Heterozygous Form. Thromb Haemost *86*, 1249–1256.

209. Mark Kahn, B.L., Diacovo, T.G., Bainton, D.F., Lanza, F., Trejo, J., and Coughlin, S.R. (1999). Glycoprotein V-Deficient Platelets Have Undiminished Thrombin Responsiveness and Do Not Exhibit a Bernard-Soulier Phenotype. Blood *94*, 4112–4121.

210. Ramakrishnan, V., Reeves, P.S., Deguzman, F., Deshpande, U., Ministri-Madrid, K., Dubridge, R.B., and Phillips, D.R. (1999). Increased thrombin responsiveness in platelets from mice lacking glycoprotein V. PNAS *96*, 13336–13341.

211. Noris, P., Arbustini, E., Spedini, P., Belletti, S., and Balduini, C.L. (1998). A new variant of Bernard-Soulier syndrome characterized by dysfunctional glycoprotein (GP) Ib and severely reduced amounts of GPIX and GPV. Br J Haematol *103*, 1004–1013. 10.1046/j.1365-2141.1998.01100.x.

212. Kimmerlin, Q., Moog, S., Ravanat, C., Strassel, C., and Lanza, F. (2022). Glycoprotein V : the unsolved GPV puzzle. Platelets *33*, 833–840. 10.1080/09537104.2021.2022114.

213. Li, C.Q., Dong, J.F., Lanza, F., Sanan, D.A., Sae-Tung, G., and Lopez, J.A. (1995). Expression of platelet glycoprotein (GP) V in heterologous cells and evidence for its association with GP Ibα in forming a GP Ib-IX-V complex on the cell surface. Journal of Biological Chemistry *270*, 16302–16307. 10.1074/jbc.270.27.16302.

214. Strassel, C., Moog, S., Baas, M.J., Cazenave, J.P., and Lanza, F. (2004). Biosynthesis of platelet glycoprotein V expressed as a single subunit or in association with GPIb-IX. Eur J Biochem *271*, 3671–3677. 10.1111/j.1432-1033.2004.04304.x.

215. Nonne, C., Hechler, B., Cazenave, J.P., Gachet, C., and Lanza, F. (2008). Reassessment of in vivo thrombus formation in glycoprotein V deficient mice backcrossed on a C57Bl/6 strain [8]. Journal of Thrombosis and Haemostasis *6*, 210–212. 10.1111/j.1538-7836.2007.02825.x.

216. Ni, H., Ramakrishnan, V., Ruggeri, Z.M., Papalia, J.M., Phillips, D.R., and Wagner, D.D. (2001). Increased thrombogenesis and embolus formation in mice lacking glycoprotein V. Blood *98*, 368–373.

217. Mohan, G., Malayala, S. v, Mehta, P., and Balla, M. (2020). A Comprehensive Review of Congenital Platelet Disorders, Thrombocytopenias and Thrombocytopathies. Cureus. 10.7759/cureus.11275.

218. Shi, Q., Wilcox, D.A., Morateck, P.A., Fahs, S.A., Kenny, D., and Montgomery, R.R. (2004). Targeting platelet GPIbα transgene expression to human megakaryocytes and forming a complete complex with endogenous GPIbβ and GPIX. Journal of Thrombosis and Haemostasis *2*, 1989–1997. 10.1111/j.1538-7836.2004.00961.x.

219. Psatha, N., Paschoudi, K., Papadopoulou, A., and Yannaki, E. (2022). In Vivo Hematopoietic Stem Cell Genome Editing: Perspectives and Limitations. Genes (Basel) *13*. 10.3390/genes13122222.

220. Wen, J., Wu, J., Cao, T., Zhi, S., Chen, Y., Aagaard, L., Zhen, P., Huang, Y., Zhong, J., and Huang, J. (2021). Methylation silencing and reactivation of exogenous genes in lentivirus-mediated transgenic mice. Transgenic Res *30*, 63–76. 10.1007/s11248-020-00224-9.

221. Wang, Y., Song, Y.T., Liu, Q., Liu, C., Wang, L.L., Liu, Y., Zhou, X. yang, Wu, J., and Wei, H. (2010). Quantitative analysis of lentiviral transgene expression in mice over seven generations. Transgenic Res *19*, 775–784. 10.1007/S11248-009-9355-Z/FIGURES/4.

222. Liu, C., Wang, L., Li, W., Zhang, X., Tian, Y., Zhang, N., He, S., Chen, T., Huang, J., and Liu, M. (2013). Highly Efficient Generation of Transgenic Sheep by Lentivirus Accompanying the Alteration of Methylation Status. PLoS One *8*. 10.1371/journal.pone.0054614.

223. Tian, Y., Li, W., Wang, L., Liu, C., Lin, J., Zhang, X., Zhang, N., He, S., Huang, J., Jia, B., et al. (2013). Expression of 2A peptide mediated tri-fluorescent protein genes were regulated by epigenetics in transgenic sheep. Biochem Biophys Res Commun *434*, 681–687. 10.1016/j.bbrc.2013.04.009.

224. Hofmann, A., Kessler, B., Ewerling, S., Kabermann, A., Brem, G., Wolf, E., and Pfeifer, A. (2006). Epigenetic regulation of lentiviral transgene vectors in a large animal model. Molecular Therapy *13*, 59–66. 10.1016/j.ymthe.2005.07.685.

225. Wen, J., Wu, J., Cao, T., Zhi, S., Chen, Y., Aagaard, L., Zhen, P., Huang, Y., Zhong, J., and Huang, J. (2021). Methylation silencing and reactivation of exogenous genes in lentivirus-mediated transgenic mice. Transgenic Res *30*, 63–76. 10.1007/S11248-020-00224-9/FIGURES/5.

226. Sauvain, M.-O., Dorr, A.P., Stevenson, B., Quazzola, A., Naef, F., Wiznerowicz, M., Schütz, F., Jongeneel, V., Duboule, D., Spitz, F., et al. (2008). Genotypic Features

of Lentivirus Transgenic Mice. J Virol *82*, 7111–7119. 10.1128/JVI.00623-08/SUPPL_FILE/TABLE_S3.XLS.

227. Herbst, F., Ball, C.R., Tuorto, F., Nowrouzi, A., Wang, W., Zavidij, O., Dieter, S.M., Fessler, S., Van Der Hoeven, F., Kloz, U., et al. (2012). Extensive methylation of promoter sequences silences lentiviral transgene expression during stem cell differentiation in vivo. Mol Ther *20*, 1014–1021. 10.1038/MT.2012.46.

228. Zhang, F., Frost, A.R., Blundell, M.P., Bales, O., Antoniou, M.N., and Thrasher, A.J. (2010). A ubiquitous chromatin opening element (UCOE) confers resistance to DNA methylation-mediated silencing of lentiviral vectors. Mol Ther *18*, 1640–1649. 10.1038/MT.2010.132.

229. Williams, S., Mustoe, T., Mulcahy, T., Griffiths, M., Simpson, D., Antoniou, M., Irvine, A., Mountain, A., and Crombie, R. (2005). CpG-island fragments from the HNRPA2B1/CBX3 genomic locus reduce silencing and enhance transgene expression from the hCMV promoter/enhancer in mammalian cells. BMC Biotechnol *5*, 17. 10.1186/1472-6750-5-17.

230. Gaszner, M., and Felsenfeld, G. (2006). Insulators: exploiting transcriptional and epigenetic mechanisms. Nat Rev Genet *7*, 703–713. 10.1038/NRG1925.

231. Jakobsson, J., Rosenqvist, N., Thompson, L., Barraud, P., and Lundberg, C. (2004). Dynamics of transgene

expression in a neural stem cell line transduced with lentiviral vectors incorporating the cHS4 insulator. Exp Cell Res *298*, 611–623. 10.1016/j.yexcr.2004.04.037.

232. Benabdellah, K., Gutierrez-Guerrero, A., Cobo, M., Muñoz, P., and Martín, F. (2014). A chimeric HS4-SAR insulator (IS2) that prevents silencing and enhances expression of lentiviral vectors in pluripotent stem cells. PLoS One *9*. 10.1371/journal.pone.0084268.

233. Shimizu, Y., Kawashiri, S.Y., Nobusue, K., Nonaka, F., Tamai, M., Honda, Y., Yamanashi, H., Nakamichi, S., Kiyama, M., Hayashida, N., et al. (2022). Association between circulating CD34-positive cell count and height loss among older men. Sci Rep *12*. 10.1038/s41598-022-11040-y.

234. Iurlo, A., Galli, N., Bucelli, C., Artuso, S., Consonni, D., and Cattaneo, D. (2022). Trend of circulating CD34+ cells in patients with myelofibrosis: Association with spleen response during ruxolitinib treatment. Br J Haematol. 10.1111/bjh.18526.

235. Mehta, A., Tahhan, A.S., Liu, C., Dhindsa, D.S., Nayak, A., Hooda, A., Moazzami, K., Islam, S.J., Rogers, S.C., Almuwaqqat, Z., et al. (2020). Circulating Progenitor Cells in Patients With Coronary Artery Disease and Renal Insufficiency. JACC Basic Transl Sci *5*, 770–782. 10.1016/j.jacbts.2020.06.006.

236. Cohn, C.S. (2020). Platelet transfusion refractoriness: how do I diagnose and manage? Hematology Am Soc Hematol Educ Program, 527–532.

237. Godeau, B., Fromont, P., Seror, T., I B Duedari A N D P H L L I P P, N.J., and Bierling, E. (1992). Platelet alloimmunization after multiple transfusions: a prospective study of 50 patients. Br J Haematol *81*, 395–400.

238. Meenaghan, M., Judson, P.A., Yousaf, K., Lewis, L., and Pamphilon, D.H. (1993). Antibodies to Platelet Glycoprotein V in Polytransfused Patients with Haematological Disease. Vox Sang *64*, 167–170. 10.1111/j.1423-0410.1993.tb05156.x.

239. Poon, M.C., and D'Oiron, R. (2018). Alloimmunization in Congenital Deficiencies of Platelet Surface Glycoproteins: Focus on Glanzmann's Thrombasthenia and Bernard-Soulier's Syndrome. Semin Thromb Hemost *44*, 604–614. 10.1055/s-0038-1648233.